Enhancing SARS-CoV-2 DNA Vaccines with CD40 Ligand and Lipid Nanoparticle Delivery

Levi Andrew Tamming

This thesis is submitted to the University of Ottawa in partial fulfillment of the requirements for the degree of Doctorate in Philosophy with specialization in Microbiology & Immunology.

Department of Biochemistry, Microbiology and Immunology,

Faculty of Medicine,

University of Ottawa

Abstract

Despite widespread vaccination, SARS-CoV-2 continues to circulate globally, with ongoing transmission driven by the emergence of immune-evasive variants and the waning of infection- and vaccine-induced immunity. Although mRNA vaccines induce strong early responses, serum neutralizing antibody (NAb) titers often wane substantially within 7–9 months post-vaccination, increasing susceptibility to breakthrough infection. While updated, variant-matched boosters can restore higher levels of protection, their overall impact is constrained by declining uptake, rollout timelines that can leave vaccines mismatched to circulating variants, and immune imprinting. Novel vaccination strategies are needed to elicit more durable and broadly protective immunity.

Multiple DNA vaccines against SARS-CoV-2 have been evaluated clinically, but most elicited only modest immune responses and often required specialized delivery systems. This thesis investigates two complementary approaches to enhance DNA vaccine performance against SARS-CoV-2: incorporation of CD40 ligand (CD40L) as a molecular adjuvant and formulation of DNA in ionizable lipid nanoparticles (DNA-LNPs). Fusing CD40L to the SARS-CoV-2 Spike enhanced the magnitude and breadth of humoral responses elicited by DNA, DNA-LNP and mRNA-LNP vaccines, while preferentially promoting Th1-skewed immunity. Encapsulation of DNA in LNPs markedly increased immunogenicity and broadened NAb activity, enabling neutralization and protection against both matched Delta and heterologous Omicron variants. This thesis also demonstrates that DNA-LNPs can afford long-term protective immunity, with durability of humoral immune response greatly exceeding those of mRNA-LNP vaccines six-months post-vaccination. Together, these findings support the feasibility and complementarity of CD40L adjuvants and LNP delivery to improve the potency, breadth, and durability of DNA vaccine-induced immunity, potentially reducing the need for frequent boosting.

Acknowledgements

To my supervisor, Dr. Sean Li, thank you for your mentorship, unique perspectives, and endless encouragement. Your support, warmth, and sense of humor have been central to this journey, and I will always remember your kindness and guidance. I'm also grateful to my co-supervisor, Dr. Lisheng Wang, and to my Thesis Advisory Committee members—Drs. Simon Sauvé, Neda Nasheri, and Anh Tran—for their thoughtful feedback and guidance.

To the Vaccine Research Lab members—Caroline, Sathya, Jianguo, and Marsha—thank you for your patience, generosity, and wisdom. To Dr. Johnston, Casey, and Grant from the Nanomedicine Lab, thank you for your dedication and hands-on help; this work truly would not have been possible without you. A special thank you to Grayson and Jessica for many stimulating lunch conversations and board game nights. I also want to extend my appreciation to everyone in the Regulatory Research Division and the Animal Care Facility who contributed to this work and helped make the Banting building feel like home.

I'm not sure I would have made it through this PhD without Dr. Pfeifle and Dr. Zhang. It has been a genuine pleasure to work alongside you both, and to share so many memorable moments along the way. Annabelle, thank you for being "the most cheerful," for all the brainstorming, and for introducing me to so many board games. Alicia, you have been a constant source of motivation and inspiration. You helped me through some of the most difficult chapters of my life and have helped me grow into the person I am today. I will forever be grateful for all you have done for me.

I'm also deeply grateful to my many friends who have supported me outside of the lab. To Filip, Justin, Julie, John, Kyle, Gaganvir, and Mack, thank you for being such a steady presence in my life for so many years. To my fellow Bell lab alumni and Slimy Seven, JD, Bri, Ashley, Jack, Natalie, and Bunz, thank you for the many new experiences and the countless memories we have made together. And thank you to Dr. Ragunath Singaravelu for always being willing to write such strong reference letters.

Lastly, thank you to my Dad, Jesse and Hayden. Knowing you will always be there for me has given me the courage to pursue my passion and the strength to keep going despite the hurdles. And to my Mom, who I know would be proud of me for reaching this milestone, thank you for everything.

List of Abbreviations

ACE2	Angiotensin-converting enzyme 2
AdV	Adenoviral-vectored
Alpha variant	B.1.1.7
Alum	Aluminum salts
ANOVA	A one-way analysis of variance
APC	Antigen-presenting cells
ARDS	Acute respiratory distress syndrome
BCA	Bicinchoninic Acid
BSL-3	biosafety level-3
CC BY	Creative Commons Attribution License
CD	Cluster of differentiation or Connector Domain
CD40L	CD40 ligand
CH	Central helix
COVID-19	Coronavirus Disease 2019
CT	Cytoplasmic tail
Delta variant	B.1.617.2
Dendritic cell	DC
DEP	Differentially expressed protein
DLinDMA	1,2-dilinoleyloxy-N,N-dimethyl-3-aminopropane
DNA-LNP	DNA in ionizable lipid nanoparticle
DODAP	1,2-dioleoyl-3-dimethylammonium-propane
DOTMA	N-[1-(2,3-dioleyloxy)propyl]-N,N,N-trimethylammonium

DOTAP	1,2-dioleoyl-3-trimethylammonium propane
DPBS	Dulbecco's phosphate-buffered saline
DPI	Days post-infection
DSPC	1,2-distearoyl-sn-glycero-3-phosphocholine
E	Envelope protein
EUA	Emergency Use Authorisation
ID	Intradermal
Ig	Immunoglobulin
IL	Interleukin
IM	Intramuscular
IPA	Ingenuity pathway analysis
Fluc	Firefly luciferase
FP	Fusion peptide
GC	Germinal centre
GFP	Green fluorescent protein
HR1	Heptad repeat 1
HR2	Heptad repeat 2
IFN	Interferon
HBV	Hepatitis B Virus
HCV	Hepatitis C Virus
HIV	Human immunodeficiency virus
KC2	DLin-KC2-DMA
KEGG	Kyoto Encyclopedia of Genes and Genomes

LLPC	Long-lived plasma cell
LNP	Lipid nanoparticle
M	Membrane protein
MERS-CoV	Middle east respiratory syndrome coronavirus
MHC	Major Histocompatibility Complex
N	Nucleocapsid protein
N1mΨ	N1-methylpseudouridine
NAb	Neutralizing antibody
NFIS	Needle-free injection system
NHP	Non-human primate
nsp	Non-structural protein
NT50	50% neutralizing titer
NTD	N-terminal domain
ORF	Open reading frame
PBS	Phosphate-buffered saline
PCA	Principal component analysis
pDNA	Plasmid DNA
PEG	Polyethylene Glycol
PFU	Plaque forming unit
qRT-PCR	quantitative real-time-PCR
R_0	Basic reproductive rate
RBD	Receptor binding domain
RBM	Receptor binding motif

R_e	Effective reproduction rate
RNP	Ribonucleoprotein
RSV	Respiratory syncytial virus
RTC	Replication transcription complex
S	Spike glycoprotein
SARS-CoV-1	Severe acute respiratory syndrome coronavirus
SARS-CoV-2	Severe acute respiratory syndrome coronavirus 2
sgmRNA	Subgenomic messenger RNA
sgRNA	Subgenomic RNA
SS	Signal sequence
STING	Stimulator of interferon genes
TBS	Tris-buffered saline
TCID50	50% Tissue Culture Infectious Dose
TCR	T cell receptor
Th1	T helper cell 1
Th2	T helper cell 2
TM	Transmembrane domain
TMPRSS2	Transmembrane protease serine 2
TNF	Tumor necrosis factor
TRAF	TNF-receptor associated factor
URT	Upper respiratory tract
VAERD	Vaccine-associated enhanced respiratory disease
VE	Vaccine efficacy

VOC	Variant of concern
VSV	Vesicular Stomatitis Virus
WHO	World Health Organization

Table of Contents

List of Figures and Tables

Chapter 1: Introduction

1.1 COVID-19

1.1.1 COVID-19 pandemic

As of June 23 2024, there had been over 775 million confirmed cases of coronavirus disease 2019 (COVID-19) and the number of reported fatalities exceeded 7 million (1). COVID-19 is caused by infection with the severe acute respiratory syndrome coronavirus 2 (SARS-CoV-2), a novel betacoronavirus that first emerged in human populations in late 2019 (2). Despite early containment efforts and lockdown measures, SARS-CoV-2 swiftly spread across the globe, prompting the World Health Organization (WHO) to declare a global pandemic on March 11, 2020 (3). The COVID-19 pandemic had broad and substantial health, social, and economic impacts (4). In response to this global emergency, an unprecedented level of resources was allocated to vaccine development, which contributed to the rapid authorization of multiple vaccines that were highly effective at reducing severe illness, hospitalization, and mortality (5,6). In May 2023, after more than 13.3 billion COVID-19 vaccine doses had been administered globally, the WHO declared the end of the COVID-19 global health emergency (7,8). However, this decision did not mark the end of SARS-CoV-2 circulation or the need for vaccination, as the virus continues to spread worldwide and remains a significant threat to vulnerable populations (9). Increasingly, SARS-CoV-2 is regarded as endemic, with expectations that the virus will persist in a manner analogous to seasonal influenza and other human coronaviruses, with recurrent waves of infection rather than complete elimination (10,11).

1.1.2 Transmission and spread

SARS-CoV-2 is highly transmissible, spreading between individuals primarily through inhalation of respiratory droplets and aerosols (12). The basic reproductive rate (R_0) of the original ancestral strain of SARS-CoV-2 is believed to have been 2–3 (13), slightly higher than that of most seasonal influenza viruses (R_0 = 1.5–2) (14). The acquisition of mutations that increase viral shedding, receptor binding and immune escape has enhanced the transmissibility of SARS-CoV-2, with the estimated R_0 of newer Omicron variants exceeding 8–10 (15). Successive waves of SARS-CoV-2 infection have occurred in many regions, driven by the emergence of these transmissible or immune-evasive variants (16). Fortunately, wide-scale immunization and natural immunity from prior infections have helped limit the effective reproduction rate (R_e) of new variants (15,17). The incubation period for SARS-CoV-2 is highly variable, ranging from 2 to 14 days, although most infected individuals develop symptoms between 4 and 6 days (18,19). Critically, SARS-CoV-2 shedding often begins prior to symptom onset, leading to substantial presymptomatic transmission (20). In addition, during asymptomatic infections, which comprise an estimated 20–40% of infections (21,22), individuals can still shed infectious virus, contributing to the “silent” spread of COVID-19 (23,24).

1.1.3 Clinical features

COVID-19 exhibits a wide clinical spectrum, spanning from asymptomatic infections to critical illness. Notably, the clinical spectrum, including the type and severity of symptoms, has continuously shifted with the emergence of new variants (25). The most common symptoms of COVID-19 include fever, cough, sore throat, fatigue, sneezing, nasal congestion and muscle soreness (26). One distinguishing symptom of COVID-19 is the loss of smell, or anosmia, caused by the virus's ability to damage the epithelium surrounding the olfactory bulb(27). SARS-CoV-2

has also been shown to infect the intestinal epithelium, causing gastrointestinal symptoms such as diarrhea and abdominal pain in a subset of patients (28). More severe cases of COVID-19 can result in difficulty with breathing, hypoxia, chest pain, severe muscle weakness, altered mental status, cyanosis and cardiac damage (26,29). SARS-CoV-2 infection can also be fatal, especially in vulnerable populations, with the primary causes of mortality including acute respiratory distress syndrome (ARDS), dysregulated systemic inflammation leading to multi-organ failure, severe thromboembolic events, and direct viral or inflammatory cardiac injury (30,31).

The severity of COVID-19 is exacerbated by various comorbidities including obesity, diabetes, immunosuppression, hypertension and pre-existing respiratory and cardiovascular diseases (32). Advanced age is the strongest risk factor for severe COVID-19, with more than 81% of COVID-19 deaths occurring in people over the age of 65 (33–35). This is primarily attributed to a combination of age-related immunological changes, including immunosenescence and inflammaging, and the higher prevalence of comorbidities in older adults (36,37). Notably, in contrast to other respiratory viruses such as influenza and respiratory syncytial virus (RSV), which are major causes of hospitalization and death in pediatric populations, pediatric SARS-CoV-2 infection is generally mild, accounting for only ~1–2% of total COVID-19 hospitalizations (38–40). Sex is also a risk factor for severe COVID-19, with men exhibiting higher rates of hospitalization and death than women, likely due to a combination of sex-dependent immune responses, differences in receptor expression and a greater prevalence of comorbidities (41–43).

SARS-CoV-2 infection can also cause Long COVID (post-acute sequelae of COVID-19 or post COVID-19 condition), which is generally defined as the continuation or development of new symptoms 3 months after COVID-19 onset, with these symptoms lasting for at least 2 months with no alternative explanation (44). Hallmark symptoms include fatigue and cognitive impairment

("brain fog"), although Long COVID can also affect neurologic, respiratory, cardiovascular, gastrointestinal, and musculoskeletal systems (45). Long COVID can result from multiple distinct pathophysiologies including persistent viral reservoirs, immune dysregulation and autoantibody formation (45,46). Risk factors for Long COVID include pre-existing comorbidities, acute disease severity, vaccination status, and sex (45). While males face a higher risk for severe acute COVID-19, females are more susceptible to Long COVID, potentially due to sex-based differences in immune response and their higher predisposition to autoimmune disorders (45,47,48). The acute and chronic manifestations of SARS-CoV-2 infection highlight the importance of effective vaccination strategies to reduce severity and long-term health impacts of COVID-19.

1.2 SARS-CoV-2

1.2.1 Coronaviridae

SARS-CoV-2 belongs to the Coronaviridae family, a group of enveloped, positive-sense single-stranded RNA viruses (49). Seven coronaviruses are known to infect humans, all of which belong to two genera: Alphacoronavirus and Betacoronavirus (50). Four of these coronaviruses are seasonal endemic viruses associated with the "common cold": the Alphacoronaviruses 229E and NL63, and the Betacoronaviruses OC43 and HKU1 (50). These four viruses are estimated to contribute to approximately 15–30% of common cold cases and typically cause mild to moderate upper respiratory tract infections, with relatively limited impact on public health (51). In contrast, the three remaining human coronaviruses — severe acute respiratory syndrome coronavirus (SARS-CoV-1), middle east respiratory syndrome coronavirus (MERS-CoV) and SARS-CoV-2 — are more virulent and capable of causing severe lower respiratory tract illness (50,52). All three are Betacoronaviruses believed to have originated from bats and spilled over to humans through

intermediate hosts (50,53). SARS-CoV-1 was responsible for the 2002-2004 SARS outbreak which affected nearly 30 countries, resulting in approximately 8,000 cases and over 700 deaths (54,55). MERS-CoV has caused recurrent outbreaks on the Arabian Peninsula, with more than 2,600 confirmed cases and over 900 reported deaths since first being identified in 2012 (56). As human-to-human transmission of MERS-CoV has been inefficient, most outbreaks have originated from repeated zoonotic spillovers from infected dromedary camels (56,57). In contrast, SARS-CoV-2 rapidly disseminated worldwide, driven through a combination of more efficient transmission, early peak viral shedding and asymptomatic spread (13,20,23).

1.2.2 Genome organization and replication

The genome of SARS-CoV-2 is approximately 29.9 kilobases in length and encodes approximately 29 proteins across 12-15 open reading frames (ORFs) (58). The largest of these are the overlapping ORF1a and ORF1b, which are translated into polyproteins pp1a and pp1ab directly from the SARS-CoV-2 positive-sense RNA genome (Figure 1.1) (58). Auto-proteolysis of these polypeptides produces 16 non-structural proteins (nsps) that form the viral replication-transcription complex (RTC) and inhibit interferon (IFN) signaling (58,59) (Figure 1.1). The RTC transcribes full-length negative-sense copies of the RNA genome within specialized double-membrane vesicles, where RNA-intermediates are secluded from host immune sensors (59). These negative-sense copies then serve as the template to generate new positive-sense viral genomes (59). The SARS-CoV-2 genome is maintained with relatively high fidelity due to the proofreading activity of nsp14, with an estimated mutation rate of $\sim 10^{-6}$ substitutions per nucleotide per replication cycle (60,61). The RTC also produces a series of shorter negative-sense subgenomic RNAs (sgRNAs) via discontinuous 5'-3' transcription which are used as templates to transcribe positive-sense subgenomic messenger RNAs (sgmRNAs) (Figure 1.1) (59). These sgmRNAs are

translated by host machinery to produce the remaining SARS-CoV-2 proteins, which include both structural and accessory proteins (59). The process of 5'-3' discontinuous transcription causes 3' proximal genes to be preferentially transcribed, helping regulate the relative expression of the viral antigens and thus influencing which are most available for immune recognition (62–64).

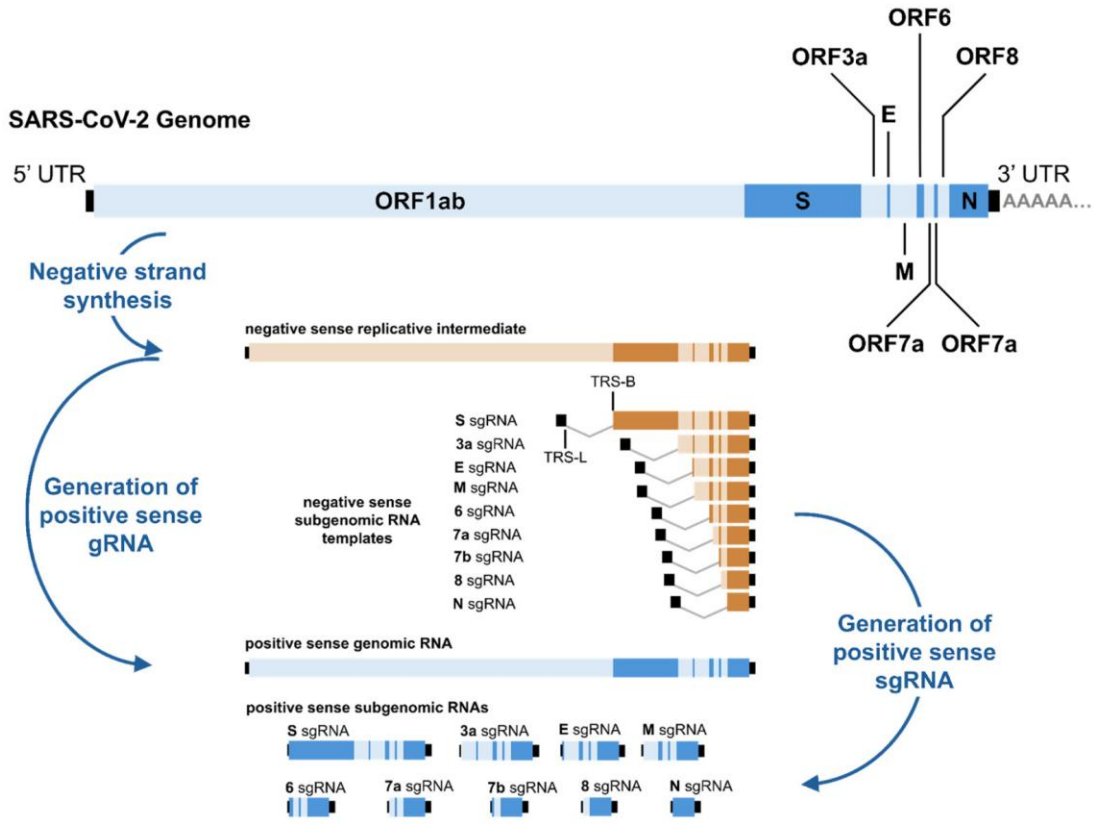

Figure 1.1. SARS-CoV-2 Genome Organization and Replication.

Following entry, the positive-sense SARS-CoV-2 genome is directly translated to produce polyproteins pp1a and pp1ab, which are proteolytically cleaved into nsps that assemble the RTC. The RTC generates negative-sense RNA intermediates that serve as templates for synthesis of new positive-sense genomes and a nested set of sgmRNAs that encode structural and accessory proteins. Reproduced from Williams, R et al. 2025 (65), in accordance with the Creative Commons Attribution 4.0 International License (CC BY 4.0) (https://creativecommons.org/licenses/by/4.0/).

1.2.3 Structural proteins and spike glycoprotein

SARS-CoV-2 encodes four structural proteins: the nucleocapsid protein (N), envelope protein (E), membrane protein (M) and spike glycoprotein (S). The N protein, the most abundant structural protein, packages the viral RNA genome into a helical ribonucleoprotein (RNP) complex that becomes enclosed by the viral envelope (66). The N protein also plays additional roles in orchestrating virion assembly, enhancing the efficiency of viral genomic RNA synthesis, and suppressing type I IFN responses (66–69). The E protein is a small integral membrane protein that acts as a calcium-selective ion channel and contributes to efficient endosomal release and virion assembly (70–72). The M protein orchestrates virion assembly, forming protein-protein interactions with itself and the other three structural proteins (73). The M protein also inhibits IFN signaling (74).

The S protein is a homotrimeric class I fusion protein that facilitates viral entry by binding host-cell receptors and mediating fusion of viral and cellular membranes (75,76) (Figure 1.2A/B). These two functions are carried out by the S1 and S2 subunits respectively. The S1 subunit includes an N-terminal signal peptide, the receptor-binding domain (RBD), and the N-terminal domain (NTD) (Figure 1.2A/B) (75). The RBD binds to the angiotensin-converting enzyme 2 (ACE2) receptor (77,78), which is highly expressed in the airway epithelium (79). ACE2 is also expressed in a range of human tissues, including the heart, kidney, vasculature, small intestine and central nervous system, contributing to the broad clinical manifestations of COVID-19 (79,80). The prefusion S protein dynamically undergoes reversible conformation changes, shifting the RBD between an “up” or “open” conformation, in which the receptor binding motif (RBM) is exposed and capable of engaging ACE2, and a “down” or “closed” conformation where the RBM is hidden and inaccessible (75) (Figure 1.2C). The NTD stabilizes the prefusion S conformation and modulates

the RBD up/down equilibrium (81,82). The NTD may also enhance viral entry through interactions with host glycans and co-receptors (83,84).

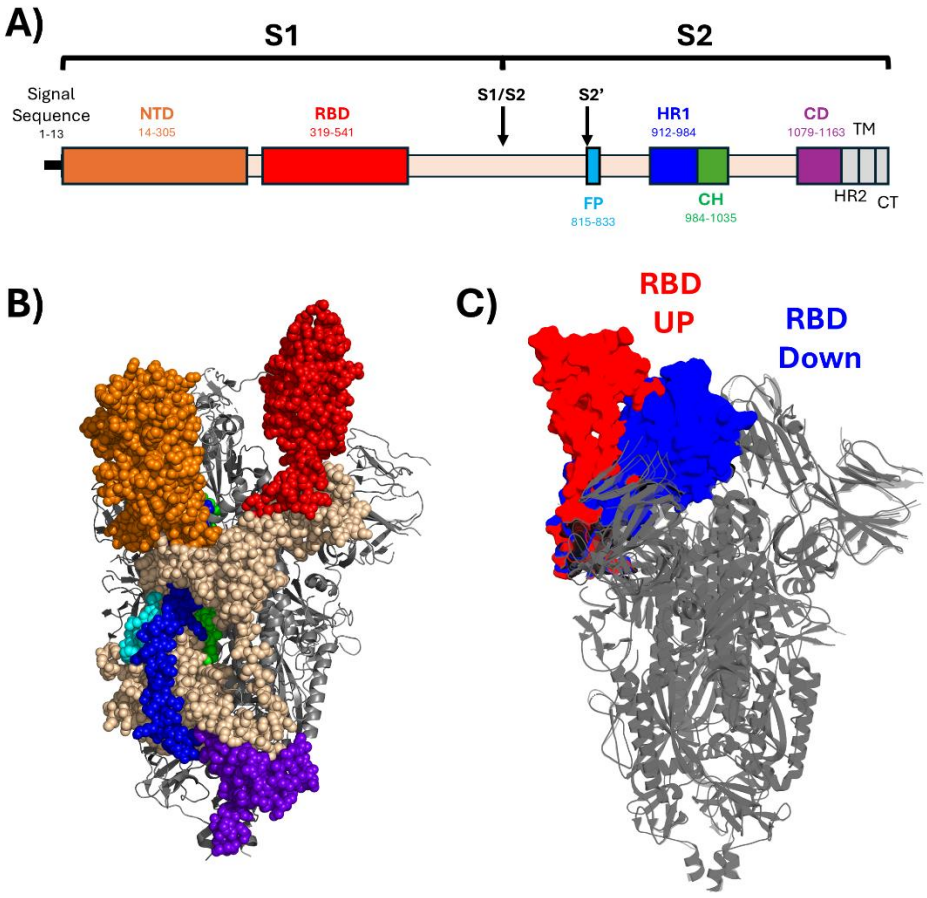

Figure 1.2. SARS-CoV-2 Spike Glycoprotein.

(A) SARS-CoV-2 Spike domain organization. NTD, N-terminal domain; RBD, receptor binding domain; FP, fusion peptide; HR1, heptad repeat 1; CH, central helix; CD, connector domain; HR2, heptad repeat 2; TM, transmembrane domain; CT, cytoplasmic tail. Arrows denote protease cleavage sites. (B) Structure of the prefusion Wuhan-Hu-1 S trimer with one RBD in the "up" (open) conformation (PDB: 6VYB). Domains of the "up" monomer are colored as follows: NTD (orange), RBD (red), FP (cyan), HR1 (blue), CH (green), CD (purple). (C) Superposition of prefusion S trimer structures in the RBD-up (red, PDB: 6VYB) and RBD-down (blue, PDB: 6VXX) conformations, highlighting the conformational difference at the RBD.

The S2 subunit is highly conserved relative to S1, reflecting significant structural constraints related to its role in membrane fusion (85). The S2 subunit is comprised of the fusion peptide (FP), heptad repeat 1 (HR1) central helix (CH), Connector Domain (CD), heptad repeat 2 (HR2), transmembrane domain (TM) and cytoplasmic tail (CT) (Figure 1.2A/B). The S1 and S2 subunits are separated by a multibasic motif referred to as the S1/S2 cleavage site (86) (Figure 1.2A/B). Proteolytic cleavage at this site primes the S protein for membrane fusion by increasing the accessibility of the downstream S2′ cleavage site (76) (Figure 1.2A/B). Cleavage at the S2′ site exposes the fusion peptide, triggering its insertion into the host membrane (76). Subsequently, the HR1 and HR2 assemble into a six-helix bundle, driving fusion of the viral and cellular membranes (87). The CT has non-fusogenic roles, regulating S protein trafficking and incorporation into virions, and contains motifs that limit its cell-surface expression (88,89).

1.2.4 Rise of Omicron and shifting entry mechanisms

Despite the relatively high replication fidelity of SARS-CoV-2, new variants with enhanced transmissibility and the ability to evade immune recognition have continued to emerge. Mutations have commonly arisen in the S1 subunit, where they have substantial effects on immune recognition, cell tropism and the efficiency and mode of viral entry (17). One of the first notable S mutations was D614G, which became globally fixed by July 2020 (90) (Figure 1.3). The D614G mutation reduced S1 shedding and increased the proportion of S proteins adopting open RBD conformations, enhancing infectivity and transmissibility (91–93). In December 2020, B.1.1.7 (Alpha) was designated the first variant of concern (VOC), a designation given to viral lineages associated with increased transmissibility, more severe disease, or reduced effectiveness of countermeasures (94). It was ~40–70% more transmissible than the ancestral strain, primarily due to the N501Y S mutation which enhanced ACE2 binding (95). The Alpha variant was displaced by

B.1.617.2 (Delta), which was associated with higher viral loads and more severe disease outcomes (96,97). The Delta variant carried additional S mutations that increased its transmissibility and fusogenicity like P681R near the S1/S2 cleavage site and mutations that aided immune escape like L452R (98,99) (Figure 1.3).

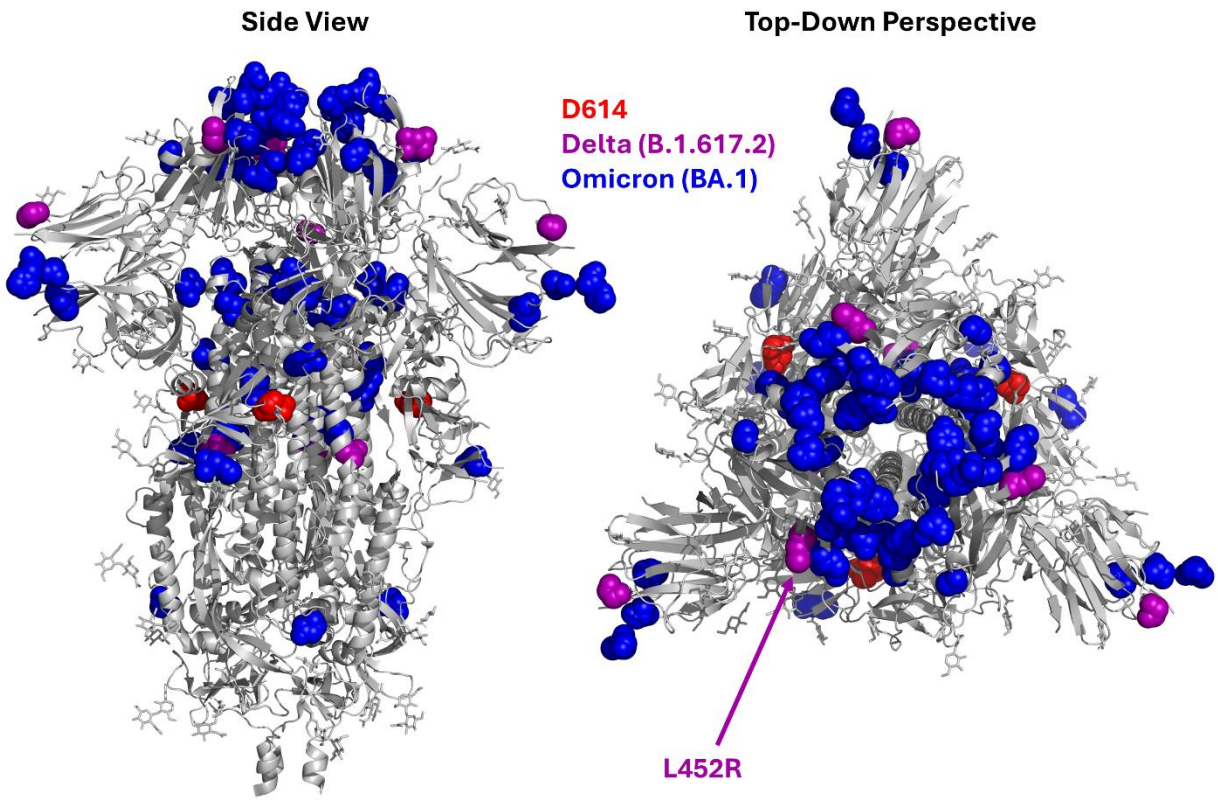

Figure 1.3. Structural mapping of SARS-CoV-2 spike protein mutations.

Side view (left) and top-down perspective (right) of the SARS-CoV-2 spike protein trimer (gray, PDB: 6VXX) with variant-defining mutations displayed as space-filling spheres. D614G (red), Delta B.1.617.2 (magenta), and Omicron BA.1 (blue). The Delta-defining substitution L452R is indicated. BA.1 carried over 30 spike mutations, with substitutions particularly concentrated in the RBD.

The most substantial jump between variants came with the sudden detection of the BA.1 (Omicron) variant in November 2021 (100). BA.1 carried more than 30 spike mutations relative to the ancestral strain and appeared without a clear intermediate form (100) (Figure 1.3). The abrupt

appearance of BA.1 and the magnitude of its evolution has led to speculation that the variant originated either in a chronically infected immunocompromised individual or through undetected circulation in a non-human host (101,102). Through a combination of increased transmissibility and avoidance of immune recognition, the Omicron lineage quickly supplanted all other SARS-CoV-2 lineages and caused a substantial surge in global infections (103,104).

Notably, several S mutations have arisen that modulate S1/S2 cleavage efficiency, consequently altering protease dependence, entry pathways, cell tropism and pathogenicity (105–107). In pre-Omicron lineages, the S1/S2 cleavage site was commonly pre-cleaved by furin-like proteases in producer cells while being trafficked through the trans-Golgi network (76,108). Infectious particles with pre-cleaved spikes would then bind ACE2 on target cells, where cell-surface proteases such as Transmembrane protease, serine 2 (TMPRSS2) would cleave the S2′ site, triggering plasma-membrane fusion (Figure 1.4) (76,109). Mutations in the Omicron lineage decreased S1/S2 cleavage efficiency, reducing TMPRSS2 usage and shifting viral entry toward cathepsin-dependent endosomal pathways (Figure 1.4) (106,107). This shift in entry mechanisms has been associated with greater upper respiratory tract (URT) tropism, potentially contributing to the reduced pathogenicity of the Omicron lineage relative to earlier variants (106,107).

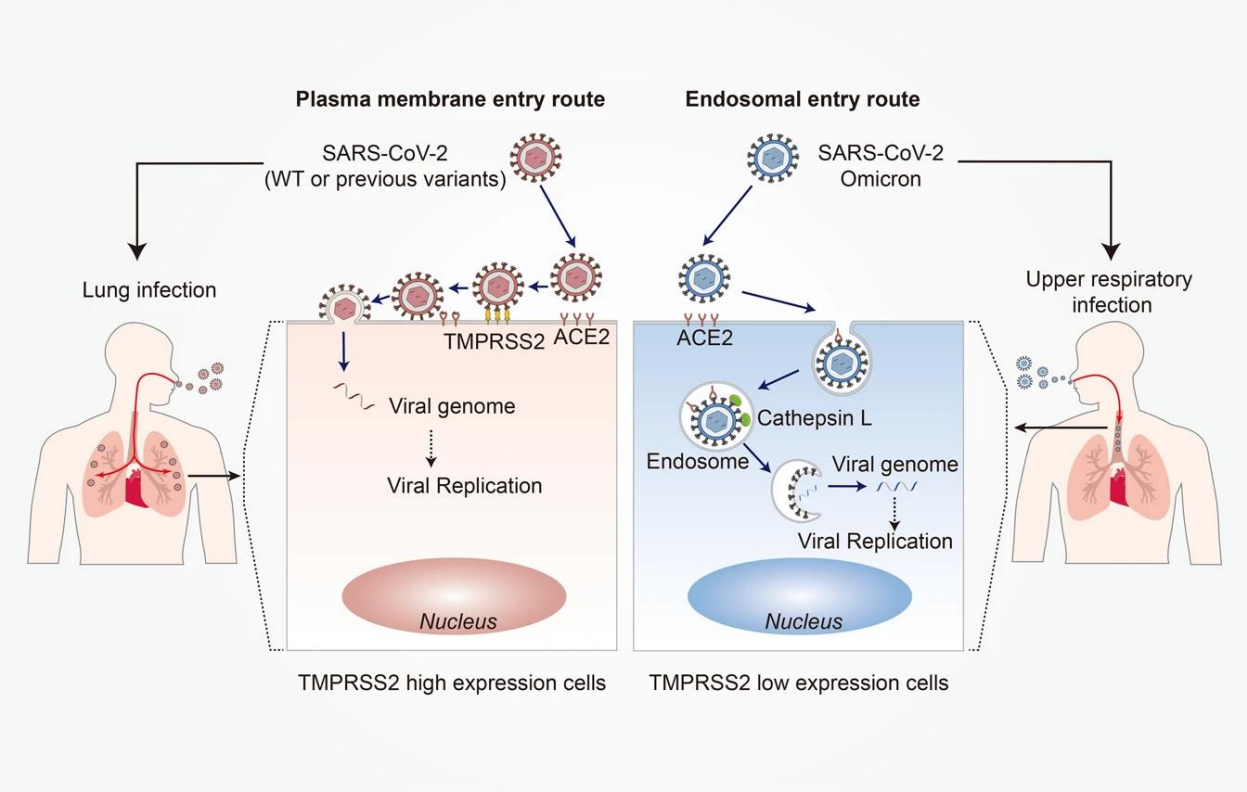

Figure 1.4. SARS-CoV-2 Entry Pathways.

SARS-CoV-2 utilizes two entry pathways: cell-surface (plasma membrane) and endosomal entry. In pre-Omicron lineages, the S1/S2 site was often pre-cleaved by furin-like proteases, priming virions for efficient cell-surface entry. After ACE2 engagement, TMPRSS2-mediated S2' cleavage triggers rapid plasma-membrane fusion and release of viral RNA. In Omicron lineages, mutations reduce S1/S2 cleavage efficiency, diminishing TMPRSS2 usage and an increasing reliance on endosomal entry pathways where acidification and endosomal proteases mediate S2' cleavage. This shift in entry has been associated with alterations in host cell tropism, decreasing lung infection and increasing URT infection and transmission. Reproduced from Fan, Y. et al. (110) in accordance with CC BY 4.0 (https://creativecommons.org/licenses/by/4.0/).

1.2.5 Post-Omicron evolution

Subsequent Omicron sublineages have caused successive waves of infection, driven by stepwise mutation accumulation and occasional recombination events. The BA.5 sublineage became predominant in mid-2022, driving major surges in multiple regions (111). BA.5 acquired mutations such as F486V, which enhanced immune escape, and re-acquired L452R, a defining mutation of the Delta lineage which increases ACE2 binding affinity (112,113). Another large surge in global

infections occurred in early 2023, driven by the emergence of the XBB lineage, which was likely generated through the recombination of co-circulating BA.2.75 and BJ.1 lineages (114) (Figure 1.5). The XBB.1.5 variant became the dominant global strain in early 2023, with the F486P mutation providing a superior balance between ACE2 binding affinity and antibody escape (115). By late 2023, the BA.2.86-descended lineage JN.1 emerged and rapidly displaced the XBB lineage, becoming predominant by early 2024 (116) (Figure 1.5). In mid-late 2024, descendants of the JN.1 lineage known as the 'FLiRT' variants (such as KP.2, KP.3 and KP.3.1.1) became dominant, characterized by immune-escaping F456L and R346T mutations (117,118) (Figure 1.5). Although global sequencing and surveillance efforts have declined dramatically, SARS-CoV-2 continued to evolve rapidly in 2025. Recombination among co-circulating lineages contributed to the rise of XEC in early 2025 (119). Shortly thereafter, the independent lineage LP.8.1 surpassed XEC in prevalence and was subsequently selected by regulators as the preferred vaccine strain for the 2025–2026 season (120,121). However, as of late 2025, LP.8.1 itself has been displaced by XFG, a recombinant lineage (122,123).

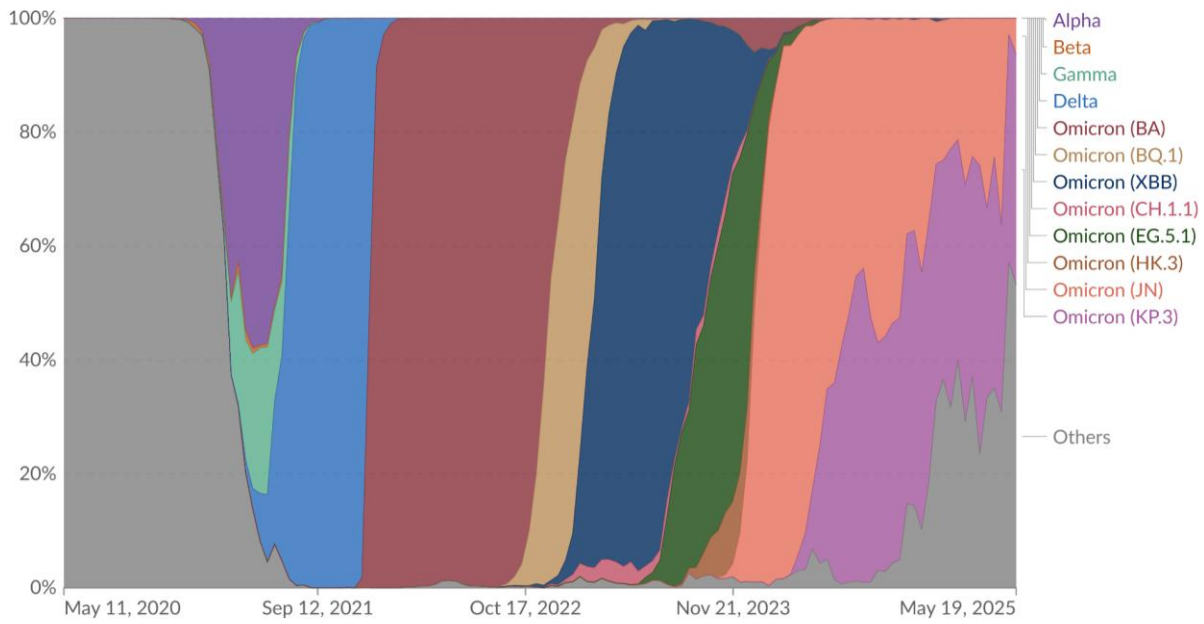

Figure 1.5. Relative Variant Abundance Canada 2020-2025.

The per variant proportion of analyzed sequences in the preceding two weeks that corresponded to each variant group. Data collected in Canada. Reproduced from Our World in Data (124) in accordance with CC BY 4.0 (https://creativecommons.org/licenses/by/4.0/).

1.3 Immunity to SARS-CoV-2

1.3.1 Humoral immunity

Most individuals infected with SARS-CoV-2 seroconvert within 10-14 days of symptom onset, with humoral responses primarily directed against the S and N proteins (125–128). Less prevalent antibody responses are also generated against the surface-exposed N-terminus of the M protein and against several non-structural proteins (129–132). Systemic immunoglobulin G (IgG) responses following SARS-CoV-2 infection are generally durable, with anti-Spike IgG detectable for at least 6 to 12 months in most individuals (125). Natural infection also elicits humoral

responses in the respiratory mucosa, with anti-Spike immunoglobulin A (IgA) readily detected in nasal secretions and saliva as early as two weeks following infection (133,134).

Antiviral antibodies can broadly be categorized into two groups: neutralizing and non-neutralizing. Neutralizing antibodies (NAbs) act by preventing viral entry into host cells. In the case of SARS-CoV-2, NAbs are primarily directed against the S protein, where they either block its interaction with ACE2 or prevent the conformational changes required for membrane fusion (135). The majority of NAbs target the RBD, although neutralizing activity has also been observed against the NTD and conserved regions of the S2 subunit (136,137). NAb titers are one of the strongest correlates of protection against SARS-CoV-2 infection and disease (138,139). While non-neutralizing antibodies do not directly block viral entry, they still contribute significantly to viral clearance by recruiting innate immune effector cells via Fc receptor engagement, triggering antibody effector functions such as phagocytosis and cytotoxicity (140). These non-neutralizing functions have been increasingly recognized as important contributors to protective immunity, particularly in the context of waning NAb titers and immune evasion by viral variants (141,142).

1.3.2 Cellular immunity

$CD8^+$ T cells, also known as cytotoxic T cells, recognize and eliminate SARS-CoV-2 infected cells (143). $CD4^+$ T cells, also known as helper T cells (T_h cells), support the development of both B and $CD8^+$ T cell responses following SARS-CoV-2 infection and vaccination (143,144). $CD4^+$ and $CD8^+$ T cell responses are detected in most infected individuals (145). In general, T cell responses are generated against every SARS-CoV-2 protein, although the majority of responses are directed against the highly expressed structural proteins (146,147). These responses are long-lived, persisting for over a year post-infection, and often exhibit memory phenotypes (148). Both infection-elicited and vaccine-elicited $CD8^+$ T cells are known to have direct protective effects.

Depletion of $CD8^+$ T cells in convalescent rhesus macaques increased susceptibility to reinfection (149). Likewise, $CD8^+$ T cell depletion in vaccinated macaques increased viral loads following challenge (150). Natural infection also induces the differentiation of lung-resident memory T cells, which persist in the respiratory mucosa and can provide a localized, rapid response upon re-infection (151).

1.3.3 Antigenic evolution and immune escape

SARS-CoV-2 has repeatedly acquired mutations that enable the virus to escape recognition from pre-existing immune responses (152–154). Immune escape has primarily been driven by mutations in the RBD and NTD domains which disrupt antibody binding (152–154). In early variants, RBM mutations such as N501Y, E484K and L452R enabled variants to partially evade NAb raised against the ancestral variant (155,156). Frequent deletions have also occurred within the NTD, disrupting neutralization by NTD supersite-targeting antibodies (157,158). Alterations in post-translational modifications (PTMs), particularly N-linked and O-linked glycosylation, also contribute to variant evolution and immune escape (152). The SARS-CoV-2 S contains many glycosylation sites, which form a "glycan shield" that can sterically mask immunodominant epitopes and limit antibody recognition (152). Consequently, mutations that introduce, remove, or alter glycosylation sites can impact immune escape both directly, by shielding epitopes, and indirectly, by reshaping conformational structure (152). The overwhelming number of S mutations in the original Omicron variant facilitated its escape from most pre-existing NAb responses (159–161). In contrast to NAbs which have been highly sensitive to antigenic evolution, non-neutralizing Ab and T cell responses have been more resilient to immune escape (162–164). As the majority of S mutations have arisen in the S1 subunit, antibodies raised against conserved S2 epitopes generally retain their ability to mediate antibody effector functions against newer variants

(162,165,166). Likewise, many immunodominant CD4 and CD8 epitopes remain conserved and are thought to contribute to sustained protection from severe disease following infection with emerging variants (164,167,168).

1.4 COVID-19 vaccines

1.4.1 Vaccination against SARS-CoV-2

Vaccination has been one of the most effective public-health measures for preventing SARS-CoV-2 infections and mitigating COVID-19 disease severity (169–171). Vaccine-induced immunity helps limit viral replication early during infection, preventing widespread inflammation and reducing most symptoms (172–174). Vaccination significantly lowers the risk of developing severe COVID-19, drastically reducing hospitalizations and deaths, especially within vulnerable populations such as the elderly and immunocompromised (175,176). Vaccination also appears to play a role in preventing Long COVID (45).

COVID-19 vaccine development proceeded at an unprecedented pace and scale. The first clinical trial began on March 16th, 2020, only two months after SARS-CoV-2 genetic sequences were first made publicly available (177,178). By March 30, 2023, the WHO reported that there were 183 candidate vaccines in clinical development (179). Numerous vaccines have been approved by national regulatory agencies and multiple have been employed in mass-immunization campaigns (180). These approved vaccines span a broad range of platforms, including traditional and next-generation approaches. As of Aug 12, 2024, an estimated 13.72 billion COVID-19 vaccine doses had been administered globally, with 70.7% of the global populations having received at least one dose (181). Early modelling estimated that vaccines saved ~14.4 million lives in the first year of their deployment (182). Recent analyses have been more conservative, suggesting COVID-19

vaccines averted ~1.5 million deaths in the WHO European Region between 2020-2023 (183) and ~2.5 million deaths globally between 2020-2024 (184).

1.4.2 mRNA vaccines

Two mRNA vaccines, mRNA-1273 (Moderna) and BNT162b2 (BioNTech/Pfizer), played a pivotal role in the global response to the COVID-19 pandemic. In their respective Phase 3 trials, mRNA-1273 and BNT162b2 demonstrated ~94-95% efficacy against symptomatic COVID-19 (185,186). Both vaccines encoded a full-length, prefusion-stabilized Spike using N1-methylpseudouridine (N1mΨ)–substituted mRNA and were delivered in ionizable lipid nanoparticles (LNPs) (187,188). N1mΨ substitution dampens innate RNA sensing and improves mRNA translation, enabling robust antigen expression (189,190). The LNPs protect the mRNA from degradation and facilitate intramuscular (IM) delivery, promoting efficient uptake and cytosolic release (191). These mRNA vaccines were highly immunogenic, generally eliciting higher NAb responses than natural infection and other vaccine platforms (139,192). They also demonstrated a favourable safety profile, eliciting mostly mild transient reactions in a small subset of individuals (185,186).

While extremely effective and a crucial component of the global pandemic response, mRNA vaccines have some limitations. Notably, their relatively high cost and stringent cold-storage requirements have limited their deployment in low-resource settings, contributing to disparities in global immunity (193–195). mRNA vaccination has also been associated with a rare risk of myocarditis and pericarditis, especially in young males (196,197), although the risk of myocarditis from COVID-19 infection remains considerably higher (198,199). Furthermore, the N1mΨ-substitution used to improve mRNA vaccine tolerability also appears capable of inducing ribosomal frame shifting, generating cellular immune responses against out of context peptides

(200). Lastly, NAb responses following mRNA vaccination undergo a relatively rapid decline, decreasing substantially in the first 6-9 months post-vaccination, coinciding with reduced protection (201–204).

1.4.3 Non-mRNA vaccines

During the pandemic, several adenoviral-vectored (AdV) vaccines, including Janssen's Ad26.COV2.S, Oxford-AstraZeneca's ChAdOx1 nCoV-19, Gamaleya Institute's Sputnik V and CanSino's Ad5-nCOV, received broad regulatory approval and underwent large-scale deployment (205–208). Over 3 billion doses of ChAdOx1 nCoV-19 alone were distributed globally (209). AdV vaccines induce robust, Th1-skewed T-cell responses, often comparable to or greater than those elicited by mRNA vaccines (210–213). In general, while AdV vaccines induce lower peak NAb responses than mRNA vaccines, their humoral responses are more durable, with minimal declines 8-months post vaccination (210,214). Concerns about anti-vector immunity blunting repeated doses has driven exploration into AdV vaccines as part of heterologous vaccination regimens (215,216). AdV vaccines are also being explored for mucosal vaccination, which aims to elicit immunity at the primary site of viral entry, thereby better reducing viral shedding and potentially providing sterilizing immunity (217). Notably, Bharat Biotech's intranasal BBV154 and CanSino's aerosolized Ad5-nCoV have received regulatory approval (218,219).

Recombinant Spike vaccines were also deployed during the pandemic. In contrast to mRNA and AdV-vaccines which are inherently immunogenic, recombinant protein vaccines typically require the co-administration of a potent adjuvant to trigger an innate immune response (220). For example, Novavax's Nuvaxovid uses Matrix-M, a saponin adjuvant which enhances antibody titers and Th1-biased cellular responses (221). In general, recombinant protein vaccines have displayed comparable efficacy and safety as mRNA and AdV vaccines in Phase 3 trials (222,223). Notably,

the rollout of variant-matched antigen updates can be significantly slower for recombinant protein vaccines, potentially requiring re-optimization of expression, purification and characterization methods, whereas mRNA and AdV platforms can be updated through simple genetic substitutions that have minimal effects of their manufacturing processes (224,225).

Inactivated vaccines also played a tremendous role in the COVID-19 pandemic, with billions of doses having been delivered by the end of 2021 (226). In general, inactivated vaccines induce lower NAb responses than next-generation platforms, such as mRNA vaccines, and additional booster doses are often required to reach comparable levels of protection (227–230). Unlike next-generation vaccines which typically target the S protein, inactivated vaccines can elicit immune responses against additional viral antigens (231,232). While this could potentially improve cross-protection against emerging variants, real-world effectiveness data generally did not show their superiority over other platforms following the emergence of Omicron (227).

1.4.4 DNA vaccines

Multiple DNA vaccines against SARS-CoV-2 were evaluated preclinically and in clinical trials. For example, Inovio's INO-4800, an electroporated plasmid DNA (pDNA)-based S vaccine, was shown to be immunogenic in BALB/c mice, Guinea pigs, and non-human primates (NHPs), generating robust NAb responses (233,234). INO-4800 was found to be safe and tolerable in Phase 1 and 2 clinical trials and induced modest immune responses (235–237). Most notably, Zydus Cadila's ZyCoV-D became the first DNA vaccine authorized for human use when it was granted emergency use authorization (EUA) in India in August 2021 (238). ZyCoV-D used the pVAX1 plasmid backbone to encode full-length, codon-optimized SARS-CoV-2 Spike with an immunoglobulin E (IgE) signal peptide (239,240). In a Phase 3 clinical trial with over 27,000 enrolled participants, three doses of ZyCoV-D were administered intradermally using a Pharmajet

Tropis® needle-free injection system (NFIS) (241). The regimen provided a modest 66% vaccine efficacy (VE), although VE estimates may have been affected by the emergence of the Delta variant (241,242). Despite its EUA representing a historic milestone for DNA vaccines, ZyCoV-D saw limited real-world use, potentially due to the availability of alternative vaccines that required fewer doses and demonstrated superior effectiveness (243).

1.5 DNA vaccines, lipid nanoparticles and adjuvants

1.5.1 DNA vaccine delivery

Early in the 1990s, Wolff et al. demonstrated that direct injection of pDNA into mouse skeletal muscle led to significant and durable transgene expression (244). Shortly afterwards, Ulmer et al. expanded on this idea, showing that IM injection of pDNA encoding influenza nucleoprotein elicited T cell responses in BALB/c mice and protected against viral challenge (245). Despite promising results in small rodent models, DNA vaccines generally displayed limited immunogenicity in larger animals and in early clinical trials, due in part to inefficient cellular uptake and limited antigen expression (246–250). These limitations spurred the investigation and development of alternative delivery strategies. For needle-based injection, intradermal (ID) delivery often yields stronger immune responses than IM delivery, owing in part to the abundance of dendritic cells and Langerhans cells in the skin (251,252). Physical delivery devices including gene guns, jet injectors, and electroporation have all been shown to improve DNA uptake and enhance vaccine immunogenicity (253–255). Despite these advancements, DNA vaccines ultimately had little impact on global COVID-19 vaccination efforts, with moderate immune responses re-highlighting persistent challenges with inefficient delivery and suboptimal

immunogenicity (256). Consequently, recent efforts have increasingly focused on adapting LNPs, the delivery technology that enabled the success of mRNA vaccines, for DNA-based vaccination.

1.5.2 LNP origins and development of ionizable Lipids

Lipid-based delivery of DNA dates back to the 1980s, when Felgner et al. demonstrated the cationic lipid N-[1-(2,3-dioleyloxy)propyl]-N,N,N-trimethylammonium (DOTMA) could efficiently deliver pDNA into mammalian cells *in vitro* (Figure 1.6) (257). Cationic lipids such as DOTMA are typically formulated into cationic liposomes that electrostatically complex with negatively charged DNA to form "lipoplexes". After binding to anionic cell membranes, lipoplexes are internalized via endocytosis and disrupt the endosomal membrane to facilitate cytosolic DNA release (258). Following the seminal work of Felgner et al., numerous cationic lipids were explored for nucleic acid delivery, the majority adopting a consistent three-component structure: a positive charged head group, a hydrophobic tail, and a linker connecting the two (259,260). In 1997, Gregoriadis et al. reported that IM injection of pDNA encoding hepatitis B surface antigen, formulated with 1,2-dioleoyl-3-trimethylammonium propane (DOTAP)-based cationic lipoplexes, elicited stronger humoral and cellular responses than naked DNA (261) (Figure 1.6).

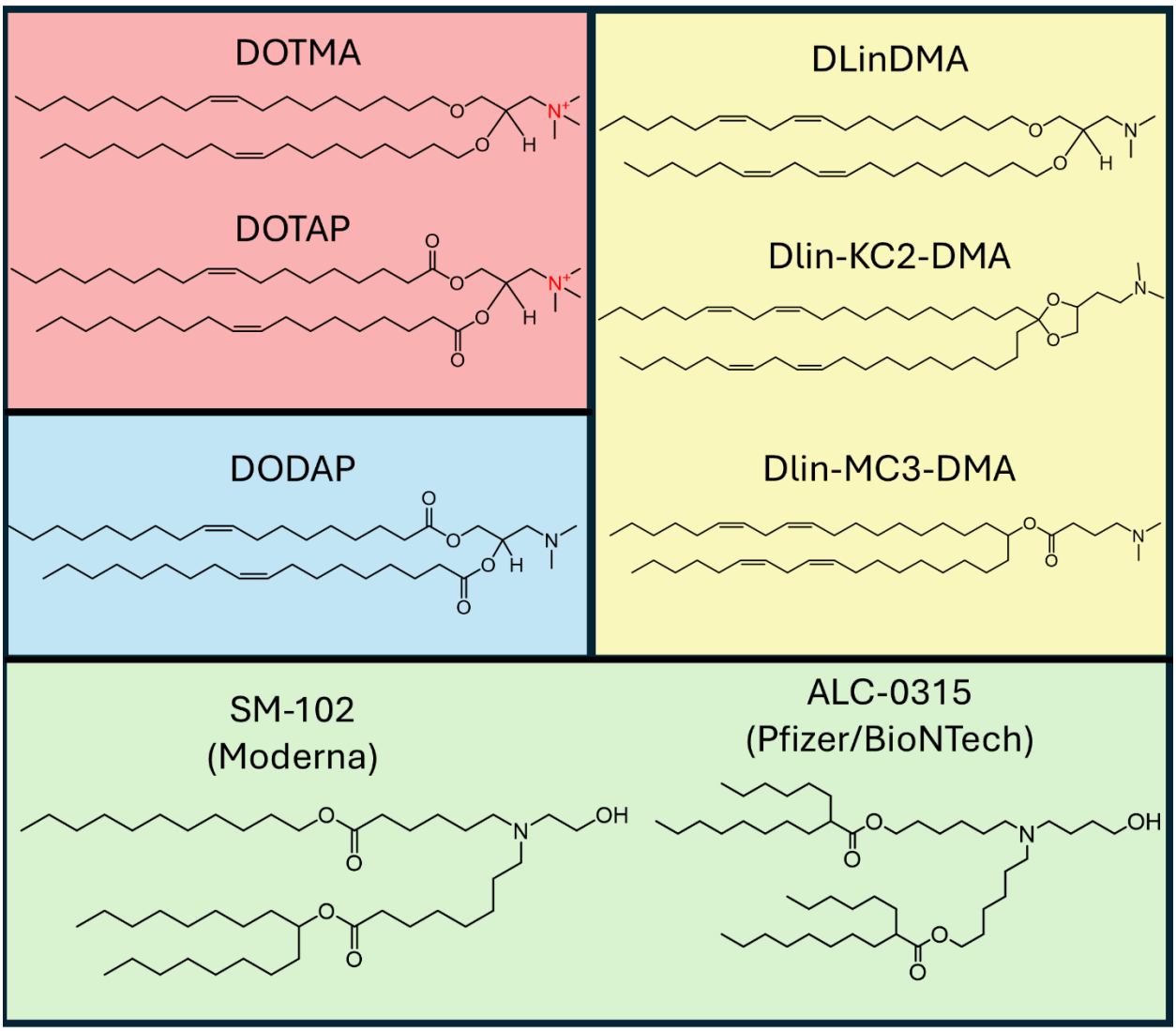

Figure 1.6. Cationic and Ionizable lipids used for nucleic acid delivery.

Chemical structures of early permanently cationic lipids (DOTMA, DOTAP; pink), an early ionizable lipid (DODAP; blue), DLinDMA-derived ionizable lipids developed for siRNA therapeutics (DLinDMA, DLin-KC2-DMA, DLin-MC3-DMA; yellow), and contemporary ionizable lipids found in COVID-19 mRNA vaccines (SM-102, ALC-0315; green).

The clinical translation of early cationic lipids such as DOTMA and DOTAP was hindered by toxicity and tolerability concerns, primarily associated with their permanently charged head groups (260,262). This limitation was addressed in 2000 when the ionizable lipid 1,2-dioleoyl-3-dimethylammonium-propane (DODAP) was used to encapsulate nucleic acids (Figure 1.6) (263).

While neutral at physiological pH, ionizable lipids become protonated in acidic endosomes, significantly increasing their tolerability (262). In 2005, screening studies revealed that ionizable lipids with higher levels of unsaturation, such as 1,2-dilinoleyloxy-N,N-dimethyl-3-aminopropane (DLinDMA) which has two double bonds per acyl tail, enhanced short interfering RNA (siRNA) delivery by improving membrane fusion and endosomal escape (264) (Figure 1.6). DLinDMA-based LNPs were a scientific breakthrough, capable of efficiently and safely mediating systemic siRNA delivery in NHPs (265). A screen of DLinDMA derivatives identified DLin-KC2-DMA as a top performer with over 10-fold greater *in vivo* hepatic gene silencing, largely attributed to adjustments to the linker and head group that enabled stronger endosomal escape (266) (Figure 1.6). DLin-MC3-DMA, a derivative of DLin-KC2-DMA served as the ionizable lipid in Onpattro (patisiran), the first FDA-approved siRNA therapeutic (267) (Figure 1.6). The 2018 approval of Onpattro validated ionizable LNPs as a clinically viable nucleic acid delivery platform and helped pave the way for LNP-formulated mRNA vaccines to play a central role in COVID-19 vaccination.

1.5.3 COVID-19 mRNA vaccine LNP composition

The mRNA-1273 (Moderna) and BNT162b2 (BioNTech/Pfizer) COVID-19 vaccines rely on the ionizable lipids SM-102 and ALC-0315, respectively (268) (Figure 1.6). In a screen of DLin-MC3-DMA derivatives, SM-102 displayed the greatest tolerability following IM administration without compromising humoral responses (269). ALC-0315 is structurally similar to SM-102, with both lipids containing branched hydrophobic tails that impart a cone-like geometry and reduce lipid packing, properties associated with enhanced endosomal membrane destabilization to better facilitate cytosolic mRNA release (191,270). In addition, both SM-102 and ALC-0315 contain hydroxylated tertiary amine head groups that help tune their apparent pKa and facilitate endosomal

escape (191,270). Both were designed with ester linkages that are susceptible to hydrolysis, thereby enhancing biodegradability and facilitating clearance (191,270).

mRNA-1273 and BNT162b2 employed a four-component LNP formulation: the ionizable lipid, 1,2-distearoyl-sn-glycero-3-phosphocholine (DSPC), cholesterol, and a Polyethylene Glycol (PEG)-lipid. The ionizable lipid represents the principal component, comprising ~50 mol% and ~46 mol% of the mRNA-1273 and BNT162b2 formulations, respectively (191). DSPC and cholesterol act as helper lipids that stabilize the LNP, improve encapsulation efficiency and promote cellular delivery (271,272). DSPC is a saturated phosphatidylcholine with a high phase transition temperature (T_m), structurally analogous to natural phospholipids, which enhances LNP stability by providing a rigid scaffold at physiological temperatures (273). Cholesterol intercalates between the branched acyl chains of the ionizable lipid and the ordered chains of DSPC, creating a liquid-ordered phase that balances rigidity and fluidity (270). This reduces membrane permeability, prevents nucleic acid leakage, limits surface protein adsorption, and prolongs circulation (270). Notably, the cholesterol used in mRNA-1273 and BNT162b2 is structurally identical to endogenous human cholesterol, enhancing their biocompatibility (191,270) PEG-lipids serve as a non-natural hydrophilic coating that limits LNP aggregation, modulate particle size and dispersity, and extend stability in both circulation and storage (270,274). While generally biocompatible, concerns have arisen regarding the induction of anti-PEG antibodies, which can accelerate nanoparticle clearance and reduce delivery efficiency upon repeated dosing (275). Together, these four components balance particle stability, biocompatibility and endosomal escape, enabling highly efficient and safe IM delivery of mRNA.

1.5.4 LNP-mediated DNA vaccination

At the onset of the COVID-19 pandemic, evidence supporting the use of novel modern LNP formulations specifically for DNA vaccine delivery was limited. In 2020, Mucker et al. demonstrated that an LNP-formulated DNA vaccine against Andes virus generated superior humoral responses than an unformulated control in rabbits and NHPs (276). These LNPs were formulated with ATX, a proprietary lipid ionizable lipid from Arcturus (277). In 2022, Algarni et al. assessed the DNA delivery efficiency of multiple LNP formulations previously developed for siRNA therapeutics (278). Notably, they observed that DLin-KC2-DMA induced greater antigen expression following IM injection than its derivative DLin-MC3-DMA, highlighting how optimizations tailored for siRNA delivery may not be beneficial for DNA delivery (278). In a similar study by our research group, SM-102 and ALC-0315 formulations were shown to induce superior *in vivo* antigen expression compared to DLin-KC2-DMA formulations following IM injection in BALB/c mice (279). Multiple preclinical studies have since demonstrated that DNA-LNPs can elicit potent immune responses against numerous pathogens, including SARS-CoV-2, influenza, Lyme disease, and human papillomavirus (HPV) (280–287).

1.5.5 DNA vaccine adjuvants

Beyond optimizing delivery, DNA vaccines have often been combined with immunostimulatory adjuvants to boost their immunogenicity. In the context of nucleic acid vaccines, immunostimulatory adjuvants fall into two main categories. The first group are traditional or classic co-formulated adjuvants delivered alongside the vaccine. Numerous traditional adjuvants licensed for use with inactivated virus or protein-based vaccine platforms have been shown to enhance DNA vaccine immune responses, including Aluminum salts (Alum) (288), Monophosphoryl lipid A (MPLA) (289), and squalene-based emulsions like MF59 (290). In

general, traditional adjuvants function by promoting antigen uptake and activating pattern recognition receptors (PRRs) (291,292). Notably, aside from mediating efficient nucleic acid delivery, ionizable lipids have also been shown to have intrinsic adjuvant activity (293–295). Combining traditional adjuvants with LNPs can pose a challenge, increasing manufacturing complexity and potentially promoting particle aggregation or destabilization.

The second category comprises genetic adjuvants: immunomodulatory proteins encoded on the same construct as the antigen or on an accompanying nucleic acid. These can include cytokines, chemokines, co-stimulatory molecules, damage-associated molecular patterns (DAMPs), pathogen-associated molecular patterns (PAMPs), or proteins that enhance antigen processing (292). Encoding these adjuvants within nucleic acid can simplify vaccine formulations and spatially and temporally localize the adjuvant effect to coincide with antigen expression, reducing off-target effects and toxicity (292,296). While genetic adjuvants are actively being investigated for both DNA and mRNA vaccines, their clinical evaluation remains limited (297–300).

1.6 CD40 ligand

1.6.1 The CD40 - CD40L immune axis

Cluster of differentiation 40 (CD40), a member of the tumor necrosis factor (TNF) receptor superfamily, is expressed on the surface of antigen-presenting cells (APCs) including dendritic cells (DCs), macrophages, and B cells (301,302). Engagement of CD40 by its ligand (CD40L) bridges innate and adaptive immune responses, promoting T cell priming, germinal-center formation, and B-cell class switching (301,302). Mechanistically, following $CD4^+$ T cell recognition of peptide–MHC II on activated DCs, T cell receptor (TCR) signaling upregulates CD40L expression on the T cell, which in turn induces CD40 clustering on the DC (303). This

clustering triggers the recruitment of TNF-receptor associated factors (TRAF2/3/5/6) and initiates canonical and non-canonical NF-κB, MAPK, and PI3K signaling pathways (303,304). This increases MHC I/II antigen presentation, upregulates co-stimulatory molecule expression (CD80, CD86, CD70), and induces pro-inflammatory cytokine production (Interleukin (IL)-12, TNFα, IL-6) (303,304) (Figure 1.7). Together, these changes enhance APC function, enabling DCs to effectively prime and activate both $CD4^+$ and $CD8^+$ T cells.

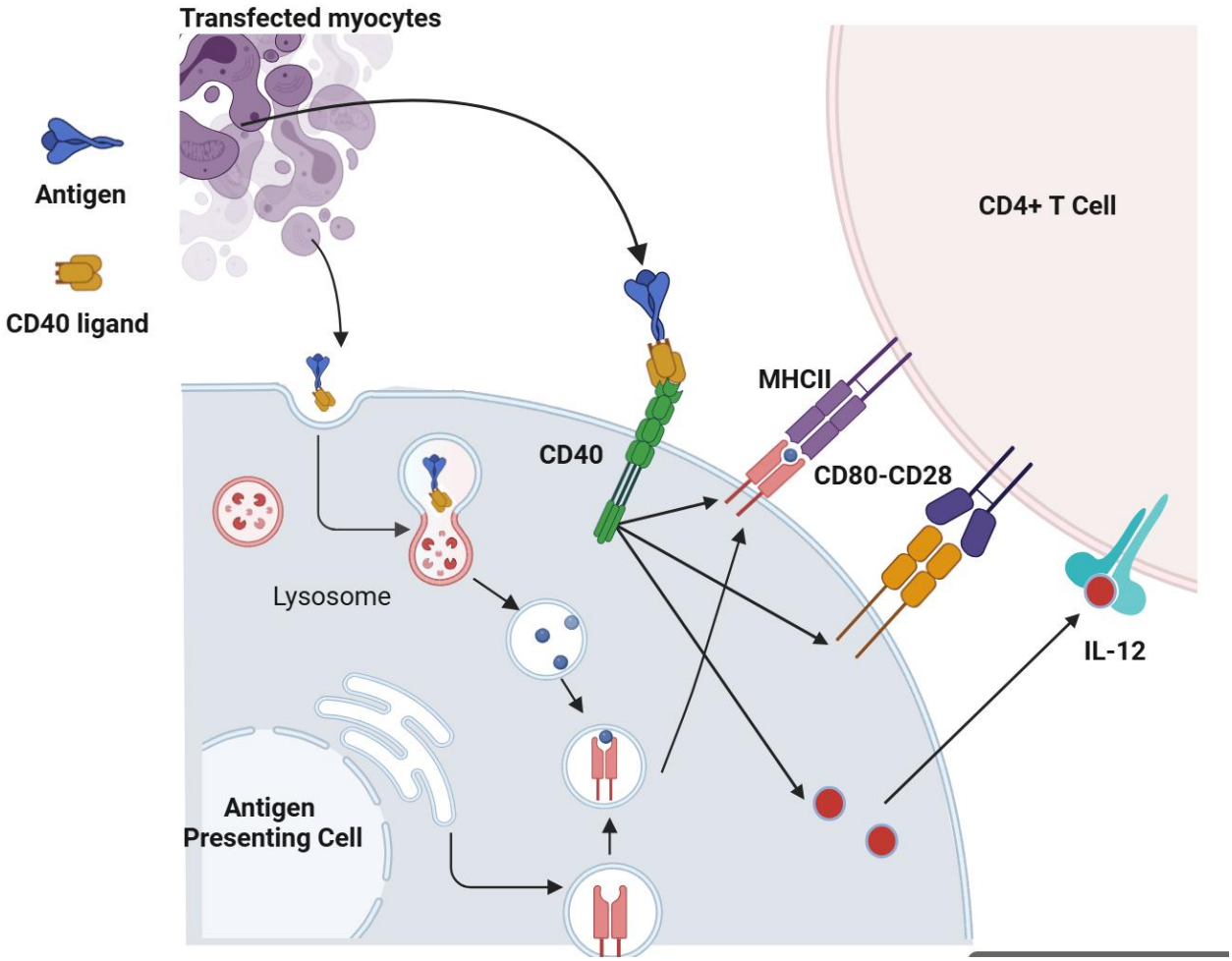

Figure 1.7. CD40L as a bifunctional vaccine adjuvant

Following IM DNA vaccination, myocytes become transfected and express the encoded antigen-CD40L fusion protein. CD40L targets the antigen to CD40-expressing APCs, promoting antigen uptake and processing for MHC II presentation. CD40 engagement simultaneously drives APC

maturation, increasing costimulatory molecule (CD80) expression and inducing cytokine secretion (IL-12). These effects enhance $CD4^+$ T cell activation, supporting stronger antigen-specific responses.

1.6.2 CD40L as a vaccine adjuvant

In 1999, Ihata et al. showed that co-administration of a plasmid encoding full-length CD40L enhanced both humoral and cellular responses to an human immunodeficiency virus (HIV) DNA vaccine (305). Li (2005) further demonstrated that directly fusing soluble CD40L to an antigen elicited superior antibody responses than co-administration of a separate CD40L-expressing plasmid (306). Similar CD40-targeted approaches across diverse vaccine platforms have proven effective against multiple pathogens, including influenza (307–309), RSV (310,311), and HIV (312,313). CD40-signaling in DCs promotes secretion of IL-12, a key driver of Th1 differentiation (301). Multiple vaccine studies have correspondingly found targeting CD40 promotes Th1-skewed immunity, biasing antibody subclasses towards IgG2a in mice and increasing production of interferon gamma (IFN-γ), IL-2, and TNFα cytokines in $CD4^+$ and $CD8^+$ T cells (305,314). Such responses are generally beneficial against intracellular pathogens, such as viruses, as they support Fc-effector functions and cytotoxic T cell immunity that can clear infected cells (315).

1.6.3 Targeting CD40 as a SARS-CoV-2 vaccine adjuvant

Prior to the COVID-19 pandemic, Hashem et al. showed that an AdV vaccine encoding MERS-CoV S1 fused to CD40L elicited significantly higher NAb titers than an S1-only control, and prevented perivascular hemorrhage after challenge in transgenic mice (316). These findings demonstrated that targeting coronavirus antigens to CD40 could enhance vaccine-induced immunity. Several groups have subsequently investigated similar CD40-targeting strategies for SARS-CoV-2 vaccination. Recombinant RBD-CD40L and N-CD40L subunit vaccines were shown to be more immunogenic than their non-adjuvanted counterparts in mice, and induced

humoral responses in NHPs when adjuvanted with Alum (317,318). Likewise, fusing RBD to the C-terminus of an anti-human CD40 antibody enhanced humoral and cellular immunity in humanized mice (319). A multi-epitope anti-CD40 construct (CD40.CoV2) elicited broad cross-reactive responses and protected transgenic mice from challenge (320), with follow-up work confirming strong Th1 $CD4^+$ responses and $CD8^+$ with stem-cell-like memory (T_{SCM}) features (321). Building on these preclinical studies, a Phase 1/2a trial was launched in June 2025 for an updated anti-CD40 vaccine (CD40.Pan.CoV) (322). A related anti-CD40 vaccine construct against HIV recently demonstrated both safety and immunogenicity in a Phase 1 study (323). Together, these studies position CD40-targetting, whether via CD40L or anti-CD40, as a broadly applicable strategy for SARS-CoV-2 vaccines.

1.7 Rationale, Hypothesis, and Objectives

1.7.1 Rationale

Despite widespread vaccination and substantial population-level immunity, SARS-CoV-2 continues to circulate globally and poses a persistent threat to vulnerable populations (324). New infections are increasingly driven by the emergence of variants that partially evade existing immune responses and the waning of infection- and vaccine-induced immunity (324). Although deploying updated boosters can refresh immunity and restore higher levels of protection, the approach is undermined by declining booster uptake, rollout timelines that can leave vaccines mismatched to circulating variants, and immune imprinting that may bias recall responses toward earlier antigens (325–328). New approaches to vaccination are essential to develop vaccines that elicit more durable and broadly protective immunity against SARS-CoV-2.

mRNA-LNP vaccines, which spearheaded COVID-19 vaccination efforts in North America and Europe, induce robust immune responses and provide high efficacy against symptomatic and severe disease (185,186,329). However, initially strong responses elicited by mRNA vaccines are generally followed by relatively rapid and marked declines in circulating antibody titers (201,330–332), with serum NAb titers exhibiting an estimated half-life of ~2 months after a two-dose vaccination regimen (333). While these vaccines continue to effectively prevent severe disease, susceptibility to infection increases significantly ~6-9 months post-vaccination (202–204).

DNA vaccines are often presented as an alternative to mRNA vaccines. DNA vaccines offer more cost-effective manufacturing and longer shelf lives at refrigerated (2–8 °C) and ambient temperatures, making them a potentially more equitable solution to address global vaccine inequities (194,334). Although multiple DNA vaccines underwent clinical evaluation during the

pandemic, none played a significant role in global vaccination efforts (235,236,241,335–338). The efficacy of DNA vaccines has historically been limited by inefficient cellular uptake and modest immunogenicity, motivating the development of improved delivery strategies and molecular adjuvants. Recent advancements in mRNA-LNP formulations, particularly the development of modern ionizable lipids, can potentially be leveraged to address the longstanding challenge of inefficient DNA vaccine delivery. Likewise, CD40L could potentially be employed to enhance the magnitude, breadth and durability of immunity induced by a SARS-CoV-2 DNA vaccine. These considerations motivate the evaluation of whether a DNA vaccine formulated in LNPs and adjuvanted with CD40L can induce and sustain cross-protective immune responses against SARS-CoV-2.

1.7.2 Hypothesis

I hypothesize that a DNA vaccine encoding the SARS-CoV-2 Spike, when formulated in LNPs and co-expressing CD40L, can provide significant protection against infection by eliciting durable and broad immune response. The ability of CD40L-adjuvanted DNA-LNPs to sustain long-term humoral immunity and protection against SARS-CoV-2 can be evaluated in comparison to mRNA-LNPs.

1.7.3 Objectives

1. Evaluate the impact of CD40L as a molecular adjuvant on the immunogenicity and protective efficacy of nucleic acid vaccines against SARS-CoV-2.
2. Assess the immunogenicity and protective efficacy of SARS-CoV-2 DNA vaccines delivered by ionizable lipid nanoparticles (DNA-LNPs).
3. Compare the durability of vaccine-induced immune responses elicited by DNA-LNPs and mRNA-LNPs.

Chapter 2: DNA Based Vaccine Expressing SARS-CoV-2 Spike-CD40L Fusion Protein Confers Protection Against Challenge in a Syrian Hamster Model

Preface: This chapter has been previously published as a research article.

Tamming L et al. DNA Based Vaccine Expressing SARS-CoV-2 Spike-CD40L Fusion Protein Confers Protection Against Challenge in a Syrian Hamster Model. ***Front Immunol***. 2022 Jan 12;12:785349. doi: 10.3389/fimmu.2021.785349.

Candidate Contribution

Levi Tamming was the primary author of this manuscript. Levi Tamming designed the experiments and vaccines. Levi Tamming performed all ELISA, pseudovirus neutralization, Western blot, CD40L bioactivity, and subgenomic mRNA experiments. Levi Tamming analyzed all data, prepared all figures, and wrote the first draft of the manuscript.

Author list

Levi A. Tamming[1,2], Diana Duque[3], Anh Tran[3*], Wanyue Zhang[1,2], Annabelle Pfeifle[1,2], Emmanuel Laryea[1,2], Jianguo Wu[1], Sathya N. Thulasi Raman[1], Caroline Gravel[1], Marsha S. Russell[1], Anwar M. Hashem[4,5], Reem M. Alsulaiman[4], Rowa Y. Alhabbab[4,6], Jun Gao[1], David Safronetz[7], Jingxin Cao[7], Lisheng Wang[2], Wangxue Chen[3], Michael J.W. Johnston[1,8], Simon Sauve[1], Michael Rosu-Myles[1,2], Xuguang Li[1,2*]

[1]Centre for Biologics Evaluation, Biologic and Radiopharmaceutical Drugs Directorate, Health Products and Food Branch, Health Canada and WHO Collaborating Center for Standardization and Evaluation of Biologicals, Ottawa, ON, Canada
[2]Department of Biochemistry, Microbiology and Immunology, Faculty of Medicine, University of Ottawa, Ottawa, ON, Canada
[3]Human Health Therapeutics Research Center, National Research Council of Canada, Ottawa, ON, Canada
[4]Vaccines and Immunotherapy Unit, King Fahd Medical Research Center, King Abdulaziz University, Jeddah, Saudi Arabia.
[5]Department of Medical Microbiology and Parasitology, Faculty of Medicine, King Abdulaziz University, Jeddah, Saudi Arabia.
[6]Department of Medical Laboratory Technology, Faculty of Applied Medical Sciences, King Abdulaziz University, Jeddah, Saudi Arabia.
[7]National Microbiology Laboratory, Public Health Agency of Canada, Winnipeg, MB, Canada
[8]Department of Chemistry, Carleton University, Ottawa, ON, Canada
*Corresponding authors

2.1 Abstract

SARS-CoV-2 infections present a tremendous threat to public health. Safe and efficacious vaccines are the most effective means in preventing the infections. A variety of vaccines have demonstrated excellent efficacy and safety around the globe. Yet, development of alternative forms of vaccines remains beneficial, particularly those with simpler production processes, less stringent storage conditions, and the capability of being used in heterologous prime/boost regimens which have shown improved efficacy against many diseases. Here we reported a novel DNA vaccine comprised of the SARS-CoV-2 spike protein fused with CD40 ligand (CD40L) serving as both a targeting ligand and molecular adjuvant. A single intramuscular injection in Syrian hamsters induced significant neutralizing antibodies 3-weeks after vaccination, with a boost substantially improving immune responses. Moreover, the vaccine also reduced weight loss and suppressed viral replication in the lungs and nasal turbinates of challenged animals. Finally, the incorporation of CD40L into the DNA vaccine was shown to reduce lung pathology more effectively than the DNA vaccine devoid of CD40L. These results collectively indicate that this DNA vaccine candidate could be further explored because of its efficacy and known safety profile.

2.2 Introduction

Since its emergence in late 2019, the severe acute respiratory syndrome-coronavirus-2 (SARS-CoV-2) has caused one of the greatest pandemics in modern history, with over 215 million confirmed infections and 4.5 million deaths (1). This global health crisis has resulted in an unprecedented push to develop safe and efficacious vaccines against SARS-CoV-2. According to the WHO, there are over 180 vaccines currently in pre-clinical development, with more than 100 having begun clinical testing (2). While more traditional vaccine technologies such as subunit and inactivated virus vaccines make up a large portion of this figure, many innovative vaccines strategies have been at the forefront of global vaccination campaigns, receiving emergency use authorization from multiple regulatory agencies. Lipid nanoparticle–formulated messenger RNA (mRNA) vaccines are one strategy that has seen widespread usage throughout the pandemic. Two mRNA vaccines in particular, Moderna's mRNA-1273 (Spikevax) (3,4) and Pfizer/BioNTech's BNT162b2 (Comirnaty) (5,6) have proven to be extremely safe and effective at preventing COVID-19 illness. With many leading regulatory bodies approving the Comirnaty vaccine (7–9), we are witnessing the beginning of a new era in vaccinology.

While unquestionably effective, the high cost and cold-storage requirements of mRNA vaccines impedes their use in both lower income countries and remote and isolated communities. Alongside protein subunit and inactivated virus vaccines, DNA vaccines present an invaluable alternative to mRNA vaccines due to their superior thermostability and reduced cost of production (10–12). Two prominent DNA vaccines against SARS-CoV-2 include Inovio pharmaceuticals' INO-4800 and Zydus Cadila's ZyCoV-D candidate vaccines, which both elicited strong humoral and cellular immune responses in their respective Phase I clinical trials (13,14). In a first for a DNA-based SARS-CoV-2 vaccine, ZyCoV-D recently received emergency use approval in India (15).

Despite promising results, some concerns remain about DNA vaccine technologies, notably their low immunogenicity and subsequent ability to produce effective immune responses. One well-tested strategy to enhance the humoral and cell-mediated immune responses to DNA vaccines is via the inclusion of the cluster of differentiation 40 (CD40) ligand (CD40L) as a molecular adjuvant (16–22). CD40, a member of the TNF-receptor superfamily, is constitutively expressed in antigen-presenting cells (APCs) as a key regulator of their activation (23–25). The CD40-CD40L interaction represents one of the most critical steps in transitioning from the innate to the adaptive immune response. Our group has previously described the benefits of using CD40L as an adjuvant for vaccines against influenza (26), respiratory syncytial virus (27) and recently, Middle East respiratory virus (MERS-CoV) (28).

Given its previously demonstrated effectiveness in inducing strong and long-lasting immune response and specifically its ability to improve the safety of a vaccine against another coronavirus, we employed CD40L as an adjuvant to develop a DNA vaccine against SARS-CoV-2. To this end, we generated a pcDNA3.1-vectored vaccine encoding a secreted pre-fusion stabilized form of the SARS-CoV-2 spike protein fused to hamster CD40L via a trimerization motif. The immunogenicity and protective efficacy of this vaccine candidate was evaluated in a Syrian hamster challenge model.

2.3 Materials and Methods

2.3.1 Cell lines and viruses

BHK-21, HEK293T and HEK293T-ACE2 cells were cultured in Dulbecco's Modified Eagle Medium (DMEM) supplemented with 25 mM HEPES, 20 U/mL Penicillin, 0.02 mg/mL Streptomycin and 10% heat-inactivated fetal-bovine serum (FBS). HEK-Blue™ CD40L cells were

cultured in DMEM supplemented with 20 U/mL Penicillin, 0.02 mg/mL Streptomycin, 100 µg/mL Normocin and 10% heat-inactivated FBS. Vero cells were cultured in DMEM supplemented with 1X non-essential amino acid, 20 U/mL Penicillin, 0.02 mg/mL Streptomycin, 1 mM sodium pyruvate and 10% heat-inactivated FBS. SARS-CoV-2 isolate Canada/ON/VIDO-01/2020 was propagated on Vero E6 cells and titered on Vero cells. Exact genetic identity to original isolate was confirmed by whole viral genome sequencing. Passage three virus stocks were used in all subsequent experiment that required live virus.

2.3.2 DNA vaccines

DNA sequences encoding the SARS-CoV-2 isolate Wuhan-Hu-1 spike (GenBank accession #MN908947) ectodomain (residues 1–1208) fused to a T4 fibritin foldon trimerization motif (YIPEAPRDGQAYVRKDGEWVLLSTFLG) without (S.dTM.PP) or with the ectodomain of *Mesocricetus auratus* CD40L (S.dTM.PP-CD40L) (GenBank accession #XM_005084522.4, residues 118-260) were commercially synthesized (BioBasic, Toronto, ON). Domains were separated by flexible glycine-serine linkers sequences "GSGG". The S ectodomains were prefusion stabilized via a "GSAS" substitution at the furin cleavage site (residues 682-685) and proline substitutions at residues 986 and 987 as previous reported (29). Coding sequences were codon optimized for expression in Syrian hamsters and subcloned into the mammalian expression plasmid pcDNA3.1 (+) using *KpnI* and *NotI* restriction enzymes (Supplemental Figure 2.1). Bulk DNA vaccine preparations were prepared with endotoxin-free gigaprep kits (Qiagen, Hilden, Germany) and the sequences were validated with Sanger sequencing.

2.3.3 *In vitro* protein expression

HEK293T cells were transiently transfected in 6-well plates with 1.6 µg of pcDNA3.1, pcDNA3.1 S.dTM.PP or pcDNA3.1 S.dTM.PP-CD40L using Lipofectamine™ 3000 Transfection Reagent

(ThermoFisher, Ottawa, ON) according to the manufacturer's instructions and incubated for 48 hours at 37°C, 5% CO_2. The cells were washed with phosphate-buffered saline (PBS) and then lysed with radioimmunoprecipitation assay buffer (ThermoFisher, Ottawa, ON). Lysates were electrophoresed on a 4-15% TGX stain-free SDS-PAGE gel (Bio-Rad, Saint-Laurent, QC) and subsequently transferred to a polyvinylidene difluoride membrane. Membranes were blocked for 1h at room temperature with tris-buffered saline (TBS) containing 0.5% Tween 20 (Sigma-Aldrich, St. Louis, MO) (V/V) (TBS-T) and 5% (W/V) non-fat milk powder then incubated overnight at 4°C in blocking buffer containing either polyclonal rabbit anti-SARS-CoV-2 Spike antibody (1:3000 dilution) (Sino Biological) or polyclonal rabbit anti-β-actin antibody (1:1000 dilution) (Cell Signaling). Membranes were then incubated for 1 hour at room temperature with goat anti-rabbit horseradish peroxidase (HRP)-conjugated secondary antibody (1:75, 000 dilution) (ThermoFisher, Ottawa, ON) in blocking buffer and developed using SuperSignal™ West Femto Maximum Sensitivity Substrate (ThermoFisher, Ottawa, ON) and a ChemiDoc MP imaging system (Bio-Rad, Saint-Laurent, QC).

2.3.4 CD40L bioactivity assay

HEK293T cells were either mock transfected or transiently transfected in a 24-well plate with 1 µg of pcDNA3.1, pcDNA3.1-S.dTM.PP or pcDNA3.1-S.dTM.PP-CD40L using Lipofectamine™ 3000 Transfection Reagent (ThermoFisher, Ottawa, ON) and incubated for 24 hours at 37°C, 5% CO_2. In a 96-well plate, 100 µL of growth media from the transfected cells was mixed with 100 µL of HEK-Blue CD40L cells (RRID:CVCL_A8CE, Invivogen, San Diego, CA) resuspended at 2.0×10^5 cells per mL in fresh media. Following a 24-hour incubation at 37°C in a 5% CO_2 incubator, 20 µL of cell culture media was mixed with 180 µL of QUANTI-Blue™ Reagent in a

96-well plate. The absorbance at 630 nm was measured periodically after a 30-minute incubation at 37°C using a Synergy™ 2 microplate reader (BioTek, Winooski, VT).

2.3.5 Hamster immunization

6-8 week old female Syrian hamsters were purchased from Charles River Laboratories (Saint-Constant, Canada). Animal experiments were approved by the National Research Council Canada (NRC) Human Health Therapeutics Animal Care Committee. Animal procedures were performed by trained staff in accordance with regulations and guidelines by the Canadian Council on Animal Care and the NRC Human Health Therapeutics Animal Care Committee. All infectious work was carried out under ABSL-3 conditions at the NRC. Animals were randomly allocated into three different experimental groups (n=12 per group) and were immunized twice with 100 µg of pcDNA3.1, pcDNA3.1 S.dTM.PP or pcDN3.1 S.dTM.PP-CD40L on days 0 and 28. The DNA vaccines were suspended in PBS at a concentration of 1 mg/mL and administered intramuscularly in the hamster's left tibialis anterior muscle with a needle syringe. Hamster serum was collected on days -7, 21 and 42. On day 49 the hamsters were intranasally challenged with 1.0×10^5 PFU of SARS-Co-2 (Canada/ON/VIDO-01/2020). Animals were euthanized by CO_2 either 2- or 7-days post-challenge and the nasal turbinate, lung and spleen were collected for determination of viral titers and histopathology analysis.

2.3.6 ELISA

Nunc MaxiSorp™ flat-bottom 96-well plates (ThermoFisher, Ottawa, ON) were coated with 1 µg/mL of either SARS-CoV-2 Spike S1+S2 ECD-His recombinant protein or SARS-CoV-2 Spike RBD-His recombinant protein (Sino Biological, Beijing, China) in PBS and incubated overnight at 4°C. Plates were washed with PBS containing 0.1% Tween-20 (PBS-T) before blocking with 3% (w/v) Bovine Serum Albumin (IgG-Free, Protease-Free) (Jackson Immuno Research, West

Grove, PA) in PBS-T for 2 hours at 37°C. The plates were washed again and two-fold serial dilutions of hamster serum, starting from 1:50 up to 1:102400 were added to the wells and incubated for 1 hour at 37°C. Plates were then washed with PBS-T and Peroxidase AffiniPure Goat Anti-Syrian Hamster IgG (H+L) (Jackson Immuno Research, West Grove, PA) was added to each well at 1:4000 and incubated at 37°C for 1h. Plates were washed again with PBS-T and 100 µL of Tetramethylbenzidine (TMB) substrate (Cell Signaling Technology, Danvers, MA) was added to each well. After a two-minute incubation at room temperature, 100 µL of 0.16 M sulfuric acid was added to terminate the reaction and absorbance was measured at 450 nm. Endpoint titers were expressed as the reciprocals of the final detectable dilution with an OD above the cut-off value, which was defined as the average OD of the pcDNA3.1-empty samples plus 3 standard deviations.

2.3.7 Pseudovirus neutralization assay

The neutralizing activity of vaccinated hamster sera was determined using a luciferase reporter SARS-CoV-2 S pseudovirus described previously (30). Briefly, pseudotyped Vesicular Stomatitis Virus (VSV) was generated by concurrently infecting HEK293T cells with G*ΔG-VSV (Kerafast, Winston-Salem, NC) and transfecting them with pCDNA3.1 encoding either SARS-CoV-2 S from the Wuhan-1 or B.1.351 (31) lineages or SΔCT from the B.1.617.2 lineage. Cell culture supernatant containing the pseudovirus was collected 24- and 48-hours post-infection before being mixed and purified by filtration through a 0.45 µm filter. In a 96-well plate, serum samples heat-inactivated at 56°C for 30 mins were serially diluted three-fold, mixed with 50 µL of pseudovirus diluted to 1.3×10^4 $TCID_{50}$/mL and incubated for 1h at 37°C, 5% CO_2. Afterwards 100 µL of 2×10^5 cells/mL of HEK293T-ACE2 was added to each well. Following an additional 24h incubation, 150 µl of supernatant was aspirated and replaced with 100 µL of Bright-Glo luciferase reagent (Promega, Madison, WS). Luminescence was measured using a Synergy™ 2 microplate reader

(BioTek, Winooski, VT). The 50% neutralization titers (NT50) were determined as previously reported (30), where the NT50 was the reciprocal of the sample dilution at which a 50% reduction in relative light units (RLU) was observed relative to the average of the no-serum control wells.

2.3.8 Lung viral titration assay

Plaque assays were performed under biosafety level-3 (BSL-3) conditions. Left lung tissues were weighed and then homogenized in 1 mL of PBS. The homogenates were centrifuged and the clarified supernatants were used in a plaque assay. In brief, a 1:10 serial dilution of clarified lung homogenate was made in infection media (DMEM supplemented with 1X non-essential amino acid, 20 U/mL Penicillin, 0.02 mg/mL Streptomycin, 1 mM sodium pyruvate, and 0.1% bovine serum albumin). Virus was adsorbed on Vero cells at 37°C and 5% CO_2 for 1h before the inoculum was removed and overlay media was added (1X infection media with 0.6% ultrapure, low-melting point agarose). The infection was incubated at 37°C and 5% CO_2 for 72h, then fixed with 10% formaldehyde and stained with crystal violet. Plaques were enumerated and PFU was determined per gram of lung tissue.

2.3.9 Subgenomic mRNA assay

SARS-CoV-2 E subgenomic mRNA (sgmRNA) levels in lungs and nasal turbinates were assessed by RT-qPCR using previously described TaqMan probes (32). SARS-CoV-2 E sgmRNA for use as a standard curve was transcribed from a commercially synthesized pcDNA3.1 E sgmRNA vector (BioBasic, Toronto, ON) using a TranscriptAid T7 High Yield Transcription Kit (ThermoFisher, Ottawa, ON) according to the manufacturer's protocol. Lung tissues were placed into RNA shield buffer (Zymo Research, Irvine, CA) and incubated overnight at 4°C to allow for reagent penetration before freezing at -80°C. Viral RNA was extracted under BSL-3 conditions from the mechanically homogenized samples using a Quick-RNA Viral Kit (Zymo Research, Irvine, CA).

Inactivated purified viral RNA was then removed from the ABSL-3 facility for subsequent qRT-PCR experiments. sgmRNA levels were assessed using a TaqMan custom gene expression assay (ThermoFisher, Ottawa, ON) (Table 2.1) and a one-step Fast Virus master mix (ThermoFisher, Ottawa, ON) according to the manufacturer's protocol. RT-qPCR reactions were conducted using an Applied Biosystems™ 7500 Fast Real-time PCR instrument. Standard curves of *in vitro* transcribed sgmRNA were used to calculated sgmRNA copiers per mL.

Table 2.1 E sgmRNA primers.

Name	Sequence
Leader_F	5'- CGATCTCTTGTAGATCTGTTCTC-3'
E_Probe	5'- ACACTAGCCATCCTTACTGCGCTTCG-3'
E_Rev	5'-FAM-ATATTGCAGCAGTACGCACACA-MGB- 3'

2.3.10 Histopathology

Right lungs were collected for histopathology analysis. The tissues were fixed for 72h in 10% neutral buffered formalin and processed by standard paraffin embedding methods (33). Sections were cut 4 µm thick, stained with hematoxylin-eosin (HE), and examined under microscopy. The severity and extent of pneumonia (the presence of inflammatory polymorphonuclear and mononuclear cells) was scored blinded by a veterinarian pathologist based on the criteria of Lien et al. (34) with modifications (Table 2.2).

Table 2.2 Histological Scoring Criteria.

Score	Histological changes
0	No significant finding
1	Minor peribronchial/bronchiolar and perivascular inflammation with slight thickening of alveolar septa with small numbers of mononuclear cell infiltration
2	Apparent inflammation and alveolus septa thickening with more interstitial mononuclear inflammatory infiltration; focal areas of consolidation
3	Multiple focal consolidation with alveolar septa thickening, and increased infiltration of inflammatory cells
4	Area of consolidation with extensive alveolar septa thickening, collapse of alveoli, restricted fusion of the thick septa, and more cell infiltration in alveolar space and the areas surrounding airways and blood vessels
5	As 4, but the lung is almost completely consolidation

2.3.11 Statistical analysis

Normality of the study data was assessed by a Shapiro-Wilk test (alpha-level=0.05). Whenever data or their log transformations were deemed not of normal distribution, a non-parametric approach was adopted. A Kruskal-Wallis H test with Holm's sequential Bonferroni adjustment was applied for pairwise (between-group) comparisons of S- and RBD-specific IgG endpoint titers, neutralizing antibody titers, lung viral burden and histology scores. A one-way analysis of variance (ANOVA) with Bonferroni's adjustment was applied for pairwise (between-group) comparisons

of CD40L bioactivity, weight loss data by day, nasal viral titer and lung subgenomic mRNA. The abovementioned analyses were performed using either SAS Enterprise Guide 7.1 or GraphPad PRISM 7. * $p < 0.05$, ** $p < 0.01$, *** $p < 0.001$, **** $p < 0.0001$.

2.4 Results

2.4.1 Recombinant antigen design, expression and bioactivity

Recombinant C-terminally truncated pre-fusion stabilized SARS-CoV-2 S proteins (S.dTM.PP) without or with a fused CD40L ectodomain (S.dTM.PP-CD40L) were generated in pcDNA3.1 vectors (Figure 2.1A&B). Western blot analysis was used to confirm the *in vitro* expression of both S.dTM.PP and S.dTM.PP-CD40L in transfected BHK-21 cells (Figure 2.1C). The western blot revealed single bands for both the S.dTM.PP and S.dTM.PP-CD40L constructs near their expected molecular weights (MW) of 137 and 152 kDa respectively. Next, a cell-based CD40 secreted embryonic alkaline phosphatase (SEAP) reporter assay was used to ensure that the fused CD40L ectodomain remained biologically active and capable of engaging with CD40 (Figure 2.1D). Cell culture media from HEK293T cells transfected with the DNA vaccines was transferred onto reporter HEK-Blue CD40L cells to test the engagement of vaccine antigen derived CD40L with CD40 from HEK-Blue cells. The S.dTM.PP-CD40L construct induced significantly higher levels CD40-CD40L signaling than the other two constructs (Figure 2.1C), confirming the bioactivity of the fused CD40L ectodomain.

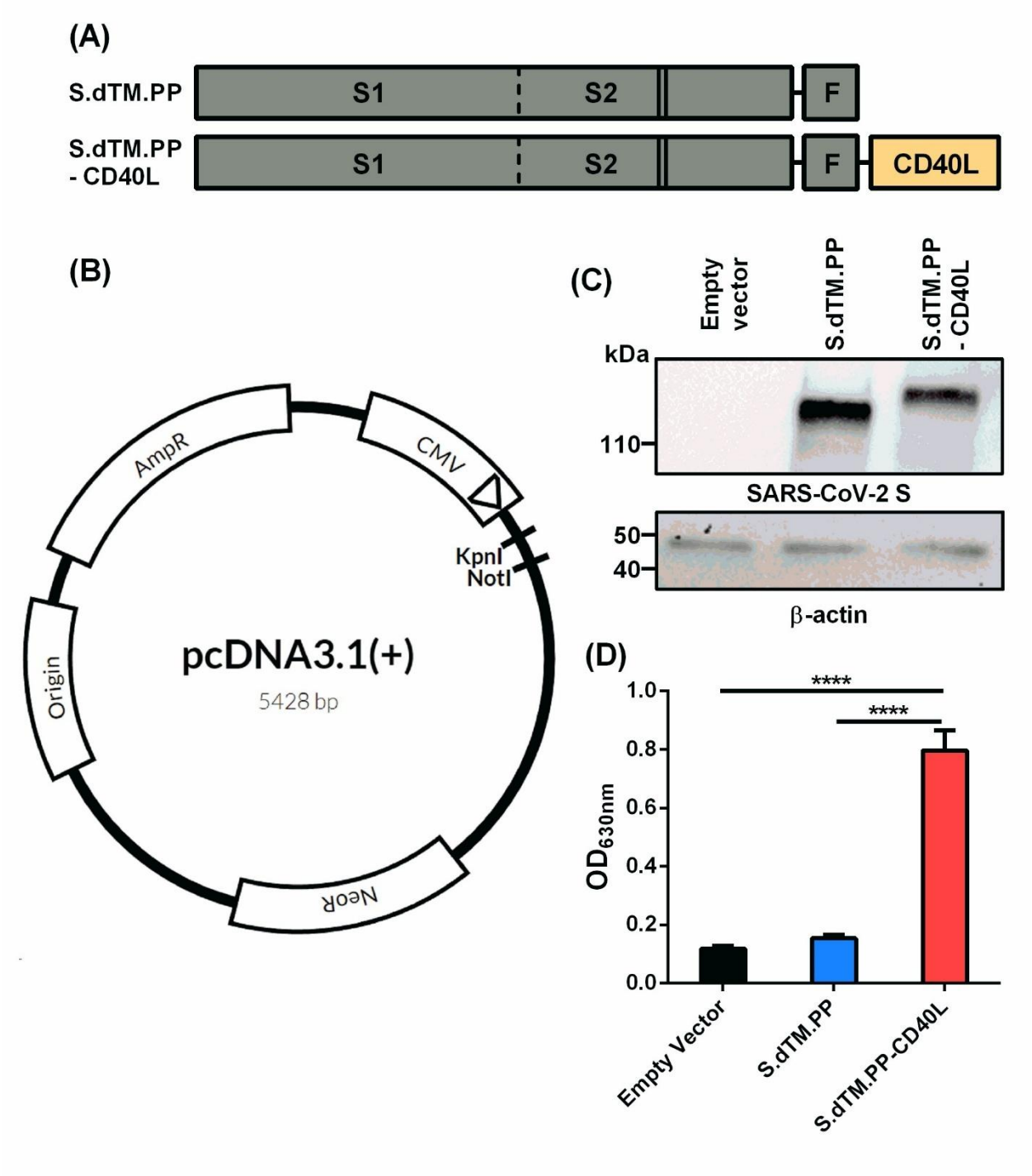

Figure 2.1 Spike-CD40L fusion antigen design and vaccine characterization.

(A) The DNA vaccine antigens were based on a truncated SARS-CoV-2 spike protein lacking the transmembrane domain and C-terminal tail. The S protein was prefusion stabilized via the introduction of two stabilizing proline mutations (solid lines) and the replacement of the furin cleavage site (dotted line). The S protein was fused to a T4 fibritin trimerization motif (F) with or

without the ectodomain of CD40L. **(B)** Antigens were subcloned into pcDNA3.1 (+) vector using KpnI and NotI restriction sites. **(C)** Antigen expression was detected in BHK-21 cells transfected with the DNA vaccines. Empty pcDNA3.1 was used as a negative control and β-actin expression was used as a loading control. kDa: kilodalton. **(D)** CD40L reporter HEK293 cells were stimulated for 24h with media collected from HEK293T cells transfected with the DNA vaccines. SEAP expression in the cell culture supernatant post-24h incubation was measured using QUANTI-Blue™ reagent. Abs_{630nm} values were measured after a 30-minute incubation. Data shown is mean ± SEM; n = 3 per group.

2.4.2 DNA vaccines elicit strong humoral responses in Syrian hamsters

Female Syrian hamsters were immunized with two 100 μg doses of pcDNA3.1-S.dTM.PP, pcDNA3.1-S.dTM.PP-CD40L or empty pcDNA3.1. The vaccines were administered intramuscularly in PBS at days 0 and 28 (Figure 2.2A). Binding antibodies against the full-length SARS-CoV-2 S (Figure 2.2B) and RBD (Figure 2.2C) were quantified 21 and 42 days after prime vaccination using an indirect ELISA. At day 21 following a single administration, S.dTM.PP-CD40L induced significantly higher antibody titers against SARS-CoV-2 RBD than its non-fusion counterpart, S.dTM.PP (Figure 2.2C). Following the boost vaccination, both vaccines elicited similar antibody titers against both full-length S (Figure 2.2B) and RBD (Figure 2.2C), at higher levels than what was observed for both on day 21. The neutralizing antibody (NAb) titer of serum collected on either day 21 or day 42 was determined using a VSV-based pseudovirus neutralization assay (Figure 2.2D). Coinciding with the increased RBD-specific IgG, after a single dose, the S.dTM.PP-CD40L vaccine induced a greater 50% neutralization titer against wild type (WT) and B.1617.2 variant pseudotyped-VSV than the S.dTM.PP vaccine (Figure 2.2D). After the boost vaccination, both spike vaccines induced significant NAb responses against WT, B.1.351 and B.1617.2 pseudotyped VSV (Figure 2.2D).

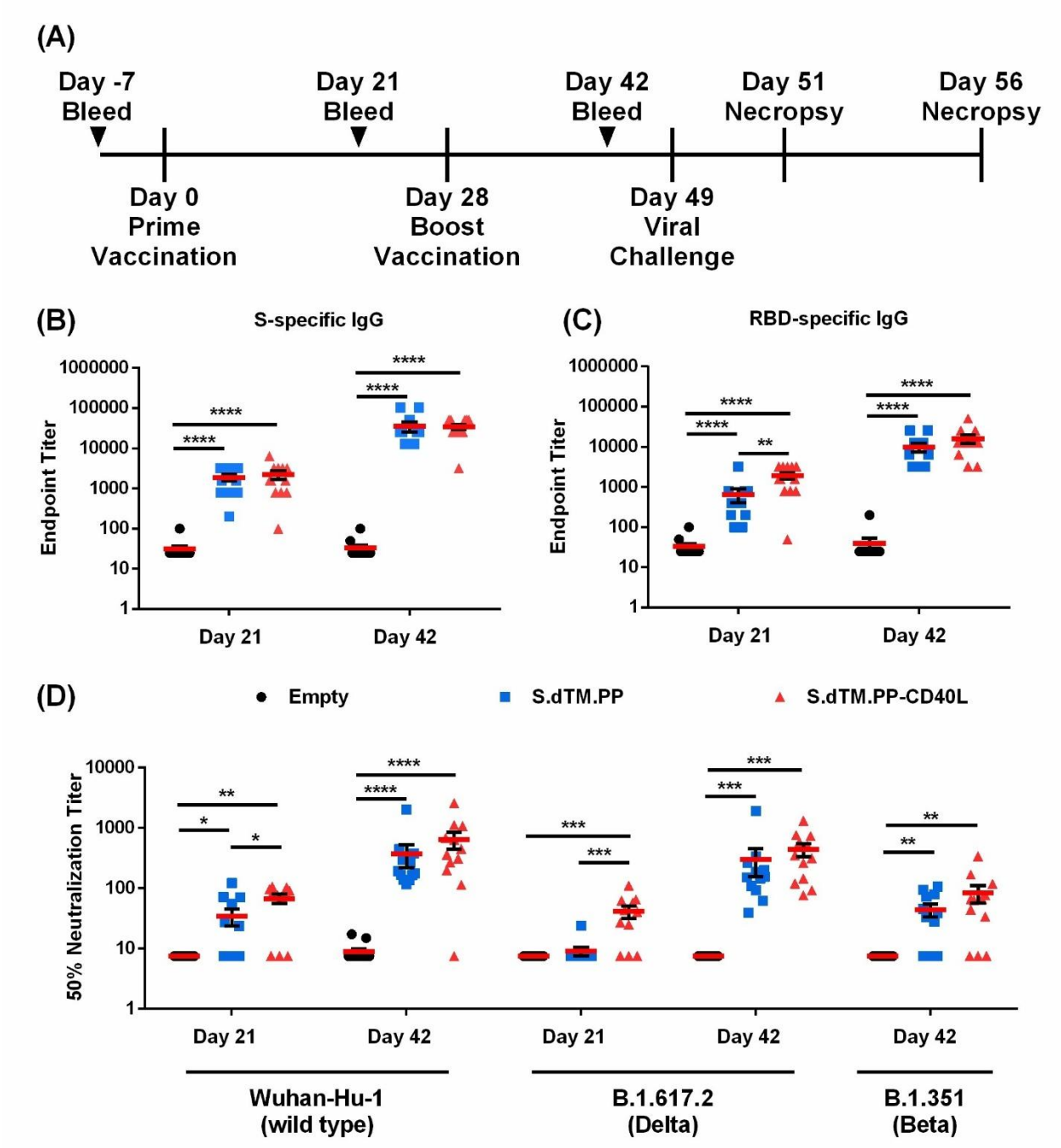

Figure 2.2. DNA vaccines induce robust humoral response.

(A) Female Syrian hamsters were randomly divided into three experimental groups (n= 12) and immunized intramuscularly on day 0 and 28 with 100 µg of pcDNA3.1, pcDNA3.1 S.dTM.PP or pcDNA3.1 S.dTM.PP-CD40L. Animals were challenged intranasally with 1×10^5 PFU of SARS-CoV-2 on day 49 and euthanized 2- and 7-days post-infection (dpi). Immunoglobulin determination of total spike **(B)** and RBD **(C)** -specific IgG in the sera of immunized hamsters was

done on days 21 and 42. **(D)** The 50% neutralization titer of immunized hamster sera at day 21 and day 42 was determined using wild type, B.1.671.2 and B.1.351 SARS-CoV-2 spike pseudotyped-VSV**.**

2.4.3 DNA vaccines protect hamsters from weight loss and reduce viral burden

On day 49, animals were challenged intranasally with 1×10^5 PFU of SARS-CoV-2 (Figure 2.2A). Changes in body weight were monitored daily post-challenge (Figure 2.3A) until animals were euthanized either 2 or 7 days post-challenge. On average, animals in the empty vector control group continued to lose body weight for 4 days post-challenge, reaching a maximum weight loss of 7.6% on day 4. Comparatively, animals immunized with the S.dTM.PP-CD40L and S.dTM.PP vaccines began to recover weight much earlier post-challenge, beginning to have significantly higher body weights than the control animals on days 3 and 4 respectively (Figure 2.3A). Viral burden in the respiratory tissues of Syrian hamsters was assessed by both plaque assay and RT-qPCR quantification of SARS-CoV-2 subgenomic mRNA (sgmRNA). On day 2 post-infection, the S.dTM.PP and S.dTM.PP-CD40L groups had significantly reduced viral burden in both lung and nasal turbinates compared to the empty vector control (Figure 2.3B/C). Although not statistically significant, there was a notable trending difference ($p=0.053$) of more than 50 folds in the mean lung viral titers between S.dTM.PP (1.4×10^7 PFU/g) and S.dTM.PP-CD40L (2.2×10^5 PFU/g). Vaccination with both S.dTM.PP and S.dTM.PP-CD40L significantly reduced the number of E sgmRNA copies in the hamster lungs 2 dpi (Figure 2.3D) relative to the empty vector control. Plaque forming units and E sgmRNA levels were below the limit of detection for all groups 7 days post-challenge (data not shown).

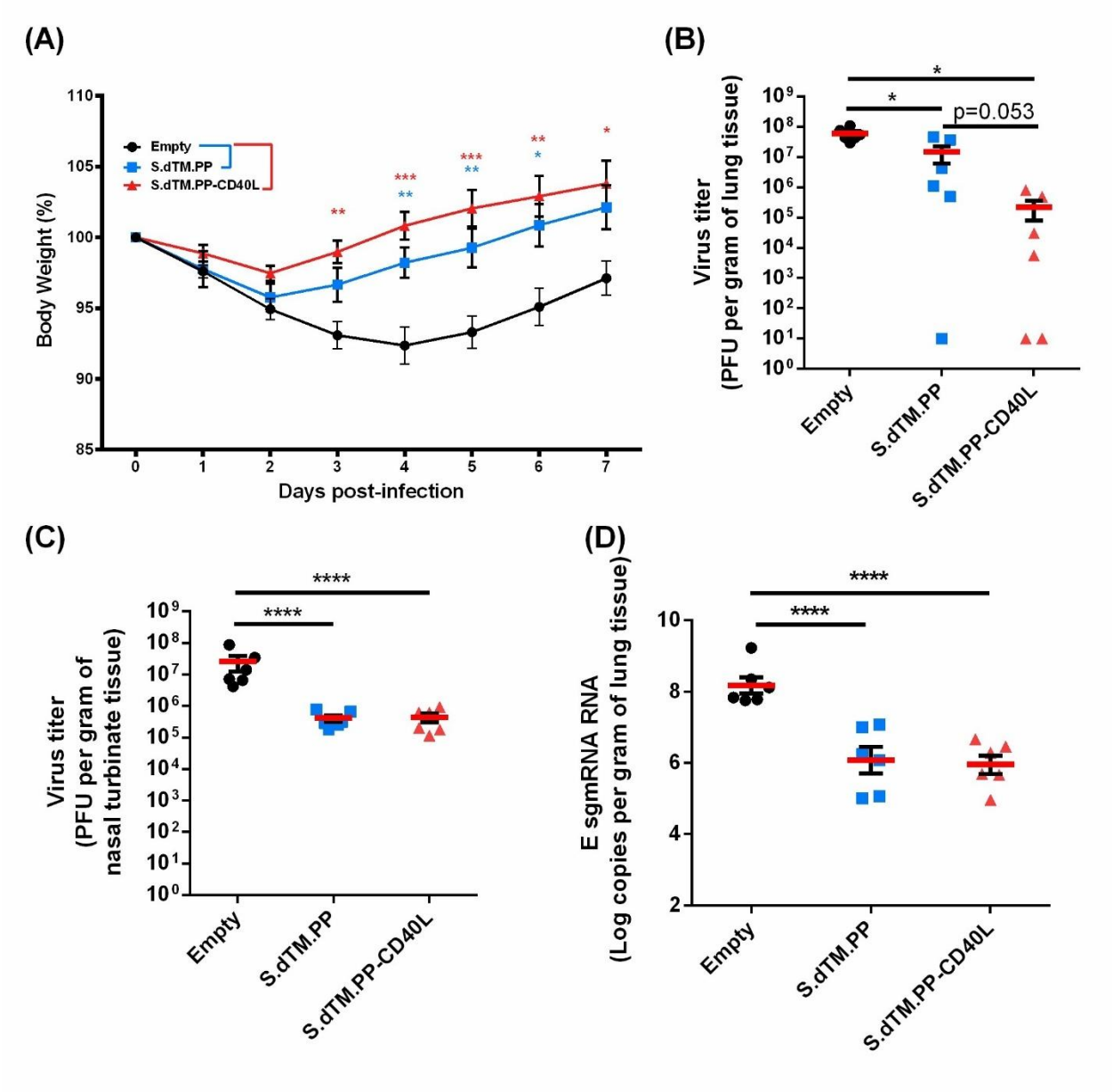

Figure 2.3. DNA vaccines reduce viral loads and improve weight recovery.

(A) Syrian hamster body weight was measured for 7-days following viral challenge (n=6). **(B)** Viral load in the lungs and nasal turbinates of SARS-CoV-2 challenged hamsters on day 2 post-infection (n=6). **(C)** Number of E sgmRNA copies in the lungs was determined via RT-qPCR 2 days post-infection (n=6). Data shown is mean ± SEM; n = 6 per group.

2.4.4 DNA vaccine expressing S-CD40L fusion protein most effectively reduced lung pathology following SARS-CoV-2 challenge

Right lung lobes were collected both 2- and 7-days post-challenge for histopathological analysis. Lungs from all infected hamsters at day 2, regardless of administered vaccine, showed mild to moderate interstitial pneumonia consisting of small to moderate numbers of mononuclear cell infiltration, thickening of the alveolar septa, and occasional presence of mixed neutrophils and mononuclear cells in the airway lumen. In addition, we detected mild to moderate infiltration of mononuclear cells in some perivascular and peribronchial areas of the lung (Figures 2.4A/B). Substantial differences in the severity of lung histopathology were observed in the infected hamsters at day 7, depending on the type of vaccine received. As anticipated, hamsters vaccinated with the empty vector showed the most severe lung histopathology. They displayed areas of consolidation due to the extensive alveolar septa thickening, collapse of alveoli, and inflammatory cell infiltration in alveolar septa and the areas surrounding airways and blood vessels. Hamsters vaccinated with S.dTM.PP showed milder lung histopathology, which were comparable to those seen at day 2 but with more apparent mononuclear inflammatory infiltration in the alveolar septa and focal areas of consolidation. The hamsters vaccinated with S.dTM.PP-CD40L showed even milder lung histopathology in their lungs than the hamsters vaccinated with S.dTM.PP (Fig. 4A/B), although the nature of the histopathological changes were similar between the two groups of hamsters. There were no overt abnormal changes in the nasal turbinate or spleen of any infected hamsters.

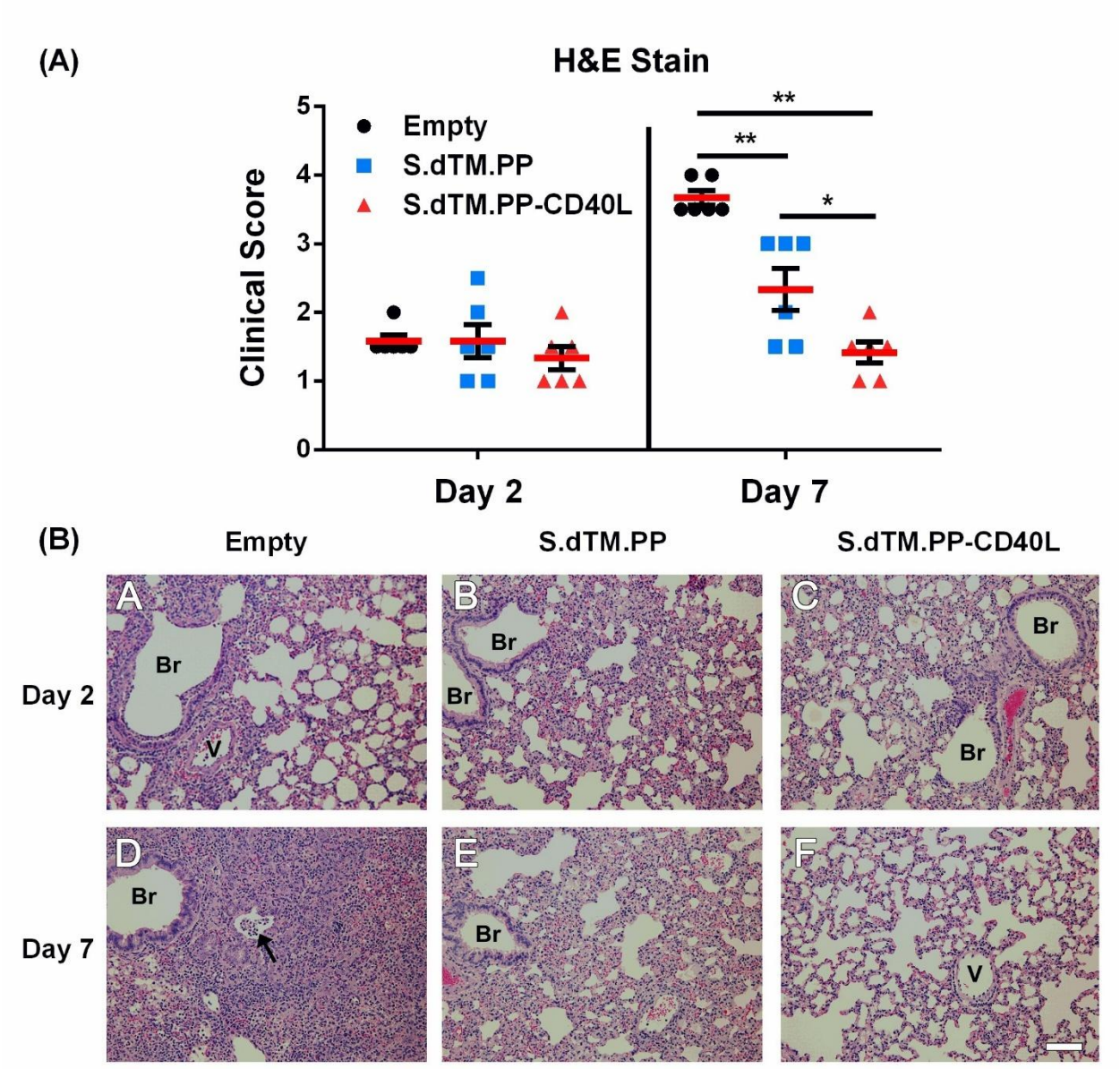

Figure 2.4. Lung Pathology following SARS-CoV-2 Challenge.

(A) Summary of histopathological scores. Data shown is mean ± SEM; n = 6 per group. **(B)** Representative photomicrographs of lung histopathology in SARS-CoV-2-infected hamsters. Groups of female golden Syrian hamsters (n=6) were intramuscularly immunized with pcDNA3.1 S.dTM.PP, pcDNA3.1 S.dTM.PP-CD40L or empty vector as a control on day 0 and 28. The hamsters were intranasally challenged with 1.0×10^5 PFU of SARS-CoV-2 on day 49 and sacrificed 2 or 7 days later. *(A-C)* Lung histopathology from infected hamsters sacrificed at day 2 post-challenge. The lungs from hamsters vaccinated with empty vector *(A),* S.dTM.PP *(B),* and S.dTM.PP-CD40L *(C)* showed mild to moderate interstitial pneumonia of similar severity. *(D-F)* Lung histopathology from infected hamsters sacrificed at day 7 post-challenge. *(D)* The lung from a hamster vaccinated with the empty vector showed areas of consolidation with the occasional

presence of mixed inflammatory cells in the bronchiolar lumen (arrow). *(E)* The lung from a hamster vaccinated with S.dTM.PP showed apparent mononuclear inflammatory infiltration in the alveolar septa and focal areas of consolidation. *(F)* The lung from a hamster vaccinated with S.dTM.PP-CD40L showed only mild interstitial pneumonia that is milder than that in the hamster vaccinated with S.dTM.PP *(E).* Br: bronchioles; V: blood vessel. H&E. Bar = 100 μm.

2.5 Discussion

Many vaccine candidates against SARS-CoV-2 have been developed in an attempt to bring a halt to the COVID-19 pandemic. While vaccination efforts are underway across the globe, there remains a need for affordable and equitable vaccines. This need is heightened by the continued emergence of SARS-CoV-2 variants with increased resistance to neutralizing antibodies (35–37). These variants of concerns and potential waning immunological memory (38) may require administration of annual booster shots, exacerbating costs. DNA vaccines present a cost-effective and temperature-stable alternative to mRNA vaccines with similar immunological characteristics. Multiple DNA vaccines against SARS-CoV-2 have been tested in various animal models and clinical trials (13,39–43). Intramuscular vaccination with 5 mg of naked pcDNA3.1 vectored vaccines encoding different variations of the SARS-CoV-2 spike protein, including S.dTM.PP, were shown to induce neutralizing antibodies and reduce levels of viral sgmRNA in the lungs of rhesus macaques (39). The pVAX-1-vectored ZyCoV-D vaccine showed strong humoral responses in mice, guinea pigs and rabbits when administered intradermally at 25 μg, 100 μg and 500 μg doses respectively (44). The ZyCoV-D vaccine was also found to be safe and immunogenic in a non-randomized phase I trial (14). INO-4800, a pGX0001-vectored Spike with an N-terminal IgE leader sequence displayed strong humoral and cell-mediated immune responses in mice and guinea pigs when administered intradermally using electroporation (43). The INO-4800 DNA vaccine was well-tolerated and immunogenic in all participants of a phase I clinical trial (13) and is now being tested in Phase II/III trials. INO-4800 is one of only a handful of candidate DNA vaccines currently

undergoing clinical testing (Supplemental Table 2.1). As DNA vaccines appear poised to become a valuable tool against COVID-19, research into overcoming their limitations and improving the technology is more essential than ever.

In this work, we evaluated the protective efficacy of a pcDNA3.1 vectored SARS-CoV-2 spike antigen fused with and without CD40L in a SARS-CoV-2 Syrian hamster challenge model. It is noted in the literature that doses of DNA vaccines vary, ranging from 50 to 200 μg with or without the use of alternative DNA vaccine delivery methods (45–47). In this study, we employed a 100 μg dose, as our study was mainly intended to compare the vaccines with or without CD40 ligand. The pcDNA3.1 S.dTM.PP-CD40L vaccine was able to induce a significant antibody response after a single dose (Figure 2.2B/C/D). Notably after a single dose, the S.dTM.PP-CD40L vaccine generated higher RBD-specific IgG antibody titers than the spike vaccine devoid of CD40L and induced a significantly greater NAb response against WT and B.1617.2 pseudoviruses (Figure 2.2D). Two weeks following the second immunization, the two spike vaccines induced similarly robust humoral responses, including the significant induction of neutralizing antibodies against WT, B.1.351 and B.1.671.2 spike pseudotyped VSV (Figure 2.2D). Post-challenge all animals experienced some level of SARS-CoV-2 related pathology. Vaccination with either spike vaccine led to a quicker recovery of body weight (Figure 2.3A) and reduced lung and nasal viral burdens (Figure 2.3B/C/D) post-challenge relative to recipients of the empty vector. While the CD40L-adjuvanted DNA vaccine did not induce statistically significant differences when compared directly to its non-adjuvanted counterpart, earlier body weight recovery and a trending decrease in pulmonary viral burden were observed for S.dTM.PP-CD40L vaccinated animals. At 2 days post-challenge all animals had comparable lung histopathology (Figure 2.4A) despite differences in lung and nasal viral burden. This result is not unexpected, as the absence of strong mucosal

immunity is likely to delay clearance of viral infection and resolution of pathological changes (48,49). In this light, CD40L seemed to contribute significantly to the recovery from damage to the lower respiratory tract. Substantial differences were noted in lung histopathology at day 7 post-challenge, where hamsters vaccinated with S.dTM.PP-CD40L had milder pathology than both the empty vector and S.dTM.PP immunized animals (Figure 2.4A). The severe lung pathology at day 7 post-challenge in hamsters vaccinated with the empty vector (Figure. 2.4A) but with no detectable viruses supports the notion that histopathology caused by the infection can persist for days after clearance of the SARS-CoV-2 infection (50).

While humoral responses and neutralizing antibodies play a critical role in vaccine-induced immunity against SARS-CoV-2 (51–53), it is important to consider strategies that also drive robust and long-lasting T cells responses. Despite not generating neutralizing antibodies, T cell epitope vaccines provide partial protection form SARS-CoV-2 challenge, suggesting T cell responses may also contribute to protection (54). Limited reagent availability for the Syrian hamster model precludes the comprehensive characterization of CD40L's effect on immune subtypes and T cell responses without the use of an additional animal model. However, mechanistic explanations for the observed reduction in lung pathology can potentially be inferred from previous work. In the past, our group and others have demonstrated that the addition of CD40L enhances antigen-specific T cell responses and improves vaccine efficacy against various viruses (21,26–28,55–57). Notably in one study, immunization with an influenza nucleoprotein CD40L fusion vaccine provided no protection against RSV challenge in BALB/c mice (27). This result highlights the inability of CD40L alone to induce protective immune responses, with its beneficial effects rather being mediated through the enhancement of antigen-specific responses. In our previous study of recombinant adenovirus-5 vectored vaccines against MERS-CoV, despite affording similar

reductions in viral burden as S1 alone, only S1-CD40L was able to prevent pulmonary perivascular hemorrhage post–MERS-CoV challenge in the transgenic Human Dipeptidyl Peptidase 4 Mouse Model (28). While pulmonary pathology did not manifest as perivascular hemorrhage in this study, owing to a variety of factors including the vaccine form, challenge virus and animal model, the reduced pulmonary pathology reported here aligns with these previous MERS-CoV findings, suggesting that a balanced protective immunity mediated by the CD40L fusion domain may have afforded additional protection from SARS-CoV-2 challenge.

Despite promising results, DNA vaccine adoption and utilization lags behind that of mRNA vaccines. Historically, the theoretical potential for DNA vaccines to integrate into the host genome has been of great concern; however, experimental evidence has shown the rate of integration to be below rates of spontaneous mutations (58,59). Similar concerns also existed about the induction of anti-DNA antibodies, although numerous pre-clinical and clinical studies have practically dismissed this concern (60). One other major concern about DNA vaccines has been their historically poor therapeutic efficacy, driven partly by low immunogenicity and the inability of unformulated DNA vaccines to avoid DNase degradation and reach the nucleus. One potential avenue for improvement is through the use of alternative immunization devices, such as jet injectors, electroporation and gene-guns, all of which have been shown to improve the uptake of DNA vaccines and their subsequent efficacy relative to needle injection (61,62). Another promising strategy is encapsulating the DNA vaccines in nanoparticles, which can improve DNA uptake, protect DNA from DNase degradation and act as an vaccine adjuvant (63–66). The successful usage of lipid-nanoparticle formulated RNA vaccines against SARS-CoV-2 lends credence to their use as a DNA vaccine delivery vector (67).

Our results underlie the need to further explore the safety and efficacy of DNA vaccines. We demonstrate the beneficial effect of using CD40L as a molecular adjuvant for a SARS-CoV-2 spike vaccine, significantly reducing lung pathology compared to a non-adjuvanted counterpart. Our work has its limitations. Specifically, while Syrian hamsters are one of the best small-animal models for vaccine evaluation against SARS-CoV-2, the scarcity of research reagents for the model precludes its use for mechanistic investigation. Further studies in mice may aim to characterize the effects of CD40L on T cell responses to determine potential molecular mechanisms underlying changes in disease pathology. Additional experiments may also investigate the potential synergism of this vaccine candidate with improved methods of DNA vaccine delivery such as lipid-nanoparticles. These experiments are currently ongoing in our laboratories.

2.6 Author Contribution

LT, MR, DS, JC, LW, WC, MJ, SS, MRM and XL contributed to the conceptualization.

LT, DD, AT, WC, JV, WZ, AP, EL, JW, CG, MR, RMA, RYA and WC conducted the experiments.

LT, AT, AH, WC, WZ, AP, EL, JW, SR, RMA, RYA and WC were involved in data curation and formal analysis.

LT and JG performed the statistical analysis.

AT, AH, DS, JC, LW, WC, MJ, SS, MRM and XL were involved in funding acquisition, supervision and project administration.

LT wrote the first draft of the manuscript.

WC and XL wrote sections of the manuscript.

All authors contributed to manuscript revision, read and approved the submitted version.

2.7 Conflict of Interest

The authors declare that the research was conducted in the absence of any commercial or financial relationships that could be construed as a potential conflict of interest.

2.8 Acknowledgments

We gratefully acknowledge Histology/Imaging/Staining services provided by the Louise Pelletier HCF at the University of Ottawa. We also gratefully acknowledge Dr. Neda Nasheri and Dr. Huixin Lu for commenting on the manuscript. This work was funded by the Government of Canada.

2.9 Supplementary Material

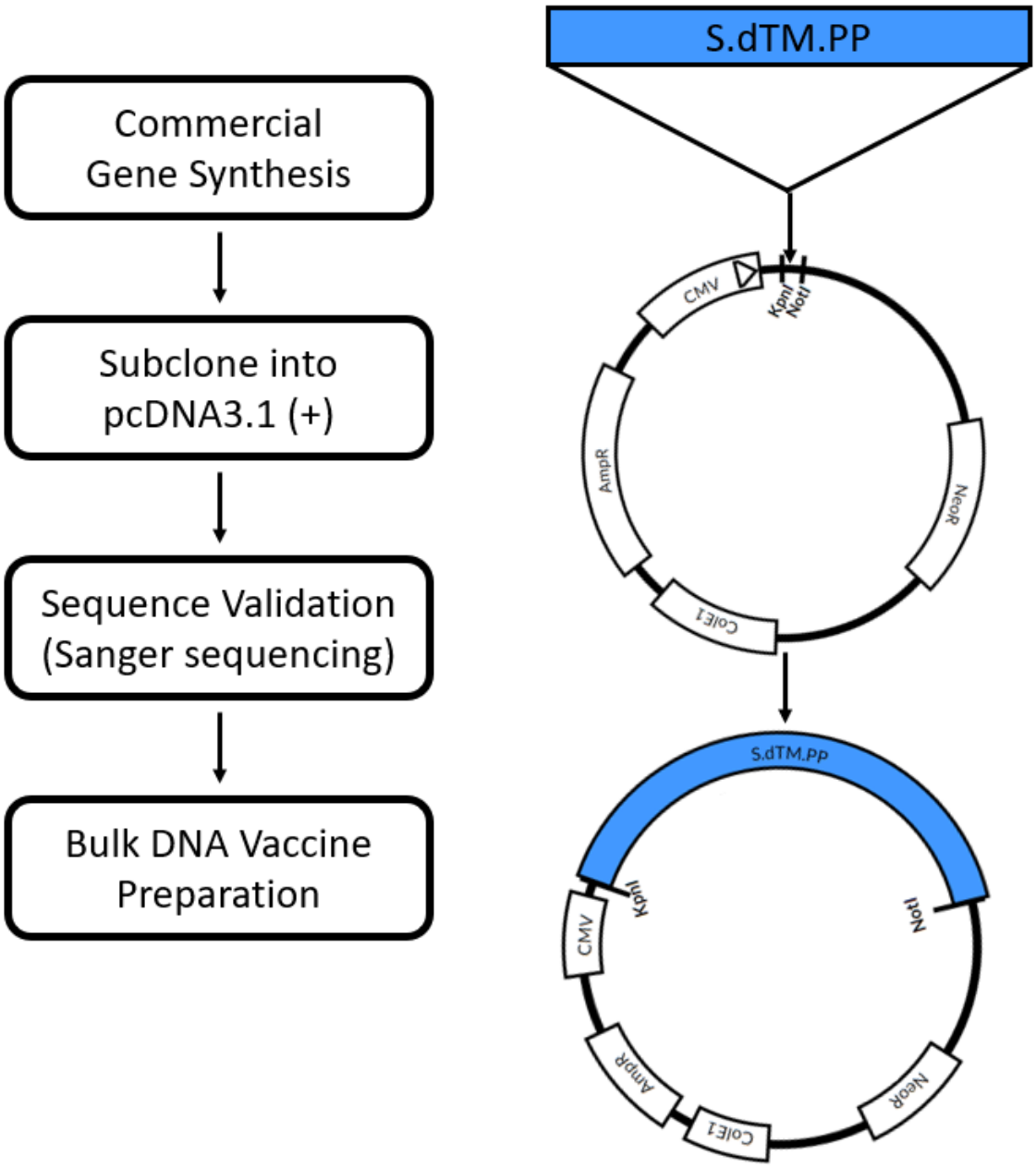

Supplemental Figure 2.1 DNA Vaccine Construction.

Commercially synthesized DNA sequences were subcloned into pcDNA3.1 (+) using KpnI and NotI restriction sites. DNA vaccines were sequenced validated before bulk preparation.

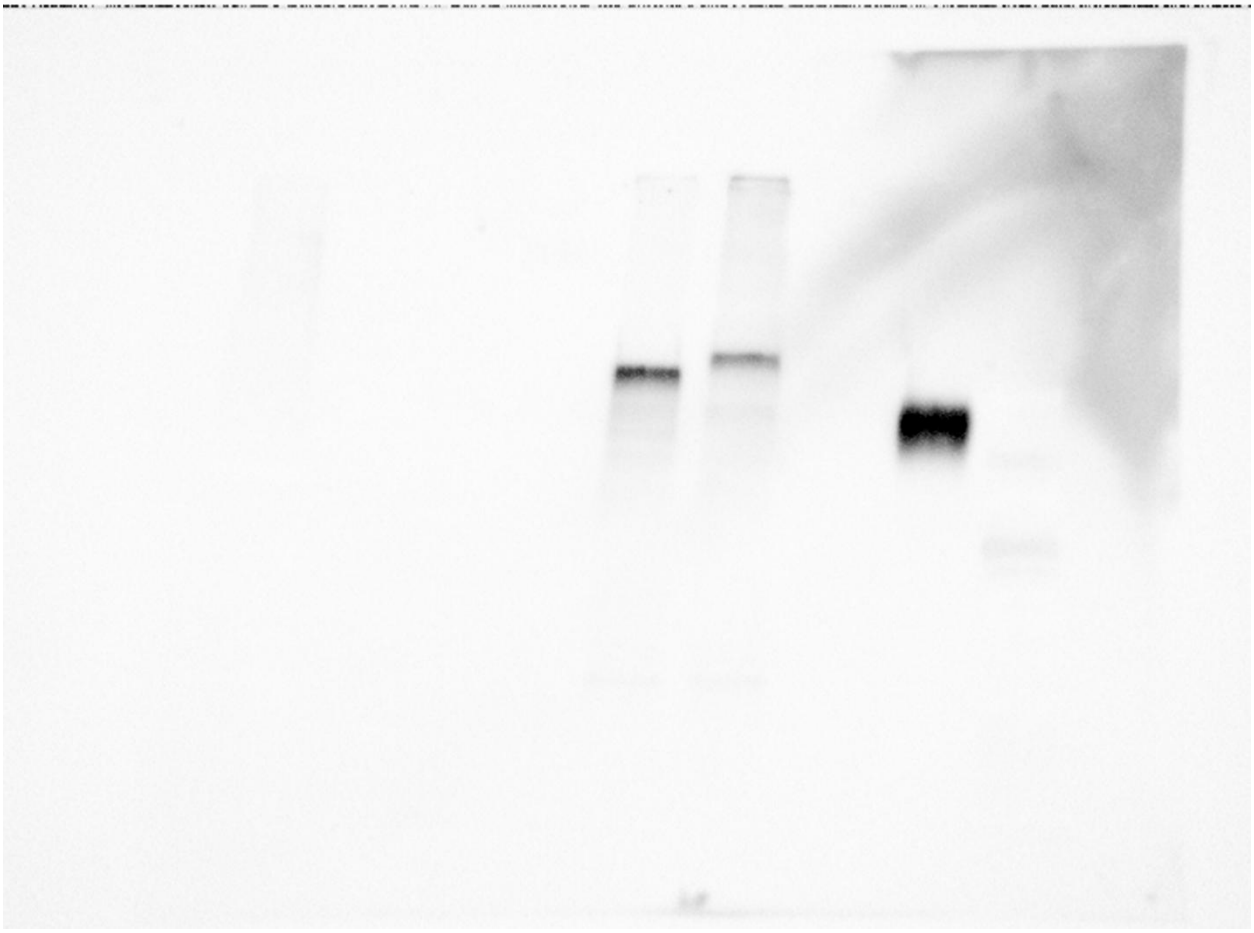

Supplemental Figure 2.2 Spike Western Blot Images.

SARS-CoV-2 (2019-nCoV) Spike Antibody, Rabbit PAb, Antigen Affinity Purified (Cat: 40591-T62, Sino Biologics). SARS-CoV-2 (2019-nCoV) Spike S1+S2 ECD-His recombinant protein (Sino Biological) used as a positive control. Chemiluminescence image of entire membrane.

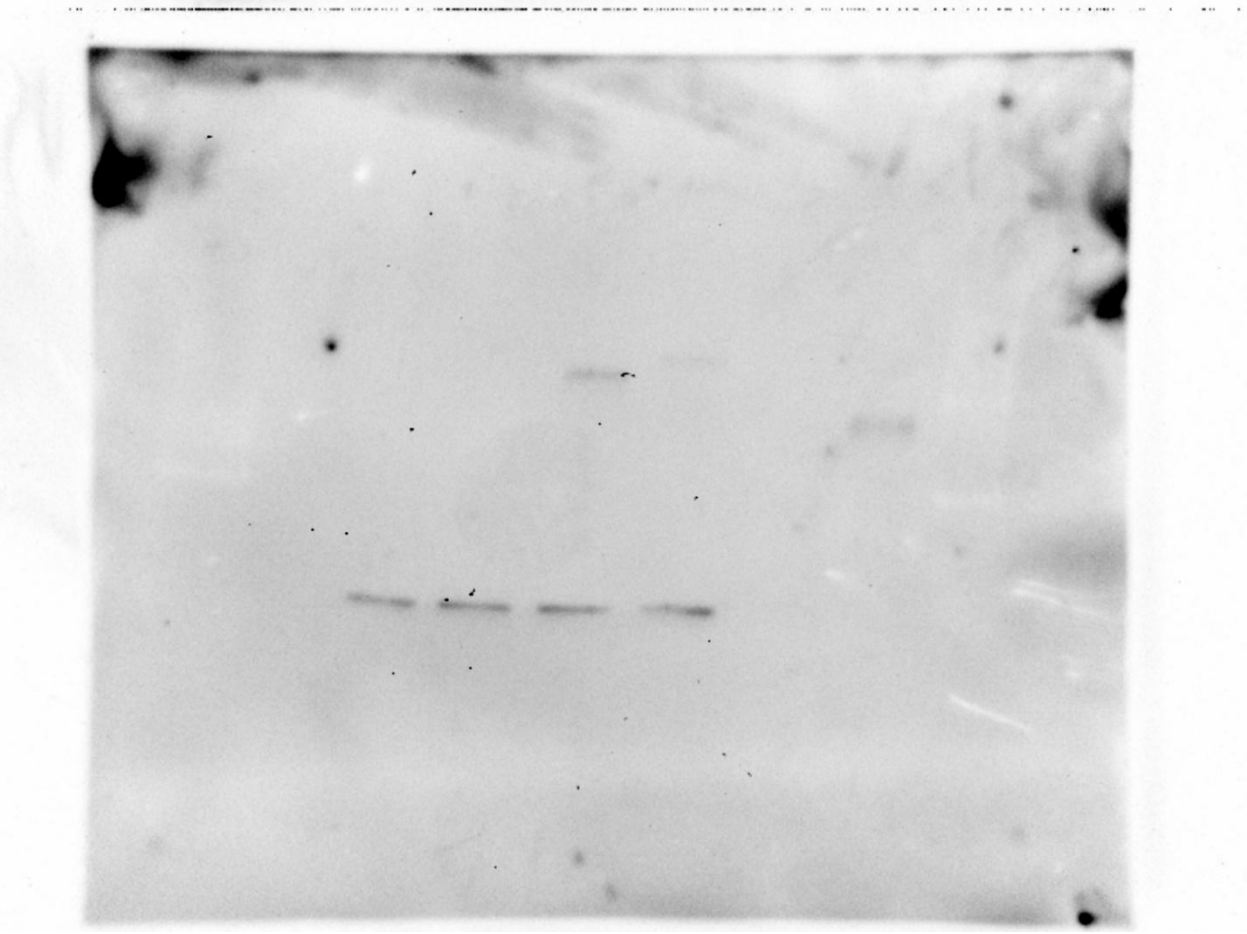

Supplemental Figure 2.3 B-actin Western Blot Image.

β-Actin Antibody (Cat: 4967, Cell Signaling). Chemiluminescence image of entire membrane.

Supplemental Table 2.1 DNA Vaccines against SARS-CoV-2 in clinical trials.

S – Spike. N – Nucleoprotein. ID – Intradermal. IM – Intramuscular. EP- Electroporation. https://clinicaltrials.gov/ accessed November 16 2021.

Vaccine Name	Vaccine Antigen	Administration Route (Doses)	Administration Device	Clinical Trial Phase	Clinical Trial Identifier
INO-4800	S	ID (2)	EP	II/III	NCT04642638
AG0302-COVID19	S	IM (2)	N/A	II/III	NCT04655625
GX-19N	S and N	IM (2)	EP	II/III	NCT05067946
VB10.2129 (C1) and VB10.2210	S or multi-antigen	IM (1 or 2)	N/A	I/II	NCT05069623
Covigenix VAX-001	S	IM (2)	N/A	I/II	NCT04591184
GLS-5310	S	ID (2)	N/A	I/II	NCT04673149
GX-19	S	IM (2)	EP or needle-free injection	I/II	NCT04445389
COVID-eVax	S	IM (1 or 2)	EP	I/II	NCT04788459
AG0301-COVID19	S	IM (1 or 2)	N/A	I/II	NCT04463472
CORVAX-12	S	IM (1)	EP	I	NCT04627675
COVIGEN	S	IM/ID (2)	needle-free injection	I	NCT04742842
COVIDITY	S and N	IM/ID (2)	needle-free injection	I	NCT05047445

2.10 References

1. Coronavirus disease (COVID-19). Available at: https://www.who.int/emergencies/diseases/novel-coronavirus-2019 [Accessed September 15, 2021]

2. COVID-19 vaccine tracker and landscape. Available at: https://www.who.int/publications/m/item/draft-landscape-of-covid-19-candidate-vaccines [Accessed September 15, 2021]

3. Corbett KS, Flynn B, Foulds KE, Francica JR, Boyoglu-Barnum S, Werner AP, et al. Evaluation of the mRNA-1273 Vaccine against SARS-CoV-2 in Nonhuman Primates. New England Journal of Medicine (2020) 383:1544–1555. doi:10.1056/NEJMoa2024671

4. Baden LR, El Sahly HM, Essink B, Kotloff K, Frey S, Novak R, et al. Efficacy and Safety of the mRNA-1273 SARS-CoV-2 Vaccine. New England Journal of Medicine (2021) 384:403–416. doi:10.1056/NEJMoa2035389

5. Polack FP, Thomas SJ, Kitchin N, Absalon J, Gurtman A, Lockhart S, et al. Safety and Efficacy of the BNT162b2 mRNA Covid-19 Vaccine. N Engl J Med (2020) 383:2603–2615. doi:10.1056/NEJMOA2034577

6. Vogel AB, Kanevsky I, Che Y, Swanson KA, Muik A, Vormehr M, et al. BNT162b vaccines protect rhesus macaques from SARS-CoV-2. Nature (2021) 592:283–289. doi:10.1038/s41586-021-03275-y

7. Health Canada authorizes first COVID-19 vaccine. Available at: https://www.canada.ca/en/health-canada/news/2020/12/health-canada-authorizes-first-covid-19-vaccine.html [Accessed September 15, 2021]

8. FDA Approves First COVID-19 Vaccine. Available at: https://www.fda.gov/news-events/press-announcements/fda-approves-first-covid-19-vaccine [Accessed September 15, 2021]

9. EMA recommends first COVID-19 vaccine for authorisation in the EU. Available at: https://www.ema.europa.eu/en/news/ema-recommends-first-covid-19-vaccine-authorisation-eu [Accessed September 15, 2021]

10. Silveira MM, Oliveira TL, Schuch RA, McBride AJA, Dellagostin OA, Hartwig DD. DNA vaccines against leptospirosis: A literature review. Vaccine (2017) 35:5559–5567. doi:10.1016/J.VACCINE.2017.08.067

11. Silveira MM, Moreira GMSG, Mendonça M. DNA vaccines against COVID-19: Perspectives and challenges. Life Sci (2021) 267:118919. doi:10.1016/J.LFS.2020.118919

12. Crommelin DJA, Anchordoquy TJ, Volkin DB, Jiskoot W, Mastrobattista E. Addressing the Cold Reality of mRNA Vaccine Stability. J Pharm Sci (2021) 110:997–1001. doi:10.1016/J.XPHS.2020.12.006

13. Tebas P, Yang S, Boyer JD, Reuschel EL, Patel A, Christensen-Quick A, et al. Safety and immunogenicity of INO-4800 DNA vaccine against SARS-CoV-2: A preliminary report of an open-label, Phase 1 clinical trial. EClinicalMedicine (2021) 31:100689. doi:10.1016/J.ECLINM.2020.100689

14. Momin T, Kansagra K, Patel H, Sharma S, Sharma B, Patel J, et al. Safety and Immunogenicity of a DNA SARS-CoV-2 vaccine (ZyCoV-D): Results of an open-label, non-randomized phase I part of phase I/II clinical study by intradermal route in healthy subjects in India. EClinicalMedicine (2021) 38:101020. doi:10.1016/J.ECLINM.2021.101020

15. DBT-BIRAC supported ZyCoV-D developed by Zydus Cadila Receives Emergency Use Authorization. (2021) Available at: https://www.pib.gov.in/PressReleasePage.aspx?PRID=1747669 [Accessed September 15, 2021]

16. Gares SL, Fischer KP, Congly SE, Lacoste S, Addison WR, Tyrrell DL, et al. Immunotargeting with CD154 (CD40 Ligand) Enhances DNA Vaccine Responses in Ducks. Clinical and Vaccine Immunology (2006) 13:958. doi:10.1128/CVI.00080-06

17. Manoj S, Griebel PJ, Babiuk LA, Hurk SVDL-V Den. Modulation of immune responses to bovine herpesvirus-1 in cattle by immunization with a DNA vaccine encoding glycoprotein D as a fusion protein with bovine CD154. Immunology (2004) 112:328–338. doi:10.1111/J.1365-2567.2004.01877.X

18. Mendoza RB, Cantwell MJ, Kipps TJ. Immunostimulatory effects of a plasmid expressing CD40 ligand (CD154) on gene immunization. The Journal of Immunology (1997) 159:5777–5781.

19. Stone GW, Barzee S, Snarsky V, Kee K, Spina CA, Yu X-F, et al. Multimeric Soluble CD40 Ligand and GITR Ligand as Adjuvants for Human Immunodeficiency Virus DNA Vaccines. J Virol (2006) 80:1762–1772. doi:10.1128/JVI.80.4.1762-1772.2006

20. Xiang R, Primus FJ, Ruehlmann JM, Niethammer AG, Silletti S, Lode HN, et al. A Dual-Function DNA Vaccine Encoding Carcinoembryonic Antigen and CD40 Ligand Trimer Induces T Cell-Mediated Protective Immunity Against Colon Cancer in Carcinoembryonic Antigen-Transgenic Mice. The Journal of Immunology (2001) 167:4560–4565. doi:10.4049/JIMMUNOL.167.8.4560

21. Kwa S, Lai L, Gangadhara S, Siddiqui M, Pillai VB, Labranche C, et al. CD40L-Adjuvanted DNA/Modified Vaccinia Virus Ankara Simian Immunodeficiency Virus SIV239 Vaccine Enhances SIV-Specific Humoral and Cellular Immunity and Improves Protection against a Heterologous SIVE660 Mucosal Challenge. J Virol (2014) 88:9579. doi:10.1128/JVI.00975-14

22. Auten MW, Huang W, Dai G, Ramsay AJ. CD40 Ligand enhances immunogenicity of vector-based vaccines in immunocompetent and CD4+ T cell deficient individuals. Vaccine (2012) 30:2768. doi:10.1016/J.VACCINE.2012.02.020

23. Ma DY, Clark EA. The role of CD40 and CD154/CD40L in dendritic cells. Semin Immunol (2009) 21:265–272. doi:10.1016/J.SMIM.2009.05.010

24. Kooten C van, Banchereau J. CD40-CD40 ligand. J Leukoc Biol (2000) 67:2–17. doi:10.1002/JLB.67.1.2

25. Fujii S, Liu K, Smith C, Bonito AJ, Steinman RM. The Linkage of Innate to Adaptive Immunity via Maturing Dendritic Cells In Vivo Requires CD40 Ligation in Addition to Antigen Presentation and CD80/86 Costimulation. Journal of Experimental Medicine (2004) 199:1607–1618. doi:10.1084/JEM.20040317

26. Fan X, Hashem AM, Chen Z, Li C, Doyle T, Zhang Y, et al. Targeting the HA2 subunit of influenza A virus hemagglutinin via CD40L provides universal protection against diverse subtypes. Mucosal Immunol (2014) 8:211–220. doi:10.1038/mi.2014.59

27. Muralidharan A, Russell M, Larocque L, Gravel C, Li C, Chen W, et al. Targeting CD40 enhances antibody- and CD8-mediated protection against respiratory syncytial virus infection. Sci Rep (2018) 8:1–13. doi:10.1038/s41598-018-34999-z

28. Hashem AM, Algaissi A, Agrawal AS, Al-amri SS, Alhabbab RY, Sohrab SS, et al. A Highly Immunogenic, Protective, and Safe Adenovirus-Based Vaccine Expressing Middle East Respiratory Syndrome Coronavirus S1-CD40L Fusion Protein in a Transgenic Human Dipeptidyl Peptidase 4 Mouse Model. J Infect Dis (2019) 220:1558–1567. doi:10.1093/INFDIS/JIZ137

29. Wrapp D, Wang N, Corbett KS, Goldsmith JA, Hsieh C-L, Abiona O, et al. Cryo-EM structure of the 2019-nCoV spike in the prefusion conformation. Science (2020) 367:1260. doi:10.1126/SCIENCE.ABB2507

30. Nie J, Li Q, Wu J, Zhao C, Hao H, Liu H, et al. Quantification of SARS-CoV-2 neutralizing antibody by a pseudotyped virus-based assay. Nat Protoc (2020) 15:3699–3715. doi:10.1038/s41596-020-0394-5

31. Wibmer CK, Ayres F, Hermanus T, Madzivhandila M, Kgagudi P, Oosthuysen B, et al. SARS-CoV-2 501Y.V2 escapes neutralization by South African COVID-19 donor plasma. Nat Med (2021) 27:622–625. doi:10.1038/s41591-021-01285-x

32. Wölfel R, Corman VM, Guggemos W, Seilmaier M, Zange S, Müller MA, et al. Virological assessment of hospitalized patients with COVID-2019. Nature 2020 (2020) 581:465–469. doi:10.1038/s41586-020-2196-x

33. Harris G, Holbein BE, Zhou H, Howard Xu H, Chen W. Potential mechanisms of mucin-enhanced acinetobacter baumannii virulence in the mouse model of intraperitoneal infection. Infect Immun (2019) 87:11. doi:10.1128/IAI.00591-19

34. Lien C-E, Lin Y-J, Chen C, Lian W-C, Kuo T-Y, Campbell JD, et al. CpG-adjuvanted stable prefusion SARS-CoV-2 spike protein protected hamsters from SARS-CoV-2 challenge. Sci Rep (2021) 11:1–7. doi:10.1038/s41598-021-88283-8

35. Wang P, Nair MS, Liu L, Iketani S, Luo Y, Guo Y, et al. Antibody resistance of SARS-CoV-2 variants B.1.351 and B.1.1.7. Nature (2021) 593:130–135. doi:10.1038/s41586-021-03398-2

36. Planas D, Veyer D, Baidaliuk A, Staropoli I, Guivel-Benhassine F, Rajah MM, et al. Reduced sensitivity of SARS-CoV-2 variant Delta to antibody neutralization. Nature (2021) 596:276–280. doi:10.1038/s41586-021-03777-9

37. Weisblum Y, Schmidt F, Zhang F, DaSilva J, Poston D, Lorenzi JCC, et al. Escape from neutralizing antibodies 1 by SARS-CoV-2 spike protein variants. Elife (2020) 9:1. doi:10.7554/ELIFE.61312

38. Thomas SJ, Moreira ED, Kitchin N, Absalon J, Gurtman A, Lockhart S, et al. Six Month Safety and Efficacy of the BNT162b2 mRNA COVID-19 Vaccine. medRxiv [Preprint] (2021). doi:10.1101/2021.07.28.21261159

39. Yu J, Tostanosk LH, Peter L, Mercad NB, McMahan K, Mahrokhia SH, et al. DNA vaccine protection against SARS-CoV-2 in rhesus macaques. Science (2020) 369:806–811. doi:10.1126/SCIENCE.ABC6284

40. Seo YB, Suh YS, Ryu JI, Jang H, Oh H, Koo B-S, et al. Soluble Spike DNA Vaccine Provides Long-Term Protective Immunity against SARS-CoV-2 in Mice and Nonhuman Primates. Vaccines (Basel) (2021) 9:307. doi:10.3390/VACCINES9040307

41. Prompetchara E, Ketloy C, Tharakhet K, Kaewpang P, Buranapraditkun S, Techawiwattanaboon T, et al. DNA vaccine candidate encoding SARS-CoV-2 spike proteins elicited potent humoral and Th1 cell-mediated immune responses in mice. PLoS One (2021) 16:e0248007. doi:10.1371/JOURNAL.PONE.0248007

42. Alamri SS, Alluhaybi KA, Alhabbab RY, Basabrain M, Algaissi A, Almahboub S, et al. Synthetic SARS-CoV-2 Spike-Based DNA Vaccine Elicits Robust and Long-Lasting Th1 Humoral and Cellular Immunity in Mice. Front Microbiol (2021) 0:2412. doi:10.3389/FMICB.2021.727455

43. Smith TRF, Patel A, Ramos S, Elwood D, Zhu X, Yan J, et al. Immunogenicity of a DNA vaccine candidate for COVID-19. Nat Commun (2020) 11:1–13. doi:10.1038/s41467-020-16505-0

44. Dey A, Chozhavel TM, Chandra H, Pericherla HPR, Kumar S, Choonia HS, et al. Immunogenic potential of DNA vaccine candidate, ZyCoV-D against SARS-CoV-2 in animal models. Vaccine (2021) 39:4108–4116. doi:10.1016/J.VACCINE.2021.05.098

45. Chai KM, Tzeng TT, Shen KY, Liao HC, Lin JJ, Chen MY, et al. DNA vaccination induced protective immunity against SARS CoV-2 infection in hamsterss. PLoS Negl Trop Dis (2021) 15:e0009374. doi:10.1371/JOURNAL.PNTD.0009374

46. Leventhal SS, Clancy C, Erasmus J, Feldmann H, Hawman DW. An Intramuscular DNA Vaccine for SARS-CoV-2 Decreases Viral Lung Load but Not Lung Pathology in Syrian Hamsters. Microorganisms (2021) 9:1040. doi:10.3390/MICROORGANISMS9051040

47. Brocato RL, Kwilas SA, Kim RK, Zeng X, Principe LM, Smith JM, et al. Protective efficacy of a SARS-CoV-2 DNA vaccine in wild-type and immunosuppressed Syrian hamsters. NPJ Vaccines (2021) 6:1–7. doi:10.1038/s41541-020-00279-z

48. Su F, Patel GB, Hu S, Chen W. Induction of mucosal immunity through systemic immunization: Phantom or reality? Hum Vaccin Immunother (2016) 12:1070. doi:10.1080/21645515.2015.1114195

49. Bricker TL, Darling TL, Hassan AO, Harastani HH, Soung A, Jiang X, et al. A single intranasal or intramuscular immunization with chimpanzee adenovirus-vectored SARS-CoV-2 vaccine protects against pneumonia in hamsters. Cell Rep (2021) 36:109400. doi:10.1016/J.CELREP.2021.109400

50. Sia SF, Yan L-M, Chin AWH, Fung K, Choy K-T, Wong AYL, et al. Pathogenesis and transmission of SARS-CoV-2 in golden hamsters. Nature 2020 583:7818 (2020) 583:834–838. doi:10.1038/s41586-020-2342-5

51. McMahan K, Yu J, Mercado NB, Loos C, Tostanoski LH, Chandrashekar A, et al. Correlates of Protection Against SARS-CoV-2 in Rhesus Macaques. Nature (2021) 590:630. doi:10.1038/S41586-020-03041-6

52. Khoury DS, Cromer D, Reynaldi A, Schlub TE, Wheatley AK, Juno JA, et al. Neutralizing antibody levels are highly predictive of immune protection from symptomatic SARS-CoV-2 infection. Nat Med (2021) 27:1205–1211. doi:10.1038/s41591-021-01377-8

53. Earle KA, Ambrosino DM, Fiore-Gartland A, Goldblatt D, Gilbert PB, Siber GR, et al. Evidence for antibody as a protective correlate for COVID-19 vaccines. Vaccine (2021) 39:4423–4428. doi:10.1016/J.VACCINE.2021.05.063

54. Zhuang Z, Lai X, Sun J, Chen Z, Zhang Z, Dai J, et al. Mapping and role of T cell response in SARS-CoV-2–infected mice. Journal of Experimental Medicine (2021) 218:e20202187. doi:10.1084/JEM.20202187

55. Tripp RA, Jones L, Anderson LJ, Brown MP. CD40 Ligand (CD154) Enhances the Th1 and Antibody Responses to Respiratory Syncytial Virus in the BALB/c Mouse. The Journal of Immunology (2000) 164:5913–5921. doi:10.4049/JIMMUNOL.164.11.5913

56. Harcourt JL, Brown MP, Anderson LJ, Tripp RA. CD40 ligand (CD154) improves the durability of respiratory syncytial virus DNA vaccination in BALB/c mice. Vaccine (2003) 21:2964–2979. doi:10.1016/S0264-410X(03)00119-1

57. Hashem AM, Gravel C, Chen Z, Yi Y, Tocchi M, Jaentschke B, et al. CD40 Ligand Preferentially Modulates Immune Response and Enhances Protection against Influenza Virus. The Journal of Immunology (2014) 193:722–734. doi:10.4049/JIMMUNOL.1300093

58. Ledwith BJ, Manam S, Troilo PJ, Barnum AB, Pauley CJ, II TGG, et al. Plasmid DNA Vaccines: Investigation of Integration into Host Cellular DNA following Intramuscular Injection in Mice. Intervirology (2000) 43:258–272. doi:10.1159/000053993

59. Sheets RL, Stein J, Manetz TS, Duffy C, Nason M, Andrews C, et al. Biodistribution of DNA Plasmid Vaccines against HIV-1, Ebola, Severe Acute Respiratory Syndrome, or West Nile Virus Is Similar, without Integration, despite Differing Plasmid Backbones or Gene Inserts. Toxicological Sciences (2006) 91:610–619. doi:10.1093/TOXSCI/KFJ169

60. Liu MA. A Comparison of Plasmid DNA and mRNA as Vaccine Technologies. Vaccines (Basel) (2019) 7:37. doi:10.3390/VACCINES7020037

61. Tebas P, Roberts CC, Muthumani K, Reuschel EL, Kudchodkar SB, Zaidi FI, et al. Safety and Immunogenicity of an Anti–Zika Virus DNA Vaccine. N Engl J Med (2017) 385:e35. doi:10.1056/NEJMOA1708120

62. Jiang J, Ramos SJ, Bangalore P, Fisher P, Germar K, Lee BK, et al. Integration of needle-free jet injection with advanced electroporation delivery enhances the magnitude, kinetics, and persistence of engineered DNA vaccine induced immune responses. Vaccine (2019) 37:3832–3839. doi:10.1016/J.VACCINE.2019.05.054

63. Mucker EM, Karmali PP, Vega J, Kwilas SA, Wu H, Joselyn M, et al. Lipid Nanoparticle Formulation Increases Efficiency of DNA-Vectored Vaccines/Immunoprophylaxis in Animals Including Transchromosomic Bovines. Sci Rep (2020) 10:1–13. doi:10.1038/s41598-020-65059-0

64. Zhang W, Yin Z, Liu N, Yang T, Wang J, Bu Z, et al. DNA–chitosan nanoparticles improve DNA vaccine-elicited immunity against Newcastle disease virus through shuttling chicken interleukin-2 gene. J Microencapsul (2010) 27:693–702. doi:10.3109/02652048.2010.507881

65. Francis JE, Skakic I, Dekiwadia C, Shukla R, Taki AC, Walduck A, et al. Solid Lipid Nanoparticle Carrier Platform Containing Synthetic TLR4 Agonist Mediates Non-Viral DNA Vaccine Delivery. Vaccines (Basel) (2020) 8:551. doi:10.3390/VACCINES8030551

66. Lim M, Badruddoza AZM, Firdous J, Azad M, Mannan A, Al-Hilal TA, et al. Engineered Nanodelivery Systems to Improve DNA Vaccine Technologies. Pharmaceutics (2020) 12:30. doi:10.3390/PHARMACEUTICS12010030

67. Shah MAA, He N, Li Z, Ali Z, Zhang L. Nanoparticles for DNA vaccine delivery. J Biomed Nanotechnol (2014) 10:2332–2349. doi:10.1166/JBN.2014.1981

Chapter 3: Lipid nanoparticle encapsulation of a Delta spike-CD40L DNA vaccine improves effectiveness against Omicron challenge in Syrian hamsters

Preface: This chapter has been previously published as a research article.

Tamming L et al. Lipid nanoparticle encapsulation of a Delta spike-CD40L DNA vaccine improves effectiveness against Omicron challenge in Syrian hamsters. ***Mol Ther Methods Clin Dev***. 2024 Aug 19;32(3):101325. doi: 10.1016/j.omtm.2024.101325.

Candidate Contribution

Levi Tamming was the primary author of this manuscript. Levi Tamming designed the experiments and vaccines. Levi Tamming prepared all plasmid constructs and performed all ELISA, pseudovirus neutralization, and subgenomic mRNA experiments. Levi Tamming performed all *in vitro* LNP transfection experiments. Levi Tamming performed all mass spectrometry sample preparation and down-stream pathway analysis. Levi Tamming analyzed all data, prepared all figures, and wrote the first draft of the manuscript.

Author list

Levi Tamming[1,2], Diana Duque[3], Jegarubee Bavananthasivam[3], Anh Tran[2,3,*], Casey Lansdell[1], Grant Frahm[1], Jianguo Wu[1], Emily EF Fekete[1], Marybeth Creskey[1], Sathya N Thulasi Raman[1], Emmanuel Laryea[1,2], Wanyue Zhang[1,2], Annabelle Pfeifle[1,2], Caroline Gravel[1], Andrew Stalker[1], Anwar M Hashem[4,5], Wangxue Chen[3], Matthew Stuible[3], Yves Durocher[3], David Safronetz[6], Jingxin Cao[6], Lisheng Wang[2], Simon Sauve[1], Michael Rosu-Myles[1,2], Xu Zhang[1], Michael JW Johnston[1,7,*], Xuguang Li[1,2,*]

[1]Centre for Oncology, Radiopharmaceuticals and Research, Biologic and Radiopharmaceutical Drugs Directorate, Health Products and Food Branch, Health Canada and World Health Organization Collaborating Center for Standardization and Evaluation of Biologicals, Ottawa, ON, Canada

[2]Department of Biochemistry, Microbiology and Immunology, Faculty of Medicine, University of Ottawa, Ottawa, ON, Canada

[3]Human Health Therapeutics Research Center, National Research Council of Canada, Ottawa, ON, Canada

[4]Vaccines and Immunotherapy Unit, King Fahd Medical Research Center, King Abdulaziz University, Jeddah, Saudi Arabia

[5]Department of Medical Microbiology and Parasitology, Faculty of Medicine, King Abdulaziz University, Jeddah, Saudi Arabia

[6]National Microbiology Laboratory, Public Health Agency of Canada, Winnipeg, MB, Canada

[7]Department of Chemistry, Carleton University, Ottawa, ON K1S 5B6, Canada

*Corresponding authors

3.1 Abstract

The effectiveness of mRNA vaccines largely depends on their lipid nanoparticle (LNP) component. Herein, we investigate the effectiveness of DLin-KC2-DMA (KC2) and SM-102-based LNPs for the intramuscular delivery of a plasmid encoding B.1.617.2 (Delta) Spike fused with CD40 ligand. LNP-encapsulation of this CD40L-adjuvanted DNA vaccine with either LNP formulation drastically enhanced antibody responses, enabling neutralization of heterologous Omicron variants. The DNA-LNP formulations provided excellent protection from homologous challenge, reducing viral replication, and preventing histopathological changes in the pulmonary tissues. Moreover, the DNA-LNP vaccines maintained a high level of protection against heterologous Omicron BA.5 challenge despite a reduced neutralizing response. In addition, we observed that DNA-LNP vaccination led to the pulmonary downregulation of interferon signaling, IL-12 signaling and macrophage response pathways following SARS-CoV-2 challenge, shedding some light on the mechanisms underlying the prevention of pulmonary injury. These results highlight the potential combination of molecular adjuvants with LNP-based vaccine delivery to induce greater and broader immune responses capable of preventing inflammatory damage and protecting against emerging variants. These findings could be informative for the future design of both DNA and mRNA vaccines.

3.2 Introduction

Since the emergence of SARS-CoV-2 and the beginning of the COVID-19 pandemic, historic amounts of time, effort, and resources have been spent on vaccine research and development. Vaccines have proven to be highly effective at reducing adverse outcomes and hospitalizations associated with SARS-CoV-2 infection (1–3), and are estimated to have prevented millions of deaths throughout the pandemic (4). Spearheading global vaccination efforts have been several mRNA lipid nanoparticle (LNP) vaccines, which have shown tremendous efficacy (5–8). A key factor contributing to the successful implementation of these mRNA vaccines has been their LNP delivery system (9,10). LNPs contribute to vaccine efficacy by reducing degradation of the nucleic acid payload and improving its cellular uptake (11–13). Additionally, the ionizable lipid component of LNP vaccines has been shown to be immunogenic (14–17), which may contribute to improved immune responses. DNA vaccines are often presented as an alternative to mRNA vaccines, sharing many properties but with a lower cost of production and a decreased likelihood to induce undesirable ribosomal frameshifting during translation (18–20). However, DNA vaccine efficacy has historically been limited by poor cellular uptake, susceptibility to DNase degradation and limited immunogenicity (21). In the wake of widespread LNP-mRNA vaccination during the COVID-19 pandemic, more research is essential to comprehend how effectively LNP delivery can be translated for use in DNA-based vaccination.

We previously described the immunogenicity and efficacy of pcDNA3.1 S.dTM.PP-CD40L, a plasmid DNA (pDNA)-vectored vaccine encoding a pre-fusion stabilized ancestral SARS-CoV-2 spike (S) ectodomain fused to the ectodomain of CD40 ligand (CD40L) (22). Engagement with CD40L on the surface of activated T cells represents a key regulator of antigen presenting cell activation (23). While the addition of CD40L to our pDNA-based vaccine improved humoral

responses following intramuscular vaccination in Syrian hamsters and afforded significant protection from challenge with an ancestral SARS-CoV-2 isolate, the adjuvanted vaccine failed to completely prevent viral replication and lung pathology. We encapsulated an updated version of our CD40L-adjuvanted vaccine based on the B.1.617.2 Delta variant, pVAX1 S-CD40L$_{B.1.617.2}$, in two different LNP formulations containing either DLin-KC2-DMA (KC2) or SM-102 ionizable lipids. We evaluated both the immunogenicity and efficacy of the LNP-encapsulated vaccines in comparison to unencapsulated pDNA in Syrian hamsters following B.1.617.2 and BA.5 SARS-CoV-2 challenge. Herein, we demonstrate that LNP-encapsulation drastically improves the strength and breadth of humoral responses induced by DNA vaccination and provides superior protection upon homologous and heterologous challenge.

3.3 Results

3.3.1 LNP-encapsulation enhances strength and breadth of DNA vaccine-induced humoral response

The B.1.617.2-based DNA construct (pVAX1 S-CD40L$_{B.1.617.2}$) differs from our previous construct in that nine mutations found in the B.1.617.2 variant S protein were introduced into the vaccine antigen (Supplemental Figure 3.1A) and the pVAX1 vector was used rather than pcDNA3.1. Due to the omission of non-essential elements the pVAX1 vector is considerably smaller than pcDNA3.1, which should allow a greater number of plasmids to be administered in an equivalent dose improving antigen expression and vaccine efficiency (24). An *in vitro* CD40 signaling bioassay confirmed the fused CD40L domain remained functional (Supplemental Figure 3.1B). To first assess DNA-LNP immunogenicity and efficacy, we immunized male Syrian hamsters intramuscularly at a 4-week interval with 5- or 20-µg of LNP-encapsulated pVAX1 S-

CD40L$_{B.1.617.2}$ (Figure 3.1A). Male hamsters were chosen as they experience more severe infection compared to females (25,26). Formulated with KC2 ionizable lipids, the DNA-LNPs had an average size distribution around 100 nm (Supplemental Table 3.1). For comparison, hamsters were also immunized with a 100-µg dose of unencapsulated pVAX1 S-CD40L$_{B.1.617.2}$, this dose of naked DNA having previously conferred significant yet incomplete protection (22). Both the 5- and 20-µg doses of KC2 LNP-encapsulated pVAX1 S-CD40L$_{B.1.617.2}$ induced greater binding antibody responses than the significantly higher 100-µg dose of unencapsulated vaccine against homologous B.1.617.2 S (Figure 3.1B) and heterologous Omicron BA.1 S (Figure 3.1C). Furthermore, the magnitude of this increase appears to rely on the fusion of CD40L (Supplemental Figure 3.1C). LNP-encapsulation also substantially improved neutralizing antibody (NAb) responses. As shown in Figure 3.1D, unlike unencapsulated pVAX1 S-CD40L$_{B.1.617.2}$, both 5- and 20-µg doses of the DNA-LNP induced significant NAb responses against B.1.617.2 pseudotyped-VSV after a single dose. Interestingly, despite having a strong binding Ab response, a single 5-µg dose of LNP-formulated pVAX1 S-CD40L$_{B.1.617.2}$ failed to elicit a detectable neutralizing response against BA.1 pseudotyped-VSV (Figure 3.1E). However, following the second vaccination, both the 5- and 20-µg doses of LNP-formulated pVAX1 S-CD40L$_{B.1.617.2}$ induced significant NAb responses against BA.1. In contrast, vaccination with naked pVAX1 S-CD40L$_{B.1.617.2}$ failed to induce a detectable omicron neutralizing response even after two vaccine doses. Notably, NAb responses following the boost vaccination were also measured against four other Omicron subvariants (Figure 3.1F). Both the 5-µg and 20-µg doses of the LNP-encapsulated vaccine induced a significant response against BA.5, while the higher dose also raised a significant response against BA.2.75. With respect to BF.7 and BQ.1, while not statistically significant relative

to control groups, vaccination with 20-μg of the DNA-LNPs did raise some neutralizing activity against these newer variants.

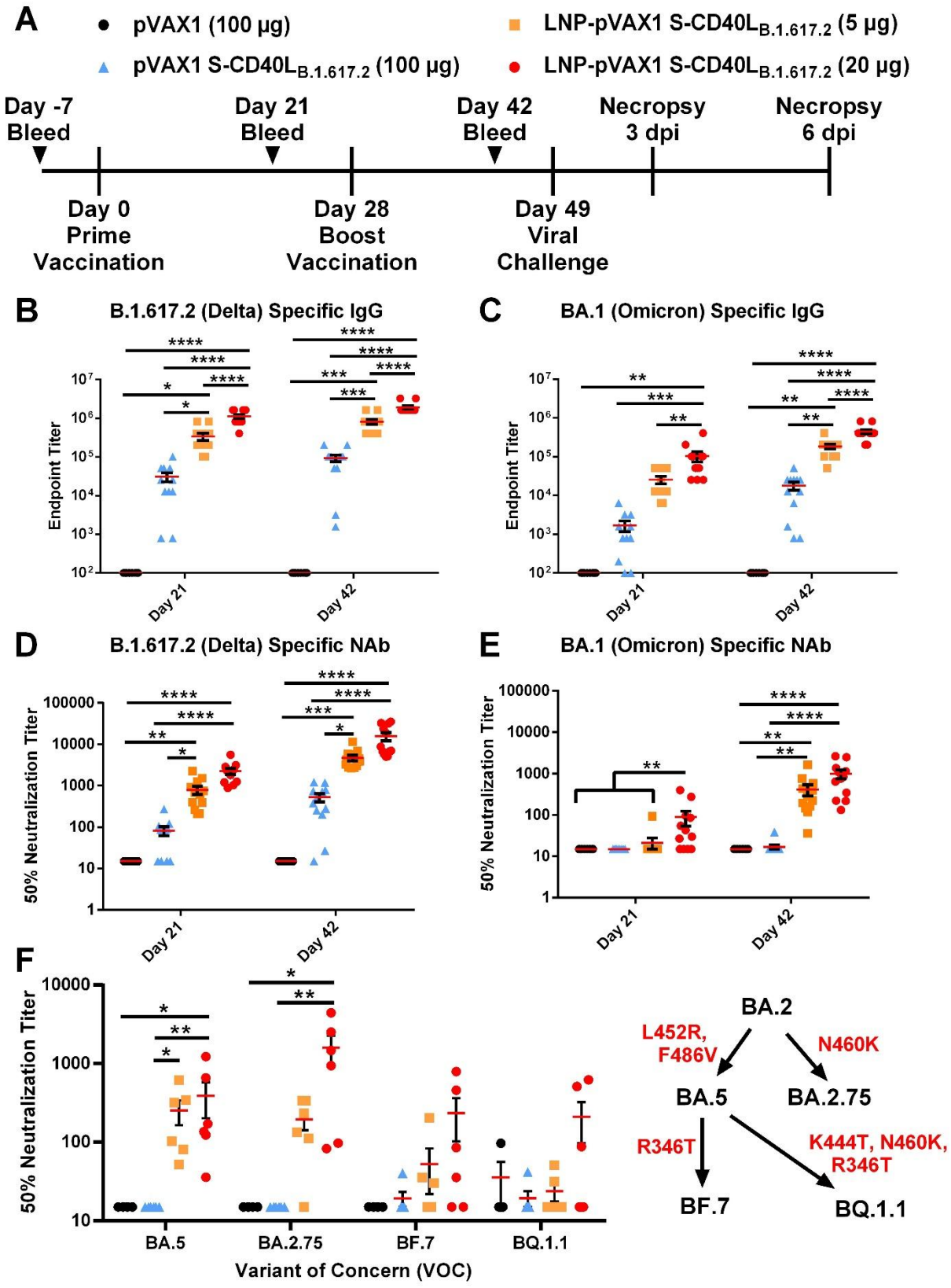
A
pVAX1 (100 µg)
pVAX1 S-CD40L B.1.617.2 (100 µg)
LNP-pVAX1 S-CD40L B.1.617.2 (5 µg)
LNP-pVAX1 S-CD40L B.1.617.2 (20 µg)
Day -7 Bleed
Day 21 Bleed
Day 42 Bleed
Necropsy 3 dpi
Necropsy 6 dpi
Day 0 Prime Vaccination
Day 28 Boost Vaccination
Day 49 Viral Challenge
B
B.1.617.2 (Delta) Specific IgG
Endpoint Titer
Day 21
Day 42
C
BA.1 (Omicron) Specific IgG
Endpoint Titer
Day 21
Day 42
D
B.1.617.2 (Delta) Specific NAb
50% Neutralization Titer
Day 21
Day 42
E
BA.1 (Omicron) Specific NAb
50% Neutralization Titer
Day 21
Day 42
F
50% Neutralization Titer
BA.5
BA.2.75
BF.7
BQ.1.1
Variant of Concern (VOC)
BA.2
L452R, F486V
N460K
BA.5
BA.2.75
R346T
K444T, N460K, R346T
BF.7
BQ.1.1

Figure 3.1 LNP-encapsulation improves humoral response to DNA vaccination

(A) Male Syrian hamsters were randomly divided into four experimental groups (n= 8 for pVAX1, n = 12 for pVAX1 S-CD40L$_{B.1.617.2}$) and immunized intramuscularly on day 0 and 28 with either 100-µg of pVAX1, 100-µg of pVAX1 S-CD40L$_{B.1.617.2}$, or 5 or 20-µg of LNP-encapsulated pVAX1 S-CD40L$_{B.1.617.2}$. Animals were challenged intranasally with 1.67 $\times 10^5$ TCID50 of a SARS-CoV-2 B.1.617.2 isolate on day 49 and euthanized 3- and 6-days post-infection (dpi). ELISA determination of total B.1.617.2 **(B)** and BA.1 **(C)** spike-specific IgG in the sera of immunized hamsters on Day 21 and 42. The 50% neutralizing titer (NT50) of immunized hamster sera on days 21 and 42 was determined using **(D)** B.1.617.2 and **(E)** BA.1 pseudotyped-VSV. **(F)** The NT50 on day 42 was also determined using BA.5, BA.2.75, BF.7 and BQ.1.1 SARS-CoV-2 spike pseudotyped-VSV. Red indicates mutations acquired in the SARS-CoV-2 Spike protein. Data shown is mean ± SEM; n= 8 for pVAX1, n = 12 for pVAX1 S-CD40L$_{B.1.617.2}$ groups, *p < 0.05, **p < 0.01, ***p < 0.001, ****p < 0.0001.

3.3.2 LNP-encapsulation protects hamsters against homologous B.1.617.2 challenge

Three weeks after the second immunization, the Syrian hamsters were challenged intranasally with 1 x 10^5 PFU of a SARS-CoV-2 B.1.617.2. Although all groups experienced slight body weight loss on the first day post-challenge, only pVAX1 control group continuously lost weight over the course of the infection, reaching a mean weight loss of 9.9 ± 4.2% on day 6 post-challenge (Figure 3.2A). In contrast, all three pVAX1 S-CD40L$_{B.1.617.2}$ vaccinated groups began recovering from the initial weight loss, importantly however, hamsters vaccinated with 5- and 20-µg of the DNA-LNP consistently lost less body weight and recovered faster than those which received 100-µg of the naked DNA vaccine. These results reflect the viral burden in the lungs and nasal turbinates of these animals. As shown in Figure 3.2B, the vaccinated groups had significant less viral burden in lungs and nasal turbinates, with no virus being detectable by plaque assay in the DNA-LNP groups. In addition to quantification of live virus, we used RT-PCR to quantify viral envelope (E) subgenomic mRNA (sgmRNA) expression in the same tissues, which revealed a similar observation. All vaccines significantly reduced E sgmRNA levels in the lung tissue relative to the pVAX1 vector control at both 3- and 6-days post-infection (dpi) (Figure 3.2C). Additionally, vaccination with the DNA-LNP also significantly reduced E sgmRNA expression in the lungs relative to unformulated

pVAX1 S-CD40L$_{B.1.617.2}$ 3-dpi (Figure 3.2C). We also observed significant decreases in nasal turbinate E sgmRNA expression in vaccinated animals (Figure 3.2D). These data demonstrated that LNP-delivered DNA vaccines afford more effective protection than naked DNA administered at much higher dose.

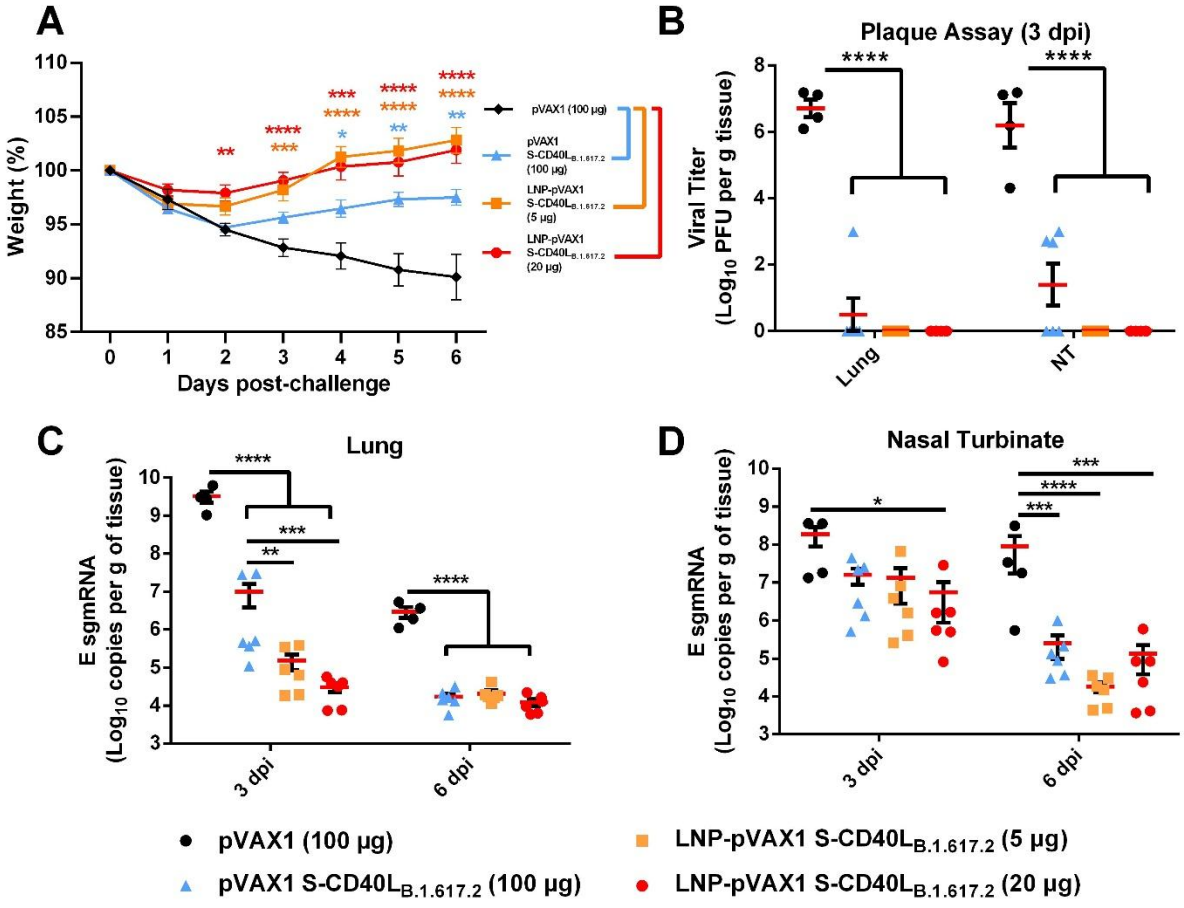

Figure 3.2 LNP-formulated DNA Vaccination greatly reduces Delta variant replication.

(A) Syrian hamster body weight was measured for 6-days following intranasal challenge with 1.67 $\times 10^5$ TCID50 of a SARS-CoV-2 B.1.617.2 isolate. **(B)** Plaque assays were used to determine the number of plaque forming units (PFU) in the lung and nasal turbinate tissue collected 3-dpi. The number of SARS-CoV-2 E sgmRNA copies in lung **(C)** and nasal turbinate **(D)** tissues was determined via RT-qPCR 3- and 6-dpi and normalized per gram of tissue. Data shown is mean ± SEM; n= 4 for pVAX1, n = 6 for pVAX1 S-CD40L$_{B.1.617.2}$ groups, *p < 0.05, **p < 0.01, ***p < 0.001, ****p < 0.0001.

3.3.3 LNP-encapsulation prevents lung pathology following homologous B.1.617.2 challenge

Next, lung samples collected from the challenged hamsters were analyzed for histopathological changes (Figure 3.3). At 3-dpi, hamsters immunized with the pVAX1 vector control or unencapsulated pVAX1 S-CD40L$_{B.1.617.2}$ vaccine developed acute bronchitis, bronchiolitis and interstitial pneumonia in their lungs. However, interstitial pneumonia in the area adjacent to the airways was generally milder in those immunized with unencapsulated pVAX1 S-CD40L$_{B.1.617.2}$ than those immunized with the pVAX1 control vector. In contrast, hamsters immunized with either dose of LNP-formulated pVAX1 S-CD40L$_{B.1.617.2}$, displayed no obvious airway or pulmonary inflammatory infiltrates or tissue damage. As anticipated, histopathological changes further progressed in the pVAX1 vector control group by 6-dpi, with the majority or entire lung tissues having become consolidated in most of the animals with very few aerated alveoli visible. At 6-dpi, the lungs of hamsters immunized with the LNP-formulated vaccines continued to display no overt histopathological changes while mild to moderate bronchopneumonia and interstitial pneumonia remained visible in some areas of lung tissues from hamsters vaccinated with unencapsulated pVAX1 S-CD40L$_{B.1.617.2}$.

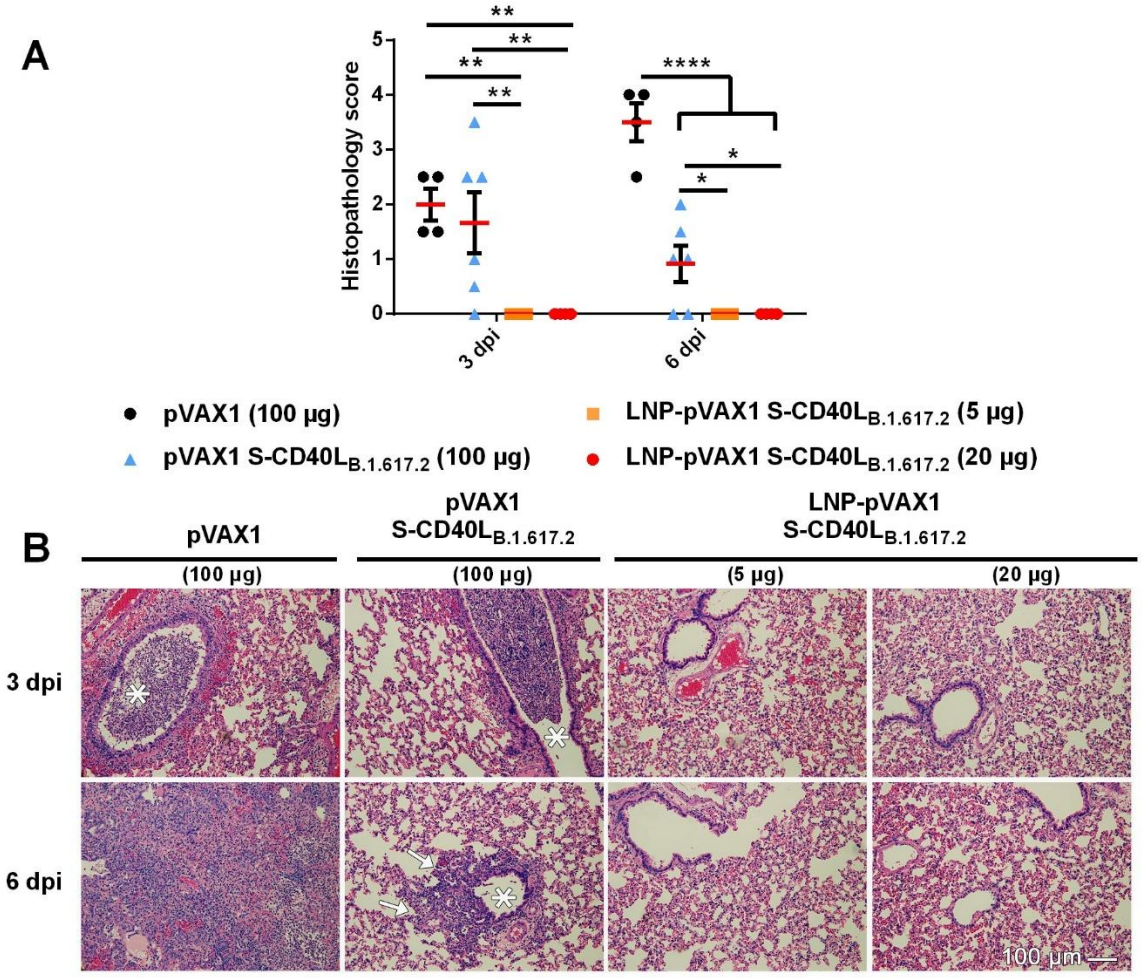

Figure 3.3 LNP-encapsulation prevents lung pathology following SARS-CoV-2 Delta variant challenge.

Histopathological changes in the lungs of hamsters immunized with different vaccine formulations and sacrificed at 3 and 6 days after being challenged intranasally with an isolate of SARS-CoV-2 B.1.617.2. **(A)** Summary of histopathological scores. Data shown is mean ± SEM; n= 4 for pVAX1, n = 6 for pVAX1 S-CD40L$_{B.1.617.2}$ groups, *p < 0.05, **p < 0.01, ****p < 0.0001. **(B)** Representative photomicrograph of H&E-stained lung tissue. * Bronchial lumen. Peribronchiolar infiltration (**arrows**). Scale Bar = 100-µm.

3.3.4 Vaccination resulted in reduced pulmonary expression of proinflammatory macromolecules

We next sought to characterize potential mechanisms underlying the prevention of lung pathology by conducting quantitative proteomic analysis of lung tissues 6-dpi, when the most severe histopathology was observed in control animals. In total, 3651 protein groups were identified and quantified. Principal component analysis (PCA) revealed a distinct separation between the protein expression profiles of the pVAX1 vector control vaccinated animals and the three pVAX1 S-CD40L$_{B.1.617.2}$ vaccinated groups (Figure 3.4A). The PCA showed no obvious overall proteome differences between the three vaccines, which was reflected by the absence of significantly differentially expressed protein (DEP) when comparing spike vaccinated groups with one another (Supplemental Table 3.3). In contrast, there were 164, 287, and 231 DEPs between the pVAX1 control group and the unencapsulated, 5-µg and 20-µg dose LNP pVAX1 S-CD40L$_{B.1.617.2}$ groups respectively (Figure 3.4B). There was considerable overlap in the three sets of DEPs (Supplemental Figure 3.2). Kyoto Encyclopedia of Genes and Genomes (KEGG) pathway analysis of these DEPs revealed an enrichment of pathways related to immune responses and viral infection for all three comparisons (Supplemental Figure 3.3 and Supplemental Table 3.4). The sets of DEPs from the LNP comparisons were additionally enriched with proteins related to other immune processes such as antigen processing, phagosomes, and cytosolic DNA-sensing. Ingenuity pathway analysis (IPA) revealed downregulation of various immune-related response pathways including interferon signaling, EIF2 signaling IL-12 signaling and macrophage responses in the pVAX1 S-CD40L$_{B.1.617.2}$ vaccinated animal lungs (Figure 3.4C and Supplemental Table 3.5). LNP-vaccinated lung tissues additionally had proteomic signatures linked to decreased macrophage

activity, including the inhibition of classical activation signaling, Fc-receptor mediated phagocytosis and Il-8 signaling.

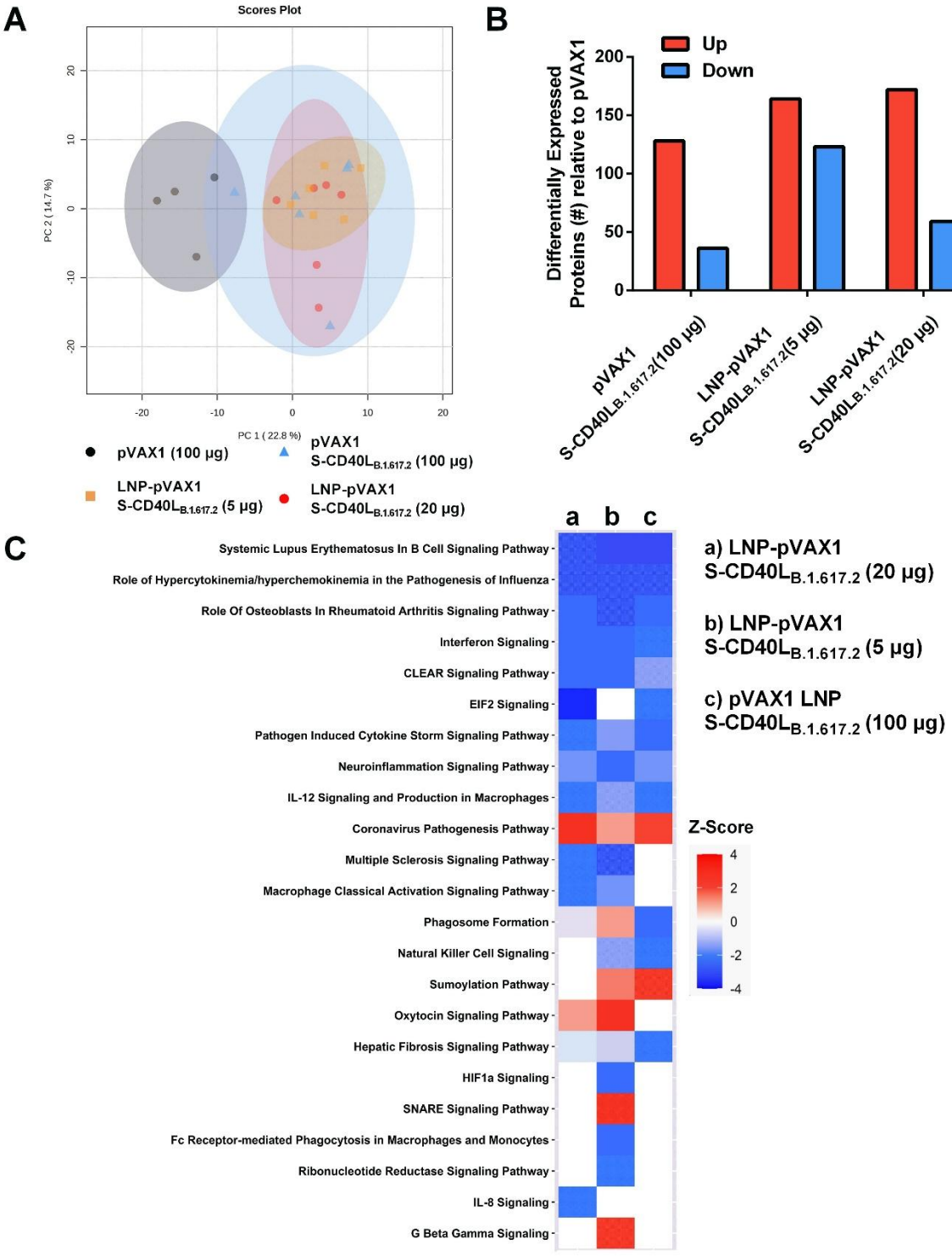

Figure 3.4 Quantitative-proteomic analysis of vaccinated hamster lung tissue post-challenge.

(A) PCA score plot of the four experimental groups. The pVAX1 vector control group demonstrates a distinct pattern relative to pVAX1 S-CD40L$_{B.1.617.2}$ vaccinated animals. **(B)** The number of differentially expressed proteins (DEPs) between the pVAX1 control and spike vaccinated groups determined by pairwise comparison. Red indicates proteins with increased expression in spike-vaccinated groups, while blue shows proteins with decreased expression. **(C)** Heatmap of the predicted activation or inhibition of canonical signaling pathways based on DEPs in the three comparisons. Color refers to the *Z*-score, where >2 indicates an activated pathway (red), while *Z*-score <−2 means the pathway is inhibited (Blue).

3.3.5 Characterization of DNA-LNP formulations *in vitro*

Having demonstrated the enhanced efficacy of DNA vaccination afforded by KC2-based LNPs, we next wanted to examine whether immunogenicity and protection would be altered when using LNPs formulated with SM-102, the ionizable lipid found in commercially approved Spikevax® COVID-19 mRNA vaccines (7,27). To this end, the potency of these two DNA-LNP formulations were first evaluated and compared *in vitro* using HEK293T cells. Across tested plasmids, KC2 and SM-102 DNA-LNPs formulations had similar size distributions and charge (Figure 3.5A). Relative to KC2, DNA LNPs formulated using SM-102 induced approximately a 10-fold increase in expression of both S-CD40L$_{B.1.617.2}$ (Figure 3.5B) and firefly luciferase (Fluc) (Figure 3.5C) 48h after transfection, mirroring previous observations (28). Using flow cytometry to measure the proportion of Green Fluorescent Protein positive (GFP+) HEK293T cells, SM-102 formulated DNA LNPs also showed a significantly greater transfection efficiency (Figure 3.5D). The intensity of GFP expression was also greater for SM-102 NDA-LNP transfected cells (Figure 3.5E).

A

Particle (50:10:38.5:1.5, mole %)	pVAX1	LNP Diameter (Mean ± SD , nm)	Zeta Potential (Mean ± SD, mV)	Encapsulation Efficiency (%)
KC2 (KC2:DOPC:Chol:DMG-PEG2000)	Parental	73.0 ± 15.5	-18.8 ± 4.5	97.9
	S-CD40L	86.1 ± 24.8	-15.9 ± 4.8	97.0
	Fluc	79.8 ± 27.2	-18.9 ± 2.1	96.0
	GFP	75.2 ± 16.2	-16.0 ± 2.6	97.2
SM-102 (SM-102:DSPC:Chol:DMG-PEG2000)	Parental	77.0 ± 17.3	-18.7 ± 3.7	89.5
	S-CD40L	83.5 ± 24.6	-14.8 ± 0.9	92.7
	Fluc	76.5 ± 15.8	-18.2 ± 1.9	93.4
	GFP	78.2 ± 16.2	-20.2 ± 2.8	96.4

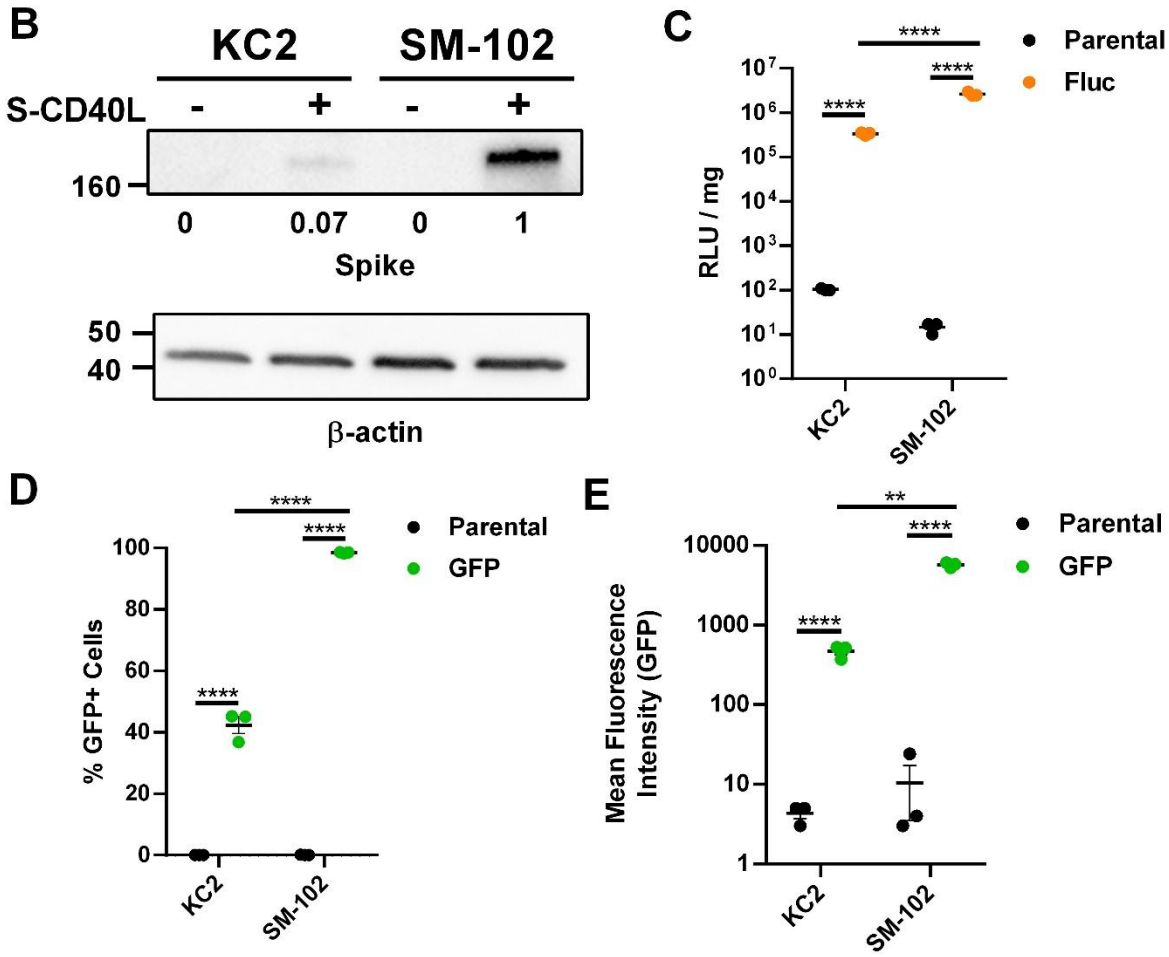

Figure 3.5 In vitro Characterization of DNA LNPs.

(A) Characterization of DNA-LNP formulations. Chol – Cholesterol. HEK293T cells were transfected in triplicate with 500 ng of each formulation. **(B)** Western blotting was done to detect SARS-CoV-2 spike expression in HEK293T cells 48h after transfection with pVAX1 S-CD40L or parental control. β-actin expression was used as a loading control and Spike expression was normalized to SM-102 pVAX1 S-CD40L. **(C)** Relative luminescence units (RLU) were measured 48h after transfection with pVAX1 Fluc or parental control. RLU was standardized per mg of protein as quantified by Bicinchoninic Acid (BCA) assay. Quantification of the **(D)** percentage of GFP+ HEK293T cells and **(E)** Mean fluorescence intensity (MFI) 48h after transfection with pVAX1 GFP or parental control. Data shown is mean ± SEM; n= 3, ****$p < 0.0001$.

3.3.6 LNP composition has minor effect on DNA vaccine immunogenicity

Syrian hamsters were vaccinated on Day 0 and 28 with 5-µg of either KC2 or SM-102 LNP-encapsulated pVAX1 S-CD40L$_{B.1.617.2}$ (Figure 3.6A). Control animals were again vaccinated with a higher dose of 100-ug of either unencapsulated pVAX1 S-CD40L$_{B.1.617.2}$ or parental pVAX1. Nanoparticle tracking analysis (NTA) showed that both DNA-LNP formulations had similar mean size distributions and encapsulation efficiencies (Supplemental Table 3.2). Compared with the naked DNA vaccine, both KC2 and SM-102 DNA-LNPs induced greater binding antibody responses against homologous B.1.617.2 (Figure 3.6B) and heterologous BA.5 (Figure 3.6C) S proteins. While the binding antibody responses induced by the two LNP formulations were quite similar, the SM-102 LNP-formulation generated higher levels of B.1.617.2 S-specific IgG on Day 21.In terms of neutralizing activity, both DNA-LNP vaccines induced a significant response against homologous B.1.617.2 (Figure 3.6D). Moreover, only the SM-102 DNA-LNPs induced a significant response relative to naked DNA (Figure 3.6D). Importantly, when assayed against heterologous BA.5, only the SM-102 formulation induced a significant NAb response despite the similar IgG levels (Figure 3.6E).

We next tested NAb responses at Day 42 against a panel of select SARS-CoV-2 variants (Figure 3.6F). Both DNA-LNP formulations induced robust NAb responses against the ancestral D614G

variant, comparable to their response against homologous B.1.617.2. However, only the SM-102 DNA-LNPs induced a significant response against both the Omicron BA.1 and BA.2.75 variants, while also inducing slightly higher, although not statistically significant, responses against BQ.1.1 and XBB.1.5.

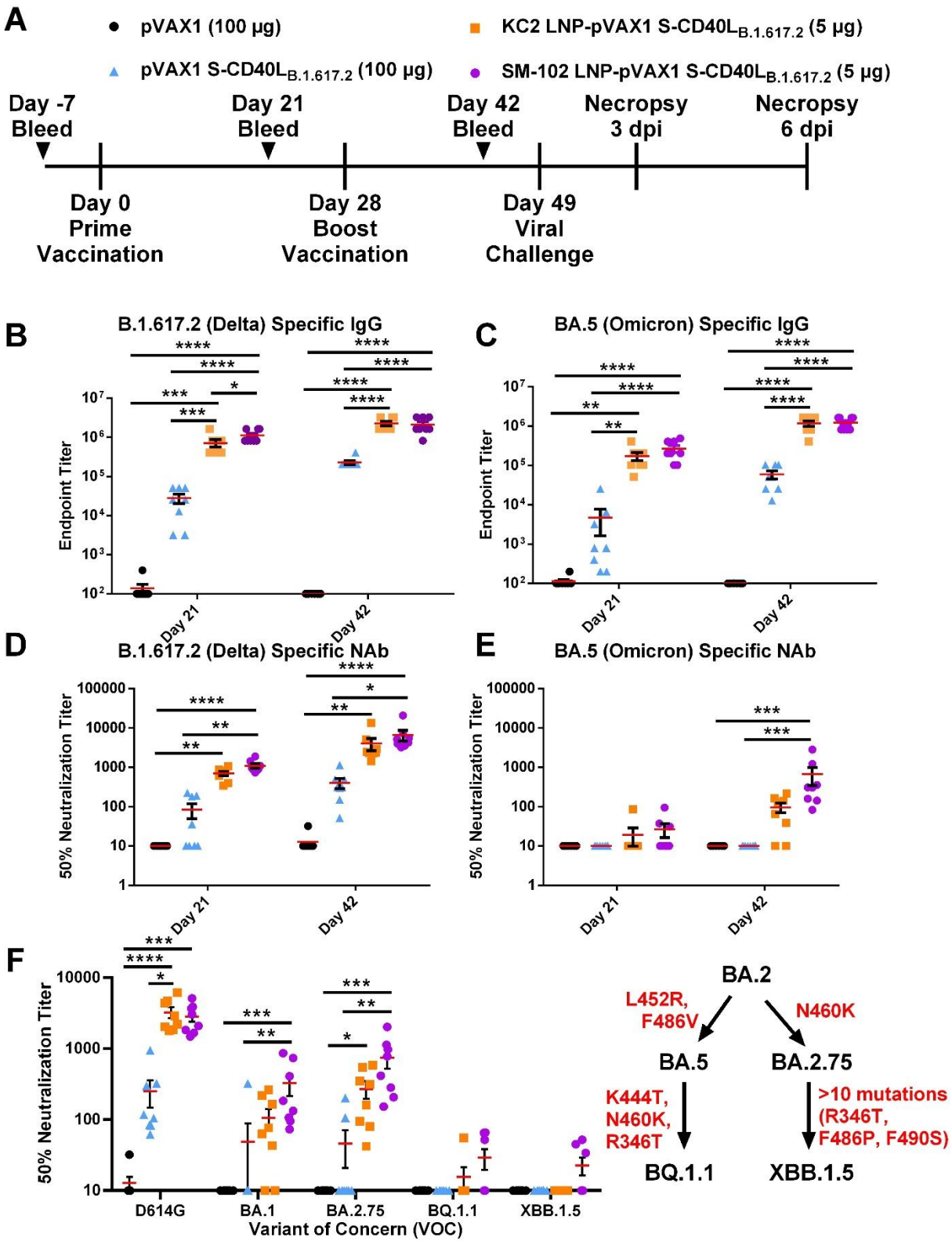
A
pVAX1 (100 µg)
KC2 LNP-pVAX1 S-CD40L B.1.617.2 (5 µg)
pVAX1 S-CD40L B.1.617.2 (100 µg)
SM-102 LNP-pVAX1 S-CD40L B.1.617.2 (5 µg)
Day -7 Bleed
Day 21 Bleed
Day 42 Bleed
Necropsy 3 dpi
Necropsy 6 dpi
Day 0 Prime Vaccination
Day 28 Boost Vaccination
Day 49 Viral Challenge
B
B.1.617.2 (Delta) Specific IgG
Endpoint Titer
Day 21
Day 42
C
BA.5 (Omicron) Specific IgG
Endpoint Titer
Day 21
Day 42
D
B.1.617.2 (Delta) Specific NAb
50% Neutralization Titer
Day 21
Day 42
E
BA.5 (Omicron) Specific NAb
50% Neutralization Titer
Day 21
Day 42
F
50% Neutralization Titer
D614G
BA.1
BA.2.75
BQ.1.1
XBB.1.5
Variant of Concern (VOC)
BA.2
L452R, F486V
N460K
BA.5
BA.2.75
K444T, N460K, R346T
>10 mutations (R346T, F486P, F490S)
BQ.1.1
XBB.1.5

Figure 3.6 DNA LNPs formulated with SM-102 induce superior humoral responses.

(A) Male Syrian hamsters were immunized intramuscularly on day 0 and 28 with either 100-µg of pVAX1, 100-µg of pVAX1 S-CD40L$_{B.1.617.2}$, or 5-µg of KC2 or SM-102 LNP-encapsulated pVAX1 S-CD40L$_{B.1.617.2}$. Animals were challenged intranasally with a SARS-CoV-2 BA.5 isolate on day 49 and euthanized 3- and 6-days post-infection (dpi). ELISA determination of the total B.1.617.2 **(B)** and BA.5 **(C)** spike-specific IgG in the sera of immunized hamsters 21- and 42-days post-vaccination. The 50% neutralizing titer (NT50) of immunized hamster sera on days 21 and 42 was determined using **(D)** B.1.617.2 and **(E)** BA.5 pseudotyped-VSV. **(F)** The NT50 on day 42 was also determined using D614G, BA.1, BA.2.75, BQ.1.1 and XBB.1.5 SARS-CoV-2 spike pseudotyped-VSV. Red indicates mutations acquired in the SARS-CoV-2 Spike protein. Data shown is mean ± SEM; n = 8, *p < 0.05, **p < 0.01, ***p < 0.001, ****p < 0.000

3.3.7 LNP-encapsulation enables DNA vaccine protection against heterologous Omicron challenge

Having characterized the humoral response induced by the two DNA-LNP formulations, we next determined the protection against heterologous Omicron challenge. Towards this, the vaccinated hamsters were challenged intranasally on Day 49 with the SARS-CoV-2 BA.5 variant. pVAX1 control vector vaccinated hamsters experienced mild weight loss, with a maximum mean weight reduction of 4.2% at 3-dpi (Figure 3.7A). Over the course of the infection, the naked DNA vaccine failed to prevent weight loss (Figure 3.7A). However, animals vaccinated with either the KC2 or SM-102 LNP-encapsulated vaccines began recovering weight at significant levels starting from 3-dpi. All three pVAX1 S-CD40L$_{B.1.617.2}$ vaccines significantly reduced viral burden in both the lung and nasal turbinates 3-dpi (Figure 3.7B), although to a greater extent with the LNP-encapsulated vaccines. Notably, both DNA-LNP formulations significantly reduced E sgmRNA expression in the lungs relative to unencapsulated pVAX1 S-CD40L$_{B.1.617.2}$ (Figure 3.7C). In the upper respiratory tract at 3-dpi, only the DNA-LNP vaccines significantly reduced E sgmRNA levels relative to the empty vector control (Figure 3.7D).

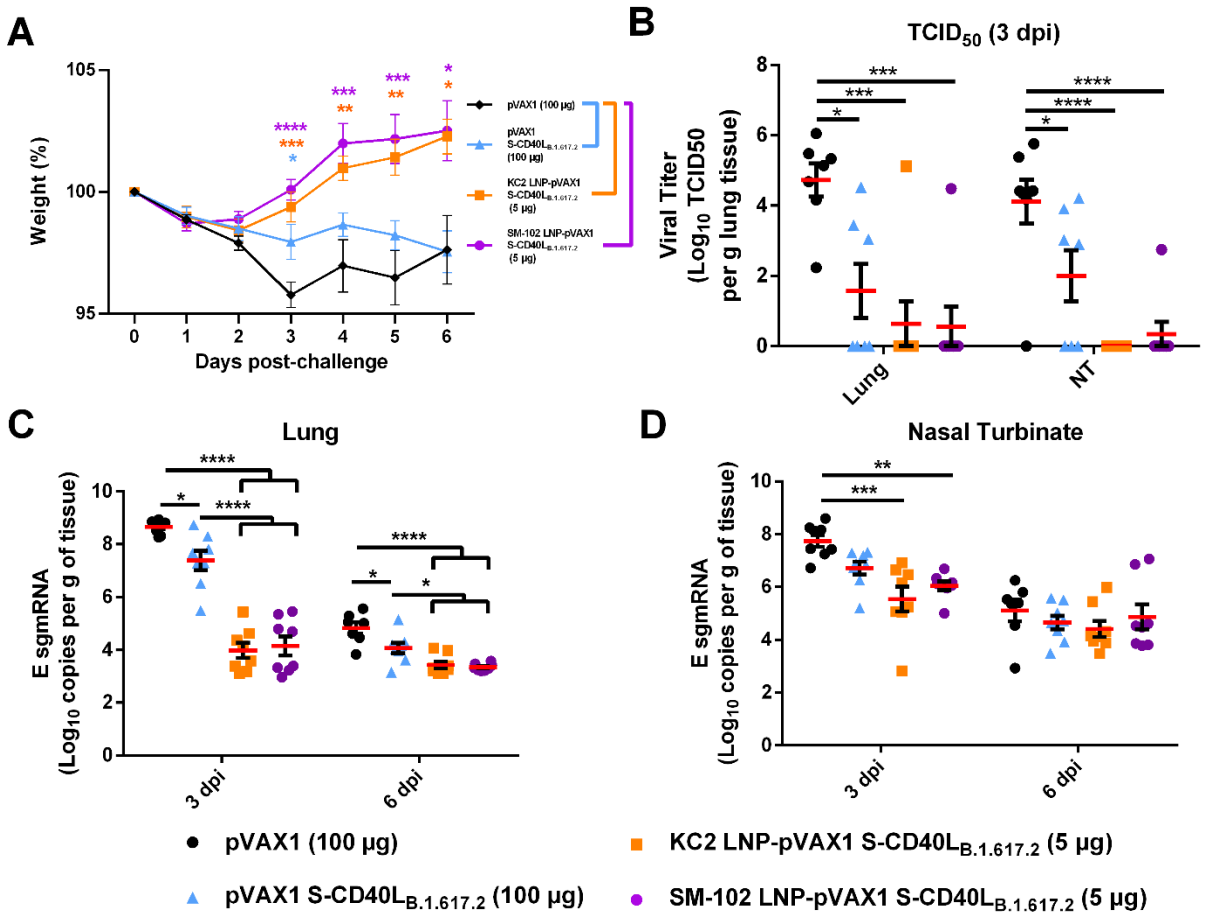

Figure 3.7 DNA LNP-encapsulation improves protection against the BA.5 Omicron variant.

Vaccinated Syrian hamsters were challenged intranasally with $1.67x10^5$ Median Tissue Culture Infectious Dose (TCID50) of a SARS-CoV-2 BA.5 isolate. **(A)** Syrian hamster body weight was measured for 6-days following challenge **B)** TCID50 was determined in the lung and nasal turbinate tissue collected 3-dpi. The number of SARS-CoV-2 E sgmRNA copies in lung **(C)** and nasal turbinate **(D)** tissues was determined via RT-qPCR 3- and 6-dpi and normalized per gram of tissue. Data shown is mean ± SEM; n = 8, *p < 0.05, **p 7< 0.01, ***p < 0.001, ****p < 0.0001.

Lastly, we again conducted histopathological of lung tissue sections collected 3- and 6-dpi (Figure 3.8).Consistent with the weight loss and viral burden, both DNA-LNP formulations reduced lung pathology relative to both the naked vaccine and control vector on both Day 3 and 6 (Figure 3.8A). Notably, the lowest histopathology scores were observed following SM-102 vaccination, with there being no overt inflammatory responses or tissue damage observable even at 3-dpi (Figure

3.8B). Collectively, these data indicate that both DNA-LNP formulations afford effective protection against heterologous challenge, with SM-2 formulation performing slightly better than KC2 as demonstrated by level of neutralizing antibodies against mismatched Omicron strains and protection from BA.5 challenge.

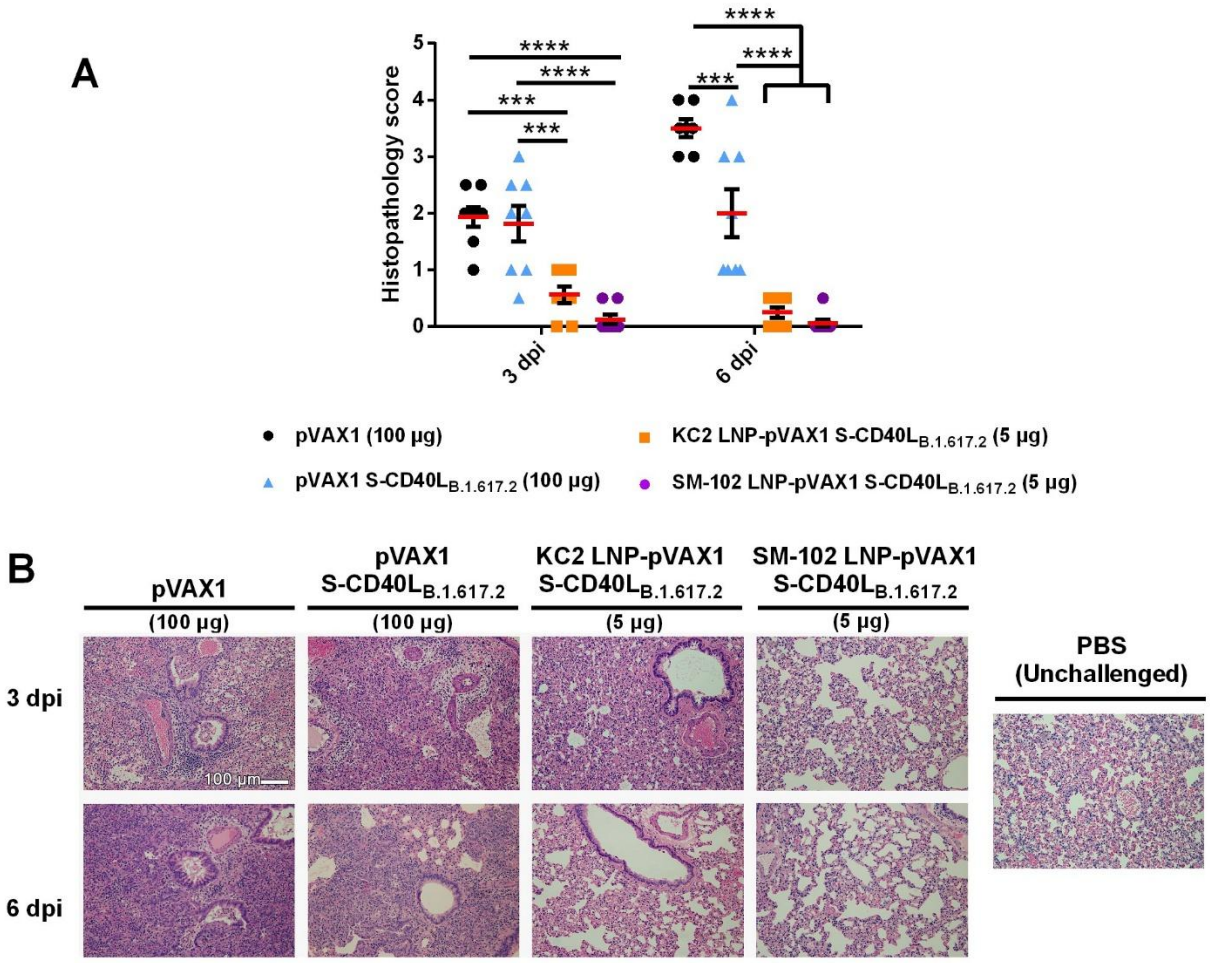

Figure 3.8 LNP-encapsulation greatly reduces lung pathology following Omicron BA.5 challenge.

Histopathological changes in the lungs of hamsters immunized with different vaccine formulations and sacrificed at 3 and 6 days after being challenged intranasally with a SARS-CoV-2 BA.5 isolate. **(A)** Summary of histopathological scores. Data shown is mean ± SEM; n = 8, *p < 0.05, **p < 0.01, ****p < 0.0001. **(B)** Representative photomicrograph of H&E-stained lung tissue. H&E. Scale bar = 100-µm.

3.4 Discussion

This current study centered on the LNP-mediated delivery of a DNA vaccine encoding SARS-CoV-2 Delta spike fused with the ectodomain of CD40L. Our approach differs from previous studies in several aspects. First, Delta spike was chosen as the vaccine antigen. While the B.1617.2 variant was one of the most virulent (29,30), it lacks most of the spike mutations found within the omicron lineage. As such, this vaccine would give us an opportunity to investigate the relationship between humoral responses and *in vivo* protection against significantly mismatched viral challenge. Secondly, we were able to directly compare the immunogenicity and efficacy two distinct LNP-formulations for DNA vaccine delivery, an approach that remains severely understudied relative to mRNA-LNP vaccination. Lastly, through the addition of CD40L, we were able to investigate the combination of a molecular adjuvant with LNP-mediated vaccine delivery, an avenue of exploration with boundless therapeutic potential for both DNA and mRNA vaccines.

The B.1.617.2 S protein does not contain many notable mutations such as K417N, N501Y, G446S, E484A, and G496S which contribute to the Omicron lineage's resistance to neutralizing antibodies (31–34). However, in our studies, encapsulation of the B.1.617.2 pDNA vaccine within KC2- or SM-102-based LNPs led to the induction of a significant NAb response against BA.1, BA.2, BA.2.75 and BA.5, albeit to a lower extent than against B.1.617.2. It is also of note that low but detectable NAb activities were observed against BF.7, BQ.1.1 and XBB.1.5, variants in which R346T, N640K, K444T and F486P, mutations are likely to further enhance neutralization resistance (35,36). These findings are largely in agreement with previous reports with respect to cross-neutralizing activities of human antisera (36,37).

To compare the two different LNP formations, we chose to assess the level of protection afforded by our B.1.617.2-based vaccine against challenge with the Omicron BA.5 variant, to which considerable but reduced NAb activities, relative to homologous B.1.617.2, were induced by both the KC-2 and SM-102 DNA-LNPs. Despite the reduced NAb response, immunization with either of the two DNA-LNP formulations led to excellent control of the heterologous BA.5 infection, comparable to that following homologous B.1.617.2 challenge, suggesting the reduced level of NAb induced by the DNA-LNP vaccines may have remained sufficient to neutralize viruses *in vivo*. Nonetheless, the future use of variants such as XBB.1.5 as a challenge strain, to which the B.1.617.2 vaccines failed to elicit a significant NAb responses, could further delineate the functional roles of neutralizing vs. non-neutralizing antibodies, along with the importance of cell-mediated immune responses.

Immune escape by emerging variants has and will likely continue to be a recurring problem for SARS-CoV-2 vaccines (38,39). Research continues to develop methods of inducing broadly neutralizing and variant-proof immune responses (40). One factor affecting the breadth of humoral immunity following vaccination is germinal center (GC) formation and subsequent B cell somatic hypermutation (41–43). While previous studies have shown CD40-targeting vaccine adjuvants to increase T follicular helper cell counts and promotes GC formation (44,45), our unencapsulated CD40L-adjuvanted pDNA vaccine was unable to overcome the hurdle of neutralizing heterologous Omicron variants. It has been shown in recent studies that SARS-CoV-2 mRNA-LNP vaccines drive strong GC responses in lymph nodes following vaccination (17,46,47). The enhanced breadth of neutralization observed in our LNP-formulated pDNA vaccines could potentially be attributed to enhanced vaccine immunogenicity, subsequently driving superior GC formation and a broader humoral response.

Finally, our proteomic analysis of lung tissues collected 6-dpi demonstrated a general decrease in innate immune and infection related response pathways in pVAX1 S-CD40L$_{B.1.617.2}$ vaccinated groups relative to the pVAX1 control vaccinated animals (Figure 3.5). Although the three vaccinated groups had similar proteomic profiles, DNA-LNP-vaccinated groups had additional DEP signatures linked to the inhibition of macrophage responses. Other transcriptomics and proteomics studies have correlated upregulated monocyte, macrophage and neutrophil signatures with disease severity during SARS-CoV-2 infection (48–52). Stronger vaccine-induced adaptive immune responses should provide better protect during the early stages of viral infection, reducing the subsequent induction of innate immune responses. Clearly, effective vaccination can attenuate the upregulation of these innate immune and inflammatory response pathways following SARS-CoV-2 infection (52–54). Altogether, these findings support the histopathological absence of pulmonary inflammatory infiltrates observed in DNA LNP-vaccinated lung tissues upon B.1.617.2 challenge.

Research demonstrating the potential therapeutic benefits of encapsulating pDNA vaccines within ionizable lipid nanoparticles is beginning to accumulate (13,55–57). During the preparation of this manuscript, Liao & Shen et al reported results of a DNA-LNP vaccine encoding ancestral or BA.1 spike which mirror our own (58). Interestingly, they also found that DNA-LNPs provided superior antibody responses and protection than mRNA-LNPs. Their results appears to be at odds with our recently published study comparing mRNA- and DNA-LNPs, where we reported that mRNA-LNPs induce superior antigen-expression and antibody responses (28). While this discrepancy remains to be understood, antigen selection, construct design, and nanoparticle fabrication could be among other unknown contributing factors. These questions, along with the rates of possible ribosomal skipping in DNA vaccines, await further investigation.

3.5 Materials and Methods

3.5.1 Cell lines and viruses

HEK293T, HEK293T-ACE2 and HEK-Blue™ CD40L cells were cultured in Dulbecco's Modified Eagle Medium (DMEM, ThermoFisher) supplemented with 25 mM HEPES, 20 U/mL Penicillin, 0.02 mg/mL Streptomycin and 10% heat-inactivated fetal-bovine serum (FBS). HEK-Blue™ CD40L media was additionally supplemented with 100-µg/mL of Normocin. Vero-TMPRSS2 cells were cultured in DMEM with L-glutamine supplemented with 1X non-essential amino acid, 1 mM sodium pyruvate and 5% FBS. SARS-CoV-2 viruses were obtained from BEI Resources. B.1.617.2 hCoV-19/USA/MD-HP05647/2021 (NR-55672) and BA.5 hCoV-19/South Africa/CERI-KRISP-K040013/2022 (NR-56798) were propagated and titered using Vero-TMPRSS2 cells and sequenced to confirm genetic fidelity. Passage four virus stocks were used in all subsequent experiments that required live virus.

3.5.2 Immunization

Animal experiments and procedures were approved by the National Research Council Canada (NRC) Human Health Therapeutics Animal Care Committee and performed by trained staff in accordance with regulations and guidelines set by the Canadian Council on Animal Care. All infectious work was carried out under ABSL-3 conditions at the NRC. 6–8-week-old male Syrian hamsters were purchased from Charles River Laboratories (Senneville, QC). Animals were randomly allocated into four experimental groups, being immunized with either 100-µg of pVAX1, 100-µg of pVAX1 S-CD40L$_{B.1.617.2}$, and 5- or 20-µg of LNP-formulated pVAX1 S-CD40L$_{B.1.617.2}$. Vaccines were suspended in 100-µL of PBS and administered intramuscularly in the hamster's left tibialis anterior muscle with a needle syringe on day 0 and day 28. Serum was collected on days

21 and 42 post-vaccination. On day 49 post-vaccination the hamsters were intranasally challenged with 1.67 $\times 10^5$ TCID50 of B.1.617.2 or BA.5. Challenge doses were found to induce significant illness in earlier dose-optimization experiments (data not shown). Animals were euthanized by CO2 either 3- or 6-days post-challenge, after which the nasal turbinate and lung tissues were collected for downstream experiments.

3.5.3 DNA Vaccine design and synthesis

The DNA vaccine was designed and prepared as previously described with minor modifications (22). A DNA sequence encoding the SARS-CoV-2 B.1.617.2 spike ectodomain (T19R, G142D, E156G, Del 157/158, L452R, T478K, D614G, P681R, D950N) fused via "GSGG" glycine-serine linkers to a T4 fibritin foldon trimerization motif and the ectodomain of *Mesocricetus auratus* CD40L (GenBank accession #XM_005084522.4, residues 118-260) was commercially synthesized (Genscript). The spike sequence was mutated to contain a "GSAS" substitution at the furin cleavage site (residues 682-685) and pre-fusion stabilizing proline substitutions at residues 986 and 987 (59). The vaccine was codon optimized for expression in Syrian hamsters and subcloned into the mammalian expression plasmid pVAX1 (ThermoFisher) using *KpnI* and *XhoI* restriction enzymes. Bulk DNA vaccine preparations were prepared with plasmid gigaprep kits (Qiagen) and sequence validated with Sanger sequencing.

3.5.4 Lipid nanoparticle (LNP) generation

LNPs were synthesized as previously described within three days of vaccination and stored at 4°C.[26,67] Briefly, pDNA-LNPs were prepared via the microfluidic mixing of an aqueous and organic phase. The aqueous phase was prepared by suspending pDNA in 25 mM acetate buffer (pH 4.0). The organic phase was prepared in ethanol and consisted of 2,2-dilinoleyl-4-dimethylaminoethyl-[1,3]-dioxolane (DLin-KC2-DMA, MedKoo Biosciences) or heptadecan-9-

yl-8-((2-hydroxyethyl)(6-oxo-6-(undecyloxy)hexyl)amino)octanoate (SM-102, MedKoo Biosciences), 1,2-distearoyl-sn-glycero-3-phosphocholine (DSPC, Avanti Polar Lipids) or 1,2-dioleoyl-sn-glycero-3-phosphocholine (DOPC, Avanti Polar Lipids), ovine cholesterol (Avanti Polar Lipids), and 1,2-dimyristoyl-rac-glycero-3-methoxypolyethylene glycol-2000 (DMG-PEG2000, Avanti Polar Lipids) at a ratio of 50:10:38.5:1.5 mole %, respectively. The two phases were mixed with a polymer amine (N = nitrogen) group to nucleic acid phosphate (P) group (N/P) ratio of 6:1 using either a NanoAssemblr BT™ instrument (Precision Nanosystems, Vancouver, BC) with a microfluidics cartridge containing a staggered herringbone mixing unit or a NanoAssemblr™ Ignite™ instrument with NxGen™ cartridges equipped with toroidal structures. LNPs were dialyzed against a 1000-fold volume of phosphate-buffered saline (PBS) (pH 7.4) for 18 hours at 4°C in a 10k MWCO cassette (ThermoFisher), passed through a 0.22-µm filter and then concentrated using an Amicon Ultra 4 10k MWCO centrifugal concentrator (Millipore Sigma). After concentration the nanoparticle size was measured via nanoparticle tracking analysis (NTA) under static conditions (NanoSight,Malvern Panalytical, Westborough, MA, USA). Five separate tracking videos (1 minute each) were taken consecutively and merged together to generate the NTA sizing data. Zeta potential was measured in 5mM phosphate buffer (pH 7.4) using disposable capillary cells on a Zetasizer Ultra instrument (Malvern Panalytical, Westborough, MA, USA). pDNA LNPs were stored at 4°C and administered within 48 hours.

3.5.5 LNP encapsulation efficiency

Nucleic acid encapsulation efficiency and vaccine dose was determined as previously described.[67] Briefly, LNPs were either untreated or disrupted with 1% Triton X-100 (Millipore Sigma) in a 96-well plate before the addition of SYBR™ Gold dye (ThermoFisher). Fluorescence (Ex/Em: 495/537 nm) was measured in each sample using a Synergy MX plate reader (BioTek). Total pDNA

concentration in each sample was determined by comparing the fluorescence relative to that of a standard curve of pDNA prepared in the same buffer. Untreated and disrupted samples were used to determine unencapsulated and total pDNA respectively. The amount of encapsulated pDNA, calculated by subtracting the amount of unencapsulated pDNA from the total amount, was used for dose calculations. Lastly, the encapsulation efficiency was determined from the amount of encapsulated pDNA relative to the total amount (Supplemental Table 3.1 & 3.2).

3.5.6 In vitro transfection

In a 24-well plate, HEK293T cells were transfected in triplicate with 500 ng of DNA-LNPs, suspended in phosphate-buffered saline (PBS) (ThermoFisher). The DNA-transfected cells were then incubated at 37 °C, 5% CO_2 for 48h prior to quantification of S-CD40L, firefly luciferase (Fluc) or Green Fluorescent Protein expression (GFP).

3.5.7 Western blotting

For determination of S-CD40L expression, transfected cells were washed with PBS and then lysed with radioimmunoprecipitation assay buffer (ThermoFisher). Lysates were electrophoresed on a 4-15% TGX stain-free SDS-PAGE gel (Bio-Rad) and then transferred to a polyvinylidene difluoride membrane. Membranes were blocked for 1 hour at room temperature with tris-buffered saline (TBS) containing 0.5% Tween 20 (Sigma-Aldrich) (V/V) (TBS-T) and 5% (W/V) non-fat milk powder then incubated overnight at 4°C in blocking buffer containing either polyclonal rabbit anti-SARS-CoV-2 Spike antibody (1:3000 dilution) (40591-T62, Sino Biological) or polyclonal rabbit anti-β-actin antibody (1:1000 dilution) (#4967, Cell Signaling Technology). Membranes were then incubated for 1 hour at room temperature with goat anti-rabbit horseradish peroxidase (HRP)-conjugated secondary antibody (1:75, 000 dilution) (ThermoFisher) in blocking buffer and

developed using SuperSignal™ West Femto Maximum Sensitivity Substrate (ThermoFisher) and a ChemiDoc MP imaging system (Bio-Rad) (Supplemental Figure 3.4 & 3.5).

3.5.8 Quantification of luciferase

Luciferase expression in cells transfected with pVAX1 Fluc DNA-LNPs was quantified as previously described (28). Briefly, media was aspirated and replaced with 200 µL of passive lysis buffer (Promega). Cells were then incubated for 30 min at room temperature on an orbital shaker at 50 rpm. Lysates were clarified via centrifugation at 15,000× *g* for 5 min at room temperature and then added in triplicate, 100 µL per well, to a white Costar 96-well plate (Corning) followed by 100 µL of room temperature Bright-Glo Reagent (Promega). Luminescence was read within 5 min and expressed as relative luminescence units/mg of protein (RLU/mg) after being normalized to total protein content as measured by a Bicinchoninic Acid (BCA) Kit (Millipore Sigma).

3.5.9 Flow cytometric analysis of GFP positive cells

HEK293T cells transfected with pVAX1 GFP DNA-LNPs were analyzed by flow cytometry (BD FACSymphony A1). Briefly, cells were lifted with PBS supplemented with 0.5 mM EDTA (ThermoFisher) for 10 minutes at 37°C. Data was acquired using the FACS DIVA software (version 9.0.2). GFP signal was measured off the 488nm blue laser, using 505 nm long-pass and 530/30 nm band-pass filters. GFP signal was used to analyze the % GFP+ HEK293T cells and measure mean fluorescence intensity (MFI) (Supplemental Figure 3.6).

3.5.10 CD40 ligand bioactivity assay

CD40L activity was assessed as previously described (22). Briefly, HEK293T cells were transfected in a 24-well plate with 1-µg of pVAX1 or pVAX1 S-CD40L$_{B.1.617.2}$ using lipofectamine 3000 (ThermoFisher). After a 24-hour incubation at 37°C and 5% CO2, 100-µL of 0.45-µm filtered

supernatant was added to a 96-well plate and mixed with 100-µL of HEK-Blue CD40L cells (InvivoGen) resuspended at 2.0×10^5 cells/mL. After 24 hours 20-µL of cell culture supernatant was mixed with 180-µL of QUANTI-Blue™ Reagent (InvivoGen) in a 96-well plate. The absorbance at 630 nm was measured after a 30-minute incubation at 37°C using a Synergy™ 2 microplate reader (BioTek).

3.5.11 ELISA

Spike protein ectodomains were obtained from the National Research Council of Canada for the following strains: B.1.617.2 (PRO7604-10 [SmT1v3 (B.1.617.2]), BA.1 (PRO7911-2 [SmT1v3-B.1.1.529]), BA.5 (PRO8213 [SmT1v3 (BA.5)]), which were produced using previously described methods (60,61). ELISAs were conducted as described previously (22). Briefly, Nunc MaxiSorp™ flat-bottom 96-well plates (ThermoFisher) were coated with 1-µg/mL of antigen diluted in PBS and incubated overnight at 4°C. Plates were washed with PBS containing 0.1% Tween-20 (PBS-T) before blocking with 3% (w/v) Bovine Serum Albumin (IgG-Free, Protease-Free) (Jackson Immuno Research) in PBS-T for 2 hours at 37°C. Plates were washed again and two-fold serial dilutions of hamster serum were prepared. After a 1-hour incubation at 37°C the plates were washed again and Peroxidase AffiniPure Goat Anti-Syrian Hamster IgG (H+L) (Jackson Immuno Research) was added to each well at 1:4000 and incubated at 37°C for 1 hour. After a final wash, 100-µL of Tetramethylbenzidine (TMB) substrate (Cell Signaling Technology) was added to each well. After a two-minute incubation at room temperature, 100-µL of 0.16 M sulfuric acid was added to terminate the reaction and absorbance was measured at 450 nm. Endpoint titers were expressed as the reciprocals of the final detectable dilution with an optical density above the cut-off value, which was defined as the average OD of the empty vector samples plus three standard deviations.

3.5.12 Pseudovirus production and neutralization

The neutralizing activity of hamster sera was determined by using a VSV-based SARS-CoV-2 S pseudovirus reporter assay as described previously (22,62). Briefly, pseudotyped VSV was generated by concurrently infecting HEK293T cells with G*ΔG-VSV (Kerafast) and transfecting them with pLV vectors encoding SARS-CoV-2 S Δ19. Vectors encoding D614G, B.1.617.2, BA.1 and BA.5 spike were purchased commercially (Invivogen) while vectors encoding BA.2.75, BF.7, BQ.1.1 and XBB.1.5 were synthesized commercially (GenScript, Brockville, ON). Supernatant containing the pseudovirus was collected 48- and 72-hours post-infection and passed through a 0.45-µm filter. In a 96-well plate, serum samples heat-inactivated at 56°C for 30 mins were serially diluted threefold and mixed with 1.3×10^4 TCID50 of pseudovirus. After a 1-hour incubation at 37°C, 5% CO2, 2×10^4 HEK293T-ACE2 cells were added to each well. After a 24-hour incubation at 37°C, 5% CO, luminescence was measured using Bright-Glo luciferase reagent (Promega) and a Synergy™ 2 microplate reader (BioTek) The 50% neutralization titers (NT50) were measured as the reciprocal of the sample dilution at which a 50% reduction in relative light units (RLU) was observed relative to the average of the no-serum control wells.

3.5.13 Quantification of viral burden

Lung and nasal turbinate tissues were homogenized in PBS using a Precellys® Evolution. Spin-clarified supernatants of the homogenates were then used for viral quantification. B.1.617.2 viral burden was determined by plaque assay as previously described (22). Briefly, a 1:10 serial dilution of clarified supernatant was prepared in infection media (DMEM supplemented with 1X non-essential amino acid, 20 U/mL Penicillin, 0.02 mg/mL Streptomycin, 1 mM sodium pyruvate, and 0.1% bovine serum albumin). Virus was adsorbed on Vero E6 cells at 37°C 5% CO2 for 1 hour before the inoculum was replaced with overlay media (1X infection media with 0.6% ultrapure,

low-melting point agarose). Cells were incubated at 37°C 5% CO2 for 72 hours, then fixed with 10% formaldehyde and stained with crystal violet. Plaques were enumerated and PFU was determined per g of tissue. BA.5 viral burden was determined by TCID50 assay on Vero-TMPRSS2 cells. Spin-clarified supernatants were serially diluted 1:10 in infection media (DMEM supplemented 1X non-essential amino acid, 1 mM sodium pyruvate and 1% FBS). Dilutions were adsorbed on Vero-TMPRSS2 cells seeded in 96-well plates for 1 hour at 37°C 5% CO2. After adsorption, inoculum was removed and 100 ml of infection media was added to each well and incubated at 37°C 5% CO2 for 5 days. Observed cytopathic effect indicates presence of infectious virus was recorded and TCID50/g of lung tissue was calculated using the Reed-Muench method (63).

3.5.14 RNA extraction and quantitative real-time-PCR (qRT-PCR)

Quantification of SARS-CoV-2 E subgenomic mRNA (sgmRNA) was completed as described previously (22). Briefly, lung and nasal turbinate tissues were placed into RNA shield buffer (Zymo Research) and incubated overnight at 4°C before freezing at -80°C. Viral RNA was extracted from the mechanically homogenized samples using a Quick-RNA Viral Kit (Zymo Research). Viral RNA expression was quantified using a one-step Fast Virus master mix (ThermoFisher) and E sgmRNA-specific primer/probe set (64). sgmRNA copy numbers were calculated by comparing sample Ct values to a standard curve of *in vitro* transcribed E sgmRNA prepared using a TranscriptAid T7 High Yield Transcription Kit (ThermoFisher) and normalized by tissue weight. All RT-qPCR reactions were conducted in MicroAmp Fast Optical 96-wells with an Applied Biosystems™ 7500 Fast Real-time PCR instrument.

3.5.15 Histopathology

Histopathology analysis was conducted as described previously (22). Briefly, right lung lobes were fixed for 72 hours in 10% neutral buffered formalin and processed by standard paraffin embedding methods (65). 4-µm thick sections were stained with hematoxylin-eosin (HE) and examined under microscopy. The severity and extent of pneumonia was scored blinded based on previously established criteria (66).

3.5.16 Mass spectrometry sample preparation and LC-MS/MS acquisition

Lung tissue was mechanically homogenized in 4% SDS supplemented with Halt™ Protease Inhibitor Cocktail (ThermoFisher) to inactivate SARS-CoV-2 virus and extract proteins. Extracted proteins were then purified using acetone precipitation, reduced using Pierce Premium-Grade TCEP HCl (ThermoFisher), and alkylated using Iodoacetamide (Sigma-Aldrich). Proteins were digested with trypsin and labeled with isobaric tags (TMT 11plex, ThermoFisher) using a dry TMT based labeling approach as described previously (67). Briefly, samples were randomly assigned to tags that were pre-aliquoted dried in 12-tube strips. A pooled sample was included in each strip for normalization between strips. After quenching the labeled peptides from each strip were combined and fractionated (Pierce High pH Reverse-Phase Peptide Fractionation Kit, ThermoFisher) into 8 fractions. Collected peptide samples were analyzed with an Orbitrap Fusion Lumos Tribrid Mass Spectrometer coupled to an Easy-nLC 1200 (ThermoFisher). For each sample 2-µl (corresponding to approximately 500 ng of peptide) were analyzed by loading onto a NanoViper Acclaim pepmap 100 trap column (75-µm 20 mm with 3-µm beads) and desalting with 0.1% formic acid in water (solvent A) before separating on a Easyspray pepmap C18 reverse-phase analytical column (50-µm 150 mm with 2-µm beads). Chromatographic separation was achieved at a flow rate of 0.300-µl/min over 100 min in five linear steps as follows (solvent B was 0.1% formic acid in 80%

acetonitrile): initial, 2% B; 80 min, 25% B; 90 min, 40% B; 95 min, 95% B; 100 min, 95% B. The eluting peptides were analyzed in data-dependent mode MSMS. An MS survey scan of 400−1600 m/z was performed in the Orbitrap at a resolution of 120000, 50ms maximum injection time and an AGC target of 4 x105. The top speed mode was used to select ions for MS2 analysis with dynamic exclusion 20 s with a ± 10 ppm window. During the MS2 analyses, precursors were isolated using a width of 0.7 m/z and fragmented by HCD at 42% collision energy, AGC target 1.25 $x10^5$ followed by Orbitrap analysis at 50000 resolutions.

3.5.17 Bioinformatics and statistical analysis pathway analysis

Raw MS data were subjected to protein identification and quantification using MaxQuant 1.6.3.3 against a *Mesocricetus auratus* (Golden Hamster) database that was downloaded from UniprotKB (https://www.uniprot.org/, downloaded 2021-08-31, 89281 entries). MaxQuant search was performed with reporter ion MS2 (TMT11) mode with the following parameters: fixed modification was set as Carbamidomethyl cysteine, variable modifications set as Oxidized methionine, protein N-term acetylation; enzyme was set as trypsin/P with maximum missing cleavage site of 2; minimal peptide length of 7 and a FDR (false discovery rates) of peptide-spectrum match (PSM) of 0.01. Isotopic impurities of each TMT channel were obtained according to the reagent lot and was used during database search to correct the purities of TMT channels for each set of TMT labeling data. MaxQuant output was then summarized and normalized using MSstatsTMT (68), using the open-source R software available on Bioconductor. Proteins in all groups were compared pairwise using a pairwise t-test. Proteins with an absolute fold change >1.5 and an adjusted p-value <0.05 were defined as differentially expressed proteins (DEPs). Principal Component Analysis (PCA) was performed with Metaboanalyst (https://www.metaboanalyst.ca/) using K-Nearest Neighbors Algorithm to estimate missing values and all other parameters set to

default. The Kyoto Encyclopedia of Genes and Genomes (KEGG) pathway enrichment analyses were performed on the DAVID Bioinformatics database (https://david.ncifcrf.gov/) with all parameter settings at their default values. DEPs were imported into Ingenuity Pathway Analysis (QIAGEN) and used to predict the activation or inhibition of canonical pathways. An enrichment score of 1.3 was considered significant. The overall predicted activation state of the biological attributes was assigned a z-score (<0: inhibition, >0: activation) and those that gave a z-score >2 or <-2 were considered significant. The results of the KEGG and IPA analysis were plotted as heat maps using RStudio.

3.5.18 Quantification and statistical analysis

Statistical analyses were performed using GraphPad Prism 9. An unpaired two-tailed t-test was used for comparisons of CD40L bioactivity. If possible, before pairwise comparison normality of the data was assessed by a Shapiro-Wilk test (alpha-level=0.05). Whenever data or their log transformations were deemed not of normal distribution, a non-parametric approach was adopted. A non-parametric Kruskal-Wallis H test with Dunn's test for multiple comparisons was applied for pairwise (between-group) comparisons of spike-specific IgG endpoint titers, neutralizing antibody titers, and plaque assay viral burden. A one-way analysis of variance (ANOVA) with Bonferroni's adjustment was applied for pairwise (between-group) comparisons of weight loss data by day, log subgenomic mRNA expression, RLU/mg, % GFP+ cells, GFP MFI and lung histopathology. The significance level and n number for each test is indicated in the Figure legends.

3.6 Data availability

All proteomics data along with the database search results were deposited to the ProteomeXchange Consortium (http://www.proteomexchange.org) via the PRIDE partner repository with the identifier PXD049053. All additional data needed to evaluate the conclusions in the paper are present in the main text and Supplementary Materials or available from the corresponding author upon request.

3.7 Author Contributions

Conceptualization, L.T., A.T., A.M.H., D.S., J.C., L.W., S.S., M.R.-M., M.J.W.J., and X.L.; Methodology, L.T., A.T., C.L., E.E.F.F., M.C., A.S., M.S., X.Z.; Formal Analysis and Data Curation, L.T., E.E.F.F., M.C., A.S., X.Z., and J.B.; Investigation, L.T., D.D., A.T., C.L., G.F, J.W., M.C., S.R., E.L., W.Z., A.P., C.G., W.C., and M.S.; Writing – Original Draft, L.T., W.C., and X.L.; Writing - Review & Editing, L.T., A.T., C.L., G.F., S.R., W.Z., A.P., C.G., A.M.H., L.W., S.S., M.R.-M., M.J.W.J., J.B., and X.L.; Resources, A.T., C.L., C.G., M.C., and Y.D. Funding Acquisition, Project administration and Supervision, A.T., Y.D., D.S., J.C., L.W., S.S., M.R.-M., M.J.W.J., and X.L.

3.8 Declaration of interests

The authors declare no competing interests.

3.9 Acknowledgement

We gratefully acknowledge the Histology and Staining services provided by the Louise Pelletier HCF at the University of Ottawa. We gratefully acknowledge the technical contribution of many members of the Mammalian Cell expression Section of the NRC-HHT for spike antigens production. We also gratefully acknowledge Dr. Lu Huixin and Dr. Roger Tam for commenting on the manuscript and Greg Harris for preparing the photomicrographs. This work is supported by the Government of Canada (Intramural funding from Health Canada) and in part by the Pandemic Response Challenge Program of the National Research Council Canada.

3.10 Supplementary Material

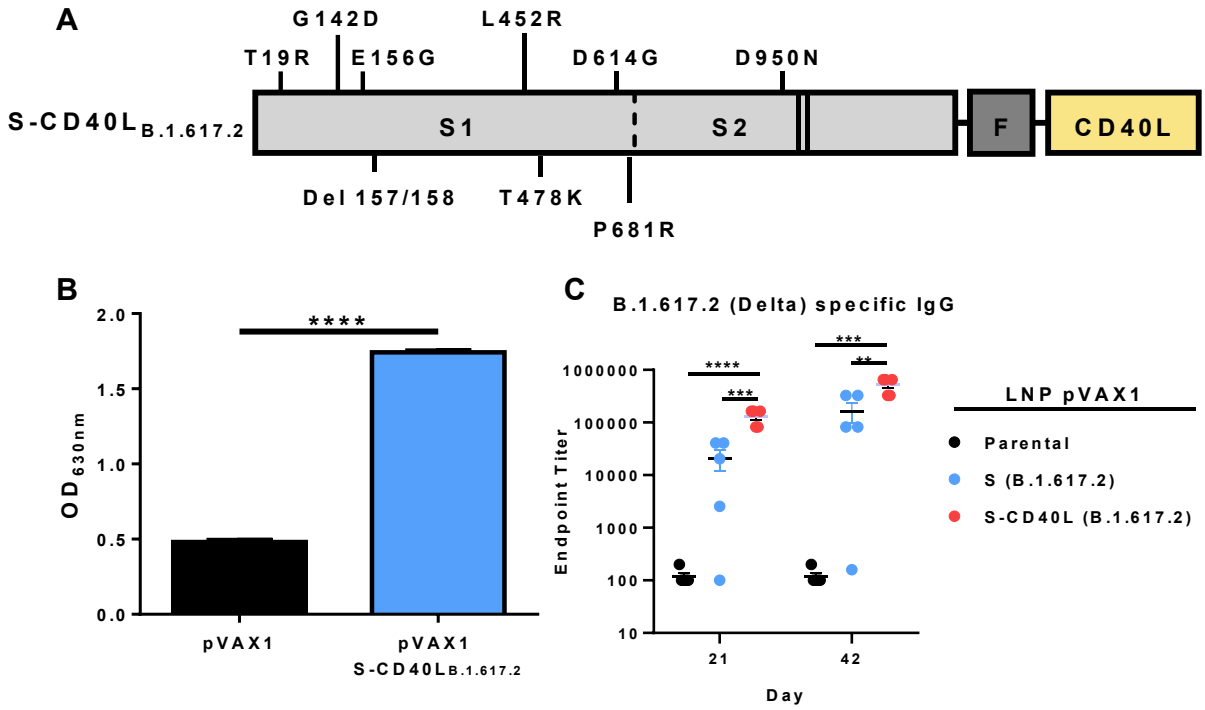

Supplemental Figure 3.1 DNA Vaccine Design and Characterization.

(A) The SARS-CoV-2 S ectodomain was prefusion stabilized via two proline mutations (solid lines) and the replacement of the furin cleavage site with "GSAS" (dotted line). The antigen was fused to a T4 fibritin trimerization motif (F) and the ectodomain of Syrian hamster CD40L (yellow). Nine mutations (T19R, G142D, E156G, Del 157/158, L452R, T478K, D614G, P681R, D950N) from the B.1.617.2 (Delta) variant were incorporated in the vaccine antigen. The codon-optimized DNA sequence encoding the fusion antigen was subcloned into a pVAX1 vector using KpnI and XhoI restriction enzymes. **(B)** CD40L reporter cells were stimulated for 24 hours with cell culture supernatant collected from HEK293T cells transfected with pVAX1 or pVAX1 S-CD40LB.1.617.2. After the stimulation, SEAP expression in the reporter cell culture supernatant was measured using QUANTI-Blue™ reagent. Abs630nm values were measured after a 30-minute incubation. Data shown is mean ± SEM; n = 3 per group, ****$p < 0.0001$ (unpaired two-tailed t-test). **(C)** Male Syrian hamsters were immunized intramuscularly on day 0 and 28 with either 100-µg of pVAX1, or 5 of SM1-20 LNP-encapsulated pVAX1 S-CD40LB.1.617.2. DNA-LNPs were generated using a NanoAssemblr™ Ignite™ instrument with NxGen™ cartridges equipped with toroidal structures. ELISA determination of total B.1.617.2 spike-specific IgG in the sera of immunized hamsters on Day 21 and 42. Data shown is mean ± SEM; n = 5 per group, **$p < 0.01$, ***$p < 0.001$, ****$p < 0.0001$.

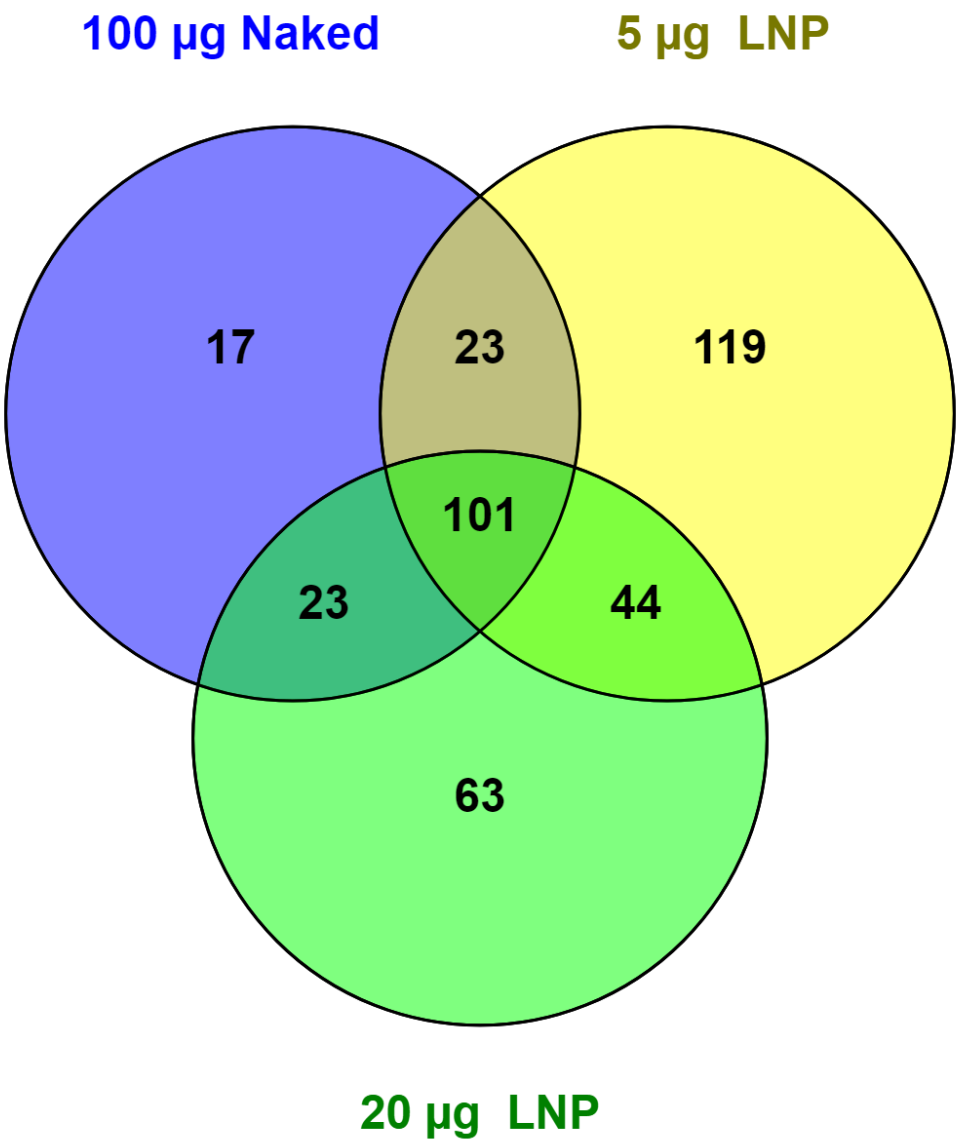

Supplemental Figure 3.2 Venn Diagram of Differentially Expressed Proteins.

Venn diagram showing overlap in DEP proteins between pVAX1 vector and pVAX1 S-CD40L$_{B.1.617.2}$ vaccinated groups. Venn diagram generated using Venny 2.1 [Oliveros, J.C. (2007-2015) Venny. An interactive tool for comparing lists with Venn's diagrams. https://bioinfogp.cnb.csic.es/tools/venny/index.html]

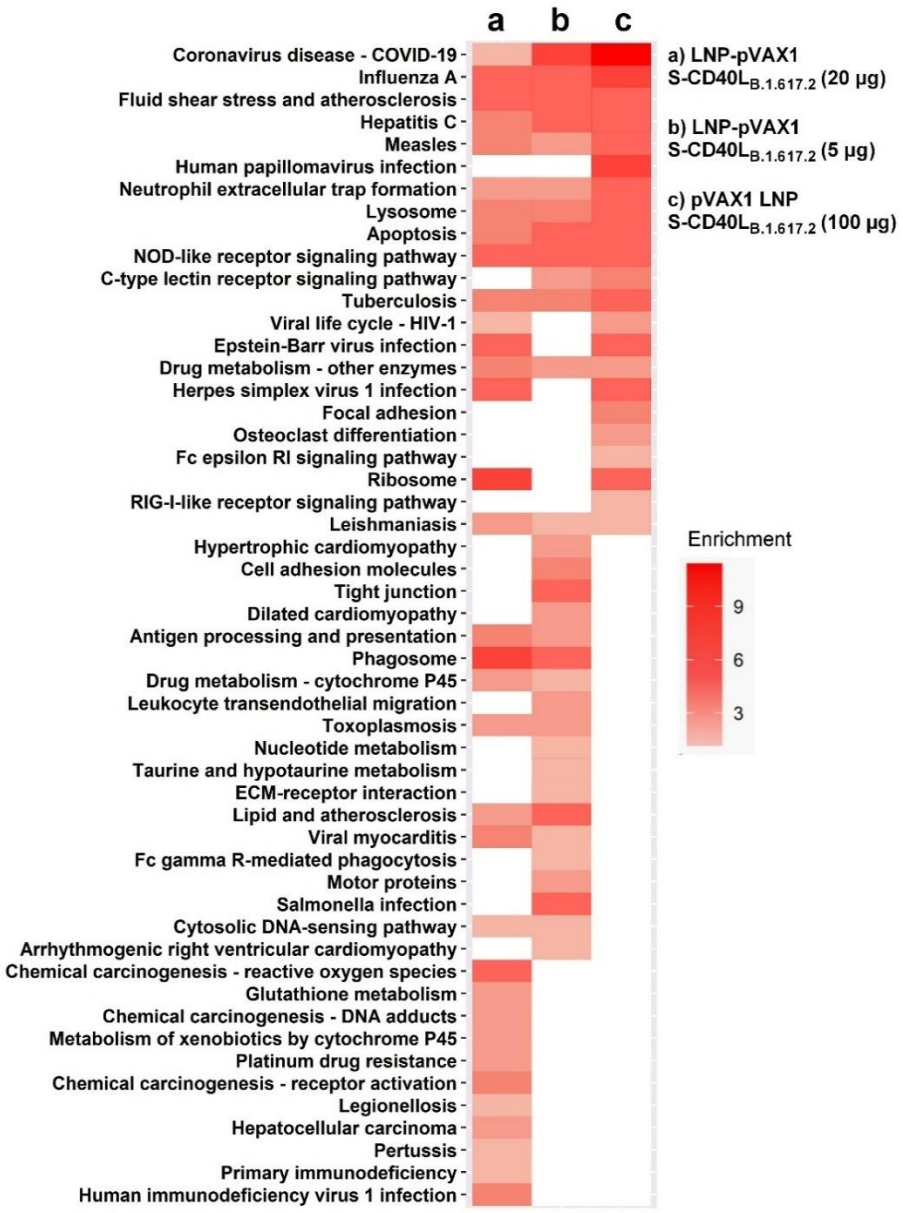

Supplemental Figure 3.3 Kyoto Encyclopedia of Genes and Genomes (KEGG) pathway enrichment analysis.

Heatmap of KEGG enrichment analysis of the differentially expressed proteins obtained from pairwise comparisons between pVAX1 and pVAX1 S-CD40L$_{B.1.617.2}$ vaccinated groups. Color refers to the enrichment score.

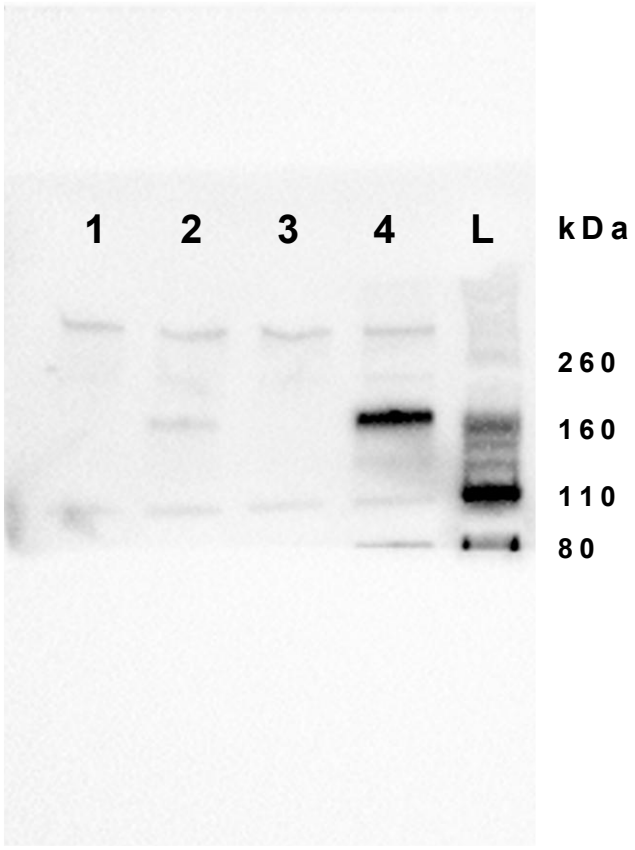

Supplemental Figure 3.4 Spike Western Blot Images.

SARS-CoV-2 (2019-nCoV) Spike Antibody, Rabbit PAb, Antigen Affinity Purified (Cat: 40591-T62, Sino Biologics). 1– KC2 pVAX1, 2- KC2 LNP pVAX1 S-CD40L$_{B.1.617.2}$, 3- SM-102 LNP pVAX1, 4- SM-102 LNP pVAX1 S-CD40L$_{B.1.617.2}$, L – Novex Sharp Pre-stained Protein Standard. Chemiluminescence image of the membrane. kDa, kiloDaltons.

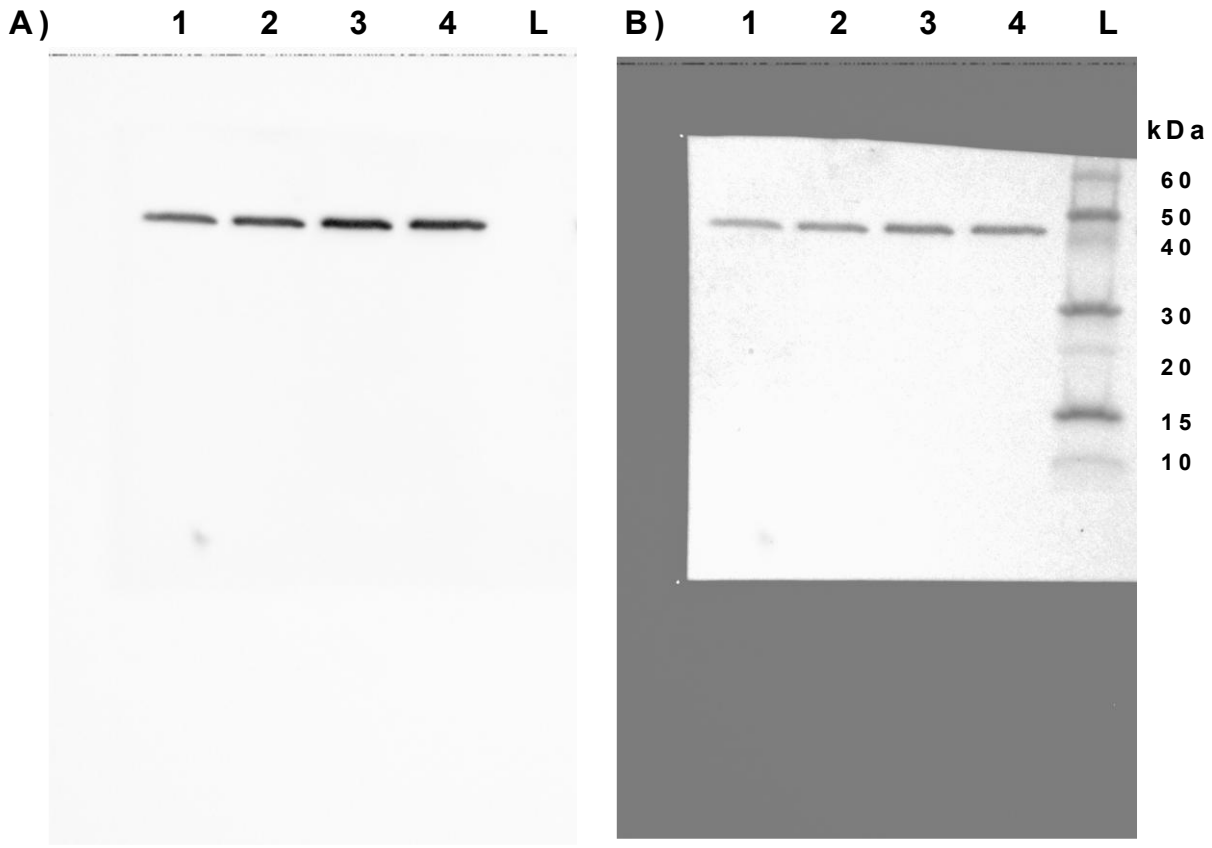

Supplemental Figure 3.5 B-actin Western Blot Image.

β-Actin Antibody (Cat: 4967, Cell Signaling). 1– KC2 pVAX1, 2- KC2 LNP pVAX1 S-CD40L$_{B.1.617.2}$, 3- SM-102 LNP pVAX1, 4- SM-102 LNP pVAX1 S-CD40L$_{B.1.617.2}$, L – Novex Sharp Pre-stained Protein Standard. kDa, kiloDaltons. **(A)** Chemiluminescence image of the membrane. **(B)** Composite chemiluminescence and colormetric image of the membrane. kDa, kiloDaltons.

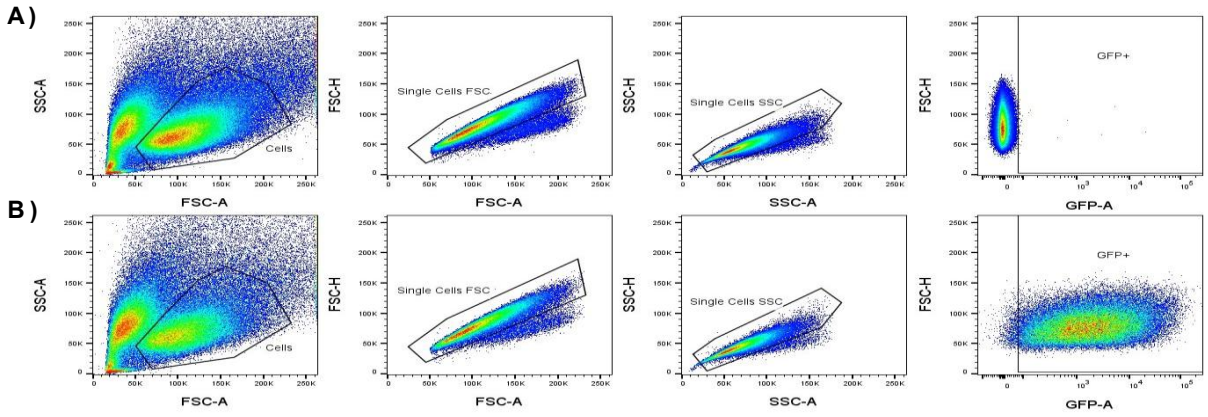

Supplemental Figure 3.6 In Vitro GFP Transfection Gating Strategy.

Representative flow cytometry gates for the analysis of GFP+ HEK293T cells transfected with **(A)** pVAX1 or **(B)** pVAX1 GFP.

Supplemental Table 3.1 KC2 LNP Characterization.

DNA-LNPs were generated using a NanoAssemblr BT™ instrument with a microfluidics cartridge containing a staggered herringbone mixing unit. Mean particle diameter measured by nanoparticle tracking analysis (NTA). Encapsulation efficiency determined by SYBR Gold assay. SD, standard deviation.

Dose	Cohort	LNP Diameter (Mean ± SD , nm)	Encapsulation Efficiency (%)
Prime	1	102.2 ± 35	>99
	2	98.3 ± 43	98.3
Boost	1	90.8 ± 34	96.1
	2	110 ± 63	97.8

Supplemental Table 3.2 KC2 and SM-102 LNP Characterization.

DNA-LNPs were generated using a NanoAssemblr BT™ instrument with a microfluidics cartridge containing a staggered herringbone mixing unit. Mean particle diameter measured by NTA. Encapsulation efficiency determined by SYBR Gold assay. SD, standard deviation.

Ionizable Lipid Component	Dose	Cohort	LNP Diameter (Mean ± SD , nm)	Encapsulation Efficiency (%)
KC2	Prime	1	83.7 ± 22	91.5
		2	84.0 ± 23	93.8
	Boost	1	90.9 ± 29	90.5
		2	84.8 ± 24.5	93.1
SM-102	Prime	1	79.0 ± 22	89.1
		2	82.1 ± 21	83.0
	Boost	1	85.0 ± 23.6	89.5
		2	80.9 ± 19	92.7

Supplemental Table 3.3 Mass-spectrometry pairwise comparisons.

Related to Figure 3.5. Protein expression in Syrian hamster lung tissue samples were compared pairwise using a pairwise t-test. Proteins with an absolute fold change >1.5 and an adjusted p-value <0.05 were defined as differentially expressed proteins (DEPs). Available online at: https://www.cell.com/cms/10.1016/j.omtm.2024.101325/attachment/b33a0bb6-d4a1-4157-a70f-1fddda8a11f0/mmc2.xlsx

Supplemental Table 3.4 GO and KEGG Analysis.

Related to Figure 3.5. Gene ontology (GO) and Kyoto Encyclopedia of Genes and Genomes (KEGG) pathway enrichment analyses were performed on the DAVID Bioinformatics database with all parameter settings at their default values. Available online at: https://www.cell.com/cms/10.1016/j.omtm.2024.101325/attachment/2b8c6cfe-707e-4cc1-b807-327d44b20ed5/mmc3.xlsx

Supplemental Table 3.5 Ingenuity Pathway Analysis.

Related to Figure 3.5. DEPs identified through pairwise t-tests were imported into Ingenuity Pathway Analysis (QIAGEN) and used to predict the activation or inhibition of canonical pathways. Available online at: https://www.cell.com/cms/10.1016/j.omtm.2024.101325/attachment/b06d2d35-8f61-485f-a8e3-c2174c6867d6/mmc4.xlsx

3.11 References

1. Moghadas SM, Vilches TN, Zhang K, Wells CR, Shoukat A, Singer BH, et al. The Impact of Vaccination on Coronavirus Disease 2019 (COVID-19) Outbreaks in the United States. *Clinical Infectious Diseases* (2021) 73:2257–2264. doi:10.1093/CID/CIAB079

2. Feikin DR, Higdon MM, Abu-Raddad LJ, Andrews N, Araos R, Goldberg Y, et al. Duration of effectiveness of vaccines against SARS-CoV-2 infection and COVID-19 disease: results of a systematic review and meta-regression. *The Lancet* (2022) 399:924–944. doi:10.1016/S0140-6736(22)00152-0

3. Bobrovitz N, Ware H, Ma X, Li Z, Hosseini R, Cao C, et al. Protective effectiveness of previous SARS-CoV-2 infection and hybrid immunity against the omicron variant and severe disease: a systematic review and meta-regression. *Lancet Infect Dis* (2023) 23:556–567. doi:10.1016/S1473-3099(22)00801-5

4. Watson OJ, Barnsley G, Toor J, Hogan AB, Winskill P, Ghani AC. Global impact of the first year of COVID-19 vaccination: a mathematical modelling study. *Lancet Infect Dis* (2022) 22:1293–1302. doi:10.1016/S1473-3099(22)00320-6

5. Baden LR, El Sahly HM, Essink B, Kotloff K, Frey S, Novak R, et al. Efficacy and Safety of the mRNA-1273 SARS-CoV-2 Vaccine. *New England Journal of Medicine* (2021) 384:403–416. doi:10.1056/NEJMOA2035389/SUPPL_FILE/NEJMOA2035389_DATA-SHARING.PDF

6. Polack FP, Thomas SJ, Kitchin N, Absalon J, Gurtman A, Lockhart S, et al. Safety and Efficacy of the BNT162b2 mRNA Covid-19 Vaccine. *N Engl J Med* (2020) 383:2603–2615. doi:10.1056/NEJMOA2034577

7. Chalkias S, Harper C, Vrbicky K, Walsh SR, Essink B, Brosz A, et al. A Bivalent Omicron-Containing Booster Vaccine against Covid-19. *New England Journal of Medicine* (2022) 387:1279–1291. doi:10.1056/NEJMOA2208343/SUPPL_FILE/NEJMOA2208343_DATA-SHARING.PDF

8. Thomas SJ, Moreira ED, Kitchin N, Absalon J, Gurtman A, Lockhart S, et al. Safety and Efficacy of the BNT162b2 mRNA Covid-19 Vaccine through 6 Months. *New England Journal of Medicine* (2021) 385:1761–1773. doi:10.1056/NEJMOA2110345/SUPPL_FILE/NEJMOA2110345_DATA-SHARING.PDF

9. Hou X, Zaks T, Langer R, Dong Y. Lipid nanoparticles for mRNA delivery. *Nature Reviews Materials 2021 6:12* (2021) 6:1078–1094. doi:10.1038/s41578-021-00358-0

10. Wilson B, Geetha KM. Lipid nanoparticles in the development of mRNA vaccines for COVID-19. *J Drug Deliv Sci Technol* (2022) 74:103553. doi:10.1016/J.JDDST.2022.103553

11. Blakney AK, McKay PF, Yus BI, Aldon Y, Shattock RJ. Inside out: optimization of lipid nanoparticle formulations for exterior complexation and in vivo delivery of saRNA. *Gene Therapy 2019 26:9* (2019) 26:363–372. doi:10.1038/s41434-019-0095-2

12. Kim J, Eygeris Y, Gupta M, Sahay G. Self-assembled mRNA vaccines. *Adv Drug Deliv Rev* (2021) 170:83–112. doi:10.1016/J.ADDR.2020.12.014

13. Mucker EM, Karmali PP, Vega J, Kwilas SA, Wu H, Joselyn M, et al. Lipid Nanoparticle Formulation Increases Efficiency of DNA-Vectored Vaccines/Immunoprophylaxis in Animals Including Transchromosomic Bovines. *Scientific Reports 2020 10:1* (2020) 10:1–13. doi:10.1038/s41598-020-65059-0

14. Connors J, Joyner D, Mege NJ, Cusimano GM, Bell MR, Marcy J, et al. Lipid nanoparticles (LNP) induce activation and maturation of antigen presenting cells in young and aged individuals. *Communications Biology 2023 6:1* (2023) 6:1–13. doi:10.1038/s42003-023-04555-1

15. Ndeupen S, Qin Z, Jacobsen S, Bouteau A, Estanbouli H, Igyártó BZ. The mRNA-LNP platform's lipid nanoparticle component used in preclinical vaccine studies is highly inflammatory. *iScience* (2021) 24: doi:10.1016/J.ISCI.2021.103479

16. Lee Y, Jeong M, Park J, Jung H, Lee H. Immunogenicity of lipid nanoparticles and its impact on the efficacy of mRNA vaccines and therapeutics. *Experimental & Molecular Medicine 2023 55:10* (2023) 55:2085–2096. doi:10.1038/s12276-023-01086-x

17. Alameh MG, Tombácz I, Bettini E, Lederer K, Sittplangkoon C, Wilmore JR, et al. Lipid nanoparticles enhance the efficacy of mRNA and protein subunit vaccines by inducing robust T follicular helper cell and humoral responses. *Immunity* (2021) 54:2877-2892.e7. doi:10.1016/j.immuni.2021.11.001

18. Kafetzis KN, Papalamprou N, McNulty E, Thong KX, Sato Y, Mironov A, et al. The Effect of Cryoprotectants and Storage Conditions on the Transfection Efficiency, Stability, and Safety of Lipid-Based Nanoparticles for mRNA and DNA Delivery. *Adv Healthc Mater* (2023) 12:2203022. doi:10.1002/ADHM.202203022

19. Liu MA. A Comparison of Plasmid DNA and mRNA as Vaccine Technologies. *Vaccines 2019, Vol 7, Page 37* (2019) 7:37. doi:10.3390/VACCINES7020037

20. Mulroney TE, Pöyry T, Yam-Puc JC, Rust M, Harvey RF, Kalmar L, et al. N1-methylpseudouridylation of mRNA causes +1 ribosomal frameshifting. *Nature 2023 625:7993* (2023) 625:189–194. doi:10.1038/s41586-023-06800-3

21. Melo AR da S, de Macêdo LS, Invenção M da CV, de Moura IA, da Gama MATM, de Melo CML, et al. Third-Generation Vaccines: Features of Nucleic Acid Vaccines and Strategies

to Improve Their Efficiency. *Genes 2022, Vol 13, Page 2287* (2022) 13:2287. doi:10.3390/GENES13122287

22. Tamming LA, Duque D, Tran A, Zhang W, Pfeifle A, Laryea E, et al. DNA Based Vaccine Expressing SARS-CoV-2 Spike-CD40L Fusion Protein Confers Protection Against Challenge in a Syrian Hamster Model. *Front Immunol* (2022) 12: doi:10.3389/FIMMU.2021.785349

23. Elgueta R, Benson MJ, De Vries VC, Wasiuk A, Guo Y, Noelle RJ. Molecular mechanism and function of CD40/CD40L engagement in the immune system. *Immunol Rev* (2009) 229:152–172. doi:10.1111/J.1600-065X.2009.00782.X

24. Harzandi N, Aghababa H, Khoramabadi N, Tabaraie T. Efficient Immunization of BALB/c Mice against Pathogenic Brucella melitensis and B. ovis: Comparing Cell-Mediated and Protective Immune Responses Elicited by pCDNA3.1 and pVAX1 DNA Vaccines Coding for Omp31 of Brucella melitensis. *Iran J Biotechnol* (2021) 19:40–47. doi:10.30498/IJB.2021.2618

25. Yuan L, Zhu H, Zhou M, Ma J, Chen R, Chen Y, et al. Gender associates with both susceptibility to infection and pathogenesis of SARS-CoV-2 in Syrian hamster. *Signal Transduction and Targeted Therapy 2021 6:1* (2021) 6:1–8. doi:10.1038/s41392-021-00552-0

26. Castellan M, Zamperin G, Franzoni G, Foiani G, Zorzan M, Drzewnioková P, et al. Host Response of Syrian Hamster to SARS-CoV-2 Infection including Differences with Humans and between Sexes. *Viruses* (2023) 15:428. doi:10.3390/V15020428/S1

27. Hassett KJ, Benenato KE, Jacquinet E, Lee A, Woods A, Yuzhakov O, et al. Optimization of Lipid Nanoparticles for Intramuscular Administration of mRNA Vaccines. *Mol Ther Nucleic Acids* (2019) 15:1–11. doi:10.1016/j.omtn.2019.01.013

28. Zhang W, Pfeifle A, Lansdell C, Frahm G, Cecillon J, Tamming L, et al. The Expression Kinetics and Immunogenicity of Lipid Nanoparticles Delivering Plasmid DNA and mRNA in Mice. *Vaccines (Basel)* (2023) 11:1580. doi:10.3390/VACCINES11101580/S1

29. Saito A, Irie T, Suzuki R, Maemura T, Nasser H, Uriu K, et al. Enhanced fusogenicity and pathogenicity of SARS-CoV-2 Delta P681R mutation. *Nature 2021 602:7896* (2021) 602:300–306. doi:10.1038/s41586-021-04266-9

30. Planas D, Veyer D, Baidaliuk A, Staropoli I, Guivel-Benhassine F, Rajah MM, et al. Reduced sensitivity of SARS-CoV-2 variant Delta to antibody neutralization. *Nature 2021 596:7871* (2021) 596:276–280. doi:10.1038/s41586-021-03777-9

31. Harvey WT, Carabelli AM, Jackson B, Gupta RK, Thomson EC, Harrison EM, et al. SARS-CoV-2 variants, spike mutations and immune escape. *Nature Reviews Microbiology 2021 19:7* (2021) 19:409–424. doi:10.1038/s41579-021-00573-0

32. Kudriavtsev A V., Vakhrusheva A V., Novoseletsky VN, Bozdaganyan ME, Shaitan K V., Kirpichnikov MP, et al. Immune Escape Associated with RBD Omicron Mutations and SARS-CoV-2 Evolution Dynamics. *Viruses 2022, Vol 14, Page 1603* (2022) 14:1603. doi:10.3390/V14081603

33. Chakraborty C, Sharma AR, Bhattacharya M, Lee SS. A Detailed Overview of Immune Escape, Antibody Escape, Partial Vaccine Escape of SARS-CoV-2 and Their Emerging Variants With Escape Mutations. *Front Immunol* (2022) 13:801522. doi:10.3389/FIMMU.2022.801522/BIBTEX

34. Liang R, Ye ZW, Ong CP, Qin Z, Xie Y, Fan Y, et al. The spike receptor-binding motif G496S substitution determines the replication fitness of SARS-CoV-2 Omicron sublineage. *Emerg Microbes Infect* (2022) 11:2093–2101. doi:10.1080/22221751.2022.2111977

35. Uraki R, Ito M, Furusawa Y, Yamayoshi S, Iwatsuki-Horimoto K, Adachi E, et al. Humoral immune evasion of the omicron subvariants BQ.1.1 and XBB. *Lancet Infect Dis* (2023) 23:30–32. doi:10.1016/S1473-3099(22)00816-7

36. Qu P, Evans JP, Faraone JN, Zheng YM, Carlin C, Anghelina M, et al. Enhanced neutralization resistance of SARS-CoV-2 Omicron subvariants BQ.1, BQ.1.1, BA.4.6, BF.7, and BA.2.75.2. *Cell Host Microbe* (2023) 31:9-17.e3. doi:10.1016/j.chom.2022.11.012

37. Qu P, Faraone JN, Evans JP, Zheng YM, Carlin C, Anghelina M, et al. Enhanced evasion of neutralizing antibody response by Omicron XBB.1.5, CH.1.1, and CA.3.1 variants. *Cell Rep* (2023) 42:112443. doi:10.1016/J.CELREP.2023.112443

38. Ao D, He X, Hong W, Wei X. The rapid rise of SARS-CoV-2 Omicron subvariants with immune evasion properties: XBB.1.5 and BQ.1.1 subvariants. *MedComm (Beijing)* (2023) 4:e239. doi:10.1002/MCO2.239

39. Willett BJ, Grove J, MacLean OA, Wilkie C, De Lorenzo G, Furnon W, et al. SARS-CoV-2 Omicron is an immune escape variant with an altered cell entry pathway. *Nature Microbiology 2022 7:8* (2022) 7:1161–1179. doi:10.1038/s41564-022-01143-7

40. Zhou J, Liu Z, Zhang G, Xu W, Xing L, Lu L, et al. Development of variant-proof severe acute respiratory syndrome coronavirus 2, pan-sarbecovirus, and pan-β-coronavirus vaccines. *J Med Virol* (2023) 95:e28172. doi:10.1002/JMV.28172

41. Kim W, Zhou JQ, Horvath SC, Schmitz AJ, Sturtz AJ, Lei T, et al. Germinal centre-driven maturation of B cell response to mRNA vaccination. *Nature 2022 604:7904* (2022) 604:141–145. doi:10.1038/s41586-022-04527-1

42. Inoue T, Shinnakasu R, Kawai C, Yamamoto H, Sakakibara S, Ono C, et al. Antibody feedback contributes to facilitating the development of Omicron-reactive memory B cells in

SARS-CoV-2 mRNA vaccinees. *Journal of Experimental Medicine* (2023) 220: doi:10.1084/JEM.20221786/213745

43. Lenart K, Hellgren F, Ols S, Yan X, Cagigi A, Cerveira RA, et al. A third dose of the unmodified COVID-19 mRNA vaccine CVnCoV enhances quality and quantity of immune responses. *Mol Ther Methods Clin Dev* (2022) 27:309–323. doi:10.1016/j.omtm.2022.10.001

44. Kwa S, Lai L, Gangadhara S, Siddiqui M, Pillai VB, Labranche C, et al. CD40L-Adjuvanted DNA/Modified Vaccinia Virus Ankara Simian Immunodeficiency Virus SIV239 Vaccine Enhances SIV-Specific Humoral and Cellular Immunity and Improves Protection against a Heterologous SIVE660 Mucosal Challenge. *J Virol* (2014) 88:9579. doi:10.1128/JVI.00975-14

45. Hashem AM, Gravel C, Chen Z, Yi Y, Tocchi M, Jaentschke B, et al. CD40 Ligand Preferentially Modulates Immune Response and Enhances Protection against Influenza Virus. *The Journal of Immunology* (2014) 193:722–734. doi:10.4049/JIMMUNOL.1300093

46. Lau JJ, Cheng SMS, Leung K, Lee CK, Hachim A, Tsang LCH, et al. Real-world COVID-19 vaccine effectiveness against the Omicron BA.2 variant in a SARS-CoV-2 infection-naive population. *Nature Medicine 2023 29:2* (2023) 29:348–357. doi:10.1038/s41591-023-02219-5

47. Turner JS, O'Halloran JA, Kalaidina E, Kim W, Schmitz AJ, Zhou JQ, et al. SARS-CoV-2 mRNA vaccines induce persistent human germinal centre responses. *Nature 2021 596:7870* (2021) 596:109–113. doi:10.1038/s41586-021-03738-2

48. Aid M, Busman-Sahay K, Vidal SJ, Maliga Z, Bondoc S, Starke C, et al. Vascular Disease and Thrombosis in SARS-CoV-2-Infected Rhesus Macaques. *Cell* (2020) 183:1354-1366.e13. doi:10.1016/j.cell.2020.10.005

49. Wendisch D, Dietrich O, Mari T, von Stillfried S, Ibarra IL, Mittermaier M, et al. SARS-CoV-2 infection triggers profibrotic macrophage responses and lung fibrosis. *Cell* (2021) 184:6243-6261.e27. doi:10.1016/J.CELL.2021.11.033/ATTACHMENT/F61754D9-B3D7-4A0E-9D20-2067CC9C519F/MMC6.XLSX

50. Nouailles G, Wyler E, Pennitz P, Postmus D, Vladimirova D, Kazmierski J, et al. Temporal omics analysis in Syrian hamsters unravel cellular effector responses to moderate COVID-19. *Nat Commun* (2021) 12: doi:10.1038/S41467-021-25030-7

51. Suresh V, Mohanty V, Avula K, Ghosh A, Singh B, Reddy RK, et al. Quantitative proteomics of hamster lung tissues infected with SARS-CoV-2 reveal host factors having implication in the disease pathogenesis and severity. *The FASEB Journal* (2021) 35:e21713. doi:10.1096/FJ.202100431R

52. Aid M, Vidal SJ, Piedra-Mora C, Ducat S, Chan CN, Bondoc S, et al. Ad26.COV2.S prevents upregulation of SARS-CoV-2 induced pathways of inflammation and thrombosis in

hamsters and rhesus macaques. *PLoS Pathog* (2022) 18:e1009990. doi:10.1371/JOURNAL.PPAT.1009990

53. Waickman AT, Victor K, Newell K, Li T, Friberg H, Foulds KE, et al. mRNA-1273 vaccination protects against SARS-CoV-2–elicited lung inflammation in nonhuman primates. *JCI Insight* (2022) 7: doi:10.1172/JCI.INSIGHT.160039

54. Meyer M, Wang Y, Edwards D, Smith GR, Rubenstein AB, Ramanathan P, et al. Attenuated activation of pulmonary immune cells in mRNA-1273–vaccinated hamsters after SARS-CoV-2 infection. *J Clin Invest* (2021) 131: doi:10.1172/JCI148036

55. Pfeifle A, Thulasi Raman SN, Lansdell C, Zhang W, Tamming L, Cecillon J, et al. DNA lipid nanoparticle vaccine targeting outer surface protein C affords protection against homologous Borrelia burgdorferi needle challenge in mice. *Front Immunol* (2023) 14:1020134. doi:10.3389/FIMMU.2023.1020134/BIBTEX

56. Algarni A, Pilkington EH, Suys EJA, Al-Wassiti H, Pouton CW, Truong NP. In vivo delivery of plasmid DNA by lipid nanoparticles: the influence of ionizable cationic lipids on organ-selective gene expression. *Biomater Sci* (2022) 10:2940–2952. doi:10.1039/D2BM00168C

57. Guimaraes LC, Costa PAC, Scalzo Júnior SRA, Ferreira HAS, Braga ACS, de Oliveira LC, et al. Nanoparticle-based DNA vaccine protects against SARS-CoV-2 variants in female preclinical models. *Nature Communications 2024 15:1* (2024) 15:1–19. doi:10.1038/s41467-024-44830-1

58. Liao H-C, Shen K-Y, Yang C-H, Chiu F-F, Chiang C-Y, Chai KM, et al. Lipid nanoparticle-encapsulated DNA vaccine robustly induce superior immune responses to the mRNA vaccine in Syrian hamsters. *Mol Ther Methods Clin Dev* (2024) 32:101169. doi:10.1016/J.OMTM.2023.101169

59. D W, N W, KS C, JA G, CL H, O A, et al. Cryo-EM structure of the 2019-nCoV spike in the prefusion conformation. *Science* (2020) 367:1255–1260. doi:10.1126/SCIENCE.ABB2507

60. Stuible M, Gervais C, Lord-Dufour S, Perret S, L'Abbé D, Schrag J, et al. Rapid, high-yield production of full-length SARS-CoV-2 spike ectodomain by transient gene expression in CHO cells. *J Biotechnol* (2021) 326:21–27. doi:10.1016/J.JBIOTEC.2020.12.005

61. Stark FC, Akache B, Deschatelets L, Tran A, Stuible M, Durocher Y, et al. Intranasal immunization with a proteosome-adjuvanted SARS-CoV-2 spike protein-based vaccine is immunogenic and efficacious in mice and hamsters. *Scientific Reports 2022 12:1* (2022) 12:1–11. doi:10.1038/s41598-022-13819-5

62. Nie J, Li Q, Wu J, Zhao C, Hao H, Liu H, et al. Quantification of SARS-CoV-2 neutralizing antibody by a pseudotyped virus-based assay. *Nature Protocols 2020 15:11* (2020) 15:3699–3715. doi:10.1038/s41596-020-0394-5

63. Reed LJ, Muench H. A simple method of estimating fifty per cent endpoints. *Am J Epidemiol* (1938) 27:493–497. doi:10.1093/OXFORDJOURNALS.AJE.A118408/2/27-3-493.PDF.GIF

64. Wölfel R, Corman VM, Guggemos W, Seilmaier M, Zange S, Müller MA, et al. Virological assessment of hospitalized patients with COVID-2019. *Nature 2020 581:7809* (2020) 581:465–469. doi:10.1038/s41586-020-2196-x

65. Harris G, Holbein BE, Zhou H, Howard Xu H, Chen W. Potential mechanisms of mucin-enhanced acinetobacter baumannii virulence in the mouse model of intraperitoneal infection. *Infect Immun* (2019) 87: doi:10.1128/IAI.00591-19/SUPPL_FILE/IAI.00591-19-S0001.PDF

66. Lien CE, Lin YJ, Chen C, Lian WC, Kuo TY, Campbell JD, et al. CpG-adjuvanted stable prefusion SARS-CoV-2 spike protein protected hamsters from SARS-CoV-2 challenge. *Scientific Reports 2021 11:1* (2021) 11:1–7. doi:10.1038/s41598-021-88283-8

67. Creskey M, Li L, Ning Z, Fekete EEF, Mayne J, Walker K, et al. An economic and robust TMT labeling approach for high throughput proteomic and metaproteomic analysis. *Proteomics* (2023) 23:2200116. doi:10.1002/PMIC.202200116

68. Huang T, Choi M, Tzouros M, Golling S, Pandya NJ, Banfai B, et al. MSstatsTMT: Statistical Detection of Differentially Abundant Proteins in Experiments with Isobaric Labeling and Multiple Mixtures. *Molecular and Cellular Proteomics* (2020) 19:1706–1723. doi:10.1074/mcp.RA120.002105

Chapter 4 Durability of DNA-LNP and mRNA-LNP Vaccine-Induced Immunity Against SARS-CoV-2 XBB.1.5

Preface: This chapter is currently under peer review. A preprint has been made publicly available.

Tamming L et al. Durability of DNA-LNP and mRNA-LNP Vaccine-Induced Immunity Against SARS-CoV-2 XBB.1.5. ***npj Vaccines*** 2026 Jan 31. doi: 10.1038/s41541-026-01382-3

Candidate Contribution

Levi Tamming was the primary author of this manuscript. Levi Tamming designed the experiments and DNA and mRNA vaccines. Levi Tamming prepared all plasmids and performed all ELISA, pseudovirus neutralization, subgenomic mRNA, ELIspot, and intracellular cytokine staining experiments. Levi Tamming analyzed all data, prepared all figures, and wrote the first draft of the manuscript.

Author list

Levi Tamming[1,2], Casey Lansdell[1], Wanyue Zhang[1,2], Diana Duque[3], Jegarubee Bavananthasivam[3], Grant Frahm[1], Annabelle Pfeifle[1,2], Sathya N. Thulasi Raman[1], Jianguo Wu[1], Caroline Gravel[1], Andrew Stalker[1], Matthew Stuible[4], Yves Durocher[4], Wangxue Chen[3], Lisheng Wang[2], Simon Sauve[1], Anh Tran[2,3]*, Michael J.W. Johnston[1,5]*, Xuguang Li[1,2]*
[1]Centre for Oncology, Radiopharmaceuticals and Research, Biologic and Radiopharmaceutical Drugs Directorate, Health Products and Food Branch, Health Canada, Ottawa, ON, Canada
[2]Department of Biochemistry, Microbiology and Immunology, Faculty of Medicine, University of Ottawa, Ottawa, ON, Canada
[3]Human Health Therapeutics Research Center, National Research Council of Canada, Ottawa, ON, Canada
[4] Human Health Therapeutics Research Center, National Research Council of Canada, Montreal, QC, Canada
[5]Department of Chemistry, Carleton University, Ottawa, ON K1S 5B6, Canada
*Corresponding authors

Copyright

4.1 Abstract

mRNA-lipid nanoparticle (LNP) vaccines induce robust adaptive immune responses and have proven highly effective against SARS-CoV-2. However, their long-term effectiveness is limited by waning humoral responses, which decline substantially within the first six months post-boost vaccination. DNA-LNPs are being investigated as an alternative vaccine platform, offering prolonged antigen expression and robust immunity. Here, we compare DNA- and mRNA-LNP vaccines encoding CD40L-adjuvanted SARS-CoV-2 XBB.1.5 Spike ($S_{XBB.1.5}$-CD40L) in a long-term in vivo challenge model. Both nucleic acid vaccines induced strong neutralizing antibody responses and conferred equivalent protection in Syrian hamsters challenged three weeks post-boost. Notably, DNA-LNP vaccination maintained high binding and neutralizing antibody titers six months post-boost, whereas mRNA-LNPs exhibited a marked decline. Correspondingly, while $S_{XBB.1.5}$-CD40L DNA-LNP vaccination completely protected from weight loss, viral replication, and lung pathology at this late timepoint, $S_{XBB.1.5}$-CD40L mRNA-LNP vaccination conferred minimal protection. These findings demonstrate that DNA-LNPs can sustain durable immunity, highlighting their potential as a next-generation vaccine platform that could reduce the need for frequent boosters.

4.2 Introduction

Ideal vaccines elicit durable immunity against their target pathogen. While mRNA vaccines have been highly effective against COVID-19, their ability to prevent symptomatic infection wanes dramatically over time (1–6). In particular, mRNA-induced antibody responses undergo an initial phase of rapid decline before stabilizing around 7-9 months post-vaccination (7–10). Although mRNA vaccination drives robust germinal center activity and affinity maturation (11), studies

show it generates only limited long-lived plasma cell (LLPC) populations in the bone marrow (12). The decay of circulating antibody titers, combined with the emergence of immune-escaping variants, has necessitated repeated booster immunizations, often on an annual basis, to sustain a high level of efficacy (13–15).

Multiple COVID-19 DNA vaccines were evaluated clinically during the pandemic, the majority of which utilized electroporation or needle-free injection systems to overcome challenges associated with inefficient delivery and limited immunogenicity in humans (16–18). Advances in lipid nanoparticle (LNP) technology were critical to the success of mRNA vaccines, both by protecting the mRNA and facilitating its cellular uptake (19,20). The ionizable lipids within these formulations also exhibit immunostimulatory properties, functioning as self-adjuvants (21,22). Recent research has highlighted how these same LNP formulations can be adapted for DNA-based vaccination (23–27). DNA- and mRNA-LNPs display distinct antigen expression kinetics and modes of innate immune activation, differences that can profoundly shape the adaptive response (26,28,29).

Here, we directly compare the immunogenicity and long-term efficacy of DNA- and mRNA-LNP vaccines against the SARS-CoV-2 XBB.1.5 variant. XBB.1.5 became globally dominant in early 2023 and was selected as the antigen for the FDA-approved monovalent mRNA-LNP vaccines deployed during the 2023–2024 season (30). We previously demonstrated that fusion of CD40 ligand (CD40L) to the SARS-CoV-2 Spike (S) enhances the immunogenicity and efficacy of DNA-based vaccines (31,32). Using this same design, both DNA- and mRNA-LNP vaccines elicited robust initial immune responses that conferred complete protection against XBB.1.5 in Syrian hamsters. However, only the DNA-LNP vaccine provided durable immunity, sustaining high levels of binding and neutralizing antibodies (NAbs) and affording near-complete protection six months

post-boost. These findings highlight the potential of DNA-LNP vaccines to confer lasting protection against emerging SARS-CoV-2 variants and emphasizes the importance of further exploring this platform.

4.3 Results

4.3.1 CD40L augments humoral and CD4$^+$ T Cell responses induced by mRNA-LNPs in mice

Building on our previous finding that CD40L enhanced the immunogenicity of a DNA-based SARS-CoV-2 S vaccine (31), we first evaluated whether this strategy could similarly augment immune responses induced by mRNA-LNP vaccination. Using our established design framework, mRNAs encoding trimerized soluble XBB.1.5 S either alone ($S_{XBB.1.5}$) or fused to the CD40L ectodomain ($S_{XBB.1.5}$-CD40L) were synthesized. BALB/c mice were immunized intramuscularly with 1.25 μg of the mRNA-LNP vaccines on days 0 and 28 before being sacrificed on day 49 for immunological analysis (Figure 4.1A). Control animals were immunized with non-coding plasmid DNA (pDNA) encapsulated in the same LNP formulation, which has previously been shown not to elicit antigen-specific responses (23,32). Both mRNA vaccines induced robust serum anti-XBB.1.5 S IgG responses compared to control mice (Figure 4.1B). Notably, the $S_{XBB.1.5}$-CD40L mRNA-LNP vaccine generated higher binding antibody levels than the non-adjuvanted vaccine. In addition, $S_{XBB.1.5}$-CD40L induced greater IgG2a responses (Figure 4.1C) without a corresponding rise in IgG1 levels (Figure 4.1D), indicative of Th1 polarization. Interestingly, both the $S_{XBB.1.5}$ and $S_{XBB.1.5}$-CD40L vaccines raised comparable levels of NAbs against XBB.1.5 (Figure 4.1E). Both $S_{XBB.1.5}$ and $S_{XBB.1.5\text{-}CD40L}$ elicited significant interferon-γ (IFNγ)-secreting splenocyte responses (Figure 4.1F). Notably, $S_{XBB.1.5}$-CD40L induced a significantly greater number of IFNγ-secreting cells than $S_{XBB.1.5}$. The inclusion of CD40L also increased the expression

of IFNγ, TNFα, and IL-2 in $CD4^+$ T cells (Figure 4.1G-I), while no statistically significant enhancement of $CD8^+$ T cell responses was observed (Figure 4.1J-L). Together, these findings demonstrate that incorporation of CD40L into mRNA-based SARS-CoV-2 S vaccines enhances Th1-biased humoral and $CD4^+$ T cell responses.

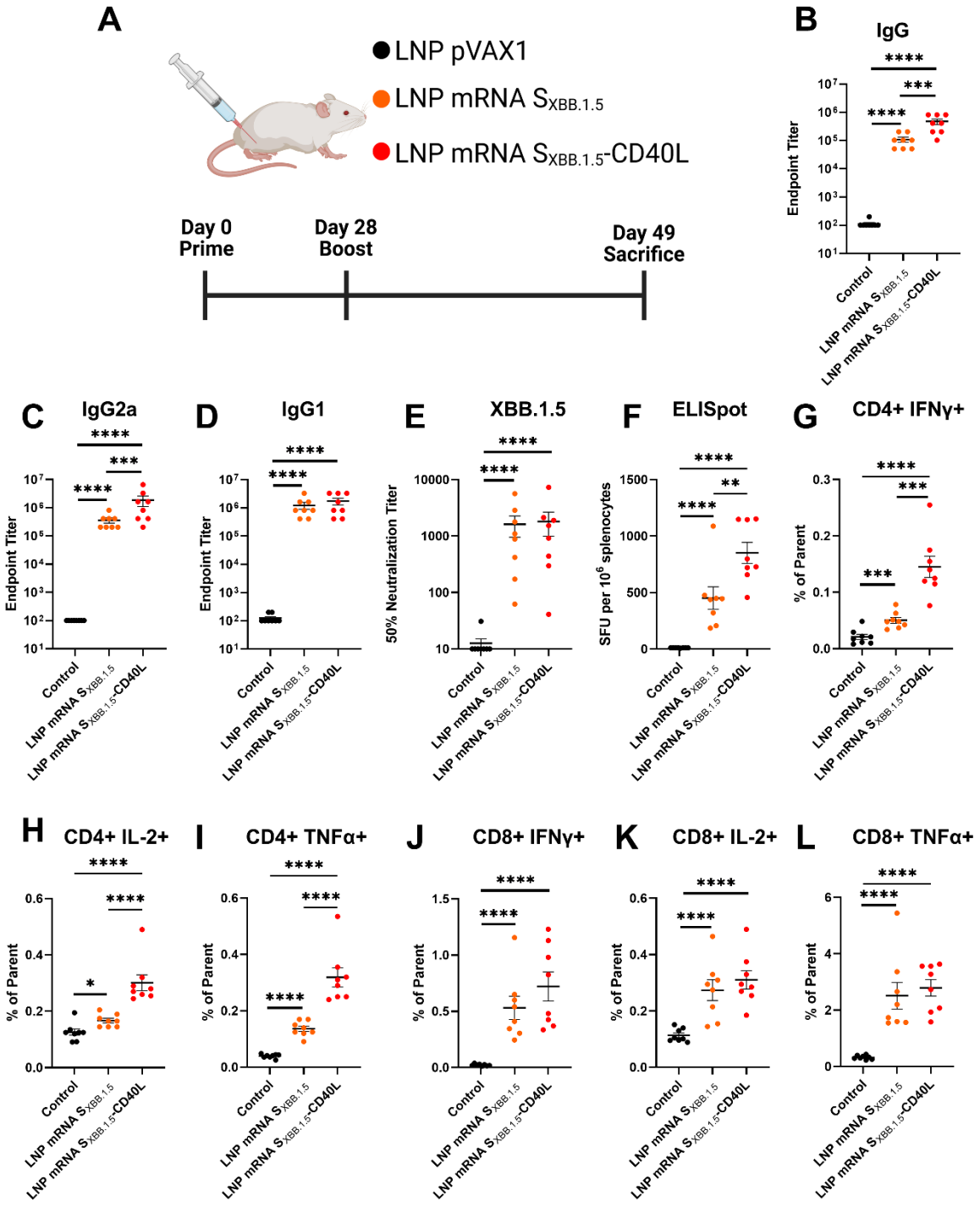
A
LNP pVAX1
LNP mRNA SXBB.1.5
LNP mRNA SXBB.1.5-CD40L
Day 0
Prime
Day 28
Boost
Day 49
Sacrifice
B
IgG
Endpoint Titer
C
IgG2a
D
IgG1
E
XBB.1.5
50% Neutralization Titer
F
ELISpot
SFU per 10^6 splenocytes
G
CD4+ IFNγ+
% of Parent
H
CD4+ IL-2+
I
CD4+ TNFα+
J
CD8+ IFNγ+
K
CD8+ IL-2+
L
CD8+ TNFα+
Control
LNP mRNA SXBB.1.5
LNP mRNA SXBB.1.5-CD40L

Figure 4.1 CD40L enhances immunogenicity of XBB.1.5 mRNA-LNP vaccines in BALB/c mice.

(A) Female BALB/c mice (n = 8 per group) were immunized intramuscularly on days 0 and 28 with 1.25 µg of $S_{XBB.1.5}$ or $S_{XBB.1.5}$-CD40L mRNA-LNPs. Control mice were vaccinated with 2.5 µg of a non-coding pVAX1 DNA-LNP. Mice were sacrificed on day 49 to assess adaptive immune responses. Created in BioRender. Tamming, L. (2026) https://BioRender.com/3cg6lmx. XBB.1.5 S-specific IgG **(B)**, IgG2a **(C)** and IgG1 **(D)** levels in the sera measured by ELISA. The 50% neutralizing titer (NT50) of mouse sera was determined using XBB.1.5 pseudotyped-VSV. Cellular immune responses were assessed by stimulating splenocytes with 1 µg/mL of an XBB.1.5 S overlapping peptide pool. (**F**) IFNγ-secreting splenocytes as determined by ELISpot. Frequency of cytokine expression by $CD4^+$ (**G-I**) and $CD8^+$ (**J-L**) T cells as determined by intracellular cytokine staining. Data shown are mean ± SEM. $^{**}p < 0.01$, $^{***}p < 0.001$, $^{****}p < 0.0001$.

4.3.2 DNA-LNP vaccines induce long-lived humoral immunity in Syrian hamsters

Given the limited durability of humoral responses observed with mRNA vaccines, we sought to assess the longevity of immunity induced by CD40L-adjuvanted DNA- and mRNA-LNP vaccines. To evaluate both immunogenicity and protection, Syrian hamsters were immunized on days 0 and 28 with either 2.5 µg of mRNA $S_{XBB.1.5}$-CD40L or 5 µg of pVAX1 $S_{XBB.1.5}$-CD40L, each formulated with the same SM-102-based LNPs (Figure 4.2A). The 5 µg DNA-LNP dose was previously established to be effective against B.1.617.2 and BA.5 challenge (32). The lower 2.5 µg mRNA dose was selected based on the higher antigen expression and immunogenicity previously observed for mRNA-LNP vaccines (28). As a negative control, animals received 5 µg non-coding pVAX1 DNA-LNP. Hamsters were subsequently challenged either on day 49 or day 203, six months post-boost. Humoral responses in the sera were assessed at days 42 and 196. On day 42, both the DNA- and mRNA-LNP vaccines elicited robust XBB.1.5 S-specific IgG responses (Figure 4.2B). While binding antibody titers in the mRNA-LNP group had declined more than 10-fold by day 196, DNA-LNP vaccinated hamsters maintained high binding antibody levels. Similarly, although both vaccines elicited comparable NAb responses against XBB.1.5 at day 42, the neutralizing activity of the mRNA-LNP group was significantly diminished relative to

the DNA-LNP six months post-boost (Figure 4.2C). To assess the breadth of immunity induced by both vaccines, we assessed the NAb response against KP.3.1.1 (Figure 4.2D), a more recent Omicron sublineage that demonstrated partial escape from XBB.1.5 vaccine-induced antibodies (33). At day 42, both DNA-LNP and mRNA-LNP immune sera neutralized KP.3.1.1, though the NAb titers were reduced compared to XBB.1.5. By day 196, neutralizing activity in the mRNA-LNP group declined to near-background levels, whereas DNA-LNP vaccinated animals retained measurable activity. Notably, immunization with DNA-LNPs encoding $S_{XBB.1.5}$ without CD40L also induced durable humoral responses, with no apparent drop in binding antibody titers six months post-boost (Supplemental Figure 4.1). Altogether, these results highlight the capacity of DNA-LNP vaccines to elicit durable and long-lived humoral immunity against SARS-CoV-2 variants.

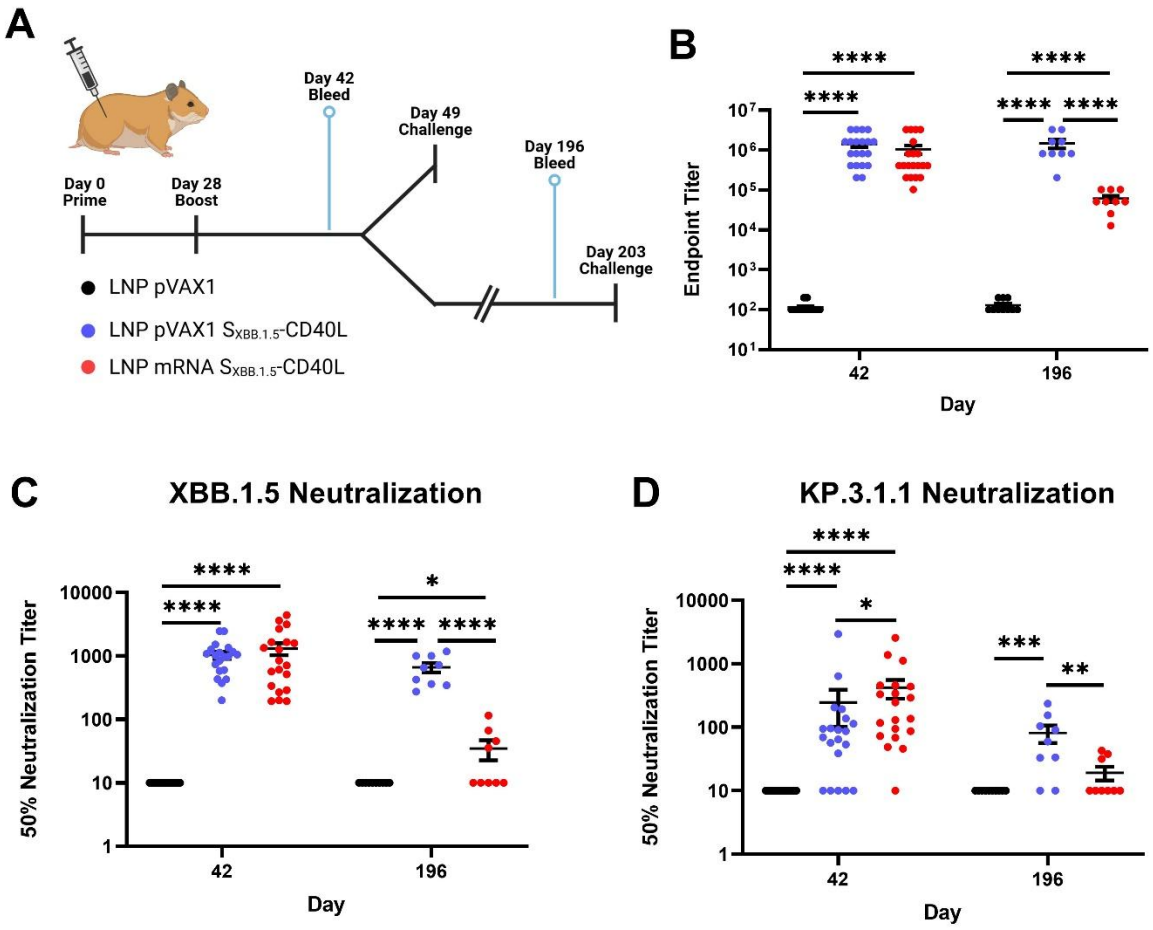

Figure 4.2 $S_{XBB.1.5}$-CD40L DNA-LNPs induce robust and durable humoral responses in Syrian hamsters.

(A) Male Syrian hamsters were immunized intramuscularly on day 0 and 28 with 5 µg of $S_{XBB.1.5}$-CD40L DNA-LNP or 2.5 µg of $S_{XBB.1.5}$-CD40L mRNA-LNP. Control hamsters were vaccinated with 5 µg of pVAX1 DNA-LNP. Animals were challenged intranasally with 1.67×10^5 TCID50 of a SARS-CoV-2 XBB.1.5 isolate on day 49 or 203. Serum was collected on day 42 (n = 20 per group) or day 196 (n = 9-10 per group) to assess humoral responses. Created in BioRender. Tamming, L. (2026) https://BioRender.com/xiodjpx. **(B)** XBB.1.5 S-specific IgG determined by ELISA. Serum NT50 determined using **(C)** XBB.1.5 pseudotyped-VSV or **(D)** KP.3.1.1. Data shown are mean ± SEM. $*p < 0.05$, $**p < 0.01$, $***p < 0.001$, $****p < 0.0001$.

4.3.3 DNA-LNPs provide long-term protection against XBB.1.5 SARS-CoV-2 challenge

Next, we evaluated the protective efficacy of the DNA- and mRNA-LNP $S_{XBB.1.5}$-CD40L vaccines.

Vaccinated Syrian hamsters were challenged with a matched SARS-CoV-2 XBB.1.5 isolate on day

49, three weeks post-boost vaccination (Figure 4.3A). The two $S_{XBB.1.5}$-CD40L vaccines conferred comparable protection against weight loss following infection (Figure 4.3B). In addition, both vaccines were highly effective at suppressing viral replication in both the upper and lower respiratory tracts, with little or no infectious particles detected in either the lungs or nasal turbinates at three days post-infection (dpi) (Figure 4.3C). Consistently, subgenomic viral mRNA (sgmRNA) levels were also reduced at both sites 3-dpi (Figure 4.3D). Histopathological analysis revealed no overt signs of inflammation or infection-associated tissue damage in the lungs collected from vaccinated animals at either 3- or 6-dpi (Figure 4.3E, Supplemental Figure 4.2). Collectively, these data show that DNA-LNP vaccination can provide a level of protection against SARS-CoV-2 challenge that is comparable with mRNA-LNP vaccination three weeks post-boost.

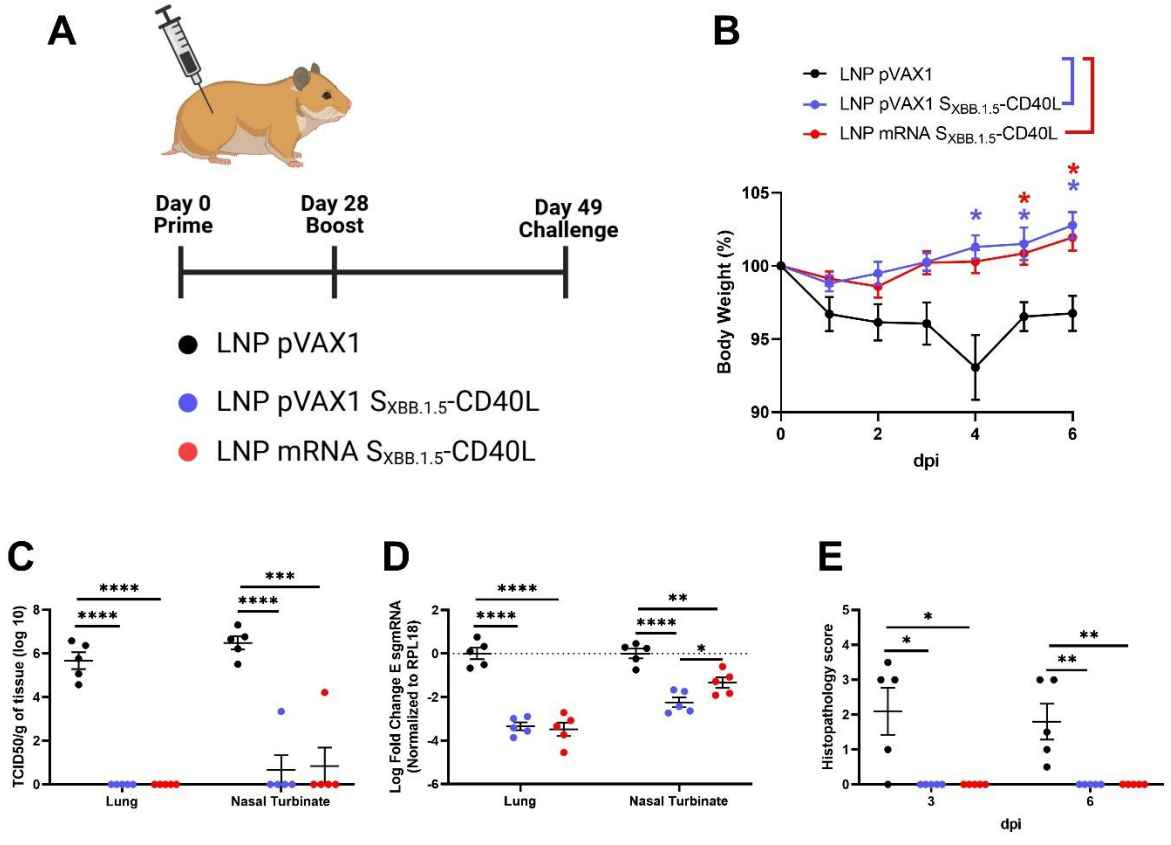

Figure 4.3 DNA- and mRNA-LNPs provide significant protection against XBB.1.5 challenge in Syrian hamsters.

(A) Immunized Syrian hamsters were challenged intranasally with 1.67×10^5 TCID50 of a SARS-CoV-2 XBB.1.5 isolate on day 49 post-vaccination and euthanized 3- (n = 5 per group) or 6-dpi (n = 5 per group). Created in BioRender. Tamming, L. (2026) https://BioRender.com/utj7sy7. **(B)** Body weight measured daily post-challenge. **(C)** TCID50 determined in lung and nasal turbinate tissues collected 3-dpi. **(D)** SARS-CoV-2 E sgmRNA expression in the lung and nasal turbinates collected 3-dpi determined via RT-qPCR. Normalized to *RPL19* mRNA expression. **(E)** Summary of pulmonary histopathological scores 3- and 6-dpi. Data shown are mean ± SEM. $**p < 0.01$, $***p < 0.001$, $****p < 0.0001$.

To assess the durability of protection, immunized hamsters were challenged with a SARS-CoV-2 XBB.1.5 isolate on day 203, approximately six months post-boost vaccination (Figure 4.4A). While the DNA-LNP continued to afford a high level of protection at this timepoint, multiple endpoints suggested that the mRNA-LNP conferred minimal protection, mirroring the observed decline in humoral immunity. Only the DNA-LNP vaccine significantly protected against weight loss following challenge (Figure 4.4B). Correspondingly, little or no infectious virus was detected in the lungs and nasal turbinates of DNA-LNP-immunized animals at 3-dpi (Figure 4.4C). In contrast, mRNA-LNP-vaccinated animals exhibited substantially higher viral burden (Figure 4.4C) and viral sgmRNA levels (Figure 4.4D). While no overt histopathological signs of infection were detected in DNA-LNP-vaccinated hamsters at both 3- and 6-dpi, lungs from mRNA-LNP–vaccinated hamsters exhibited pronounced inflammatory cell infiltration and tissue consolidation 6-dpi (Figure 4.4E, Supplemental Figure 4.3 & 4.4 and Supplemental Table 4.1). Together, these findings demonstrate that DNA-LNP vaccination sustains robust protective efficacy for at least six months post-boost vaccination.

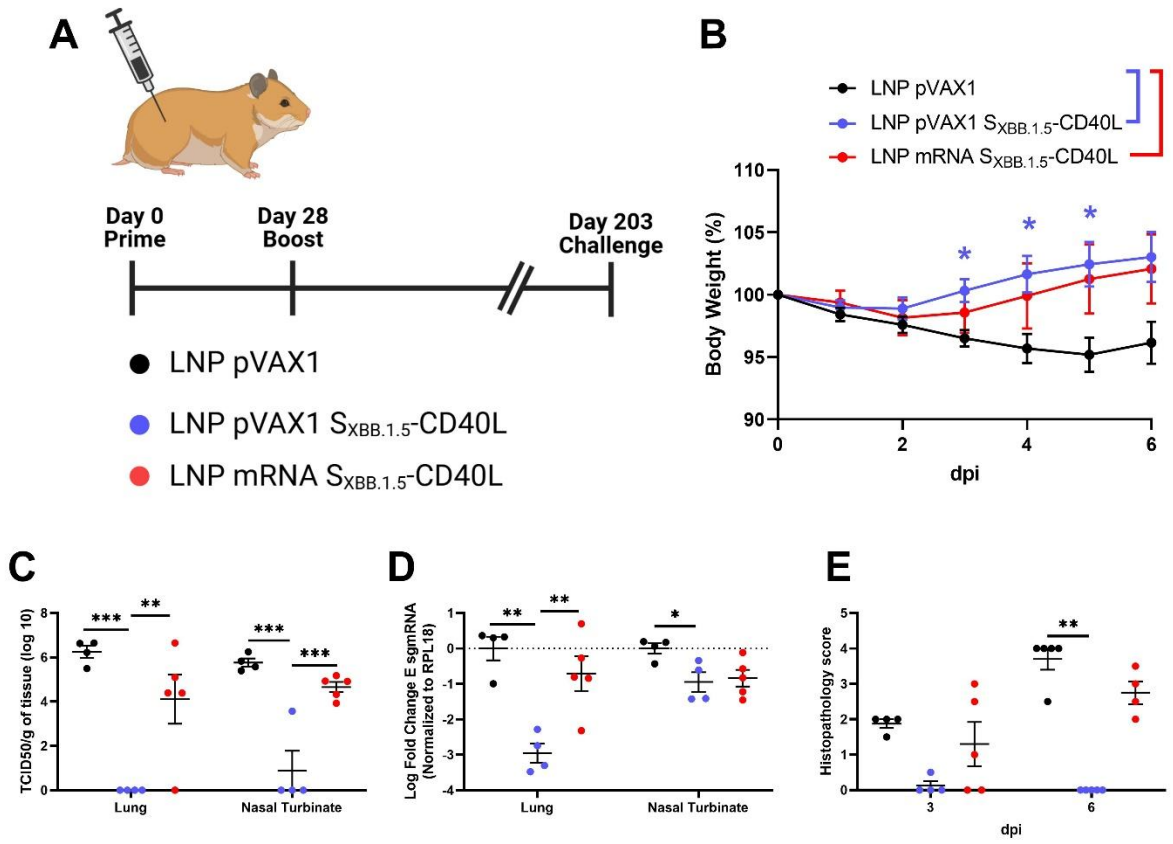

Figure 4.4 $S_{XBB.1.5}$-CD40L DNA-LNPs provide durable protection 6-months post-boost in Syrian hamsters.

(A) Immunized Syrian hamsters were challenged intranasally with 1.67×10^5 TCID50 of a SARS-CoV-2 XBB.1.5 isolate on day 203 post-vaccination and euthanized 3- (n = 4-5 per group) or 6-dpi (n = 4-5 per group). Created in BioRender. Tamming, L. (2026) https://BioRender.com/79on9si. **(B)** Body weight measured daily post-challenge. **(C)** TCID50 determined in lung and nasal turbinate tissues collected 3-dpi. **(D)** SARS-CoV-2 E sgmRNA expression in the lung and nasal turbinates collected 3-dpi determined via RT-qPCR. Normalized to *RPL19* mRNA expression. **(E)** Summary of pulmonary histopathological scores 3- and 6-dpi. Data shown are mean ± SEM. $*p < 0.05$, $**p < 0.01$, $***p < 0.001$, $****p < 0.0001$.

4.4 Discussion

In this study, we demonstrate that DNA-LNP vaccines provide durable immunity against the SARS-CoV-2 XBB.1.5 variant, affording better long-term protection than a similar mRNA-LNP

formulation. Recent studies have highlighted DNA-LNPs as a promising next-generation vaccine platform (23–27,34–37). Some of these studies have demonstrated that DNA-LNPs are capable of inducing comparable or even superior immune responses than mRNA-LNPs (25,26) . Notably, these studies have also highlighted how DNA- and mRNA-LNPs differ in terms of their antigen kinetics and immune engagement. Whereas mRNA-LNPs generate potent but short-lived antigen expression, DNA-LNPs sustain expression for much longer, with detectable expression often persisting beyond one month (26,28,29). DNA-LNPs also appear to be more inflammatory than nucleoside-modified mRNA-LNPs, triggering strong innate immune responses through STING-sensing pathways (26,29). How these factors influence the overall adaptive immune response induced by DNA-LNPs remains to be fully elucidated. While a few studies have reported the durability of humoral and cellular responses elicited by DNA-LNPs (25,26), none to our knowledge have directly demonstrated their ability to confer long-term protection against viral challenge.

We have previously established that fusion of CD40L to the SARS-CoV-2 S enhances the magnitude and breadth of humoral responses induced by DNA and DNA-LNP vaccines (31,32). As such, we first assessed whether the benefits of this approach extended to mRNA-LNP vaccines. Consistent with other platforms, $S_{XBB.1.5}$-CD40L mRNA-LNPs induced greater humoral and CD4+ T cell responses. This enhancement appeared to primarily affect Th1 responses, which are critical for protection against intracellular pathogens such as SARS-CoV-2. To the best of our knowledge, this is the first report of an antigen-CD40L fusion delivered by mRNA-LNP vaccination against an infectious pathogen. Prior studies investigating CD40L as a molecular adjuvant have shown its capacity to promote germinal centre (GC) formation (38). GC reactions are linked to the generation of high-affinity LLPCs which are the primary producers of circulating antibodies (39). Despite this

link, the $S_{XBB.1.5}$-CD40L mRNA-LNP vaccine did not sustain a long-lived humoral response, with antibody levels waning markedly by six months post-boost vaccination, and correspondingly appeared to afford only minimal protection at this later point. Co-administration of mRNA encoding interleukin (IL)-12p70 or IL-7 has been shown to enhance GC activity and increase the durability of humoral responses, although such adjuvanted vaccines still exhibit substantial waning over extended follow-up (40,41). Together, these observations suggest that while molecular adjuvants can strengthen GC responses, they may not fully overcome durability limitations intrinsic to mRNA-LNPs.

In contrast, both $S_{XBB.1.5}$ and $S_{XBB.1.5}$-CD40L DNA-LNP vaccines maintained robust antibody responses over the same six-month period and preserved a high level of protection. Consistent with our observations, Tursi et al. reported that DNA-LNP induced immune responses were more durable than mRNA-LNP induced responses, having greater $CD8^+$ T cell recall responses in mice one-year post-vaccination and stronger humoral responses in rabbits after six months (26). Paradoxically, Tursi et al. also observed that DNA-LNPs generated weaker GC responses than mRNA-LNPs, suggesting that the sustained humoral immunity may be driven by other factors (26). The half-life of nucleoside modified mRNA upon intramuscular injection is estimated to be less than 24 h, which is reflected by its short antigen expression window (42). Circular RNA vaccines, which are intrinsically more resistant to degradation because of their closed-loop structure, prolong antigen expression and induce superior and more durable humoral responses (43–45). Likewise, mRNA-1723 readenylation by TENT5a in a subset of innate immune cells has been shown to delay transcript degradation, prolonging expression and enhancing humoral responses (46). These findings from mRNA vaccine studies indicate that prolonged antigen expression, whether achieved through molecular design or cellular processes, can strongly

influence vaccine durability. Further studies are required to define the full duration of DNA-LNP antigen expression *in vivo*, to identify which cell populations sustain this expression, and to determine whether it is the critical factor supporting the durable immunity observed here and in previous studies(25,26). Fate-mapping approaches have demonstrated that the accumulation of LLPCs in the bone marrow scales with the duration of immune responses(47). The prolonged antigen expression following DNA-LNP vaccination may extend GC activity and thereby increase LLPC recruitment to the bone marrow. It also remains unclear how DNA-LNP vaccination affects the quality of humoral responses, and whether it drives the generation of higher-avidity antibodies which can enhance the potency and breadth of SARS-CoV-2 NAbs(48). Future work should assess GC activity, bone marrow LLPC numbers and antibody avidity at multiple times following DNA-LNP vaccination.

A key limitation of this study is the limited number of DNA- and mRNA-LNP doses evaluated. Notably, most published studies comparing DNA- and mRNA-LNPs have done so using equivalent nucleic acid masses(25,26) , although this can represent substantial differences in both the molar amount of each nucleic acid delivered and in the quantity of immunogenic lipids administered. Relative to mRNA vaccines, which can immediately be translated upon endosomal escape, DNA vaccines must additionally cross the nuclear membrane to enable transcription of the encoded antigen. Even when administered at a 25-fold mass excess relative to mRNA-LNPs, DNA-LNPs induce over 10-fold less antigen expression within the first four weeks (28). On this basis, we selected a 5 μg DNA-LNP dose and a 2.5 μg mRNA-LNP dose, with the goal of assessing the relative durability of each platform following an approximately equivalent initial immune response. While previous reports suggest equivalent mass doses would yield similar results (25,26), this was not assessed in the present work. In addition, this study was limited by relatively

small group sizes (n = 4-5), which may limit the robustness of individual protection endpoints. Future studies should employ a more rigorous approach, systematically comparing the two platforms across a broad range of doses, including molar nucleic acid equivalents and doses controlling for equivalent total lipid mass, to definitively evaluate the relative strengths and limitations of each platform.

Assessing the durability of DNA-LNP-induced immunity across multiple animal models will be critical. Liao et al. reported marked differences in the magnitude and duration of DNA- and mRNA-LNP responses across species, with DNA-LNPs eliciting the strongest immunity in hamsters (25). Notably, DNA-LNPs have displayed different reactogenicities in different models and can elicit highly inflammatory responses(29,37). Additional studies in diverse models, genetic backgrounds and, ultimately, in humans will be essential to delineate the true potential and limitations of this platform. Future studies should also determine whether DNA-LNPs are compatible with high-risk or immunocompromised populations, in whom excessive inflammation could pose safety concerns.

In summary, this study establishes that DNA-LNP vaccines can provide durable protection against the SARS-CoV-2 XBB.1.5 variant, outperforming an otherwise comparable mRNA-LNP vaccine. We demonstrate that DNA-LNP vaccination maintains antibody responses and protective outcomes for at least six months post-boost vaccination in Syrian hamsters. These findings position DNA-LNPs as a promising next-generation vaccine modality with the potential to address the issue of rapidly declining antibody responses observed with current mRNA vaccines.

4.5 Methods

4.5.1 Cell lines and viruses

BHK-21 (RRID:CVCL_1915) and HEK293T-ACE2 (SL221; RRID:CVCL_C9BE) cells were cultured in Dulbecco's modified Eagle's medium (DMEM, Thermo Fisher) supplemented with 25 mM HEPES, 1X non-essential amino acid (NEAA), 20 U/mL penicillin, 0.02 mg/mL streptomycin, and 10% heat-inactivated fetal bovine serum (FBS). Vero-TMPRSS2 cells (RRID:CVCL_YQ49) were cultured in DMEM with L-glutamine supplemented with 1X NEAA, 1 mM sodium pyruvate, and 5% FBS. The XBB.1.5 SARS-CoV-2 viral isolate hCoV-19/USA/MD-HP40900/2022 (NR-59104) was obtained from BEI resources. The virus was propagated and titered using Vero-TMPRSS2 cells and sequenced to confirm genetic fidelity. Passage four virus stocks were used for all experiments that required live virus.

4.5.2 Animal care

Animal experiments and procedures were either approved by the Animal Care Committee at Health Canada or at National Research Council Canada (NRC). All work was performed by trained staff in accordance with regulations and guidelines set by the Canadian Council on Animal Care. All infectious work was carried out under ABSL-3 conditions at the NRC. All animals were purchased from Charles River Laboratories (Senneville, QC). Euthanasia was performed by cardiac puncture exsanguination and cervical dislocation under isoflurane anesthesia.

4.5.3 DNA and mRNA vaccine design and synthesis

The vaccine antigens were designed as previously described (31). Briefly, the SARS-CoV-2 XBB.1.5 S (GenBank: UZG29433.1) ectodomain (residues 1-1199) was mutated to have a "GSAS" substitution at the furin cleavage site (residues 678-681) and pre-fusion stabilizing proline

substitutions at residues 982 and 983. The antigen was trimerized by fusion to a T4 fibritin foldon domain. The antigen was then optionally fused to the CD40L ectodomain of Mesocricetus auratus (GenBank: XM_005084522.4, residues 118-260) or of Mus musculus (GenBank accession #NM_011616, residues 118-260). Domains were separated by flexible glycine-serine linkers sequences “GSGG”. Domain coding sequences were individually codon optimized for expression in Mus musculus and Mesocricetus auratus by GenScript. DNA coding sequences were commercially synthesized (Genscript) and then subcloned into pVAX1 (Invitrogen) using KpnI/XhoI or KpnI/NotI restriction enzymes. Bulk DNA vaccine preparations were prepared using endotoxin-free gigaprep kits (Qiagen). mRNA vaccines with matching coding sequences were commercially synthesized by TriLink Biotechnologies with a CleanCap®AG Cap 1 structure and a 120A polyadenylated tail. mRNA was DNAse and phosphatase treated and purified by silica membrane. All mRNA was fully substituted with N1-methyl-pseudouridine.

4.5.4 DNA-LNP and mRNA-LNP preparation

DNA- and mRNA-LNPs were synthesized as previously described within 48 h of vaccination and stored at 4°C (28,32). Briefly, the aqueous phase was prepared by suspending DNA in 25 mM acetate buffer (pH 4.0) or mRNA in 50 mM citrate buffer (pH 4.0). The organic phase was prepared in ethanol and consisted of SM-102 (MedKoo Biosciences), 1,2-distearoyl-sn-glycero-3-phosphocholine (DSPC, Avanti Polar Lipids), ovine cholesterol (Cholesterol, Millipore Sigma), and DMG-PEG2000 (Millipore Sigma) at a 50:10:38.5:1.5 percent molar ratio respectively. The aqueous and organic phases were mixed with a polymer amine (N = nitrogen) group to nucleic acid phosphate (P) group (N/P) ratio of 6:1 using a NanoAssemblr Ignite instrument (Precision Nanosystems). LNPs were dialyzed against Dulbecco's phosphate-buffered saline (DPBS) for 18 h at 4°C in a 10kDa MWCO cassette (Thermo Fisher). Prior to vaccination, LNPs were passed

through a 0.22 μm filter and concentrated using an Amicon Ultra 4 10 k MWCO centrifugal concentrator (Millipore Sigma). Nanoparticle size was measured using a NanoSight NS300 (Malvern Panalytical). LNP encapsulation efficiency was measured by disrupting LNPs with 1% Triton X-100 (Millipore Sigma) and adding SYBR™ Gold dye (Thermo Fisher) (Supplemental Table 4.2 & 4.3).

4.5.5 Immunization and SARS-CoV-2 challenge

All animals were randomly divided into experimental groups. Female BALB/c mice (6-8 weeks-old) were vaccinated with 2.5 μg of DNA-LNPs or 1.25 μg of mRNA-LNPs, resuspended in 50 μL of PBS. Male Syrian hamsters (6-8 weeks old) were vaccinated with 5 μg of DNA-LNPs or 2.5 μg of mRNA-LNPs, resuspended in 100 μL of PBS. Injection volumes were divided evenly between both tibialis anterior muscles with a needle syringe on day 0 and day 28. Animals were bled at the time points indicated in the figure legends/text to assess antibody responses. On day 49 or 203 post-vaccination the hamsters were intranasally challenged with 1.67 ×105 TCID50 of XBB.1.5 SARS-CoV-2. Hamsters were weighed daily and euthanized either 3- or 6-days post-challenge to assess viral burden and pathology.

4.5.6 Enzyme-linked immunosorbent assay (ELISA)

S-specific antibody titers were determined as previously described (31). Briefly, Nunc MaxiSorp flat-bottom 96-well plates (Thermo Fisher) were coated with 1 μg/mL of recombinant XBB.1.5 S protein diluted in PBS overnight at 4°C. Recombinant XBB.1.5 S protein (PRO8581 [SmT2v3 (XBB.1.5)] was obtained from the National Research Council of Canada, which was produced as previously described (49). Plates were washed with PBS containing 0.1% Tween 20 (PBS-T) before blocking with 3% (w/v) bovine serum albumin (BSA, IgG-free) (Jackson ImmunoResearch) in PBS-T for 2 h at 37°C. After washing, plates were incubated for 1 h at 37°C

with mouse or hamster serum serially diluted in blocking buffer. After additional washes, the plates were incubated with either 1:2000 HRP-conjugated anti-mouse IgG (RRID:AB_772210) or 1:4000 HRP-conjugated anti-hamster IgG (RRID:AB_2337454) for 1 h at 37°C. After a final wash, plates were developed for 5 minutes using tetramethylbenzidine (TMB) substrate (Cell Signaling Technology) before being stopped with the addition of 0.16 M sulfuric acid. Absorbance values were measured at 450 nm with a Synergy 2 (BioTek) plate reader. Endpoint titers were expressed as the reciprocals of the final detectable dilution with an optical density (OD) above the cutoff value (average OD of control samples plus three standard deviations).

4.5.7 Pseudovirus neutralization assay

SARS-CoV-2 S-pseudotyped VSV was generated by concurrently infecting BHK-21 cells with G∗ΔG-VSV (Kerafast, EH1020-PM) and transfecting them pDNA vectors encoding SARS-CoV-2 S Δ19 as previously described (50). A pLV vector encoding XBB.1.5 was synthesized commercially by Genscript. A vector encoding KP.3.1.1 was a gift from David Nemazee (Addgene plasmid #233342). After 48 and 72 h, supernatant was collected, passed through a 0.45 μm filter and stored at -80°C until use. For neutralization assays, heat inactivated serum samples were serially diluted in a white 96-well plate and incubated with the pseudovirus for 1 h at 37°C. After, 6×10^4 HEK293T-ACE2 cells were added and plates were incubated for 24 h at 37°C 5% CO_2. Luminescence was measured using Bright-Glo luciferase reagent (Promega) and a Synergy 2 (BioTek) plate reader. 50% neutralization titers (NT50) were measured as the reciprocal dilution at which a 50% reduction in relative light units (RLU) was observed relative to no-serum controls.

4.5.8 Quantification of viral burden

XBB.1.5 SARS-CoV-2 viral burden was determined as previously described (32). Briefly, lung and nasal turbinate tissues were homogenized in PBS using a Precellys Evolution. Spin-clarified

supernatants were serially diluted before being adsorbed on Vero-TMPRSS2 cells seeded in 96-well plates for 1 h at 37°C, 5% CO_2. After the incubation, the media was replaced and the plates were incubated at 37°C, 5% CO_2 for 5 days. Observed cytopathic effects were recorded and the 50% Tissue Culture Infectious Dose (TCID50) was calculated per g of tissue using the Reed-Muench method (51).

4.5.9 RNA extraction and quantitative reverse-transcription PCR (qRT-PCR)

Lung and nasal turbinate tissues were homogenized in RNA shield buffer (Zymo Research) using a Precellys Evolution. RNA was extracted from the homogenized samples using a Quick-RNA Viral Kit (Zymo Research). RNA expression was quantified using a one-step Fast Virus master mix (Thermo Fisher) and either an E sgmRNA- or RPL18-specific TaqMan primer/probe set (52,53). E sgmRNA expression was normalized to RPL18 expression using the ddCT method (54). All RT-qPCR reactions were conducted in MicroAmp Fast Optical 96 wells with an Applied Biosystems 7500 Fast Real-time PCR instrument.

4.5.10 Histopathology

Histopathology processing and analysis was conducted as described previously (31). Briefly, right lung lobes were fixed for 72 h in 10% neutral buffered formalin and processed by routine paraffin embedding methods (55). Four-micrometer-thick sections were stained with hematoxylin-eosin (H&E) and examined under microscopy. The severity and extent of pneumonia was scored blinded based on previously established criteria, sampling five fields per lung(56). For the long-term study 6 dpi timepoint, the severity and extent of pneumonia in individual lung lobes was also scored (**Supplemental Table 4.1**). Representative histopathology images are shown in **Supplemental Figure 4.2-4.4**.

4.5.11 Mouse Tissue Processing

Spleens from vaccinated mice were collected three weeks post-boost vaccination and homogenized with a gentleMACS™ Dissociator (Miltenyi Biotec) using the m_spleen_01 program. Splenocytes were filtered using a 70 μm cell-strainer before being resuspended in ACK lysis buffer for 3 minutes at room temperature. Lysis was quenched by the addition of PBS and splenocytes were resuspended in RPMI 1640 media (Thermo Fisher) supplemented with 20 U/mL penicillin, 0.02 mg/mL streptomycin, and 10% heat-inactivated FBS. Splenocytes were counted using a Sysmex XT-2000iV haematology analyzer and then used in downstream assays.

4.5.12 Enzyme-linked immunosorbent spot (ELISpot) assay

IFNγ secretion from splenocytes was measured using a Murine IFNγ Single-Color Enzymatic ELISPOT assay (ImmunoSpot) according to the manufacturer's protocol. For stimulation, splenocytes were stimulated with 1 μg/mL of an overlapping SARS-CoV-2 Omicron XBB.1.5.X Spike Protein Peptide Pool (StemCell Technologies Cat# 100-1422). DMSO was used as a negative control. Plates were incubated for 20 h at 37°C 5% CO_2 before being developed. Spots were counted using an ImmunoSpot® S6 Analyzer and reported per million splenocytes.

4.5.13 Intracellular Cytokine Staining

Splenocytes were stimulated with 1 μg/mL of an overlapping peptide pool (as in ELISpot) for 5 h at 37 °C, 5% CO_2. Samples were supplemented with GolgiPlug and GolgiStop Protein Transport Inhibitors (BD Bioscience) 45 minutes into the stimulation. Stimulated cells were washed with PBS and then incubated with a viability stain and surface marker antibody cocktail for 30 minutes at 4°C. The cocktail contained LIVE/DEAD™ Fixable Violet Dead Cell Stain (Thermo Fisher), anti-CD3 PerCP-Vio® 700 REAfinity™ (Miltenyi Biotec Cat# 130-120-826,

RRID:AB_2752207), anti-CD4 VioGreen™ REAfinity™ (Miltenyi Biotec Cat# 130-118-693, RRID:AB_2734087), and anti-CD8a PE-Vio® 770 REAfinity™ (Miltenyi Biotec Cat# 130-118-946, RRID:AB_2733251). Stained cells were washed with PBS + 0.5% BSA + 2 mM EDTA (FACS buffer) and then fixed/permeabilized using BD cytofix/cytoperm (BD Biosciences) for 20 minutes at 4°C. Cells were washed in Perm/Wash (BD Bioscience) and then stained with intracellular antibody cocktail for 20 minutes at 4°C. This cocktail contained anti-IFNγ FITC REAfinity™ (Miltenyi Biotec Cat# 130-123-283, RRID:AB_2819467), anti-TNF-α PE REAfinity™ (Miltenyi Biotec Cat# 130-119-561, RRID:AB_2784485), and anti- IL-2 APC REAfinity™ (Miltenyi Biotec Cat# 130-129-192, RRID:AB_2922001). Cells were resuspended in FACS buffer and stored at 4°C prior to analysis by flow cytometry (FACSymphoney A1) the next day. Data analysis was completed using FlowJo version 10.10.0 (RRID:SCR_008520). Gating strategy is shown in Supplementary Figure 4.5.

4.5.14 Quantification and statistical analysis

Statistical analyses were performed using GraphPad Prism 9 (RRID:SCR_002798). Normality and homoscedasticity of raw or log-transformed data were assessed using the Shapiro–Wilk test and Brown–Forsythe test, respectively ($\alpha = 0.05$). A repeated-measures two-way analysis of variance (RM two-way ANOVA) with Tukey's multiple-comparisons test was used for pairwise (between-group) comparisons of body-weight data. A non-parametric Kruskal–Wallis test with Dunn's multiple-comparison correction was used for pairwise comparisons of histopathology scores. For all other data, a one-way ANOVA with Tukey's multiple-comparisons test was applied to raw data (subgenomic mRNA) or log-transformed data (ELISA, NT50, ELISpot, ICS, TCID50, Fold Change). The number of samples for each graph is indicated in the figure legends. In all datasets, $*p < 0.05$, $**p < 0.01$, $***p < 0.001$, $****p < 0.0001$

4.6 Data Availability

All data supporting the conclusions of this study are present in the main text and supplementary materials. Additional information is available from the corresponding authors upon request.

4.7 Acknowledgements

We gratefully acknowledge the histology and staining services provided by the Louise Pelletier HCF at the University of Ottawa. We gratefully acknowledge the technical contribution of Simon Lord-Dufour, Brian Cass and Louis Bisson at the NRC-HHT for recombinant S production. We also would like to acknowledge the assistance provided by the Animal Care Facility staff at Health Canada and the National Research Council of Canada. We thank Dr. Lu Huixin and Dr. Roger Tam for commenting on the manuscript and Greg Beaudoin for preparing the photomicrographs. Schematic representations were created in BioRender. This work is supported by the Government of Canada (intramural funding from Health Canada).

4.8 Author contribution statement

Conceptualization, L.T., A.T., M.J.W.J., X.L.; Methodology, L.T., C.L., W.Z., G.F., M.S., A.T.; Formal Analysis and Visualization, L.T., A.S.; Investigation, L.T., C.L., W.Z., D.D., J.B., G.F., A.P., S.N.R. J.W., C.G., A.S., W.C.; Resources, C.L., S.N.R., C.G., M.S., Y.D., A.T.; Writing - Original Draft, L.T.; Writing - Review & Editing, L.T., C.L., W.Z., D.D., J.B., G.F., A.P., S.N.R. J.W., C.G., A.S., M.S., Y.D., W.C., L.W., S.S., A.T., M.J.W.J., X.L.; Supervision, Y.D., L.W., S.S., A.T., M.J.W.J., X.L.; Project Administration L.T., A.T., M.J.W.J., X.L.; Funding Acquisition, Y.D., L.W., S.S., A.T., M.J.W.J., X.L.;

4.9 Competing interests

The Authors declare no Competing Financial or Non-Financial Interests.

4.10 Supplementary Information

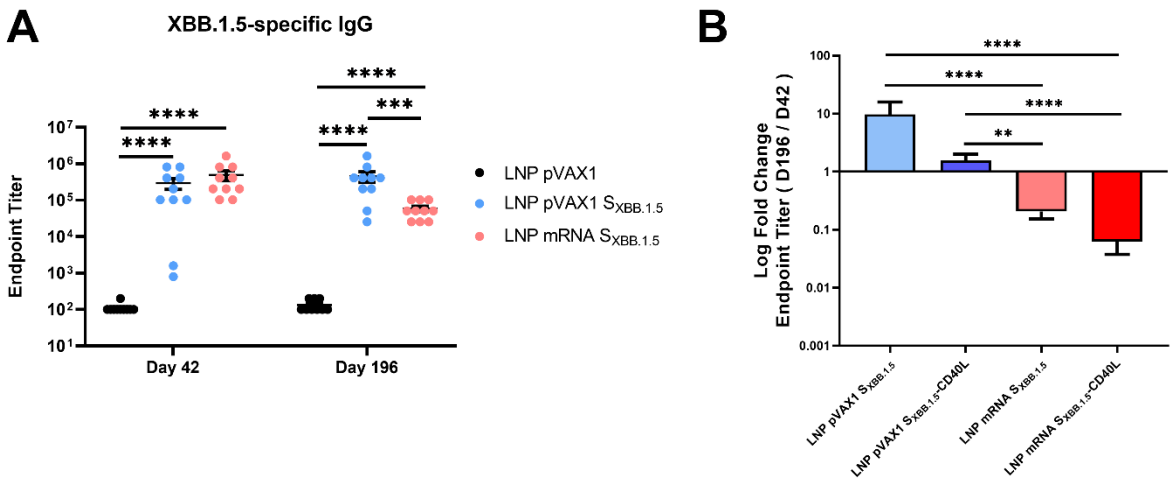

Supplemental Figure 4.1 Longevity of DNA-LNP immunity is independent of CD40L.

(A) Male Syrian hamsters were immunized intramuscularly on day 0 and 28 with 5 µg of $S_{XBB.1.5}$ DNA-LNP or 2.5 µg of $S_{XBB.1.5}$ mRNA-LNP. Control hamsters were vaccinated with 5 µg of pVAX1 DNA-LNP. XBB.1.5 Spike-specific IgG in the serum was determined by ELISA on day 42 or 196 post-vaccination. **(B)** Log fold change in endpoint titers between days 42 and 196 (D196/D42) for $S_{XBB.1.5}$ and $S_{XBB.1.5}$-CD40L (See Figure 4.2) vaccines. Data shown are mean ± SEM, n= 10. $^{**}p < 0.01$, $^{***}p < 0.001$, $^{****}p < 0.0001$.

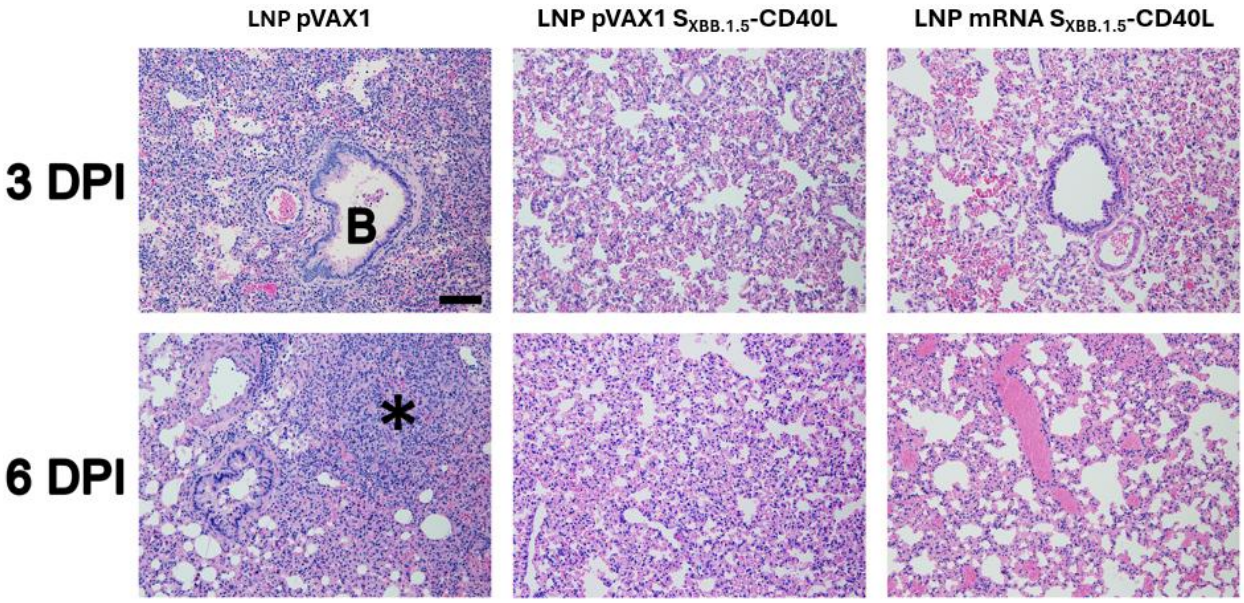

Supplemental Figure 4.2 Short-Term Lung Pathology.

Representative photomicrograph of H&E stained lung tissues. Immunized Syrian hamsters were intranasally challenged with an isolate of SARS-CoV-2 XBB.1.5 on day 49. B, bronchioles; *, area of inflammatory cell infiltration and tissue consolidation. Scale bar, 100 μm. Related to Figure 4.3.

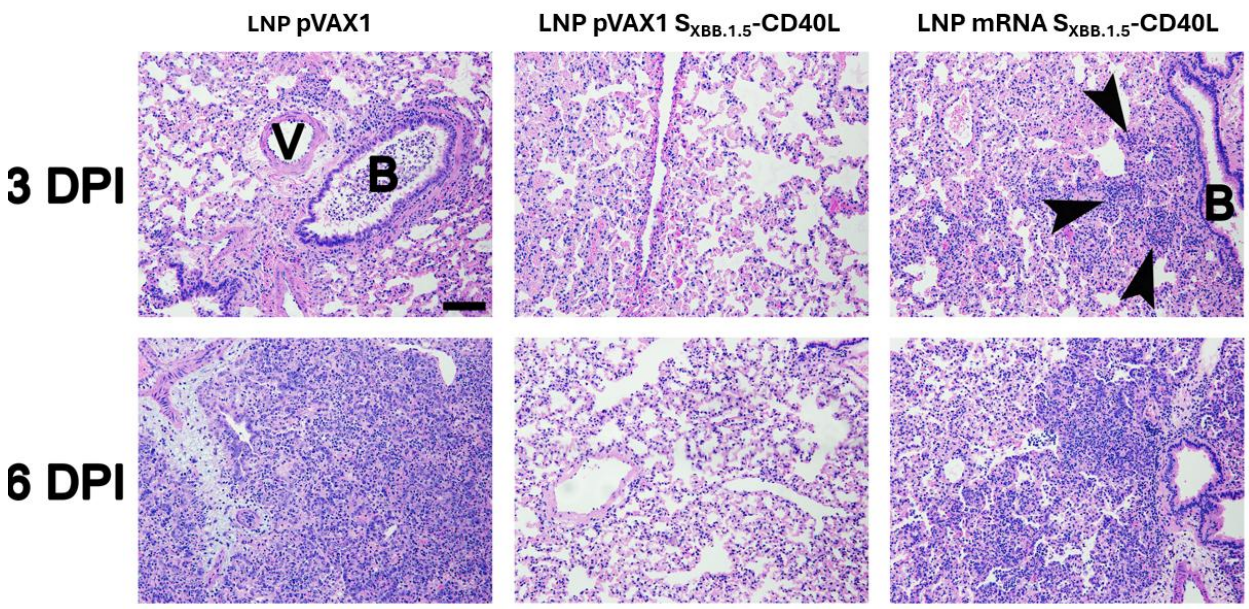

Supplemental Figure 4.3 High Magnification Long-Term Lung Pathology.

Representative photomicrograph of H&E-stained lung tissues. Immunized Syrian hamsters were intranasally challenged with an isolate of SARS-CoV-2 XBB.1.5 on day 203. B, exudate of inflammatory cells in the lumen of a bronchus; V, blood vessel. Arrows, peri-airway inflammatory cell infiltration and tissue consolidation. Scale bar, 100 μm. Related to Figure 4.4.

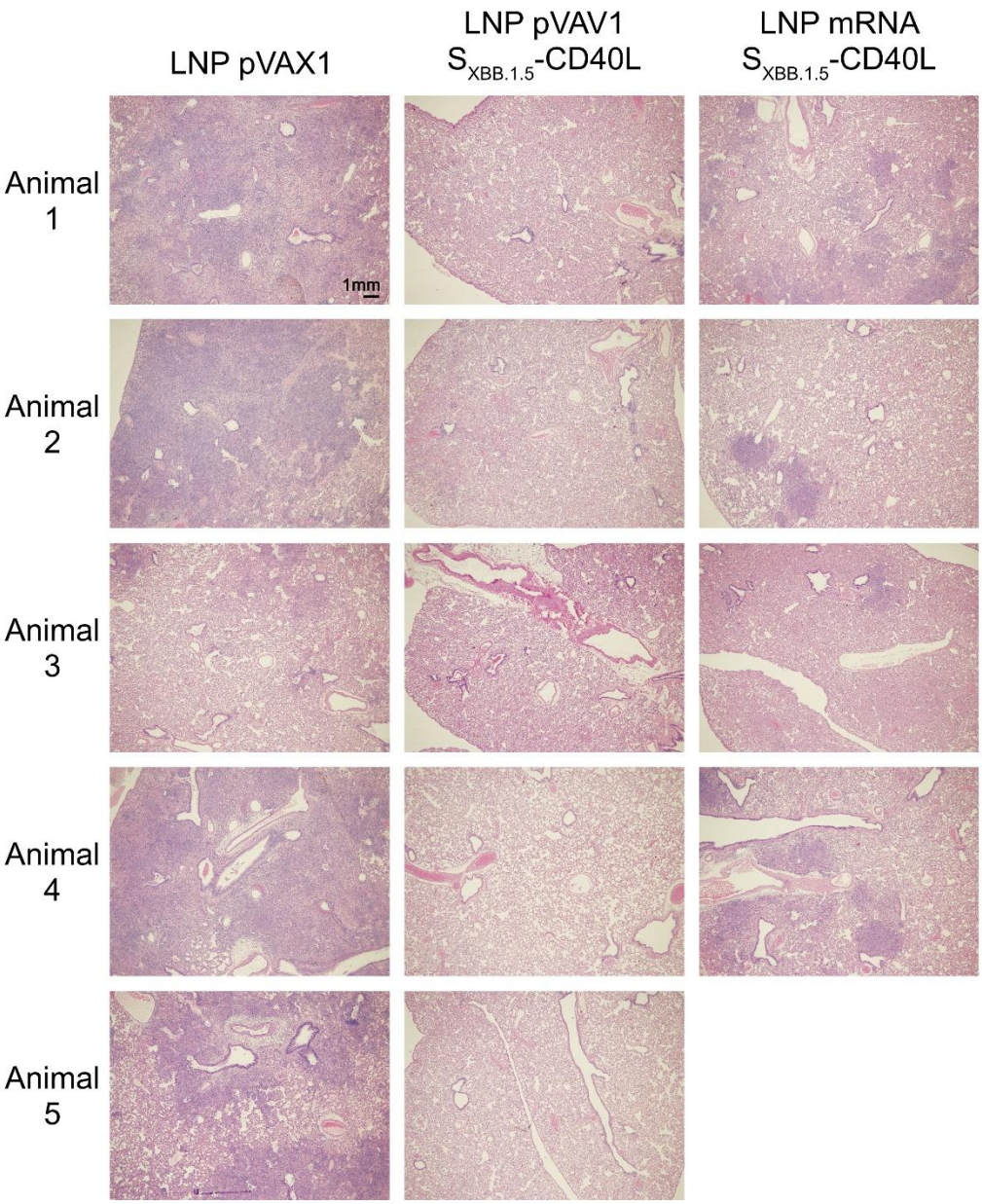

Supplemental Figure 4.4 Low Magnification Long-Term Lung Pathology.

Representative photomicrograph of H&E-stained lung tissues at 1X magnification, demonstrating global lung morphology at 6-dpi. Immunized Syrian hamsters were intranasally challenged with an isolate of SARS-CoV-2 XBB.1.5 on day 203. Related to Figure 4.4.

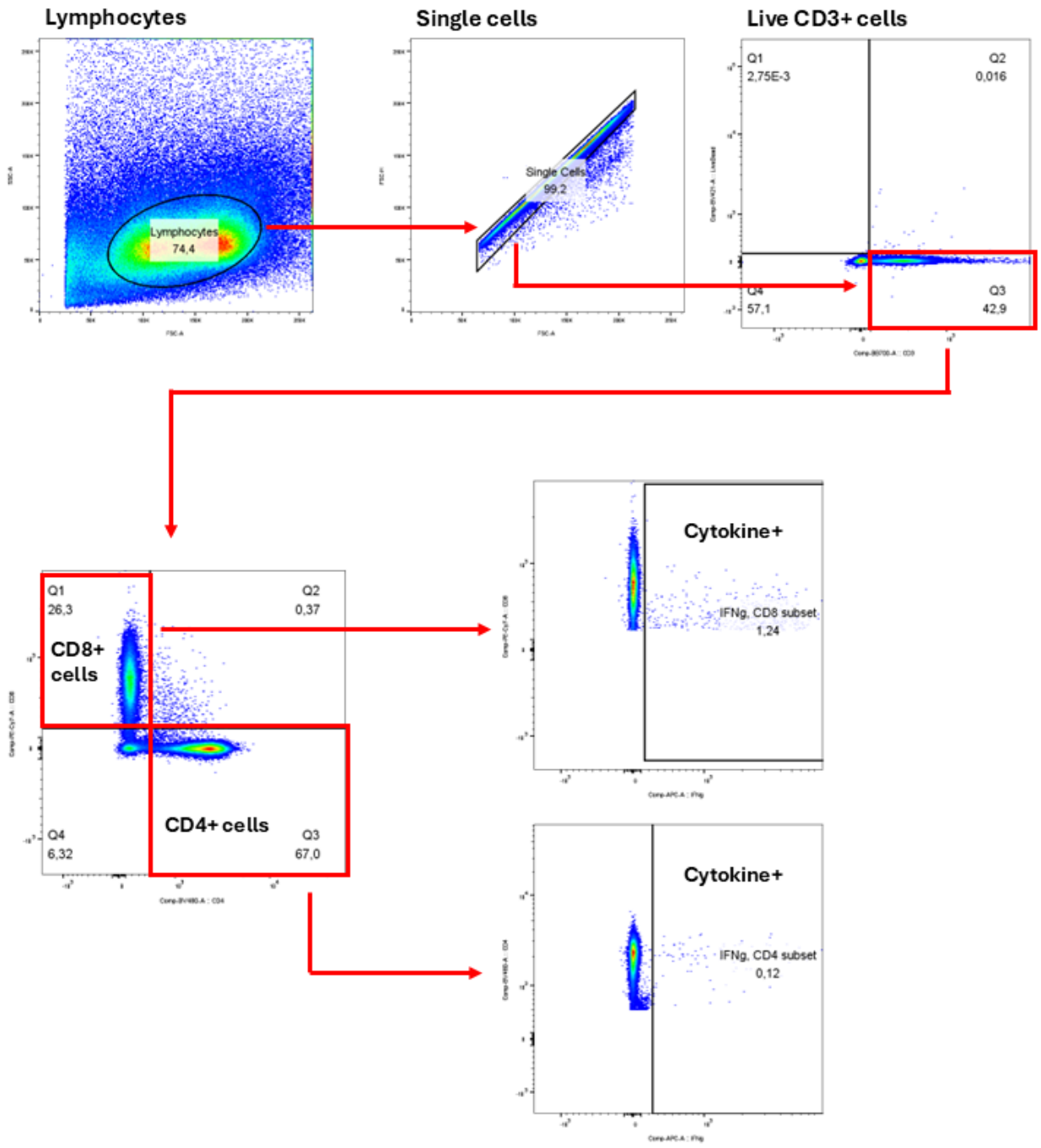

Supplemental Figure 4.5 T cell gating strategy.

Gating strategy for cytokine expression in $CD4^+$ and $CD8^+$ T cells isolated from BALB/c spleens. Representative plots from a $S_{XBB.1.5}$-CD40L mRNA-LNPs vaccinated mouse. Related to Figure 4.1.

Supplemental Table 4.1 Long-Term Lung Pathology Per Lobe.

Immunized Syrian hamsters were intranasally challenged with an isolate of SARS-CoV-2 XBB.1.5 on day 203. At 6-dpi, the severity and extent of pneumonia was assessed independently for each right lung lobe (labeled arbitrarily from A-D). Related to Figure 4.4.

	LNP pVAX1					LNP pVAX1 $S_{XBB.1.5}$-CD40L					LNP mRNA $S_{XBB.1.5}$-CD40L			
Lobe	1	2	3	4	5	1	2	3	4	5	1	2	3	4
A	4	4	0.5	4	4	0	0	0	0	0	4	2.5	1.5	3
B	4	4	3	4	4	0	0	0	0	0	3.5	3	1.5	3
C	4	4	2.5	3	4	0	0	0	0	0	2	1	2	3
D	3	-	-	4	3	0	0	0	-	0	0	-	2	3

Supplemental Table 4.2 Characterization of mouse DNA- and mRNA-LNP vaccines.

Biophysical characterization parameters of DNA- and mRNA-LNP vaccines used in BALB/c studies. Mean particle diameter measured by nanoparticle tracking analysis (NTA). Encapsulation efficiency determined by SYBR™ Gold assay. NT, nucleotides. BP, base pairs. SD, standard deviation. Related to Figure 4.1.

Vaccine (length, NT or BP)	Prime/Boost	LNP Diameter (Mean ± SD , nm)	Encapsulation efficiency (%)
pVAX1 (2999)	Prime	67.5 ± 10.7	97.6
	Boost	69.1 ± 12.1	96.0
mRNA $S_{XBB.1.5}$ (3659)	Prime	69.2 ± 13.0	88.5
	Boost	74.0 ± 14.9	86.0
mRNA $S_{XBB.1.5}$-CD40L (4102)	Prime	72.2 ± 14.8	83.9
	Boost	75.4 ± 17.6	80.7

Supplemental Table 4.3 Characterization of hamster DNA- and mRNA-LNP vaccines.

Biophysical characterization parameters of DNA- and mRNA-LNP vaccines used in Syrian hamster studies. Mean particle diameter measured by NTA. Encapsulation efficiency determined by SYBR™ Gold assay. NT, nucleotides. BP, base pairs. SD, standard deviation. Related to Figure 4.2-4.4 and Supplemental Figure 4.1.

Vaccine (length, NT or BP)	Prime/Boost	LNP Diameter (Mean ± SD , nm)	Encapsulation efficiency (%)
pVAX1 (2999)	Prime	72.2 ± 14.6	93.4
	Boost	71.3 ± 14.2	94.0
pVAX1 SXBB.1.5 (6658)	Prime	79.7 ± 18.2	92.4
	Boost	78.5 ± 18.7	91.8
pVAX1 SXBB.1.5-CD40L (7101)	Prime	81.3 ± 19.5	94.3
	Boost	81.7 ± 20.9	93.1
mRNA SXBB.1.5 (3659)	Prime	71.6 ± 15.2	83.8
	Boost	71.7 ± 13.3	88.4
mRNA SXBB.1.5-CD40L (4102)	Prime	72.2 ± 16.7	80.7
	Boost	72.2 ± 16.1	85.2

4.11 References

1. Lasrado N, Collier ARY, Miller J, Hachmann NP, Liu J, Anand T, et al. Waning immunity and IgG4 responses following bivalent mRNA boosting. *Sci Adv* (2024) 10:9945. doi:10.1126/SCIADV.ADJ9945

2. Föhse K, Geckin B, Zoodsma M, Kilic G, Liu Z, Röring RJ, et al. The impact of BNT162b2 mRNA vaccine on adaptive and innate immune responses. *Clinical Immunology* (2023) 255:109762. doi:10.1016/J.CLIM.2023.109762

3. Ishii T, Hamada K, Jubishi D, Hashimoto H, Okamoto K, Hisasue N, et al. Waning cellular immune responses and predictive factors in maintaining cellular immunity against SARS-CoV-2 six months after BNT162b2 mRNA vaccination. *Sci Rep* (2023) 13:1–12. doi:10.1038/S41598-023-36397-6;SUBJMETA

4. Haq MA, Roy AK, Ahmed R, Kuddusi RU, Sinha M, Hossain MS, et al. Antibody longevity and waning following COVID-19 vaccination in a 1-year longitudinal cohort in Bangladesh. *Sci Rep* (2024) 14:1–11. doi:10.1038/S41598-024-61922-6;SUBJMETA

5. Tong X, McNamara RP, Avendaño MJ, Serrano EF, García-Salum T, Pardo-Roa C, et al. Waning and boosting of antibody Fc-effector functions upon SARS-CoV-2 vaccination. *Nature Communications 2023 14:1* (2023) 14:1–15. doi:10.1038/s41467-023-39189-8

6. Moore M, Anderson L, Schiffer JT, Matrajt L, Dimitrov D. Durability of COVID-19 vaccine and infection induced immunity: A systematic review and meta-regression analysis. *Vaccine* (2025) 54:126966. doi:10.1016/J.VACCINE.2025.126966

7. Srivastava K, Carreño JM, Gleason C, Monahan B, Singh G, Abbad A, et al. SARS-CoV-2-infection- and vaccine-induced antibody responses are long lasting with an initial waning phase followed by a stabilization phase. *Immunity* (2024) 57:587-599.e4. doi:10.1016/j.immuni.2024.01.017

8. Widge AT, Rouphael NG, Jackson LA, Anderson EJ, Roberts PC, Makhene M, et al. Durability of Responses after SARS-CoV-2 mRNA-1273 Vaccination. *New England Journal of Medicine* (2021) 384:80–82. doi:10.1056/NEJMC2032195

9. Doria-Rose N, Suthar MS, Makowski M, O'Connell S, McDermott AB, Flach B, et al. Antibody Persistence through 6 Months after the Second Dose of mRNA-1273 Vaccine for Covid-19. *New England Journal of Medicine* (2021) 384:2259–2261. doi:10.1056/NEJMC2103916

10. Pegu A, O'Connell SE, Schmidt SD, O'Dell S, Talana CA, Lai L, et al. Durability of mRNA-1273 vaccine–induced antibodies against SARS-CoV-2 variants. *Science (1979)* (2021) 373:1372–1377. doi:10.1126/SCIENCE.ABJ4176

11. Kim W, Zhou JQ, Horvath SC, Schmitz AJ, Sturtz AJ, Lei T, et al. Germinal centre-driven maturation of B cell response to mRNA vaccination. *Nature 2022 604:7904* (2022) 604:141–145. doi:10.1038/s41586-022-04527-1

12. Nguyen DC, Hentenaar IT, Morrison-Porter A, Solano D, Haddad NS, Castrillon C, et al. SARS-CoV-2-specific plasma cells are not durably established in the bone marrow long-lived compartment after mRNA vaccination. *Nat Med* (2025) 31:235–244. doi:10.1038/S41591-024-03278-Y;SUBJMETA

13. Florea A, Sy LS, Qian L, Ackerson BK, Luo Y, Tubert JE, et al. Effectiveness of Messenger RNA-1273 Vaccine Booster Against Coronavirus Disease 2019 in Immunocompetent Adults. *Clinical Infectious Diseases* (2023) 76:252–262. doi:10.1093/CID/CIAC785

14. Abu-Raddad LJ, Chemaitelly H, Ayoub HH, AlMukdad S, Yassine HM, Al-Khatib HA, et al. Effect of mRNA Vaccine Boosters against SARS-CoV-2 Omicron Infection in Qatar. *New England Journal of Medicine* (2022) 386:1804–1816. doi:10.1056/NEJMOA2200797

15. Ackerson BK, Bruxvoort KJ, Qian L, Sy LS, Qiu S, Tubert JE, et al. Effectiveness and durability of mRNA-1273 BA.4/BA.5 bivalent vaccine (mRNA-1273.222) against SARS-CoV-2 BA.4/BA.5 and XBB sublineages. *Hum Vaccin Immunother* (2024) 20: doi:10.1080/21645515.2024.2335052

16. Maslow JN, Kwon I, Kudchodkar SB, Kane D, Tadesse A, Lee H, et al. DNA Vaccines for Epidemic Preparedness: SARS-CoV-2 and Beyond. *Vaccines 2023, Vol 11, Page 1016* (2023) 11:1016. doi:10.3390/VACCINES11061016

17. Blakney AK, Bekker LG. DNA vaccines join the fight against COVID-19. *The Lancet* (2022) 399:1281–1282. doi:10.1016/S0140-6736(22)00524-4

18. Feliciano L-, Chapman C;, Hooper R;, Elma JW;, Zehrung K;, Brennan D;, et al. Improved DNA Vaccine Delivery with Needle-Free Injection Systems. *Vaccines 2023, Vol 11, Page 280* (2023) 11:280. doi:10.3390/VACCINES11020280

19. Sabnis S, Kumarasinghe ES, Salerno T, Mihai C, Ketova T, Senn JJ, et al. A Novel Amino Lipid Series for mRNA Delivery: Improved Endosomal Escape and Sustained Pharmacology and Safety in Non-human Primates. *Molecular Therapy* (2018) 26:1509–1519. doi:10.1016/j.ymthe.2018.03.010

20. Hassett KJ, Benenato KE, Jacquinet E, Lee A, Woods A, Yuzhakov O, et al. Optimization of Lipid Nanoparticles for Intramuscular Administration of mRNA Vaccines. *Mol Ther Nucleic Acids* (2019) 15:1–11. doi:10.1016/j.omtn.2019.01.013

21. Connors J, Joyner D, Mege NJ, Cusimano GM, Bell MR, Marcy J, et al. Lipid nanoparticles (LNP) induce activation and maturation of antigen presenting cells in young and

aged individuals. *Communications Biology 2023 6:1* (2023) 6:1–13. doi:10.1038/s42003-023-04555-1

22. Alameh MG, Tombácz I, Bettini E, Lederer K, Sittplangkoon C, Wilmore JR, et al. Lipid nanoparticles enhance the efficacy of mRNA and protein subunit vaccines by inducing robust T follicular helper cell and humoral responses. *Immunity* (2021) 54:2877-2892.e7. doi:10.1016/j.immuni.2021.11.001

23. Pfeifle A, Thulasi Raman SN, Lansdell C, Zhang W, Tamming L, Cecillon J, et al. DNA lipid nanoparticle vaccine targeting outer surface protein C affords protection against homologous Borrelia burgdorferi needle challenge in mice. *Front Immunol* (2023) 14:1020134. doi:10.3389/FIMMU.2023.1020134/BIBTEX

24. Guimaraes LC, Costa PAC, Scalzo Júnior SRA, Ferreira HAS, Braga ACS, de Oliveira LC, et al. Nanoparticle-based DNA vaccine protects against SARS-CoV-2 variants in female preclinical models. *Nature Communications 2024 15:1* (2024) 15:1–19. doi:10.1038/s41467-024-44830-1

25. Liao HC, Shen KY, Yang CH, Chiu FF, Chiang CY, Chai KM, et al. Lipid nanoparticle-encapsulated DNA vaccine robustly induce superior immune responses to the mRNA vaccine in Syrian hamsters. *Mol Ther Methods Clin Dev* (2024) 32:101169. doi:10.1016/j.omtm.2023.101169

26. Tursi NJ, Tiwari S, Bedanova N, Kannan T, Parzych E, Okba N, et al. Modulation of lipid nanoparticle-formulated plasmid DNA drives innate immune activation promoting adaptive immunity. *Cell Rep Med* (2025) 6:102035. doi:10.1016/J.XCRM.2025.102035

27. Li M, Liu L, Li X, Li J, Zhao C, Zhao Y, et al. Lipid Nanoparticles Outperform Electroporation in Delivering Therapeutic HPV DNA Vaccines. *Vaccines (Basel)* (2024) 12:666. doi:10.3390/VACCINES12060666/S1

28. Zhang W, Pfeifle A, Lansdell C, Frahm G, Cecillon J, Tamming L, et al. The Expression Kinetics and Immunogenicity of Lipid Nanoparticles Delivering Plasmid DNA and mRNA in Mice. *Vaccines (Basel)* (2023) 11:1580. doi:10.3390/VACCINES11101580/S1

29. Patel MN, Tiwari S, Wang Y, O'Neill S, Wu J, Omo-Lamai S, et al. Safer non-viral DNA delivery using lipid nanoparticles loaded with endogenous anti-inflammatory lipids. *Nature Biotechnology 2025* (2025)1–11. doi:10.1038/s41587-025-02556-5

30. FDA Takes Action on Updated mRNA COVID-19 Vaccines to Better Protect Against Currently Circulating Variants | FDA. Available at: https://www.fda.gov/news-events/press-announcements/fda-takes-action-updated-mrna-covid-19-vaccines-better-protect-against-currently-circulating [Accessed October 5, 2025]

31. Tamming LA, Duque D, Tran A, Zhang W, Pfeifle A, Laryea E, et al. DNA Based Vaccine Expressing SARS-CoV-2 Spike-CD40L Fusion Protein Confers Protection Against Challenge in a Syrian Hamster Model. *Front Immunol* (2022) 12: doi:10.3389/FIMMU.2021.785349

32. Tamming L, Duque D, Tran A, Lansdell C, Frahm G, Wu J, et al. Lipid nanoparticle encapsulation of a Delta spike-CD40L DNA vaccine improves effectiveness against Omicron challenge in Syrian hamsters. *Mol Ther Methods Clin Dev* (2024) 32:101325. doi:10.1016/j.omtm.2024.101325

33. Kaku Y, Uriu K, Okumura K, Ito J, Sato K. Virological characteristics of the SARS-CoV-2 KP.3.1.1 variant. *Lancet Infect Dis* (2024) 24:e609. doi:10.1016/S1473-3099(24)00505-X

34. Nunes da Silva W, Dias Moura Prazeres PH, Goulart Guimarães PP. PLA-PEG as an alternative to PEGylated lipids for nanoparticle-based DNA vaccination against SARS-CoV-2. *Mol Ther Nucleic Acids* (2024) 35:102293. doi:10.1016/j.omtn.2024.102293

35. Lai DC, Nguyen TN, Trinh GP, Steffen D, Vu HLX. Lipid nanoparticle-encapsulated DNA vaccine induces balanced antibody and T-cell responses in pigs with maternally derived antibodies. *J Virol* (2025) doi:10.1128/JVI.01123-25

36. Lai DC, Nguyen TN, Poonsuk K, McVey DS, Vu HLX. Lipid nanoparticle-encapsulated DNA vaccine encoding African swine fever virus p54 antigen elicits robust immune responses in pigs. *Vet Microbiol* (2025) 305:110508. doi:10.1016/J.VETMIC.2025.110508

37. Mucker EM, Karmali PP, Vega J, Kwilas SA, Wu H, Joselyn M, et al. Lipid Nanoparticle Formulation Increases Efficiency of DNA-Vectored Vaccines/Immunoprophylaxis in Animals Including Transchromosomic Bovines. *Scientific Reports 2020 10:1* (2020) 10:8764-. doi:10.1038/s41598-020-65059-0

38. AM H, C G, Z C, Y Y, M T, B J, et al. CD40 ligand preferentially modulates immune response and enhances protection against influenza virus. *J Immunol* (2014) 193:722–734. doi:10.4049/JIMMUNOL.1300093

39. Kometani K, Kurosaki T. Differentiation and maintenance of long-lived plasma cells. *Curr Opin Immunol* (2015) 33:64–69. doi:10.1016/J.COI.2015.01.017

40. Brook B, Duval V, Barman S, Speciner L, Sweitzer C, Khanmohammed A, et al. Adjuvantation of a SARS-CoV-2 mRNA vaccine with controlled tissue-specific expression of an mRNA encoding IL-12p70. *Sci Transl Med* (2024) 16: doi:10.1126/SCITRANSLMED.ADM8451;PAGE:STRING:ARTICLE/CHAPTER

41. Wang L, Wan J, He W, Wang Z, Wu Q, Zhou M, et al. IL-7 promotes mRNA vaccine-induced long-term immunity. *Journal of Nanobiotechnology 2024 22:1* (2024) 22:716-. doi:10.1186/S12951-024-02993-5

42. Pardi N, Tuyishime S, Muramatsu H, Kariko K, Mui BL, Tam YK, et al. Expression kinetics of nucleoside-modified mRNA delivered in lipid nanoparticles to mice by various routes. *Journal of Controlled Release* (2015) 217:345–351. doi:10.1016/J.JCONREL.2015.08.007

43. Swingle KL, Hamilton AG, Han X, Liao KC, Safford HC, Thatte AS, et al. Circular RNA lipid nanoparticle vaccine against SARS-CoV-2. *Proceedings of the National Academy of Sciences* (2025) 122:e2505718122. doi:10.1073/PNAS.2505718122

44. Qu L, Yi Z, Shen Y, Lin L, Chen F, Xu Y, et al. Circular RNA vaccines against SARS-CoV-2 and emerging variants. *Cell* (2022) 185:1728-1744.e16. doi:10.1016/j.cell.2022.03.044

45. Wan J, Wang Z, Wang L, Wu L, Zhang C, Zhou M, et al. Circular RNA vaccines with long-term lymph node-targeting delivery stability after lyophilization induce potent and persistent immune responses. *mBio* (2024) 15: doi:10.1128/MBIO.01775-23

46. Krawczyk PS, Mazur M, Orzeł W, Gewartowska O, Jeleń S, Antczak W, et al. Re-adenylation by TENT5A enhances efficacy of SARS-CoV-2 mRNA vaccines. *Nature* (2025) 641:984–992. doi:10.1038/S41586-025-08842-1;TECHMETA

47. Robinson MJ, Dowling MR, Pitt C, O'Donnell K, Webster RH, Hill DL, et al. Long-lived plasma cells accumulate in the bone marrow at a constant rate from early in an immune response. *Sci Immunol* (2022) 7: doi:10.1126/SCIIMMUNOL.ABM8389

48. Muecksch F, Weisblum Y, Barnes CO, Schmidt F, Schaefer-Babajew D, Wang Z, et al. Affinity maturation of SARS-CoV-2 neutralizing antibodies confers potency, breadth, and resilience to viral escape mutations. *Immunity* (2021) 54:1853-1868.e7. doi:10.1016/j.immuni.2021.07.008

49. Colwill K, Galipeau Y, Stuible M, Gervais C, Arnold C, Rathod B, et al. A scalable serology solution for profiling humoral immune responses to SARS-CoV-2 infection and vaccination. *Clin Transl Immunology* (2022) 11:e1380. doi:10.1002/CTI2.1380

50. Nie J, Li Q, Wu J, Zhao C, Hao H, Liu H, et al. Quantification of SARS-CoV-2 neutralizing antibody by a pseudotyped virus-based assay. *Nature Protocols 2020 15:11* (2020) 15:3699–3715. doi:10.1038/s41596-020-0394-5

51. Reed LJ, Muench H. A simple method of estimating fifty per cent endpoints. *Am J Epidemiol* (1938) 27:493–497. doi:10.1093/OXFORDJOURNALS.AJE.A118408/2/27-3-493.PDF.GIF

52. Wölfel R, Corman VM, Guggemos W, Seilmaier M, Zange S, Müller MA, et al. Virological assessment of hospitalized patients with COVID-2019. *Nature 2020 581:7809* (2020) 581:465–469. doi:10.1038/s41586-020-2196-x

53. Zivcec M, Safronetz D, Haddock E, Feldmann H, Ebihara H. Validation of assays to monitor immune responses in the Syrian golden hamster (Mesocricetus auratus). *J Immunol Methods* (2011) 368:24–35. doi:10.1016/J.JIM.2011.02.004

54. Livak KJ, Schmittgen TD. Analysis of Relative Gene Expression Data Using Real-Time Quantitative PCR and the 2−ΔΔCT Method. *Methods* (2001) 25:402–408. doi:10.1006/METH.2001.1262

55. Harris G, Holbein BE, Zhou H, Howard Xu H, Chen W. Potential mechanisms of mucin-enhanced acinetobacter baumannii virulence in the mouse model of intraperitoneal infection. *Infect Immun* (2019) 87: doi:10.1128/IAI.00591-19/SUPPL_FILE/IAI.00591-19-S0001.PDF

56. Lien CE, Lin YJ, Chen C, Lian WC, Kuo TY, Campbell JD, et al. CpG-adjuvanted stable prefusion SARS-CoV-2 spike protein protected hamsters from SARS-CoV-2 challenge. *Scientific Reports 2021 11:1* (2021) 11:1–7. doi:10.1038/s41598-021-88283-8

Chapter 5: Discussion and Conclusion

Waning immunity and the emergence of immune-escaping variants have continually rendered vaccinated individuals susceptible to breakthrough infections and reinfection with SARS-CoV-2. NAb responses in particular, are often short-lived and rapidly evaded by new variants, necessitating periodic updated boosters to maintain high circulating titer and to keep pace with viral evolution (202,203,339). DNA vaccines garnered significant interest during the COVID-19 pandemic, with numerous candidates having undergone clinical evaluation (235,236,241,300,335–338). The majority of these candidates relied on electroporation or NFISs for delivery, approaches that require costly proprietary equipment and could be difficult to deploy at scale (340). Moreover, even with these delivery approaches, DNA vaccines generally elicited weaker immune responses than commercial mRNA-LNP vaccines (241,335,336,338,341), highlighting the need for alternative strategies to bolster their immunogenicity. This thesis evaluates two strategies to enhance DNA-vaccine performance against SARS-CoV-2: first, fusing CD40L to the antigen as a molecular adjuvant to improve the potency and breadth of humoral responses; second, formulating DNA in LNPs to overcome inefficient delivery and thereby improve expression, immunogenicity, and protection. Together, these studies provide practical design principles for DNA vaccines and outline strategies to generate more durable immunity.

5.1 CD40 Ligand as a Vaccine Adjuvant

The first objective of this thesis was to assess how incorporating CD40L into nucleic acid-based vaccines would alter immune responses against SARS-CoV-2. Previously, our group evaluated an Ad5-vectored MERS-CoV vaccine in which trimerized S1 was fused to CD40L (316). The addition of CD40L enhanced vaccine immunogenicity and prevented pulmonary perivascular hemorrhage

post-challenge (316). Early reports during the COVID-19 pandemic indicated that the S1 subunit alone was less effective as a vaccine antigen than full-length S, which induced greater NAb responses (342,343). Accordingly, in Chapter 2 a pDNA vaccine was generated encoding soluble prefusion-stabilized SARS-CoV-2 S fused to the CD40L ectodomain (Figure 2.1). Following IM administration in Syrian hamsters, the pcDNA3.1 S-CD40L vaccine elicited higher binding and neutralizing antibody responses than pcDNA3.1 S (Figure 2.2). Notably, after a single dose the naked CD40L-adjuvanted DNA vaccine induced a detectable NAb response against heterologous B.1.617.2 S (Figure 2.2). Despite being more immunogenic, the pcDNA3.1 S-CD40L vaccine did not reduce weight loss and viral burden following SARS-CoV-2 challenge relative to pCDNA3.1 S (Figure 2.3). However, the CD40L-adjuvanted vaccine did confer better protection against lung histopathology at 7-dpi (Figure 2.4), potentially reflecting enhanced viral control. In line with previous reports against other pathogens, the work in Chapter 2 demonstrated that CD40L could enhance the immunogenicity and efficacy of SARS-CoV-2 vaccines. However, the addition of CD40L alone was not sufficient to confer complete protection from challenge, potentially due to inefficient DNA delivery following naked administration.

The effect of CD40L inclusion was also assessed in DNA-LNP and mRNA-LNP platforms, where nucleic acid delivery is more efficient. In Chapter 3, SM-102 LNP-encapsulated pVAX1 S-CD40L$_{B.1.617.2}$ induced greater binding antibody responses than SM-102 LNP-encapsulated pVAX1 S$_{B.1.617.2}$ in Syrian hamsters after the first and second doses (Supplemental Figure 3.1). In Chapter 4, mRNA-LNPs encoding S$_{XBB.1.5}$-CD40L elicited superior binding antibody responses in mice than S$_{XBB.1.5}$ mRNA-LNPs (Figure 4.1). Notably, in Chapter 4 CD40L preferentially increased titers of IgG2a rather than IgG1 (Figure 4.1), indicative of a Th1-biased response (344). Likewise, S$_{XBB.1.5}$-CD40L mRNA-LNPs elicited greater Th1-associated cytokine (IFNy, IL-2 and

TNFα) expression in $CD4^+$ T cells than the unadjuvanted vaccine (Figure 4.1). These results mirror previous characterizations of CD40L-adjuvanted vaccines, which predominantly elicit Th1-skewed responses (305,311,314,345). While there have been no reports of vaccine-associated enhanced respiratory disease (VAERD) in humans, preclinical COVID-19 models have shown that Th2-biased responses can be associated with enhanced eosinophilic immunopathology following viral challenge (346–348). As such, a Th1-driving adjuvant such as CD40L could be particularly advantageous.

In Chapter 4, while $S_{XBB.1.5}$-CD40L mRNA-LNP vaccination elicited a robust early humoral response, it showed limited durability, as NAb titers in vaccinated hamsters dropped substantially by 6 months post-vaccination (Figure 4.2). Previously, a CD40L-adjuvanted AdV vaccine targeting influenza nucleoprotein was shown to induce earlier and more persistent germinal centre responses than its unadjuvanted counterpart, coinciding with enhanced protection 4 months post-vaccination (307). Despite evidence that CD40L can enhance long-term immunity in other vaccine platforms, its addition was insufficient to overcome the limited durability of mRNA-LNP–induced responses in this hamster model (Figure 4.2). Notably, co-administration of BNT162b2 with mRNA encoding IL-12p70 not only increased the magnitude of humoral responses but also better sustained responses 373 days post-vaccination (349). Likewise, co-administration of mRNA encoding IL-7 with a rabies glycoprotein mRNA vaccine enhanced NAb six months post-vaccination (350). Both adjuvants augmented germinal centre responses, increasing the proportional area of B cell zones and enhancing Tfh and GC B cell frequencies, respectively (349,350). Importantly, although these adjuvants enhanced the relative durability of humoral responses, antibody titers still declined significantly within a few months post-vaccination. Collectively, this may suggest that encoded adjuvants may be insufficient on their own to fully overcome intrinsic limitations of the mRNA-

LNP platform. Notably, although CD40L did not improve the stability of circulating antibody levels, it could still have provided benefits through enhanced memory B and T cell formation and improved recall capacity. Further work will be needed to evaluate these additional aspects of immune memory alongside GC responses following CD40L-adjuvanted mRNA-LNP vaccination.

Recently, two CD40-targeted vaccines progressed into early-phase clinical trials. In a Phase 1 study of CD40.HIVRI.Env, an anti-CD40 IgG4 monoclonal antibody fused at the heavy-chain C terminus to the HIV Envelope protein (Env), Env-specific $CD4^+$ T cells and IgG responses were detected in all participants (323). While the use of agonistic anti-CD40 antibodies has been associated with systemic cytokine-release symptoms and platelet activation (351–353), these adverse effects typically result from high-dose systemic administration. In contrast, the IM administered CD40.HIVRI.Env demonstrated an acceptable safety profile across all evaluated doses (323). An ongoing Phase 1/2a trial is currently evaluating CD40.RBDv as a booster for SARS-CoV-2, where NAb will be measured as a primary immunogenic endpoint (322). Taken together, the abundance of preclinical studies and these early clinical evaluations support the feasibility of CD40L- and anti-CD40–based antigens for human vaccination.

5.2 Lipid Nanoparticle Vaccines

Advances in ionizable lipids and LNP formulations have enabled the effective delivery of siRNA therapeutics and mRNA vaccines (191,354). In Chapter 3, to assess whether these advances could be translated to DNA vaccination, the immunogenicity and efficacy of naked and LNP-encapsulated pVAX1-S-CD40L$_{B.1.617.2}$ was assessed in Syrian hamsters. Encapsulation in KC2-based LNPs markedly enhanced humoral responses, increasing the magnitude of Spike-specific IgG and NAb responses (Figure 3.2). Notably, the Delta-based DNA-LNP also elicited significant

NAb titers against the Omicron subvariants BA.2.75 and BA.5 (Figure 3.2). The immunogenic DNA-LNP vaccine was highly protective, with vaccinated hamsters displaying minimal viral burden and no overt signs of lung histopathology (Figure 3.2 & 3.3).

DLin-KC2-DMA was identified for its ability to mediate hepatic gene silencing after systemic administration (266), and thus was not tailored for IM delivery. In contrast, SM-102, used in Moderna's Spikevax COVID-19 vaccine, was optimized for IM mRNA vaccination (269). Under the assumption that an DNA vaccine would benefit from these same optimizations, Syrian hamsters were immunized with pVAX1-S-CD40L$_{B.1.617.2}$ formulated in either KC2- or SM-102–based LNPs. While both DNA-LNPs elicited robust humoral responses, the SM-102 DNA-LNPs elicited greater NAb responses against Omicron subvariants (Figure 3.6). Both DNA-LNPs afforded significant protection against heterologous challenge with the BA.5 variant, although there were modest numerical advantages for the SM-102 formulation across most endpoints (Figure 3.6). Transfection experiments with pVAX1 encoding green fluorescent protein or firefly luciferase demonstrated the superiority of the SM-102 formulation for *in vitro* pDNA delivery (Figure 3.5). Concurrently, our group showed that SM-102 DNA-LNPs induced higher and more durable luciferase expression than KC2 DNA-LNPs in BALB/c mice (279). Notably, the SM-102 DNA-LNPs induced significantly lower antigen expression than a lower dose of mRNA-LNPs (279). This likely reflects the fact that, whereas mRNA-LNPs are primarily limited by endosomal escape, DNA-LNPs must also migrate through the cytosol and enter the nucleus prior to transcription, well-recognized bottlenecks limiting non-viral DNA delivery (355). Overcoming these challenges may require specialized strategies, such as incorporating DNA nuclear targeting sequences (286,355,356) or developing LNPs that release DNA in condensed supramolecular cores (357).

In Chapter 4, Syrian hamsters were immunized with DNA or mRNA vaccines encoding $S_{XBB.1.5}$-CD40L, formulated in identical SM-102–based LNPs. Both vaccines induced similar humoral responses three weeks post-boost (Figure 4.2), and both provided near-complete protection from challenge with the XBB.1.5 variant four weeks post-boost (Figure 4.3). Given that waning immunity has limited the long-term effectiveness of mRNA vaccines (202–204,358), the ability of DNA-LNPs to elicit durable immunity was assessed by challenging immunized hamsters six months post-boost. Consistent with existing literature, NAb titers decreased dramatically following mRNA-LNP vaccination (Figure 4.2), coinciding with substantially reduced protection (Figure 4.4). In contrast, DNA-LNP vaccination generated a sustained NAb response (Figure 4.2) and continued to afford a significant level of protection at this later time point (Figure 4.4).

The observed superior durability of DNA-LNP-induced immunity mirrors recent reports from other groups. Liao et al. showed that DNA-LNP vaccination elicited anti-Spike IgG and NAb responses that were more stably maintained than mRNA-LNP–induced responses over 20 weeks in BALB/c mice and Syrian hamsters (280). Similarly, Tursi et al. demonstrated that DNA-LNP-induced stronger humoral responses than mRNA-LNPs in rabbits six months post-vaccination (281). The mechanisms underlying the superior durability of DNA-LNP induced humoral responses remain unclear. Long-lived plasma cells (LLPCs), particularly those residing in the bone marrow, are the principal source of sustained antibody secretion long after vaccination, and their generation is usually linked to strong and sustained GC reactions, which are critical for affinity maturation (359). While mRNA-LNPs have been shown to induce strong early GC responses (360), these responses contract substantially within a month (361). Accordingly, mRNA-LNP vaccinations fail to durably establish bone marrow LLPC populations (362) , potentially due to the transient nature of mRNA-encoded antigen expression. Tursi et al. reported that, relative to

mRNA-LNPs, DNA-LNPs induced weaker germinal center responses (281), suggesting that the longevity of humoral responses is not a consequence of augmented early GC activity. It has now been well-established that DNA-LNPs drive prolonged antigen expression (279,281,363). This sustained antigenic stimulus may support long-term antibody production through mechanisms that do not rely solely on strong early GC responses, for example by maintaining low-level B cell activation over time.

5.3 Combatting SARS-CoV-2 Immune Escape

Newly emerging SARS-CoV-2 variants continue to subvert existing immune responses, necessitating novel vaccination strategies to induce broad and sustained protection. This thesis demonstrates that CD40L and LNP encapsulation can increase the NAb breadth induced by DNA vaccines encoding SARS-CoV-2 S. In chapter 2, the addition of CD40L enabled the induction of NAb against the Delta variant after a single dose when vaccinating with the ancestral S (Figure 2.2). In Chapter 3, LNP-encapsulation of a pVAX1 S-CD40L$_{B.1.617.2}$ enabled the neutralization of multiple Omicron subvariants, with detectable responses extending to the BQ.1 variant (Figure 3.6). LNP-encapsulated pVAX1 S-CD40L$_{B.1.617.2}$ also afforded near-complete protection from heterologous BA.5 challenge, demonstrating robust cross-protection (Figure 3.7 & 3.8). Lastly, in Chapter 4, DNA-LNPs targeting XBB.1.5 S induced durable NAb responses against the JN.1 variant six months post-vaccination, a time point at which mRNA-LNPs had largely lost NAb activity (Figure 4.2). These findings suggest that alternative platforms such as CD40L-adjuvanted DNA-LNPs may help sustain cross-variant NAb responses over longer intervals.

In practice, several national health authorities have and continue to recommend the use of antigen-matched seasonal boosters to improve protection against circulating SARS-CoV-2 variants

(364,365). However, the effectiveness of repeated boosters has been hindered by immune imprinting (328,366–368), the propensity of the immune system to amplify pre-existing responses upon re-exposure to related antigens rather than generate de novo responses. Although imprinting can boost responses against conserved regions, it can impair responses targeted towards newly mutated epitopes, which in the case of SARS-CoV-2 often correspond to key neutralizing regions of S (369). For example, immune responses in individuals boosted with bivalent mRNA vaccines encoding both ancestral and BA.5 S are dominated by ancestral recall, yielding neutralization profiles similar to those boosted with monovalent ancestral vaccines (328). Likewise, updated monovalent XBB.1.5 boosters preferentially elicit recall of pre-existing ancestral-reactive memory B cells (368). Nonetheless, evidence indicates that repeated exposure to Omicron strains can shift immune responses away from the ancestral strain (370,371). Clonal analyses suggest that this shift is driven largely by the redirection of pre-existing ancestral-imprinted memory B cells toward Omicron epitopes through somatic hypermutation, rather than the generation of de novo Omicron-specific clones (372). Notably, immune imprinting is not a uniform phenomenon, with different vaccine platforms and the severity of infection inducing distinct magnitudes and patterns of imprinting (369,373). To what extent DNA-LNPs, and their persistent antigen expression, shape immune imprinting remains to be determined.

Despite challenges with immune imprinting and the immune evasion of emerging SARS-CoV-2 variants, current vaccination strategies have maintained a high level of protection against severe outcomes, likely through the contribution of cross-reactive T cell responses and non-neutralizing antibodies (140,374,375). T cell depletion and adoptive transfer studies have demonstrated that vaccine-elicited T cells are critical for controlling viral replication and mitigating disease in settings where neutralizing Ab titers are low or where variants partially escape humoral recognition

(150,376). Peptide-based vaccines, like CoVac-1 (377,378), represent an alternative vaccination strategy designed to specifically induce robust T cell responses against multiple conserved epitopes derived from different SARS-CoV-2 proteins. While often more resistant to immune escape, peptide vaccines often suffer from lower immunogenicity and typically require potent adjuvants (379).

Experiments have likewise demonstrated the importance of Fc effector mechanisms against SARS-CoV-2 (166,380). Most notably, vaccination with mRNA-1273 failed to protect against Omicron BA.5 challenge in mice lacking FcγRIII, demonstrating the importance of Fc effector mechanisms when neutralizing antibody responses are suboptimal (166). To what extent cross-reactive T-cell and non-neutralizing Ab responses played in the cross-protection observed in Chapter 2 remains unclear. Transfer and depletion studies could therefore be used in future work to determine their contribution to DNA-LNP–mediated immunity.

5.4 Future Directions

This thesis demonstrates that DNA-LNP vaccines can elicit potent and durable immunity against SARS-CoV-2, highlighting their potential as a next-generation vaccine platform. However, important questions remain regarding the mechanistic basis of their prolonged immunity, their translational potential in humans, and how best to optimize both the DNA cargo and the LNP formulation for vaccination. Addressing these knowledge gaps will be essential to fully realize the clinical potential of DNA-LNP vaccines.

5.4.1 Mechanism of durable immunity

As shown in Chapter 4, a key advantage of DNA-LNP vaccines is their ability to elicit prolonged humoral immunity, exemplified by the maintenance of high circulating NAb titers six-months post-

vaccination (Figure 4.2). Additional studies are needed to determine whether this durability is directly driven by sustained antigen expression (279,281). Incorporating inducible expression or conditional excision systems into DNA vaccine constructs could theoretically enable precise control and termination of antigen production (381,382). Measuring the resulting NAb decay kinetics and quantifying changes in LLPC accumulation in the bone marrow at extended time points would help clarify the contribution of prolonged antigen expression to DNA-LNP–mediated durability.

Moreover, the impact of persistent antigen expression on DNA-LNP induced immune responses remains unknown beyond one year. In the context of chronic viral infections sustained antigen loads have been linked to T cell exhaustion (383–385). Tursi et al. found that DNA-LNPs elicited stronger T cell responses in BALB/c mice one year after vaccination, although exhaustion markers were not assessed (281). Thus, it is important to assess how sustained antigen-expression from DNA-LNPs might shape long-term T cell differentiation and function.

Defining the cellular tropism of DNA-LNPs will also be critical, as emerging evidence continues to highlight the importance of antigen expression within non-myocyte populations following mRNA-LNP vaccination. Contrary to a primarily phagocytosis-focused view of APCs as sentinels that scavenge and process exogenous antigen, de novo antigen expression within APCs appears to be critical for mRNA-LNP responses (386,387). A recent study using mRNA-LNPs embedded with miRNA-targeting sites demonstrated that while antigen expression within myocytes was largely dispensable, knockdown of expression within innate immune cells significantly impaired $CD4^+$ T cell and humoral responses (387). Furthermore, a significant portion of LNPs escape the injection site via the vasculature and lymphatic systems, distributing systemically (388,389). For many LNP formulations, this leads to significant liver accumulation (279,390). This systemic

dissemination can also deliver LNPs to draining lymph nodes and other secondary lymphoid organs, where both immune cells and long-lived stromal subsets can be transfected (391–393). Antigen expression within such compartments could contribute to superior antigen availability and, in turn, support sustained immune responses (394). Accordingly, future studies should define the cellular tropism of DNA-LNPs, quantify the duration of antigen expression across tissues, and determine how expression in specific compartments contributes to the long-term durability of immunity.

5.4.2 Translational relevance

Important questions remain regarding their safety and potential clinical translation of DNA-LNP vaccines, particularly given significant species-specific differences in immunogenicity and reactogenicity. While Liao et al. noted that DNA-LNPs afforded stronger humoral responses than mRNA-LNPs in BALB/c mice and Syrian hamsters, they observed the opposite pattern in rats and rabbits (280). Similarly, Guimarães et al. reported that, in Syrian hamsters, a DNA-LNP elicited protective efficacy and immunogenicity comparable to those of the BNT162b2 mRNA vaccine (395). However, in K18-hACE2 mice, the same DNA-LNP induced inferior responses (395) . These studies highlight how the relative performance of each platform can be model-dependent, potentially requiring re-optimization of doses or formulations for use in different species. Notably, doses of DNA-LNPs that are well tolerated in BALB/c mice can trigger severe systemic inflammation, pronounced cytokinemia, and mortality in C57BL/6 mice (363,396). Mechanistically, DNA-LNPs induce robust STING (Stimulator of Interferon Genes) signaling (281,357,363). STING inhibition can attenuate these inflammatory responses and improves tolerability (357,363), although the consequences for vaccine immunogenicity remain unclear. Interestingly, DNA-LNPs have been reported to be effective and generally well tolerated in rhesus

macaques (276). Future studies are required to define the contribution of STING signaling to DNA-LNP immunogenicity and to determine whether this platform can achieve an acceptable safety profile in humans.

5.4.3 Platform optimization

This thesis represents a preliminary investigation of DNA-LNP formulations, relying on KC2- and SM-102–based particles that were originally developed for siRNA and mRNA applications, respectively (266,269). Future studies should prioritize optimizing LNP formulations specifically for DNA vaccines. Relative to mRNA-LNPs, higher nitrogen to phosphate (N/P) ratios have been shown to be beneficial for DNA-LNPs, increasing the frequency of GC B cells, likely reflecting differences in nucleic acid structure and charge distribution (281). Barcoded pDNA constructs have been used identifying LNP compositions that maximize tissue-specific delivery (395). In addition, improved mixing approaches can generate more uniform DNA-LNPs and have been reported to increase *in vivo* transgene expression by 2–3 orders of magnitude (357). Collectively, these findings suggest that tuning of ionizable lipid chemistry, N/P ratios, and assembly parameters could substantially improve the potency of next-generation DNA-LNP vaccines.

There also remains substantial room to optimize DNA vaccine constructs themselves. One advantage of mRNA vaccines is that they consist only of coding sequences and essential untranslated regions, lacking bacterial backbones and selectable marker sequences required for plasmid propagation. Although pVAX1 is considered a “minimal” plasmid backbone, it still contains exogenous bacterial DNA, including a ColE1 origin of replication and a kanamycin resistance cassette, which are unnecessary to elicit vaccine responses *in vivo*. Multiple next-generation DNA vectors are being explored to further minimize or eliminate these elements, including covalently closed linear DNA (Doggy bone, ministering, midge) (397,398), mini circle

DNA (399), and nanoplasmids (400). Many of these vectors can also be synthesized enzymatically, eliminating the need for bacterial propagation and thereby reducing the amount of unmethylated cytosine-phosphate-guanine (CpG) motifs which could act as unwanted TLR9 agonists (401,402). The smaller size of these minimal vectors can also improve trafficking to and through the nuclear pore complex (403,404).

Lastly, DNA-LNPs should be investigated for mucosal vaccination. Mucosal immunity is of particular interest because it acts directly at the site of pathogen entry and offers the greatest potential to prevent infection and reduce transmission (405). Several studies have explored the intranasal administration of mRNA-LNP vaccines; however, they often require reformulation and substantially higher doses to only achieve relatively modest immune responses (406,407). Incorporation of mucoadhesive chitosan and APC-targeting mannose moieties has been shown to enhance immune responses following intranasal mRNA-LNP vaccination (408,409). To our knowledge, the use of DNA-LNP formulations for intranasal vaccination has not yet been systematically examined and could represent a promising new avenue to elicit localized and potentially more durable mucosal immunity.

5.5 Final Remarks

This thesis explored the use of DNA vaccines against SARS-CoV-2, investigating the benefits of incorporating the molecular adjuvant CD40L and of encapsulating DNA vaccines within LNPs. These studies demonstrate that CD40L can substantially enhance the breadth and potency of DNA vaccine responses, and that LNP encapsulation can overcome key delivery limitations associated with naked DNA immunization. DNA-LNP formulations generated long-lived NAb responses and provided durable immunity against SARS-CoV-2. Collectively, these findings will help guide the

design of next-generation DNA vaccines, with the potential to improve protection against SARS-CoV-2 and to be adapted for use against other emerging and re-emerging pathogens.

References

1. Emerging Diseases and Zoonoses (EZD), Epidemic and Pandemic Preparedness and Prevention (EPP). COVID-19 epidemiological update – 15 July 2024. (2024). Available at: https://www.who.int/publications/m/item/covid-19-epidemiological-update-edition-169 [Accessed December 31, 2025]

2. Hui DS, I Azhar E, Madani TA, Ntoumi F, Kock R, Dar O, et al. The continuing 2019-nCoV epidemic threat of novel coronaviruses to global health — The latest 2019 novel coronavirus outbreak in Wuhan, China. *International Journal of Infectious Diseases* (2020) 91:264–266. doi:10.1016/j.ijid.2020.01.009

3. WHO. Virtual press conference on COVID-19 – 11 March 2020. Available at: https://www.who.int/docs/default-source/coronaviruse/transcripts/who-audio-emergencies-coronavirus-press-conference-full-and-final-11mar2020.pdf [Accessed December 31, 2025]

4. Impact of COVID-19 on people's livelihoods, their health and our food systems. Available at: https://www.who.int/news/item/13-10-2020-impact-of-covid-19-on-people's-livelihoods-their-health-and-our-food-systems [Accessed December 31, 2025]

5. Huang HY, Wang SH, Tang Y, Sheng W, Zuo CJ, Wu DW, et al. Landscape and progress of global COVID-19 vaccine development. *Hum Vaccin Immunother* (2021) 17:3276–3280. doi:10.1080/21645515.2021.1945901

6. Barouch DH. Covid-19 Vaccines — Immunity, Variants, Boosters. *New England Journal of Medicine* (2022) 387:1011–1020. doi:10.1056/NEJMRA2206573;PAGEGROUP:STRING:PUBLICATION

7. WHO Director-General's opening remarks at the media briefing – 5 May 2023. Available at: https://www.who.int/news-room/speeches/item/who-director-general-s-opening-remarks-at-the-media-briefing---5-may-2023 [Accessed December 31, 2025]

8. WHO chief declares end to COVID-19 as a global health emergency | UN News. Available at: https://news.un.org/en/story/2023/05/1136367 [Accessed December 31, 2025]

9. COVID-19 - Global Situation. Available at: https://www.who.int/emergencies/disease-outbreak-news/item/2025-DON572 [Accessed December 31, 2025]

10. Otto SP, MacPherson A, Colijn C. Endemic does not mean constant as SARS-CoV-2 continues to evolve. *Evolution (N Y)* (2024) 78:1092–1108. doi:10.1093/EVOLUT/QPAE041

11. Bartha I, Maher C, Lavrenko V, Chen YP, Tao Q, di Iulio J, et al. Morbidity of SARS-CoV-2 in the evolution to endemicity and in comparison with influenza. *Communications Medicine 2024 4:1* (2024) 4:244-. doi:10.1038/s43856-024-00633-5

12. Rahman HS, Aziz MS, Hussein RH, Othman HH, Salih Omer SH, Khalid ES, et al. The transmission modes and sources of COVID-19: A systematic review. *International Journal of Surgery Open* (2020) 26:125–136. doi:10.1016/J.IJSO.2020.08.017

13. Liu Y, Gayle AA, Wilder-Smith A, Rocklöv J. The reproductive number of COVID-19 is higher compared to SARS coronavirus. *J Travel Med* (2020) 27:1–4. doi:10.1093/JTM/TAAA021

14. Biggerstaff M, Cauchemez S, Reed C, Gambhir M, Finelli L. Estimates of the reproduction number for seasonal, pandemic, and zoonotic influenza: A systematic review of the literature. *BMC Infect Dis* (2014) 14:480-. doi:10.1186/1471-2334-14-480/FIGURES/5

15. Liu Y, Rocklöv J. The effective reproductive number of the Omicron variant of SARS-CoV-2 is several times relative to Delta. *J Travel Med* (2022) 29:1–4. doi:10.1093/JTM/TAAC037

16. Silva ACE, Bernardes AT, Barbosa EAG, Das Chagas IAS, Dáttilo W, Reis AB, et al. Successive Pandemic Waves with Different Virulent Strains and the Effects of Vaccination for SARS-CoV-2. *Vaccines (Basel)* (2022) 10: doi:10.3390/VACCINES10030343/S1

17. Carabelli AM, Peacock TP, Thorne LG, Harvey WT, Hughes J, de Silva TI, et al. SARS-CoV-2 variant biology: immune escape, transmission and fitness. *Nature Reviews Microbiology 2023 21:3* (2023) 21:162–177. doi:10.1038/s41579-022-00841-7

18. McAloon C, Collins Á, Hunt K, Barber A, Byrne AW, Butler F, et al. Incubation period of COVID-19: a rapid systematic review and meta-analysis of observational research. *BMJ Open* (2020) 10:e039652. doi:10.1136/BMJOPEN-2020-039652

19. Wu Y, Kang L, Guo Z, Liu J, Liu M, Liang W. Incubation Period of COVID-19 Caused by Unique SARS-CoV-2 Strains: A Systematic Review and Meta-analysis. *JAMA Netw Open* (2022) 5:e2228008–e2228008. doi:10.1001/JAMANETWORKOPEN.2022.28008

20. Tindale LC, Stockdale JE, Coombe M, Garlock ES, Lau WYV, Saraswat M, et al. Evidence for transmission of covid-19 prior to symptom onset. *Elife* (2020) 9:1–34. doi:10.7554/ELIFE.57149

21. Ma Q, Liu J, Liu Q, Kang L, Liu R, Jing W, et al. Global Percentage of Asymptomatic SARS-CoV-2 Infections Among the Tested Population and Individuals

With Confirmed COVID-19 Diagnosis: A Systematic Review and Meta-analysis. *JAMA Netw Open* (2021) 4:e2137257–e2137257. doi:10.1001/JAMANETWORKOPEN.2021.37257

22. Wang B, Andraweera P, Elliott S, Mohammed H, Lassi Z, Twigger A, et al. Asymptomatic SARS-CoV-2 Infection by Age: A Global Systematic Review and Meta-analysis. *Pediatric Infectious Disease Journal* (2023) 42:232–239. doi:10.1097/INF.0000000000003791

23. Almadhi MA, Abdulrahman A, Sharaf SA, AlSaad D, Stevenson NJ, Atkin SL, et al. The high prevalence of asymptomatic SARS-CoV-2 infection reveals the silent spread of COVID-19. *International Journal of Infectious Diseases* (2021) 105:656–661. doi:10.1016/j.ijid.2021.02.100

24. Sah P, Fitzpatrick MC, Zimmer CF, Abdollahi E, Juden-Kelly L, Moghadas SM, et al. Asymptomatic SARS-CoV-2 infection: A systematic review and meta-analysis. *Proc Natl Acad Sci U S A* (2021) 118:e2109229118. doi:10.1073/PNAS.2109229118;WGROUP:STRING:PUBLICATION

25. Gili R, Burioni R. SARS-CoV-2 before and after Omicron: two different viruses and two different diseases? *Journal of Translational Medicine 2023 21:1* (2023) 21:251-. doi:10.1186/S12967-023-04095-6

26. Baj J, Karakuła-Juchnowicz H, Teresiński G, Buszewicz G, Ciesielka M, Sitarz R, et al. COVID-19: Specific and Non-Specific Clinical Manifestations and Symptoms: The Current State of Knowledge. *Journal of Clinical Medicine 2020, Vol 9,* (2020) 9:1–22. doi:10.3390/JCM9061753

27. Tsukahara T, Brann DH, Datta SR. Mechanisms of SARS-CoV-2-associated anosmia. *https://doi.org/101152/physrev000122023* (2023) 103: doi:10.1152/PHYSREV.00012.2023

28. Villapol S. Gastrointestinal symptoms associated with COVID-19: impact on the gut microbiome. *Translational Research* (2020) 226:57–69. doi:10.1016/J.TRSL.2020.08.004

29. Thevarajan I, Buising KL, Cowie BC. Clinical presentation and management of COVID-19. *Medical Journal of Australia* (2020) 213:134–139. doi:10.5694/MJA2.50698;PAGE:STRING:ARTICLE/CHAPTER

30. Elezkurtaj S, Greuel S, Ihlow J, Michaelis EG, Bischoff P, Kunze CA, et al. Causes of death and comorbidities in hospitalized patients with COVID-19. *Scientific Reports 2021 11:1* (2021) 11:4263-. doi:10.1038/s41598-021-82862-5

31. de Roquetaillade C, Bredin S, Lascarrou JB, Soumagne T, Cojocaru M, Chousterman BG, et al. Timing and causes of death in severe COVID-19 patients. *Critical Care 2021 25:1* (2021) 25:224-. doi:10.1186/S13054-021-03639-W

32. Ng WH, Tipih T, Makoah NA, Vermeulen JG, Goedhals D, Sempa JB, et al. Comorbidities in SARS-CoV-2 patients: A systematic review and meta-analysis. *mBio* (2021) 12:1–12. doi:10.1128/MBIO.03647-20;REQUESTEDJOURNAL:JOURNAL:MBIO;PAGE:STRING:ARTICLE/CHAPTER

33. People with Certain Medical Conditions and COVID-19 Risk Factors | Covid | CDC. Available at: https://www.cdc.gov/covid/risk-factors/index.html [Accessed December 31, 2025]

34. Underlying Conditions and the Higher Risk for Severe COVID-19 | Covid | CDC. Available at: https://www.cdc.gov/covid/hcp/clinical-care/underlying-conditions.html [Accessed December 31, 2025]

35. Tejada-Vera B, Kramarow EA. Key findings Data from the National Vital Statistics System. (2020) Available at: https://www.cdc.gov/nchs/products/index.htm. [Accessed December 31, 2025]

36. Gallo A, Pero E, Pellegrino S, Macerola N, Murace CA, Ibba F, et al. How can Biology of Aging Explain the Severity of COVID-19 in Older Adults. *Clin Geriatr Med* (2022) 38:461–472. doi:10.1016/j.cger.2022.04.002

37. Pietrobon AJ, Teixeira FME, Sato MN. I mmunosenescence and Inflammaging: Risk Factors of Severe COVID-19 in Older People. *Front Immunol* (2020) 11:579220. doi:10.3389/FIMMU.2020.579220/FULL

38. Jorgensen SCJ, Hernandez A, Buchan SA, Fitzpatrick T, Guttmann A, Morris SK, et al. Burden of Illness Associated With Respiratory Syncytial Virus, Influenza, and Coronavirus Disease 2019 in Infants and Young Children in Ontario, Canada, 2018–2023: A Population-Based Canadian Immunization Research Network Study. *Open Forum Infect Dis* (2024) 11: doi:10.1093/OFID/OFAE601

39. Dhochak N, Singhal T, Kabra SK, Lodha R. Pathophysiology of COVID-19: Why Children Fare Better than Adults? *The Indian Journal of Pediatrics 2020 87:7* (2020) 87:537–546. doi:10.1007/S12098-020-03322-Y

40. Laris-González A, Avilés-Robles M, Domínguez-Barrera C, Parra-Ortega I, Sánchez-Huerta JL, Ojeda-Diezbarroso K, et al. Influenza vs. COVID-19: Comparison of Clinical Characteristics and Outcomes in Pediatric Patients in Mexico City. *Front Pediatr* (2021) 9:676611. doi:10.3389/FPED.2021.676611/BIBTEX

41. Twitchell DK, Christensen MB, Hackett G, Morgentaler A, Saad F, Pastuszak AW. Examining Male Predominance of Severe COVID-19 Outcomes: A Systematic Review. *https://home.liebertpub.com/andro* (2022) 3:41–53. doi:10.1089/ANDRO.2022.0006

42. Pradhan A, Olsson PE. Sex differences in severity and mortality from COVID-19: are males more vulnerable? *Biology of Sex Differences 2020 11:1* (2020) 11:53-. doi:10.1186/S13293-020-00330-7

43. Peckham H, de Gruijter NM, Raine C, Radziszewska A, Ciurtin C, Wedderburn LR, et al. Male sex identified by global COVID-19 meta-analysis as a risk factor for death and ITU admission. *Nature Communications 2020 11:1* (2020) 11:6317-. doi:10.1038/s41467-020-19741-6

44. Soriano JB, Murthy S, Marshall JC, Relan P, Diaz J V. A clinical case definition of post-COVID-19 condition by a Delphi consensus. *Lancet Infect Dis* (2022) 22:e102–e107. doi:10.1016/S1473-3099(21)00703-9

45. Greenhalgh T, Sivan M, Perlowski A, Nikolich J. Long COVID: a clinical update. *The Lancet* (2024) 404:707–724. doi:10.1016/S0140-6736(24)01136-X

46. Davis HE, McCorkell L, Vogel JM, Topol EJ. Long COVID: major findings, mechanisms and recommendations. *Nature Reviews Microbiology 2023 21:3* (2023) 21:133–146. doi:10.1038/s41579-022-00846-2

47. Gorenshtein A, Leibovitch L, Liba T, Stern S, Stern Y. Gender Disparities in Neurological Symptoms of Long COVID: A Systematic Review and Meta-Analysis. *Neuroepidemiology* (2025) 59:426–440. doi:10.1159/000540919

48. Bai F, Tomasoni D, Falcinella C, Barbanotti D, Castoldi R, Mulè G, et al. Female gender is associated with long COVID syndrome: a prospective cohort study. *Clinical Microbiology and Infection* (2022) 28:611.e9-611.e16. doi:10.1016/j.cmi.2021.11.002

49. Masters PS. The Molecular Biology of Coronaviruses. *Adv Virus Res* (2006) 66:193–292. doi:10.1016/S0065-3527(06)66005-3

50. Tang G, Liu Z, Chen D. Human coronaviruses: Origin, host and receptor. *Journal of Clinical Virology* (2022) 155:105246. doi:10.1016/J.JCV.2022.105246

51. Liu DX, Liang JQ, Fung TS. "Human Coronavirus-229E, -OC43, -NL63, and -HKU1 (Coronaviridae)," in *Encyclopedia of Virology: Volume 1-5, Fourth Edition* (Academic Press), 428–440. doi:10.1016/B978-0-12-809633-8.21501-X

52. Pormohammad A, Ghorbani S, Khatami A, Farzi R, Baradaran B, Turner DL, et al. Comparison of confirmed COVID-19 with SARS and MERS cases - Clinical characteristics, laboratory findings, radiographic signs and outcomes: A systematic review

and meta-analysis. *Rev Med Virol* (2020) 30:e2112. doi:10.1002/RMV.2112;WGROUP:STRING:PUBLICATION

53. Cui J, Li F, Shi ZL. Origin and evolution of pathogenic coronaviruses. *Nat Rev Microbiol* (2019) 17:181–192. doi:10.1038/S41579-018-0118-9;SUBJMETA

54. Cherry JD, Krogstad P. SARS: The First Pandemic of the 21st Century. *Pediatric Research 2004 56:1* (2004) 56:1–5. doi:10.1203/01.pdr.0000129184.87042.fc

55. Lam WK, Zhong NS, Tan WC. Overview on SARS in Asia and the World. *Respirology* (2003) 8:S2–S5. doi:10.1046/J.1440-1843.2003.00516.X;PAGE:STRING:ARTICLE/CHAPTER

56. Islam MM, Khanom H, Farag E, Mim ZT, Naidoo P, Mkhize-Kwitshana ZL, et al. Global patterns of Middle East respiratory syndrome coronavirus (MERS-CoV) prevalence and seroprevalence in camels: A systematic review and meta-analysis. *One Health* (2023) 16:100561. doi:10.1016/J.ONEHLT.2023.100561

57. Sikkema RS, Farag EABA, Islam M, Atta M, Reusken CBEM, Al-Hajri MM, et al. Global status of Middle East respiratory syndrome coronavirus in dromedary camels: a systematic review. *Epidemiol Infect* (2019) 147:e84. doi:10.1017/S095026881800345X

58. Gorkhali R, Koirala P, Rijal S, Mainali A, Baral A, Bhattarai HK. Structure and Function of Major SARS-CoV-2 and SARS-CoV Proteins. *Bioinform Biol Insights* (2021) 15: doi:10.1177/11779322211025876;PAGEGROUP:STRING:PUBLICATION

59. V'kovski P, Kratzel A, Steiner S, Stalder H, Thiel V. Coronavirus biology and replication: implications for SARS-CoV-2. *Nature Reviews Microbiology 2020 19:3* (2020) 19:155–170. doi:10.1038/s41579-020-00468-6

60. Takada K, Ueda MT, Shichinohe S, Kida Y, Ono C, Matsuura Y, et al. Genomic diversity of SARS-CoV-2 can be accelerated by mutations in the nsp14 gene. *iScience* (2023) 26:106210. doi:10.1016/j.isci.2023.106210

61. Amicone M, Borges V, Alves MJ, Isidro J, Zé-Zé L, Duarte S, et al. Mutation rate of SARS-CoV-2 and emergence of mutators during experimental evolution. *Evol Med Public Health* (2022) 10:142–155. doi:10.1093/EMPH/EOAC010

62. Brant AC, Hu Z, Chen AZ, Majerciak V, Yewdell J, Zheng Z-M. Discontinuous template switching generates coronavirus subgenomic RNAs from the 3′ viral genome end by 5′ to 3′ transcription. *J Virol* (2025) 99: doi:10.1128/JVI.01438-25;WGROUP:STRING:PUBLICATION

63. Chen Z, Ng RWY, Lui G, Ling L, Chow C, Yeung ACM, et al. Profiling of SARS-CoV-2 Subgenomic RNAs in Clinical Specimens. *Microbiol Spectr* (2022) 10: doi:10.1128/SPECTRUM.00182-22;CTYPE:STRING:JOURNAL

64. Kim D, Lee JY, Yang JS, Kim JW, Kim VN, Chang H. The Architecture of SARS-CoV-2 Transcriptome. *Cell* (2020) 181:914-921.e10. doi:10.1016/j.cell.2020.04.011

65. Williams R, Hales J, Collier W, Gould P, Williams R, Hales J, et al. Coronavirus Replication: Genomes, Subgenomic RNAs, and Defective Viral Genomes. *Viruses 2025, Vol 17,* (2025) 17: doi:10.3390/V17060767

66. Bai Z, Cao Y, Liu W, Li J, Bai Z, Cao Y, et al. The SARS-CoV-2 Nucleocapsid Protein and Its Role in Viral Structure, Biological Functions, and a Potential Target for Drug or Vaccine Mitigation. *Viruses 2021, Vol 13,* (2021) 13: doi:10.3390/V13061115

67. Lu S, Ye Q, Singh D, Cao Y, Diedrich JK, Yates JR, et al. The SARS-CoV-2 nucleocapsid phosphoprotein forms mutually exclusive condensates with RNA and the membrane-associated M protein. *Nature Communications 2021 12:1* (2021) 12:502-. doi:10.1038/s41467-020-20768-y

68. Cong Y, Ulasli M, Schepers H, Mauthe M, V'kovski P, Kriegenburg F, et al. Nucleocapsid Protein Recruitment to Replication-Transcription Complexes Plays a Crucial Role in Coronaviral Life Cycle. *J Virol* (2020) 94: doi:10.1128/JVI.01925-19;REQUESTEDJOURNAL:JOURNAL:JVI;JOURNAL:JOURNAL:JVI;PAGE:STRING:ARTICLE/CHAPTER

69. Mu J, Fang Y, Yang Q, Shu T, Wang A, Huang M, et al. SARS-CoV-2 N protein antagonizes type I interferon signaling by suppressing phosphorylation and nuclear translocation of STAT1 and STAT2. *Cell Discovery 2020 6:1* (2020) 6:65-. doi:10.1038/s41421-020-00208-3

70. Wang WA, Carreras-Sureda A, Demaurex N. SARS-CoV-2 infection alkalinizes the ERGIC and lysosomes through the viroporin activity of the viral envelope protein. *J Cell Sci* (2023) 136: doi:10.1242/JCS.260685/297320

71. Breitinger U, Farag NS, Sticht H, Breitinger HG. Viroporins: Structure, function, and their role in the life cycle of SARS-CoV-2. *Int J Biochem Cell Biol* (2022) 145:106185. doi:10.1016/J.BIOCEL.2022.106185

72. Medeiros-Silva J, Dregni AJ, Somberg NH, Duan P, Hong M. Atomic structure of the open SARS-CoV-2 E viroporin. *Sci Adv* (2023) 9: doi:10.1126/SCIADV.ADI9007;CSUBTYPE:STRING:SPECIAL;PAGE:STRING:ARTICLE/CHAPTER

73. Zhang Z, Nomura N, Muramoto Y, Ekimoto T, Uemura T, Liu K, et al. Structure of SARS-CoV-2 membrane protein essential for virus assembly. *Nature Communications 2022 13:1* (2022) 13:4399-. doi:10.1038/s41467-022-32019-3

74. Zheng Y, Zhuang MW, Han L, Zhang J, Nan ML, Zhan P, et al. Severe acute respiratory syndrome coronavirus 2 (SARS-CoV-2) membrane (M) protein inhibits type I and III interferon production by targeting RIG-I/MDA-5 signaling. *Signal Transduction and Targeted Therapy 2021 5:1* (2020) 5:299-. doi:10.1038/s41392-020-00438-7

75. Wrapp D, Wang N, Corbett KS, Goldsmith JA, Hsieh C-L, Abiona O, et al. Cryo-EM structure of the 2019-nCoV spike in the prefusion conformation. *Science (1979)* (2020) 367:1260–1263. doi:10.1126/SCIENCE.ABB2507;WEBSITE:WEBSITE:AAAS-SITE;ISSUE:ISSUE:DOI

76. Jackson CB, Farzan M, Chen B, Choe H. Mechanisms of SARS-CoV-2 entry into cells. *Nature Reviews Molecular Cell Biology 2021 23:1* (2021) 23:3–20. doi:10.1038/s41580-021-00418-x

77. Walls AC, Park YJ, Tortorici MA, Wall A, McGuire AT, Veesler D. Structure, Function, and Antigenicity of the SARS-CoV-2 Spike Glycoprotein. *Cell* (2020) 181:281-292.e6. doi:10.1016/J.CELL.2020.02.058

78. Lan J, Ge J, Yu J, Shan S, Zhou H, Fan S, et al. Structure of the SARS-CoV-2 spike receptor-binding domain bound to the ACE2 receptor. *Nature 2020 581:7807* (2020) 581:215–220. doi:10.1038/s41586-020-2180-5

79. Hamming I, Timens W, Bulthuis MLC, Lely AT, Navis GJ, van Goor H. Tissue distribution of ACE2 protein, the functional receptor for SARS coronavirus. A first step in understanding SARS pathogenesis. *Journal of Pathology* (2004) 203:631–637. doi:10.1002/PATH.1570;CTYPE:STRING:JOURNAL

80. Hikmet F, Méar L, Edvinsson Å, Micke P, Uhlén M, Lindskog C. The protein expression profile of ACE2 in human tissues. *Molecular Systems Biology 2020 16:7* (2020) 16:MSB209610-. doi:10.15252/MSB.20209610

81. Pang YT, Acharya A, Lynch DL, Pavlova A, Gumbart JC. SARS-CoV-2 spike opening dynamics and energetics reveal the individual roles of glycans and their collective impact. *Communications Biology 2022 5:1* (2022) 5:1170-. doi:10.1038/s42003-022-04138-6

82. Gobeil SMC, Janowska K, McDowell S, Mansouri K, Parks R, Stalls V, et al. Effect of natural mutations of SARS-CoV-2 on spike structure, conformation, and antigenicity. *Science (1979)* (2021) 373: doi:10.1126/SCIENCE.ABI6226;WEBSITE:WEBSITE:AAAS-SITE;JOURNAL:JOURNAL:SCIENCE;WGROUP:STRING:PUBLICATION

83. Díaz-Salinas MA, Jain A, Durham ND, Munro JB. Single-molecule imaging reveals allosteric stimulation of SARS-CoV- 2 spike receptor binding domain by host

sialic acid. *Sci Adv* (2024) 10:4920. doi:10.1126/SCIADV.ADK4920;PAGEGROUP:STRING:PUBLICATION

84. Tomris I, Unione L, Nguyen L, Zaree P, Bouwman KM, Liu L, et al. SARS-CoV-2 Spike N-Terminal Domain Engages 9-O-Acetylated α2–8-Linked Sialic Acids. *ACS Chem Biol* (2023) 18:1180–1191. doi:10.1021/ACSCHEMBIO.3C00066

85. Olmedillas E, Rajamanickam RR, Avalos RD, Ana-Sosa-Batiz F, Zyla D, Zandonatti MA, et al. Structure of a SARS-CoV-2 spike S2 subunit in a pre-fusion, open conformation. *Cell Rep* (2025) 44:116052. doi:10.1016/j.celrep.2025.116052

86. Johnson BA, Xie X, Bailey AL, Kalveram B, Lokugamage KG, Muruato A, et al. Loss of furin cleavage site attenuates SARS-CoV-2 pathogenesis. *Nature 2021 591:7849* (2021) 591:293–299. doi:10.1038/s41586-021-03237-4

87. Cai Y, Zhang J, Xiao T, Peng H, Sterling SM, Walsh RM, et al. Distinct conformational states of SARS-CoV-2 spike protein. *Science (1979)* (2020) 369: doi:10.1126/SCIENCE.ABD4251;PAGE:STRING:ARTICLE/CHAPTER

88. Li Q, Liu Y, Zhang L. Cytoplasmic tail determines the membrane trafficking and localization of SARS-CoV-2 spike protein. *Front Mol Biosci* (2022) 9:1004036. doi:10.3389/FMOLB.2022.1004036/BIBTEX

89. Dey D, Qing E, He Y, Chen Y, Jennings B, Cohn W, et al. A single C-terminal residue controls SARS-CoV-2 spike trafficking and incorporation into VLPs. *Nature Communications 2023 14:1* (2023) 14:8358-. doi:10.1038/s41467-023-44076-3

90. Yurkovetskiy L, Wang X, Pascal KE, Tomkins-Tinch C, Nyalile TP, Wang Y, et al. Structural and Functional Analysis of the D614G SARS-CoV-2 Spike Protein Variant. *Cell* (2020) 183:739-751.e8. doi:10.1016/j.cell.2020.09.032

91. Plante JA, Liu Y, Liu J, Xia H, Johnson BA, Lokugamage KG, et al. Spike mutation D614G alters SARS-CoV-2 fitness. *Nature 2020 592:7852* (2020) 592:116–121. doi:10.1038/s41586-020-2895-3

92. Zhou B, Thao TTN, Hoffmann D, Taddeo A, Ebert N, Labroussaa F, et al. SARS-CoV-2 spike D614G change enhances replication and transmission. *Nature 2021 592:7852* (2021) 592:122–127. doi:10.1038/s41586-021-03361-1

93. Mansbach RA, Chakraborty S, Nguyen K, Montefiori DC, Korber B, Gnanakaran S. The SARS-CoV-2 Spike variant D614G favors an open conformational state. *Sci Adv* (2021) 7:3671–3687. doi:10.1126/SCIADV.ABF3671;JOURNAL:JOURNAL:SCIADV;WEBSITE:WEBSITE:AAAS-

SITE;REQUESTEDJOURNAL:JOURNAL:SCIADV;WGROUP:STRING:PUBLICATIO
N

94. Hill V, Plessis L Du, Peacock TP, Aggarwal D, Colquhoun R, Carabelli AM, et al. The origins and molecular evolution of SARS-CoV-2 lineage B.1.1.7 in the UK. *Virus Evol* (2022) 8: doi:10.1093/VE/VEAC080

95. Liu Y, Liu J, Plante KS, Plante JA, Xie X, Zhang X, et al. The N501Y spike substitution enhances SARS-CoV-2 infection and transmission. *Nature 2021 602:7896* (2021) 602:294–299. doi:10.1038/s41586-021-04245-0

96. Bolze A, Luo S, White S, Cirulli ET, Wyman D, Dei Rossi A, et al. SARS-CoV-2 variant Delta rapidly displaced variant Alpha in the United States and led to higher viral loads. *Cell Rep Med* (2022) 3:100564. doi:10.1016/J.XCRM.2022.100564

97. Twohig KA, Nyberg T, Zaidi A, Thelwall S, Sinnathamby MA, Aliabadi S, et al. Hospital admission and emergency care attendance risk for SARS-CoV-2 delta (B.1.617.2) compared with alpha (B.1.1.7) variants of concern: a cohort study. *Lancet Infect Dis* (2022) 22:35–42. doi:10.1016/S1473-3099(21)00475-8

98. Mlcochova P, Kemp SA, Dhar MS, Papa G, Meng B, Ferreira IATM, et al. SARS-CoV-2 B.1.617.2 Delta variant replication and immune evasion. *Nature 2021 599:7883* (2021) 599:114–119. doi:10.1038/s41586-021-03944-y

99. Motozono C, Toyoda M, Zahradnik J, Saito A, Nasser H, Tan TS, et al. SARS-CoV-2 spike L452R variant evades cellular immunity and increases infectivity. *Cell Host Microbe* (2021) 29:1124-1136.e11. doi:10.1016/J.CHOM.2021.06.006

100. Viana R, Moyo S, Amoako DG, Tegally H, Scheepers C, Althaus CL, et al. Rapid epidemic expansion of the SARS-CoV-2 Omicron variant in southern Africa. *Nature 2022 603:7902* (2022) 603:679–686. doi:10.1038/s41586-022-04411-y

101. Wei C, Shan KJ, Wang W, Zhang S, Huan Q, Qian W. Evidence for a mouse origin of the SARS-CoV-2 Omicron variant. *Journal of Genetics and Genomics* (2021) 48:1111–1121. doi:10.1016/J.JGG.2021.12.003

102. Mallapaty S. Where did Omicron come from? Three key theories. *Nature* (2022) 602:26–28. doi:10.1038/D41586-022-00215-2;SUBJMETA

103. Willett BJ, Grove J, MacLean OA, Wilkie C, De Lorenzo G, Furnon W, et al. SARS-CoV-2 Omicron is an immune escape variant with an altered cell entry pathway. *Nature Microbiology 2022 7:8* (2022) 7:1161–1179. doi:10.1038/s41564-022-01143-7

104. Daria S, Islam MR. The SARS-CoV-2 omicron wave is indicating the end of the pandemic phase but the COVID-19 will continue. *J Med Virol* (2022) 94:2343–2345. doi:10.1002/JMV.27635;JOURNAL:JOURNAL:10969071;ISSUE:ISSUE:DOI

105. Saito A, Irie T, Suzuki R, Maemura T, Nasser H, Uriu K, et al. Enhanced fusogenicity and pathogenicity of SARS-CoV-2 Delta P681R mutation. *Nature 2021 602:7896* (2021) 602:300–306. doi:10.1038/s41586-021-04266-9

106. Mykytyn AZ, Breugem TI, Geurts MH, Beumer J, Schipper D, Acker R van, et al. SARS-CoV-2 Omicron entry is type II transmembrane serine protease-mediated in human airway and intestinal organoid models. *J Virol* (2023) 97: doi:10.1128/JVI.00851-23

107. Meng B, Abdullahi A, Ferreira IATM, Goonawardane N, Saito A, Kimura I, et al. Altered TMPRSS2 usage by SARS-CoV-2 Omicron impacts infectivity and fusogenicity. *Nature 2022 603:7902* (2022) 603:706–714. doi:10.1038/s41586-022-04474-x

108. Papa G, Mallery DL, Albecka A, Welch LG, Cattin-Ortolá J, Luptak J, et al. Furin cleavage of SARS-CoV-2 Spike promotes but is not essential for infection and cell-cell fusion. *PLoS Pathog* (2021) 17:e1009246. doi:10.1371/JOURNAL.PPAT.1009246

109. Hoffmann M, Kleine-Weber H, Schroeder S, Krüger N, Herrler T, Erichsen S, et al. SARS-CoV-2 Cell Entry Depends on ACE2 and TMPRSS2 and Is Blocked by a Clinically Proven Protease Inhibitor. *Cell* (2020) 181:271-280.e8. doi:10.1016/j.cell.2020.02.052

110. Fan Y, Li X, Zhang L, Wan S, Zhang L, Zhou F. SARS-CoV-2 Omicron variant: recent progress and future perspectives. *Signal Transduction and Targeted Therapy 2022 7:1* (2022) 7:141-. doi:10.1038/s41392-022-00997-x

111. Rössler A, Netzl A, Knabl L, Schäfer H, Wilks SH, Bante D, et al. BA.2 and BA.5 omicron differ immunologically from both BA.1 omicron and pre-omicron variants. *Nature Communications 2022 13:1* (2022) 13:7701-. doi:10.1038/s41467-022-35312-3

112. Wang Q, Guo Y, Iketani S, Nair MS, Li Z, Mohri H, et al. Antibody evasion by SARS-CoV-2 Omicron subvariants BA.2.12.1, BA.4 and BA.5. *Nature 2022 608:7923* (2022) 608:603–608. doi:10.1038/s41586-022-05053-w

113. Cao Y, Yisimayi A, Jian F, Song W, Xiao T, Wang L, et al. BA.2.12.1, BA.4 and BA.5 escape antibodies elicited by Omicron infection. *Nature 2022 608:7923* (2022) 608:593–602. doi:10.1038/s41586-022-04980-y

114. Tamura T, Ito J, Uriu K, Zahradnik J, Kida I, Anraku Y, et al. Virological characteristics of the SARS-CoV-2 XBB variant derived from recombination of two Omicron subvariants. *Nature Communications 2023 14:1* (2023) 14:2800-. doi:10.1038/s41467-023-38435-3

115. Qu P, Faraone JN, Evans JP, Zheng YM, Carlin C, Anghelina M, et al. Enhanced evasion of neutralizing antibody response by Omicron XBB.1.5, CH.1.1, and CA.3.1 variants. *Cell Rep* (2023) 42:112443. doi:10.1016/J.CELREP.2023.112443

116. Naveed Siddiqui A, Musharaf I, Gulumbe BH. The JN.1 variant of COVID-19: immune evasion, transmissibility, and implications for global health. *Ther Adv Infect Dis* (2025) 12: doi:10.1177/20499361251314763;CTYPE:STRING:JOURNAL

117. Wang Q, Mellis IA, Ho J, Bowen A, Kowalski-Dobson T, Valdez R, et al. Recurrent SARS-CoV-2 spike mutations confer growth advantages to select JN.1 sublineages. *Emerg Microbes Infect* (2024) 13: doi:10.1080/22221751.2024.2402880;ISSUE:ISSUE:DOI

118. Hu Y, Zou J, Nguyen MD, Chang HC, Yeung J, Hao H, et al. Comparative analysis of replication and immune evasion among SARS-CoV-2 subvariants BA.2.86, JN.1, KP.2, and KP.3. *mBio* (2025) 16: doi:10.1128/MBIO.03503-24;WEBSITE:WEBSITE:ASMJ;ISSUE:ISSUE:DOI

119. Aljabali AAA, Lundstrom K, Hromić-Jahjefendić A, El-Baky NA, Nawn D, Hassan SkS, et al. The XEC Variant: Genomic Evolution, Immune Evasion, and Public Health Implications. *Viruses 2025, Vol 17,* (2025) 17: doi:10.3390/V17070985

120. Liu J, Yu Y, Yang S, Jian F, Song W, Yu L, et al. Virological and antigenic characteristics of SARS-CoV-2 variants LF.7.2.1, NP.1, and LP.8.1. *Lancet Infect Dis* (2025) 25:e128–e130. doi:10.1016/S1473-3099(25)00015-5

121. COVID-19 Vaccines (2025-2026 Formula) for Use in the United States Beginning in Fall 2025 | FDA. Available at: https://www.fda.gov/vaccines-blood-biologics/industry-biologics/covid-19-vaccines-2025-2026-formula-use-united-states-beginning-fall-2025 [Accessed December 31, 2025]

122. Guo C, Yu Y, Liu J, Jian F, Yang S, Song W, et al. Antigenic and virological characteristics of SARS-CoV-2 variants BA.3.2, XFG, and NB.1.8.1. *Lancet Infect Dis* (2025) 25:e374–e377. doi:10.1016/S1473-3099(25)00308-1

123. Mellis IA, Wu M, Hong H, Tzang CC, Bowen A, Wang Q, et al. Antibody evasion and receptor binding of SARS-CoV-2 LP.8.1.1, NB.1.8.1, XFG, and related subvariants. *Cell Rep* (2025) 44:116440. doi:10.1016/J.CELREP.2025.116440

124. SARS-CoV-2 variants in analyzed sequences, Canada. Available at: https://ourworldindata.org/grapher/covid-variants-area?country=~CAN [Accessed December 31, 2025]

125. Premkumar L, Segovia-Chumbez B, Jadi R, Martinez DR, Raut R, Markmann AJ, et al. The receptor-binding domain of the viral spike protein is an immunodominant and highly specific target of antibodies in SARS-CoV-2 patients. *Sci Immunol* (2020) 5:8413. doi:10.1126/SCIIMMUNOL.ABC8413;WEBSITE:WEBSITE:AAAS-SITE;WGROUP:STRING:PUBLICATION

126. Guthmiller JJ, Stovicek O, Wang J, Changrob S, Li L, Halfmann P, et al. SARS-CoV-2 infection severity is linked to superior humoral immunity against the spike. *mBio* (2021) 12:1–13. doi:10.1128/MBIO.02940-20;PAGE:STRING:ARTICLE/CHAPTER

127. Noble CCA, McDonald E, Nicholson S, Biering-Sørensen S, Pittet LF, Byrne AL, et al. Characterising the SARS-CoV-2 nucleocapsid (N) protein antibody response. *Journal of Infection* (2025) 90:106436. doi:10.1016/j.jinf.2025.106436

128. Amrun SN, Lee CYP, Lee B, Fong SW, Young BE, Chee RSL, et al. Linear B-cell epitopes in the spike and nucleocapsid proteins as markers of SARS-CoV-2 exposure and disease severity. *EBioMedicine* (2020) 58:102911. doi:10.1016/j.ebiom.2020.102911

129. Heffron AS, McIlwain SJ, Amjadi MF, Baker DA, Khullar S, Armbrust T, et al. The landscape of antibody binding in SARS-CoV-2 infection. *PLoS Biol* (2021) 19:e3001265. doi:10.1371/JOURNAL.PBIO.3001265

130. Li Y, Xu Z, Lei Q, Lai D yun, Hou H, Jiang H wei, et al. Antibody landscape against SARS-CoV-2 reveals significant differences between non-structural/accessory and structural proteins. *Cell Rep* (2021) 36:109391. doi:10.1016/j.celrep.2021.109391

131. Hachim A, Gu H, Kavian O, Mori M, Kwan MYW, Chan WH, et al. SARS-CoV-2 accessory proteins reveal distinct serological signatures in children. *Nature Communications 2022 13:1* (2022) 13:2951-. doi:10.1038/s41467-022-30699-5

132. Jörrißen P, Schütz P, Weiand M, Vollenberg R, Schrempf IM, Ochs K, et al. Antibody Response to SARS-CoV-2 Membrane Protein in Patients of the Acute and Convalescent Phase of COVID-19. *Front Immunol* (2021) 12:679841. doi:10.3389/FIMMU.2021.679841/BIBTEX

133. Cervia C, Nilsson J, Zurbuchen Y, Valaperti A, Schreiner J, Wolfensberger A, et al. Systemic and mucosal antibody responses specific to SARS-CoV-2 during mild versus severe COVID-19. *Journal of Allergy and Clinical Immunology* (2021) 147:545-557.e9. doi:10.1016/j.jaci.2020.10.040

134. Sterlin D, Mathian A, Miyara M, Mohr A, Anna F, Claër L, et al. IgA dominates the early neutralizing antibody response to SARS-CoV-2. *Sci Transl Med* (2021) 13:2223. doi:10.1126/SCITRANSLMED.ABD2223;CTYPE:STRING:JOURNAL

135. Morales-Núñez JJ, Muñoz-Valle JF, Torres-Hernández PC, Hernández-Bello J, Morales-Núñez JJ, Muñoz-Valle JF, et al. Overview of Neutralizing Antibodies and Their Potential in COVID-19. *Vaccines 2021, Vol 9,* (2021) 9: doi:10.3390/VACCINES9121376

136. Chen Y, Zhao X, Zhou H, Zhu H, Jiang S, Wang P. Broadly neutralizing antibodies to SARS-CoV-2 and other human coronaviruses. *Nature Reviews Immunology 2022 23:3* (2022) 23:189–199. doi:10.1038/s41577-022-00784-3

137. Li CJ, Chang SC. SARS-CoV-2 spike S2-specific neutralizing antibodies. *Emerg Microbes Infect* (2023) 12: doi:10.1080/22221751.2023.2220582;JOURNAL:JOURNAL:TEMI20;REQUESTEDJOURNAL:JOURNAL:TEMI20;ISSUE:ISSUE:DOI

138. Cromer D, Steain M, Reynaldi A, Schlub TE, Wheatley AK, Juno JA, et al. Neutralising antibody titres as predictors of protection against SARS-CoV-2 variants and the impact of boosting: a meta-analysis. *Lancet Microbe* (2022) 3:e52–e61. doi:10.1016/S2666-5247(21)00267-6

139. Khoury DS, Cromer D, Reynaldi A, Schlub TE, Wheatley AK, Juno JA, et al. Neutralizing antibody levels are highly predictive of immune protection from symptomatic SARS-CoV-2 infection. *Nature Medicine 2021 27:7* (2021) 27:1205–1211. doi:10.1038/s41591-021-01377-8

140. Zhang A, Stacey HD, D'Agostino MR, Tugg Y, Marzok A, Miller MS. Beyond neutralization: Fc-dependent antibody effector functions in SARS-CoV-2 infection. *Nature Reviews Immunology 2022 23:6* (2022) 23:381–396. doi:10.1038/s41577-022-00813-1

141. Tong X, McNamara RP, Avendaño MJ, Serrano EF, García-Salum T, Pardo-Roa C, et al. Waning and boosting of antibody Fc-effector functions upon SARS-CoV-2 vaccination. *Nat Commun* (2023) 14:1–15. doi:10.1038/S41467-023-39189-8;TECHMETA

142. Bartsch YC, Tong X, Kang J, Avendano MJ, Serrano EF, García-Salum T, et al. Omicron variant Spike-specific antibody binding and Fc activity are preserved in recipients of mRNA or inactivated COVID-19 vaccines. *Sci Transl Med* (2022) 14:9243. doi:10.1126/SCITRANSLMED.ABN9243;JOURNAL:JOURNAL:STM;PAGE:STRING:ARTICLE/CHAPTER

143. Sette A, Crotty S. Adaptive immunity to SARS-CoV-2 and COVID-19. *Cell* (2021) 184:861–880. doi:10.1016/J.CELL.2021.01.007

144. Yong L, Hutchings C, Barnes E, Klenerman P, Provine NM. Distinct Requirements for CD4+ T Cell Help for Immune Responses Induced by mRNA and Adenovirus-Vector SARS-CoV-2 Vaccines. *Eur J Immunol* (2025) 55:e202451142. doi:10.1002/EJI.202451142;PAGE:STRING:ARTICLE/CHAPTER

145. Sekine T, Perez-Potti A, Rivera-Ballesteros O, Strålin K, Gorin JB, Olsson A, et al. Robust T Cell Immunity in Convalescent Individuals with Asymptomatic or Mild COVID-19. *Cell* (2020) 183:158-168.e14. doi:10.1016/j.cell.2020.08.017

146. Grifoni A, Weiskopf D, Ramirez SI, Mateus J, Dan JM, Moderbacher CR, et al. Targets of T Cell Responses to SARS-CoV-2 Coronavirus in Humans with COVID-19

Disease and Unexposed Individuals. *Cell* (2020) 181:1489-1501.e15. doi:10.1016/j.cell.2020.05.015

147. Tarke A, Sidney J, Kidd CK, Dan JM, Ramirez SI, Yu ED, et al. Comprehensive analysis of T cell immunodominance and immunoprevalence of SARS-CoV-2 epitopes in COVID-19 cases. *Cell Rep Med* (2021) 2:100204. doi:10.1016/J.XCRM.2021.100204

148. Cohen KW, Linderman SL, Moodie Z, Czartoski J, Lai L, Mantus G, et al. Longitudinal analysis shows durable and broad immune memory after SARS-CoV-2 infection with persisting antibody responses and memory B and T cells. *Cell Rep Med* (2021) 2:100354. doi:10.1016/J.XCRM.2021.100354

149. McMahan K, Yu J, Mercado NB, Loos C, Tostanoski LH, Chandrashekar A, et al. Correlates of protection against SARS-CoV-2 in rhesus macaques. *Nature 2020 590:7847* (2020) 590:630–634. doi:10.1038/s41586-020-03041-6

150. Liu J, Yu J, McMahan K, Jacob-Dolan C, He X, Giffin V, et al. CD8 T cells contribute to vaccine protection against SARS-CoV-2 in macaques. *Sci Immunol* (2022) 7: doi:10.1126/SCIIMMUNOL.ABQ7647

151. Grau-Expósito J, Sánchez-Gaona N, Massana N, Suppi M, Astorga-Gamaza A, Perea D, et al. Peripheral and lung resident memory T cell responses against SARS-CoV-2. *Nature Communications 2021 12:1* (2021) 12:3010-. doi:10.1038/s41467-021-23333-3

152. Harvey WT, Carabelli AM, Jackson B, Gupta RK, Thomson EC, Harrison EM, et al. SARS-CoV-2 variants, spike mutations and immune escape. *Nature Reviews Microbiology 2021 19:7* (2021) 19:409–424. doi:10.1038/s41579-021-00573-0

153. Roederer AL, Cao Y, St. Denis K, Sheehan ML, Li CJ, Lam EC, et al. Ongoing evolution of SARS-CoV-2 drives escape from mRNA vaccine-induced humoral immunity. *Cell Rep Med* (2024) 5:101850. doi:10.1016/J.XCRM.2024.101850

154. Markov P V., Ghafari M, Beer M, Lythgoe K, Simmonds P, Stilianakis NI, et al. The evolution of SARS-CoV-2. *Nature Reviews Microbiology 2023 21:6* (2023) 21:361–379. doi:10.1038/s41579-023-00878-2

155. Wibmer CK, Ayres F, Hermanus T, Madzivhandila M, Kgagudi P, Oosthuysen B, et al. SARS-CoV-2 501Y.V2 escapes neutralization by South African COVID-19 donor plasma. *Nat Med* (2021) 27:622–625. doi:10.1038/s41591-021-01285-x

156. Planas D, Veyer D, Baidaliuk A, Staropoli I, Guivel-Benhassine F, Rajah MM, et al. Reduced sensitivity of SARS-CoV-2 variant Delta to antibody neutralization. *Nature 2021 596:7871* (2021) 596:276–280. doi:10.1038/s41586-021-03777-9

157. Duyvesteyn HME, Dijokaite-Guraliuc A, Liu C, Supasa P, Kronsteiner B, Jeffery K, et al. Concerted deletions eliminate a neutralizing supersite in SARS-CoV-2 BA.2.87.1 spike. *Structure* (2024) 32:1594-1602.e6. doi:10.1016/j.str.2024.07.020

158. McCallum M, De Marco A, Lempp FA, Tortorici MA, Pinto D, Walls AC, et al. N-terminal domain antigenic mapping reveals a site of vulnerability for SARS-CoV-2. *Cell* (2021) 184:2332-2347.e16. doi:10.1016/J.CELL.2021.03.028

159. Cao Y, Wang J, Jian F, Xiao T, Song W, Yisimayi A, et al. Omicron escapes the majority of existing SARS-CoV-2 neutralizing antibodies. *Nature 2021 602:7898* (2021) 602:657–663. doi:10.1038/s41586-021-04385-3

160. Wilhelm A, Widera M, Grikscheit K, Toptan T, Schenk B, Pallas C, et al. Limited neutralisation of the SARS-CoV-2 Omicron subvariants BA.1 and BA.2 by convalescent and vaccine serum and monoclonal antibodies. *EBioMedicine* (2022) 82:104158. doi:10.1016/j.ebiom.2022.104158

161. Evans JP, Zeng C, Qu P, Faraone J, Zheng YM, Carlin C, et al. Neutralization of SARS-CoV-2 Omicron sub-lineages BA.1, BA.1.1, and BA.2. *Cell Host Microbe* (2022) 30:1093-1102.e3. doi:10.1016/j.chom.2022.04.014

162. Bartsch YC, Tong X, Kang J, Avendano MJ, Serrano EF, García-Salum T, et al. Omicron variant Spike-specific antibody binding and Fc activity are preserved in recipients of mRNA or inactivated COVID-19 vaccines. *Sci Transl Med* (2022) 14:9243. doi:10.1126/SCITRANSLMED.ABN9243;JOURNAL:JOURNAL:STM;PAGE:STRING:ARTICLE/CHAPTER

163. Tarke A, Sidney J, Methot N, Yu ED, Zhang Y, Dan JM, et al. Impact of SARS-CoV-2 variants on the total CD4+ and CD8+ T cell reactivity in infected or vaccinated individuals. *Cell Rep Med* (2021) 2:100355. doi:10.1016/J.XCRM.2021.100355

164. Mazzoni A, Vanni A, Spinicci M, Capone M, Lamacchia G, Salvati L, et al. SARS-CoV-2 Spike-Specific CD4+ T Cell Response Is Conserved Against Variants of Concern, Including Omicron. *Front Immunol* (2022) 13:801431. doi:10.3389/FIMMU.2022.801431/BIBTEX

165. Kaplonek P, Fischinger S, Cizmeci D, Bartsch YC, Kang J, Burke JS, et al. mRNA-1273 vaccine-induced antibodies maintain Fc effector functions across SARS-CoV-2 variants of concern. *Immunity* (2022) 55:355-365.e4. doi:10.1016/j.immuni.2022.01.001

166. Mackin SR, Desai P, Whitener BM, Karl CE, Liu M, Baric RS, et al. Fc-γR-dependent antibody effector functions are required for vaccine-mediated protection against antigen-shifted variants of SARS-CoV-2. *Nature Microbiology 2023 8:4* (2023) 8:569–580. doi:10.1038/s41564-023-01359-1

167. Riou C, Keeton R, Moyo-Gwete T, Hermanus T, Kgagudi P, Baguma R, et al. Escape from recognition of SARS-CoV-2 variant spike epitopes but overall preservation of T cell immunity. *Sci Transl Med* (2022) 14:6824. doi:10.1126/SCITRANSLMED.ABJ6824;PAGE:STRING:ARTICLE/CHAPTER

168. Choi SJ, Kim DU, Noh JY, Kim S, Park SH, Jeong HW, et al. T cell epitopes in SARS-CoV-2 proteins are substantially conserved in the Omicron variant. *Cellular & Molecular Immunology 2022 19:3* (2022) 19:447–448. doi:10.1038/s41423-022-00838-5

169. Mohammed I, Nauman A, Paul P, Ganesan S, Chen KH, Jalil SMS, et al. The efficacy and effectiveness of the COVID-19 vaccines in reducing infection, severity, hospitalization, and mortality: a systematic review. *Hum Vaccin Immunother* (2022) 18: doi:10.1080/21645515.2022.2027160;WGROUP:STRING:PUBLICATION

170. Zhou G, Dael N, Verweij S, Balafas S, Mubarik S, Rengerink KO, et al. Effectiveness of COVID-19 vaccines against SARS-CoV-2 infection and severe outcomes in adults: a systematic review and meta-analysis of European studies published up to 22 January 2024. *European Respiratory Review* (2025) 34: doi:10.1183/16000617.0222-2024

171. Wong BK-F, Mabbott NA. Systematic review and meta-analysis of COVID-19 mRNA vaccine effectiveness against hospitalizations in adults. *Immunotherapy Advances* (2024) 4:ltae011. doi:10.1093/IMMADV/LTAE011

172. Tan ST, Kwan AT, Rodríguez-Barraquer I, Singer BJ, Park HJ, Lewnard JA, et al. Infectiousness of SARS-CoV-2 breakthrough infections and reinfections during the Omicron wave. *Nature Medicine 2023 29:2* (2023) 29:358–365. doi:10.1038/s41591-022-02138-x

173. Bramante CT, Proper JL, Boulware DR, Karger AB, Murray T, Rao V, et al. Vaccination Against SARS-CoV-2 Is Associated With a Lower Viral Load and Likelihood of Systemic Symptoms. *Open Forum Infect Dis* (2022) 9: doi:10.1093/OFID/OFAC066

174. Abu-Raddad LJ, Chemaitelly H, Ayoub HH, Tang P, Coyle P, Hasan MR, et al. Relative infectiousness of SARS-CoV-2 vaccine breakthrough infections, reinfections, and primary infections. *Nature Communications 2022 13:1* (2022) 13:532-. doi:10.1038/s41467-022-28199-7

175. Cai M, Xie Y, Al-Aly Z. Association of 2024–2025 Covid-19 Vaccine with Covid-19 Outcomes in U.S. Veterans. *New England Journal of Medicine* (2025) 393:1612–1623. doi:10.1056/NEJMOA2510226;ISSUE:ISSUE:DOI

176. Liang CK, Lee WJ, Peng LN, Meng LC, Hsiao FY, Chen LK. COVID-19 Vaccines in Older Adults: Challenges in Vaccine Development and Policy Making. *Clin Geriatr Med* (2022) 38:605–620. doi:10.1016/j.cger.2022.03.006

177. Study Details | NCT04283461 | Safety and Immunogenicity Study of 2019-nCoV Vaccine (mRNA-1273) for Prophylaxis of SARS-CoV-2 Infection (COVID-19) | ClinicalTrials.gov. Available at: https://clinicaltrials.gov/study/NCT04283461 [Accessed December 31, 2025]

178. Khare S, Gurry C, Freitas L, Schultz MB, Bach G, Diallo A, et al. GISAID's Role in Pandemic Response. *China CDC Wkly* (2021) 3:1049. doi:10.46234/CCDCW2021.255

179. COVID-19 vaccine tracker and landscape. Available at: https://www.who.int/publications/m/item/draft-landscape-of-covid-19-candidate-vaccines [Accessed December 31, 2025]

180. Magalhães B de AP, Medeiros Minasi J, Lobato RC, Lemos LC, de Britto LS, Barros RM, et al. Globally approved vaccines for COVID-19: a systematic review. *Brazilian Journal of Microbiology 2024 56:1* (2025) 56:511–527. doi:10.1007/S42770-024-01600-X

181. Coronavirus (COVID-19) Vaccinations - Our World in Data. Available at: https://ourworldindata.org/covid-vaccinations [Accessed December 31, 2025]

182. Watson OJ, Barnsley G, Toor J, Hogan AB, Winskill P, Ghani AC. Global impact of the first year of COVID-19 vaccination: a mathematical modelling study. *Lancet Infect Dis* (2022) 22:1293–1302. doi:10.1016/S1473-3099(22)00320-6

183. Meslé MMI, Brown J, Mook P, Katz MA, Hagan J, Pastore R, et al. Estimated number of lives directly saved by COVID-19 vaccination programmes in the WHO European Region from December, 2020, to March, 2023: a retrospective surveillance study. *Lancet Respir Med* (2024) 12:714–727. doi:10.1016/S2213-2600(24)00179-6

184. Ioannidis JPA, Pezzullo AM, Cristiano A, Boccia S. Global Estimates of Lives and Life-Years Saved by COVID-19 Vaccination During 2020-2024. *JAMA Health Forum* (2025) 6:e252223–e252223. doi:10.1001/JAMAHEALTHFORUM.2025.2223

185. Polack FP, Thomas SJ, Kitchin N, Absalon J, Gurtman A, Lockhart S, et al. Safety and Efficacy of the BNT162b2 mRNA Covid-19 Vaccine. *N Engl J Med* (2020) 383:2603–2615. doi:10.1056/NEJMOA2034577

186. Baden LR, El Sahly HM, Essink B, Kotloff K, Frey S, Novak R, et al. Efficacy and Safety of the mRNA-1273 SARS-CoV-2 Vaccine. *New England Journal of Medicine* (2021) 384:403–416. doi:10.1056/NEJMoa2035389

187. Walsh EE, Frenck RW, Falsey AR, Kitchin N, Absalon J, Gurtman A, et al. Safety and Immunogenicity of Two RNA-Based Covid-19 Vaccine Candidates. *New England Journal of Medicine* (2020) 383:2439–2450. doi:10.1056/NEJMOA2027906;WGROUP:STRING:MMS

188. Jackson LA, Anderson EJ, Rouphael NG, Roberts PC, Makhene M, Coler RN, et al. An mRNA Vaccine against SARS-CoV-2 — Preliminary Report. *New England Journal of Medicine* (2020) 383:1920–1931. doi:10.1056/NEJMOA2022483;WGROUP:STRING:MMS

189. Nance KD, Meier JL. Modifications in an Emergency: The Role of N1-Methylpseudouridine in COVID-19 Vaccines. *ACS Cent Sci* (2021) 7:748–756. doi:10.1021/ACSCENTSCI.1C00197

190. Andries O, Mc Cafferty S, De Smedt SC, Weiss R, Sanders NN, Kitada T. N1-methylpseudouridine-incorporated mRNA outperforms pseudouridine-incorporated mRNA by providing enhanced protein expression and reduced immunogenicity in mammalian cell lines and mice. *Journal of Controlled Release* (2015) 217:337–344. doi:10.1016/J.JCONREL.2015.08.051

191. Schoenmaker L, Witzigmann D, Kulkarni JA, Verbeke R, Kersten G, Jiskoot W, et al. mRNA-lipid nanoparticle COVID-19 vaccines: Structure and stability. *Int J Pharm* (2021) 601:120586. doi:10.1016/J.IJPHARM.2021.120586

192. Liu X, Shaw RH, Stuart ASV, Greenland M, Aley PK, Andrews NJ, et al. Safety and immunogenicity of heterologous versus homologous prime-boost schedules with an adenoviral vectored and mRNA COVID-19 vaccine (Com-COV): a single-blind, randomised, non-inferiority trial. *The Lancet* (2021) 398:856–869. doi:10.1016/S0140-6736(21)01694-9

193. Light DW, Lexchin J. The costs of coronavirus vaccines and their pricing. *J R Soc Med* (2021) 114:502–504. doi:10.1177/01410768211053006;WGROUP:STRING:PUBLICATION

194. Uddin MN, Roni MA, Uddin MN, Roni MA. Challenges of Storage and Stability of mRNA-Based COVID-19 Vaccines. *Vaccines 2021, Vol 9,* (2021) 9: doi:10.3390/VACCINES9091033

195. Santangelo OE, Provenzano S, Martino G Di, Ferrara P, Santangelo OE, Provenzano S, et al. COVID-19 Vaccination and Public Health: Addressing Global, Regional, and Within-Country Inequalities. *Vaccines 2024, Vol 12,* (2024) 12: doi:10.3390/VACCINES12080885

196. Stowe J, Miller E, Andrews N, Whitaker HJ. Risk of myocarditis and pericarditis after a COVID-19 mRNA vaccine booster and after COVID-19 in those with and without prior SARS-CoV-2 infection: A self-controlled case series analysis in England. *PLoS Med* (2023) 20:e1004245. doi:10.1371/JOURNAL.PMED.1004245

197. Oster ME, Shay DK, Su JR, Gee J, Creech CB, Broder KR, et al. Myocarditis Cases Reported After mRNA-Based COVID-19 Vaccination in the US From December 2020 to August 2021. *JAMA* (2022) 327:331–340. doi:10.1001/JAMA.2021.24110

198. Fairweather DL, Beetler DJ, Di Florio DN, Musigk N, Heidecker B, Cooper LT. COVID-19, Myocarditis and Pericarditis. *Circ Res* (2023) 132:1302–1319. doi:10.1161/CIRCRESAHA.123.321878

199. Elizalde MU, Eguinoa FJG, de las Huertas AGL, Jiménez-González M, Ramírez E. Myocarditis and pericarditis risk with mRNA COVID-19 vaccination compared to unvaccinated individuals: A retrospective cohort study in a Spanish Tertiary Hospital. *Biomedicine & Pharmacotherapy* (2024) 171:116181. doi:10.1016/J.BIOPHA.2024.116181

200. Mulroney TE, Pöyry T, Yam-Puc JC, Rust M, Harvey RF, Kalmar L, et al. N1-methylpseudouridylation of mRNA causes +1 ribosomal frameshifting. *Nature 2023 625:7993* (2023) 625:189–194. doi:10.1038/s41586-023-06800-3

201. Shrotri M, Navaratnam AMD, Nguyen V, Byrne T, Geismar C, Fragaszy E, et al. Spike-antibody waning after second dose of BNT162b2 or ChAdOx1. *The Lancet* (2021) 398:385–387. doi:10.1016/S0140-6736(21)01642-1

202. Mizrahi B, Lotan R, Kalkstein N, Peretz A, Perez G, Ben-Tov A, et al. Correlation of SARS-CoV-2-breakthrough infections to time-from-vaccine. *Nature Communications 2021 12:1* (2021) 12:6379-. doi:10.1038/s41467-021-26672-3

203. Chemaitelly H, Tang P, Hasan MR, AlMukdad S, Yassine HM, Benslimane FM, et al. Waning of BNT162b2 Vaccine Protection against SARS-CoV-2 Infection in Qatar. *New England Journal of Medicine* (2021) 385: doi:10.1056/NEJMOA2114114;SUBPAGE:STRING:FULL

204. Patalon T, Saciuk Y, Peretz A, Perez G, Lurie Y, Maor Y, et al. Waning effectiveness of the third dose of the BNT162b2 mRNA COVID-19 vaccine. *Nature Communications 2022 13:1* (2022) 13:3203-. doi:10.1038/s41467-022-30884-6

205. Falsey AR, Sobieszczyk ME, Hirsch I, Sproule S, Robb ML, Corey L, et al. Phase 3 Safety and Efficacy of AZD1222 (ChAdOx1 nCoV-19) Covid-19 Vaccine. *New England Journal of Medicine* (2021) 385:2348–2360. doi:10.1056/NEJMOA2105290;WGROUP:STRING:MMS

206. Sadoff J, Gray G, Vandebosch A, Cárdenas V, Shukarev G, Grinsztejn B, et al. Final Analysis of Efficacy and Safety of Single-Dose Ad26.COV2.S. *New England Journal of Medicine* (2022) 386:847–860. doi:10.1056/NEJMOA2117608;WGROUP:STRING:MMS

207. Logunov DY, Dolzhikova I V., Shcheblyakov D V., Tukhvatulin AI, Zubkova O V., Dzharullaeva AS, et al. Safety and efficacy of an rAd26 and rAd5 vector-based heterologous prime-boost COVID-19 vaccine: an interim analysis of a randomised controlled phase 3 trial in Russia. *The Lancet* (2021) 397:671–681. doi:10.1016/S0140-6736(21)00234-8

208. Zhu FC, Li YH, Guan XH, Hou LH, Wang WJ, Li JX, et al. Safety, tolerability, and immunogenicity of a recombinant adenovirus type-5 vectored COVID-19 vaccine: a dose-escalation, open-label, non-randomised, first-in-human trial. *The Lancet* (2020) 395:1845–1854. doi:10.1016/S0140-6736(20)31208-3

209. Oxford vaccine saved most lives in its first year of rollout | University of Oxford. Available at: https://www.ox.ac.uk/news/2022-07-15-oxford-vaccine-saved-most-lives-its-first-year-rollout [Accessed December 31, 2025]

210. Collier AY, Yu J, McMahan K, Liu J, Chandrashekar A, Maron JS, et al. Differential Kinetics of Immune Responses Elicited by Covid-19 Vaccines. *New England Journal of Medicine* (2021) 385:2010–2012. doi:10.1056/NEJMC2115596;WGROUP:STRING:MMS

211. Barbeau DJ, Martin JM, Carney E, Dougherty E, Doyle JD, Dermody TS, et al. Comparative analysis of human immune responses following SARS-CoV-2 vaccination with BNT162b2, mRNA-1273, or Ad26.COV2.S. *npj Vaccines 2022 7:1* (2022) 7:77-. doi:10.1038/s41541-022-00504-x

212. Maringer Y, Nelde A, Schroeder SM, Schuhmacher J, Hörber S, Peter A, et al. Durable spike-specific T cell responses after different COVID-19 vaccination regimens are not further enhanced by booster vaccination. *Sci Immunol* (2022) 7: doi:10.1126/SCIIMMUNOL.ADD3899;WEBSITE:WEBSITE:AAAS-SITE;WGROUP:STRING:PUBLICATION

213. Awakoaiye B, Li S, Sanchez S, Dangi T, Irani N, Arroyo L, et al. Comparative analysis of adenovirus, mRNA, and protein vaccines reveals context-dependent immunogenicity and efficacy. *JCI Insight* (2025) 10: doi:10.1172/JCI.INSIGHT.198069

214. Barouch DH, Stephenson KE, Sadoff J, Yu J, Chang A, Gebre M, et al. Durable Humoral and Cellular Immune Responses 8 Months after Ad26.COV2.S Vaccination. *New England Journal of Medicine* (2021) 385:951–953. doi:10.1056/NEJMC2108829;PAGEGROUP:STRING:PUBLICATION

215. Murray SM, Amini A, Ferry H, Garner LC, Pudjohartono MF, Kronsteiner B, et al. Dosing interval is a major factor determining the quality of T cells induced by SARS-CoV-2 mRNA and adenoviral vector vaccines. *Sci Immunol* (2025) 10:eadu4610. doi:10.1126/SCIIMMUNOL.ADU4610

216. Klemis V, Schmidt T, Schub D, Mihm J, Marx S, Abu-Omar A, et al. Comparative immunogenicity and reactogenicity of heterologous ChAdOx1-nCoV-19-priming and BNT162b2 or mRNA-1273-boosting with homologous COVID-19 vaccine regimens. *Nature Communications 2022 13:1* (2022) 13:4710-. doi:10.1038/s41467-022-32321-0

217. Li J, Wu G, Huang Z, Hu J, Tie X, Wu H, et al. Advances and prospects of respiratory mucosal vaccines: mechanisms, technologies, and clinical applications. *npj Vaccines 2025 10:1* (2025) 10:230-. doi:10.1038/s41541-025-01280-0

218. Akula VR, Bhate AS, Gillurkar CS, Kushwaha JS, Singh AP, Singh C, et al. Effect of heterologous intranasal iNCOVACC® vaccination as a booster to two-dose intramuscular Covid-19 vaccination series: a randomized phase 3 clinical trial. *Communications Medicine 2025 5:1* (2025) 5:133-. doi:10.1038/s43856-025-00818-6

219. Jia S, Liu Y, He Q, Pan H, Liang Z, Zhou J, et al. Effectiveness of a booster dose of aerosolized or intramuscular adenovirus type 5 vectored COVID-19 vaccine in adults: a multicenter, partially randomized, platform trial in China. *Nature Communications 2025 16:1* (2025) 16:2969-. doi:10.1038/s41467-025-58327-y

220. Facciolà A, Visalli G, Laganà A, Pietro A Di, Facciolà A, Visalli G, et al. An Overview of Vaccine Adjuvants: Current Evidence and Future Perspectives. *Vaccines 2022, Vol 10,* (2022) 10: doi:10.3390/VACCINES10050819

221. Stertman L, Palm AKE, Zarnegar B, Carow B, Lunderius Andersson C, Magnusson SE, et al. The Matrix-M™ adjuvant: A critical component of vaccines for the 21st century. *Hum Vaccin Immunother* (2023) 19: doi:10.1080/21645515.2023.2189885;ISSUE:ISSUE:DOI

222. Heath PT, Galiza EP, Baxter DN, Boffito M, Browne D, Burns F, et al. Safety and Efficacy of the NVX-CoV2373 Coronavirus Disease 2019 Vaccine at Completion of the Placebo-Controlled Phase of a Randomized Controlled Trial. *Clinical Infectious Diseases* (2023) 76:398–407. doi:10.1093/CID/CIAC803

223. Thuluva S, Paradkar V, Gunneri SR, Yerroju V, Mogulla R, Suneetha PV, et al. Immunogenicity and safety of Biological E's CORBEVAX™ vaccine compared to COVISHIELD™ (ChAdOx1 nCoV-19) vaccine studied in a phase-3, single blind, multicentre, randomized clinical trial. *Hum Vaccin Immunother* (2023) 19: doi:10.1080/21645515.2023.2203632;JOURNAL:JOURNAL:KHVI19;PAGE:STRING:ARTICLE/CHAPTER

224. Sookhoo JRV, Schiffman Z, Ambagala A, Kobasa D, Pardee K, Babiuk S. Protein Expression Platforms and the Challenges of Viral Antigen Production. *Vaccines 2024, Vol 12,* (2024) 12: doi:10.3390/VACCINES12121344

225. Fda. FDA Briefing Document Vaccines and Related Biological Products Advisory Committee Meeting Selection of the 2025-2026 Formula for COVID-19 Vaccines. (2025).

226. China's COVID vaccines have been crucial — now immunity is waning. Available at: https://www.nature.com/articles/d41586-021-02796-w [Accessed January 1, 2026]

227. Lau JJ, Cheng SMS, Leung K, Lee CK, Hachim A, Tsang LCH, et al. Real-world COVID-19 vaccine effectiveness against the Omicron BA.2 variant in a SARS-CoV-2 infection-naive population. *Nature Medicine 2023 29:2* (2023) 29:348–357. doi:10.1038/s41591-023-02219-5

228. Maher S, Assaly NME, Aly DM, Atta S, Fteah AM, Badawi H, et al. Comparative study of neutralizing antibodies titers in response to different types of COVID-19 vaccines among a group of egyptian healthcare workers. *Virology Journal 2024 21:1* (2024) 21:277-. doi:10.1186/S12985-024-02546-0

229. Lim WW, Mak L, Leung GM, Cowling BJ, Peiris M. Comparative immunogenicity of mRNA and inactivated vaccines against COVID-19. *Lancet Microbe* (2021) 2:e423. doi:10.1016/S2666-5247(21)00177-4

230. Zuo F, Abolhassani H, Du L, Piralla A, Bertoglio F, de Campos-Mata L, et al. Heterologous immunization with inactivated vaccine followed by mRNA-booster elicits strong immunity against SARS-CoV-2 Omicron variant. *Nature Communications 2022 13:1* (2022) 13:2670-. doi:10.1038/s41467-022-30340-5

231. Lim JME, Hang SK, Hariharaputran S, Chia A, Tan N, Lee ES, et al. A comparative characterization of SARS-CoV-2-specific T cells induced by mRNA or inactive virus COVID-19 vaccines. *Cell Rep Med* (2022) 3:100793. doi:10.1016/J.XCRM.2022.100793

232. Huang R, Ying L, Wang J, Xia J, Zhang Y, Mao H, et al. Non-spike and spike-specific memory T cell responses after the third dose of inactivated COVID-19 vaccine. *Front Immunol* (2023) 14:1139620. doi:10.3389/FIMMU.2023.1139620/BIBTEX

233. Smith TRF, Patel A, Ramos S, Elwood D, Zhu X, Yan J, et al. Immunogenicity of a DNA vaccine candidate for COVID-19. *Nat Commun* (2020) 11: doi:10.1038/S41467-020-16505-0

234. Walters JN, Schouest B, Patel A, Reuschel EL, Schultheis K, Parzych E, et al. Prime-boost vaccination regimens with INO-4800 and INO-4802 augment and broaden immune responses against SARS-CoV-2 in nonhuman primates. *Vaccine* (2022) 40:2960–2969. doi:10.1016/J.VACCINE.2022.03.060

235. Tebas P, Yang SP, Boyer JD, Reuschel EL, Patel A, Christensen-Quick A, et al. Safety and immunogenicity of INO-4800 DNA vaccine against SARS-CoV-2: A preliminary report of an open-label, Phase 1 clinical trial. *EClinicalMedicine* (2021) 31:100689. doi:10.1016/j.eclinm.2020.100689

236. Kraynyak KA, Blackwood E, Agnes J, Tebas P, Giffear M, Amante D, et al. SARS-CoV-2 DNA Vaccine INO-4800 Induces Durable Immune Responses Capable of Being Boosted in a Phase 1 Open-Label Trial. *J Infect Dis* (2022) 225:1923–1932. doi:10.1093/INFDIS/JIAC016

237. Jia S, Shao C, Cheng X, Pan H, Wang Z, Xia Y, et al. Immunogenicity and safety of a COVID-19 DNA vaccine in healthy adults and elderly: A randomized, observer-blind, placebo-controlled phase 2 trial. *Hum Vaccin Immunother* (2025) 21: doi:10.1080/21645515.2024.2448405;WGROUP:STRING:PUBLICATION

238. Press Release:Press Information Bureau. Available at: https://www.pib.gov.in/PressReleasePage.aspx?PRID=1747669&reg=3&lang=2 [Accessed January 1, 2026]

239. Dey A, Chozhavel TM, Chandra H, Pericherla HPR, Kumar S, Choonia HS, et al. Immunogenic potential of DNA vaccine candidate, ZyCoV-D against SARS-CoV-2 in animal models. *Vaccine* (2021) 39:4108–4116. doi:10.1016/J.VACCINE.2021.05.098

240. Momin T, Kansagra K, Patel H, Sharma S, Sharma B, Patel J, et al. Safety and Immunogenicity of a DNA SARS-CoV-2 vaccine (ZyCoV-D): Results of an open-label, non-randomized phase I part of phase I/II clinical study by intradermal route in healthy subjects in India. *EClinicalMedicine* (2021) 38:101020. doi:10.1016/J.ECLINM.2021.101020

241. Khobragade A, Bhate S, Ramaiah V, Deshpande S, Giri K, Phophle H, et al. Efficacy, safety, and immunogenicity of the DNA SARS-CoV-2 vaccine (ZyCoV-D): the interim efficacy results of a phase 3, randomised, double-blind, placebo-controlled study in India. *The Lancet* (2022) 399:1313–1321. doi:10.1016/S0140-6736(22)00151-9

242. Novelli G, Colona VL, Pandolfi PP, Novelli G, Colona VL, Pandolfi PP. A focus on the spread of the delta variant of SARS-CoV-2 in India. *Indian Journal of Medical Research* (2025) 153:537–541. doi:10.4103/IJMR.IJMR_1353_21

243. Purohit N, Chugh Y, Bahuguna P, Prinja S. COVID-19 management: The vaccination drive in India. *Health Policy Technol* (2022) 11:100636. doi:10.1016/J.HLPT.2022.100636

244. Wolff JA, Malone RW, Williams P, Chong W, Acsadi G, Jani A, et al. Direct gene transfer into mouse muscle in vivo. *Science (1979)* (1990) 247:1465–1468.

doi:10.1126/SCIENCE.1690918;JOURNAL:JOURNAL:SCIENCE;WGROUP:STRING:PUBLICATION

245. Ulmer JB, Donnelly JJ, Parker SE, Rhodes GH, Felgner PL, Dwarki VJ, et al. Heterologous protection against influenza by injection of DNA encoding a viral protein. *Science (1979)* (1993) 259:1745–1749. doi:10.1126/SCIENCE.8456302;REQUESTEDJOURNAL:JOURNAL:SCIENCE;CTYPE:STRING:JOURNAL

246. MacGregor RR, Boyer JD, Ugen KE, Lacy KE, Gluckman SJ, Bagarazzi ML, et al. First Human Trial of a DNA-Based Vaccine for Treatment of Human Immunodeficiency Virus Type 1 Infection: Safety and Host Response. *J Infect Dis* (1998) 178:92–100. doi:10.1086/515613

247. Tacket CO, Roy MJ, Widera G, Swain WF, Broome S, Edelman R. Phase 1 safety and immune response studies of a DNA vaccine encoding hepatitis B surface antigen delivered by a gene delivery device. *Vaccine* (1999) 17:2826–2829. doi:10.1016/S0264-410X(99)00094-8

248. Le TP, Coonan KM, Hedstrom RC, Charoenvit Y, Sedegah M, Epstein JE, et al. Safety, tolerability and humoral immune responses after intramuscular administration of a malaria DNA vaccine to healthy adult volunteers. *Vaccine* (2000) 18:1893–1901. doi:10.1016/S0264-410X(99)00407-7

249. Otten G, Schaefer M, Doe B, Liu H, Srivastava I, Zur Megede J, et al. Enhancement of DNA vaccine potency in rhesus macaques by electroporation. *Vaccine* (2004) 22:2489–2493. doi:10.1016/J.VACCINE.2003.11.073

250. Widera G, Austin M, Rabussay D, Goldbeck C, Barnett SW, Chen M, et al. Increased DNA Vaccine Delivery and Immunogenicity by Electroporation In Vivo. *The Journal of Immunology* (2000) 164:4635–4640. doi:10.4049/JIMMUNOL.164.9.4635

251. Boyle JS, Silva A, Brady JL, Lew AM. DNA immunization: Induction of higher avidity antibody and effect of route on T cell cytotoxicity. *Proc Natl Acad Sci U S A* (1997) 94:14626–14631. doi:10.1073/PNAS.94.26.14626;WEBSITE:WEBSITE:PNAS-SITE;ISSUE:ISSUE:DOI

252. Condon C, Watkins SC, Celluzzi CM, Thompson K, Falo LD. DNA–based immunization by in vivo transfection of dendritic cells. *Nature Medicine 1996 2:10* (1996) 2:1122–1128. doi:10.1038/nm1096-1122

253. Wang S, Zhang C, Zhang L, Li J, Huang Z, Lu S. The relative immunogenicity of DNA vaccines delivered by the intramuscular needle injection, electroporation and gene gun methods. *Vaccine* (2008) 26:2100–2110. doi:10.1016/J.VACCINE.2008.02.033

254. Bodles-Brakhop AM, Heller R, Draghia-Akli R. Electroporation for the delivery of DNA-based vaccines and immunotherapeutics: Current clinical developments. *Molecular Therapy* (2009) 17:585–592. doi:10.1038/mt.2009.5

255. Suschak JJ, Williams JA, Schmaljohn CS. Advancements in DNA vaccine vectors, non-mechanical delivery methods, and molecular adjuvants to increase immunogenicity. *Hum Vaccin Immunother* (2017) 13:2837–2848. doi:10.1080/21645515.2017.1330236

256. Cagigi A, Douradinha B. Have mRNA vaccines sentenced DNA vaccines to death? *Expert Rev Vaccines* (2023) 22:1154–1167. doi:10.1080/14760584.2023.2282065;JOURNAL:JOURNAL:IERV20;WGROUP:STRING:PUBLICATION

257. Felgner PL, Gadek TR, Holm M, Roman R, Chan HW, Wenz M, et al. Lipofection: a highly efficient, lipid-mediated DNA-transfection procedure. *Proc Natl Acad Sci U S A* (1987) 84:7413–7417. doi:10.1073/PNAS.84.21.7413;PAGE:STRING:ARTICLE/CHAPTER

258. Zelphati O, Szoka FC. Mechanism of oligonucleotide release from cationic liposomes. *Proc Natl Acad Sci U S A* (1996) 93:11493–11498. doi:10.1073/PNAS.93.21.11493;WGROUP:STRING:PUBLICATION

259. Zhang S, Xu Y, Wang B, Qiao W, Liu D, Li Z. Cationic compounds used in lipoplexes and polyplexes for gene delivery. *Journal of Controlled Release* (2004) 100:165–180. doi:10.1016/J.JCONREL.2004.08.019

260. Lv H, Zhang S, Wang B, Cui S, Yan J. Toxicity of cationic lipids and cationic polymers in gene delivery. *Journal of Controlled Release* (2006) 114:100–109. doi:10.1016/J.JCONREL.2006.04.014

261. Gregoriadis G, Saffie R, De Souza JB. Liposome-mediated DNA vaccination. *FEBS Lett* (1997) 402:107–110. doi:10.1016/S0014-5793(96)01507-4

262. Martin B, Sainlos M, Aissaoui A, Oudrhiri N, Hauchecorne M, Vigneron J-P, et al. The Design of Cationic Lipids for Gene Delivery. *Curr Pharm Des* (2005) 11:375–394. doi:10.2174/1381612053382133

263. Semple SC, Klimuk SK, Harasym TO, Dos Santos N, Ansell SM, Wong KF, et al. Efficient encapsulation of antisense oligonucleotides in lipid vesicles using ionizable aminolipids: formation of novel small multilamellar vesicle structures. *Biochimica et Biophysica Acta (BBA) - Biomembranes* (2001) 1510:152–166. doi:10.1016/S0005-2736(00)00343-6

264. Heyes J, Palmer L, Bremner K, MacLachlan I. Cationic lipid saturation influences intracellular delivery of encapsulated nucleic acids. *Journal of Controlled Release* (2005) 107:276–287. doi:10.1016/J.JCONREL.2005.06.014

265. Zimmermann TS, Lee ACH, Akinc A, Bramlage B, Bumcrot D, Fedoruk MN, et al. RNAi-mediated gene silencing in non-human primates. *Nature 2006 441:7089* (2006) 441:111–114. doi:10.1038/nature04688

266. Semple SC, Akinc A, Chen J, Sandhu AP, Mui BL, Cho CK, et al. Rational design of cationic lipids for siRNA delivery. *Nature Biotechnology 2010 28:2* (2010) 28:172–176. doi:10.1038/nbt.1602

267. Akinc A, Maier MA, Manoharan M, Fitzgerald K, Jayaraman M, Barros S, et al. The Onpattro story and the clinical translation of nanomedicines containing nucleic acid-based drugs. *Nature Nanotechnology 2019 14:12* (2019) 14:1084–1087. doi:10.1038/s41565-019-0591-y

268. Chaudhary N, Weissman D, Whitehead KA. mRNA vaccines for infectious diseases: principles, delivery and clinical translation. *Nature Reviews Drug Discovery 2021 20:11* (2021) 20:817–838. doi:10.1038/s41573-021-00283-5

269. Hassett KJ, Benenato KE, Jacquinet E, Lee A, Woods A, Yuzhakov O, et al. Optimization of Lipid Nanoparticles for Intramuscular Administration of mRNA Vaccines. *Mol Ther Nucleic Acids* (2019) 15:1–11. doi:10.1016/j.omtn.2019.01.013

270. Hou X, Zaks T, Langer R, Dong Y. Lipid nanoparticles for mRNA delivery. *Nature Reviews Materials 2021 6:12* (2021) 6:1078–1094. doi:10.1038/s41578-021-00358-0

271. Kulkarni JA, Witzigmann D, Leung J, Tam YYC, Cullis PR. On the role of helper lipids in lipid nanoparticle formulations of siRNA. *Nanoscale* (2019) 11:21733–21739. doi:10.1039/C9NR09347H

272. Kulkarni JA, Myhre JL, Chen S, Tam YYC, Danescu A, Richman JM, et al. Design of lipid nanoparticles for in vitro and in vivo delivery of plasmid DNA. *Nanomedicine* (2017) 13:1377–1387. doi:10.1016/J.NANO.2016.12.014

273. Chen W, Duša F, Witos J, Ruokonen SK, Wiedmer SK. Determination of the Main Phase Transition Temperature of Phospholipids by Nanoplasmonic Sensing. *Scientific Reports 2018 8:1* (2018) 8:14815-. doi:10.1038/s41598-018-33107-5

274. Zhang L, Seow BYL, Bae KH, Zhang Y, Liao KC, Wan Y, et al. Role of PEGylated lipid in lipid nanoparticle formulation for in vitro and in vivo delivery of mRNA vaccines. *Journal of Controlled Release* (2025) 380:108–124. doi:10.1016/J.JCONREL.2025.01.071

275. Ju Y, Carreño JM, Simon V, Dawson K, Krammer F, Kent SJ. Impact of anti-PEG antibodies induced by SARS-CoV-2 mRNA vaccines. *Nature Reviews Immunology 2022 23:3* (2022) 23:135–136. doi:10.1038/s41577-022-00825-x

276. Mucker EM, Karmali PP, Vega J, Kwilas SA, Wu H, Joselyn M, et al. Lipid Nanoparticle Formulation Increases Efficiency of DNA-Vectored Vaccines/Immunoprophylaxis in Animals Including Transchromosomic Bovines. *Scientific Reports 2020 10:1* (2020) 10:8764-. doi:10.1038/s41598-020-65059-0

277. Ramaswamy S, Tonnu N, Tachikawa K, Limphong P, Vega JB, Karmali PP, et al. Systemic delivery of factor IX messenger RNA for protein replacement therapy. *Proc Natl Acad Sci U S A* (2017) 114:E1941–E1950. doi:10.1073/PNAS.1619653114;PAGE:STRING:ARTICLE/CHAPTER

278. Algarni A, Pilkington EH, Suys EJA, Al-Wassiti H, Pouton CW, Truong NP. In vivo delivery of plasmid DNA by lipid nanoparticles: the influence of ionizable cationic lipids on organ-selective gene expression. *Biomater Sci* (2022) 10:2940–2952. doi:10.1039/D2BM00168C

279. Zhang W, Pfeifle A, Lansdell C, Frahm G, Cecillon J, Tamming L, et al. The Expression Kinetics and Immunogenicity of Lipid Nanoparticles Delivering Plasmid DNA and mRNA in Mice. *Vaccines (Basel)* (2023) 11:1580. doi:10.3390/VACCINES11101580/S1

280. Liao HC, Shen KY, Yang CH, Chiu FF, Chiang CY, Chai KM, et al. Lipid nanoparticle-encapsulated DNA vaccine robustly induce superior immune responses to the mRNA vaccine in Syrian hamsters. *Mol Ther Methods Clin Dev* (2024) 32:101169. doi:10.1016/j.omtm.2023.101169

281. Tursi NJ, Tiwari S, Bedanova N, Kannan T, Parzych E, Okba N, et al. Modulation of lipid nanoparticle-formulated plasmid DNA drives innate immune activation promoting adaptive immunity. *Cell Rep Med* (2025) 6:102035. doi:10.1016/J.XCRM.2025.102035

282. Lai DC, Nguyen TN, Poonsuk K, McVey DS, Vu HLX. Lipid nanoparticle-encapsulated DNA vaccine encoding African swine fever virus p54 antigen elicits robust immune responses in pigs. *Vet Microbiol* (2025) 305:110508. doi:10.1016/J.VETMIC.2025.110508

283. Nguyen TN, Lai DC, Sillman S, Petro-Turnquist E, Weaver EA, Vu HLX. Lipid nanoparticle-encapsulated DNA vaccine confers protection against swine and human-origin H1N1 influenza viruses. *mSphere* (2024) 9: doi:10.1128/MSPHERE.00283-24;SUBPAGE:STRING:FULL

284. Li M, Liu L, Li X, Li J, Zhao C, Zhao Y, et al. Lipid Nanoparticles Outperform Electroporation in Delivering Therapeutic HPV DNA Vaccines. *Vaccines (Basel)* (2024) 12: doi:10.3390/VACCINES12060666/S1

285. Pfeifle A, Thulasi Raman SN, Lansdell C, Zhang W, Tamming L, Cecillon J, et al. DNA lipid nanoparticle vaccine targeting outer surface protein C affords protection against homologous Borrelia burgdorferi needle challenge in mice. *Front Immunol* (2023) 14:1020134. doi:10.3389/FIMMU.2023.1020134/BIBTEX

286. Chai D, Wang J, Lim JM, Xie X, Yu X, Zhao D, et al. Lipid nanoparticles deliver DNA-encoded biologics and induce potent protective immunity. *Molecular Cancer 2025 24:1* (2025) 24:12-. doi:10.1186/S12943-024-02211-8

287. Nguyen TN, Kumari S, Sillman S, Chaudhari J, Lai DC, Vu HLX, et al. A Single-Dose Intramuscular Immunization of Pigs with Lipid Nanoparticle DNA Vaccines Based on the Hemagglutinin Antigen Confers Complete Protection against Challenge Infection with the Homologous Influenza Virus Strain. *Vaccines 2023, Vol 11,* (2023) 11: doi:10.3390/VACCINES11101596

288. Ulmer JB, Dewitt CM, Chastain M, Friedman A, Donnelly JJ, McClements WL, et al. Enhancement of DNA vaccine potency using conventional aluminum adjuvants. *Vaccine* (1999) 18:18–28. doi:10.1016/S0264-410X(99)00151-6

289. Sasaki S, Tsuji T, Hamajima K, Fukushima J, Ishii N, Kaneko T, et al. Monophosphoryl lipid A enhances both humoral and cell- mediated immune responses to DNA vaccination against human immunodeficiency virus type 1. *Infect Immun* (1997) 65:3520–3528. doi:10.1128/IAI.65.9.3520-3528.1997;ISSUE:ISSUE:DOI

290. Ott G, Singh M, Kazzaz J, Briones M, Soenawan E, Ugozzoli M, et al. A cationic sub-micron emulsion (MF59/DOTAP) is an effective delivery system for DNA vaccines. *Journal of Controlled Release* (2002) 79:1–5. doi:10.1016/S0168-3659(01)00545-4

291. Zhao T, Cai Y, Jiang Y, He X, Wei Y, Yu Y, et al. Vaccine adjuvants: mechanisms and platforms. *Signal Transduction and Targeted Therapy 2023 8:1* (2023) 8:283-. doi:10.1038/s41392-023-01557-7

292. Spunde K, Korotkaja K, Sominskaya I, Zajakina A. Genetic adjuvants: A paradigm shift in vaccine development and immune modulation. *Mol Ther Nucleic Acids* (2025) 36:102536. doi:10.1016/J.OMTN.2025.102536

293. Ndeupen S, Qin Z, Jacobsen S, Bouteau A, Estanbouli H, Igyártó BZ. The mRNA-LNP platform's lipid nanoparticle component used in preclinical vaccine studies is highly inflammatory. *iScience* (2021) 24:103479. doi:10.1016/j.isci.2021.103479

294. Alameh MG, Tombácz I, Bettini E, Lederer K, Sittplangkoon C, Wilmore JR, et al. Lipid nanoparticles enhance the efficacy of mRNA and protein subunit vaccines by inducing robust T follicular helper cell and humoral responses. *Immunity* (2021) 54:2877-2892.e7. doi:10.1016/j.immuni.2021.11.001

295. Zelkoski AE, Lu Z, Sukumar G, Dalgard C, Said H, Alameh MG, et al. Ionizable lipid nanoparticles of mRNA vaccines elicit NF-κB and IRF responses through toll-like receptor 4. *npj Vaccines 2025 10:1* (2025) 10:73-. doi:10.1038/s41541-025-01124-x

296. Hojecki CE, Tursi NJ, Livingston C, Weiner DB, Gary EN. Advances in molecular adjuvants for nucleic acid vaccines. *Front Immunol* (2025) 16:1646800. doi:10.3389/FIMMU.2025.1646800/FULL

297. Kalams SA, Parker S, Jin X, Elizaga M, Metch B, Wang M, et al. Safety and Immunogenicity of an HIV-1 Gag DNA Vaccine with or without IL-12 and/or IL-15 Plasmid Cytokine Adjuvant in Healthy, HIV-1 Uninfected Adults. *PLoS One* (2012) 7:e29231. doi:10.1371/JOURNAL.PONE.0029231

298. Elizaga ML, Li SS, Kochar NK, Wilson GJ, Allen MA, Hong Van NT, et al. Safety and tolerability of HIV-1 multiantigen pDNA vaccine given with IL-12 plasmid DNA via electroporation, boosted with a recombinant vesicular stomatitis virus HIV Gag vaccine in healthy volunteers in a randomized, controlled clinical trial. *PLoS One* (2018) 13:e0202753. doi:10.1371/JOURNAL.PONE.0202753

299. de Rosa SC, Edupuganti S, Huang Y, Han X, Elizaga M, Swann E, et al. Robust antibody and cellular responses induced by DNA-only vaccination for HIV. *JCI Insight* (2020) 5: doi:10.1172/JCI.INSIGHT.137079

300. Wong YC, Hang Ho DH, Zhou R, Zhang R, Woo KF, Cheng WY, et al. An open-label study on the safety and immunogenicity of a PD-1-enhanced DNA vaccine used as a T cell booster for COVID-19. *EBioMedicine* (2025) 115:105699. doi:10.1016/j.ebiom.2025.105699

301. Quezada SA, Jarvinen LZ, Lind EF, Noelle RJ. CD40/CD154 interactions at the interface of tolerance and immunity. *Annu Rev Immunol* (2004) 22:307–328. doi:10.1146/ANNUREV.IMMUNOL.22.012703.104533/CITE/REFWORKS

302. Elgueta R, Benson MJ, De Vries VC, Wasiuk A, Guo Y, Noelle RJ. Molecular mechanism and function of CD40/CD40L engagement in the immune system. *Immunol Rev* (2009) 229:152–172. doi:10.1111/J.1600-065X.2009.00782.X;REQUESTEDJOURNAL:JOURNAL:1600065X;CSUBTYPE:STRING:SPECIAL;PAGE:STRING:ARTICLE/CHAPTER

303. Ma DY, Clark EA. The role of CD40 and CD154/CD40L in dendritic cells. *Semin Immunol* (2009) 21:265–272. doi:10.1016/J.SMIM.2009.05.010

304. Bishop GA, Moore CR, Xie P, Stunz LL, Kraus ZJ. TRAF Proteins in CD40 Signaling. *Adv Exp Med Biol* (2007) 597:131–151. doi:10.1007/978-0-387-70630-6_11

305. Ihata A, Watabe S, Sasaki S, Shirai A, Fukushima J, Hamajima K, et al. Immunomodulatory effect of a plasmid expressing CD40 ligand on DNA vaccination against human immunodeficiency virus type-1. *Immunology* (1999) 98:436–442. doi:10.1046/J.1365-2567.1999.00879.X;PAGEGROUP:STRING:PUBLICATION

306. Li W. Synergistic antibody induction by antigen-CD40 ligand fusion protein as improved immunogen. *Immunology* (2005) 115:215–222. doi:10.1111/J.1365-2567.2005.02141.X;WEBSITE:WEBSITE:PERICLES;ISSUE:ISSUE:DOI

307. Hashem AM, Gravel C, Chen Z, Yi Y, Tocchi M, Jaentschke B, et al. CD40 Ligand Preferentially Modulates Immune Response and Enhances Protection against Influenza Virus. *The Journal of Immunology* (2014) 193:722–734. doi:10.4049/JIMMUNOL.1300093

308. Pose AG, Gómez JN, Sánchez AV, Redondo AV, Rodríguez ER, Seguí RM, et al. Subunit influenza vaccine candidate based on CD154 fused to HAH5 increases the antibody titers and cellular immune response in chickens. *Vet Microbiol* (2011) 152:328–337. doi:10.1016/J.VETMIC.2011.05.033

309. Fan X, Hashem AM, Chen Z, Li C, Doyle T, Zhang Y, et al. Targeting the HA2 subunit of influenza A virus hemagglutinin via CD40L provides universal protection against diverse subtypes. *Mucosal Immunol* (2015) 8:211–220. doi:10.1038/mi.2014.59

310. Muralidharan A, Russell M, Larocque L, Gravel C, Li C, Chen W, et al. Targeting CD40 enhances antibody- and CD8-mediated protection against respiratory syncytial virus infection. *Sci Rep* (2018) 8:1–13. doi:10.1038/s41598-018-34999-z

311. Tripp RA, Jones L, Anderson LJ, Brown MP. CD40 Ligand (CD154) Enhances the Th1 and Antibody Responses to Respiratory Syncytial Virus in the BALB/c Mouse. *The Journal of Immunology* (2000) 164:5913–5921. doi:10.4049/JIMMUNOL.164.11.5913

312. Gupta S, Termini JM, Raffa FN, Williams C-A, Kornbluth RS, Stone GW. Vaccination with a Fusion Protein That Introduces HIV-1 Gag Antigen into a Multitrimer CD40L Construct Results in Enhanced CD8 + T Cell Responses and Protection from Viral Challenge by Vaccinia-Gag . *J Virol* (2014) 88:1492–1501. doi:10.1128/JVI.02229-13;WGROUP:STRING:PUBLICATION

313. Melchers M, Matthews K, de Vries RP, Eggink D, van Montfort T, Bontjer I, et al. A stabilized HIV-1 envelope glycoprotein trimer fused to CD40 ligand targets and activates dendritic cells. *Retrovirology 2011 8:1* (2011) 8:48-. doi:10.1186/1742-4690-8-48

314. Sin JI, Kim JJ, Zhang D, Weiner DB. Modulation of Cellular Responses by Plasmid CD40L: CD40L Plasmid Vectors Enhance Antigen-Specific Helper T Cell Type 1 CD4+ T Cell-Mediated Protective Immunity against Herpes Simplex Virus Type 2 in Vivo. *https://home.liebertpub.com/hum* (2004) 12:1091–1102. doi:10.1089/104303401750214302

315. Romagnani S. T-cell subsets (Th1 versus Th2). *Annals of Allergy, Asthma and Immunology* (2000) 85:9–18. doi:10.1016/S1081-1206(10)62426-X

316. Hashem AM, Algaissi A, Agrawal AS, Al-amri SS, Alhabbab RY, Sohrab SS, et al. A Highly Immunogenic, Protective, and Safe Adenovirus-Based Vaccine Expressing Middle East Respiratory Syndrome Coronavirus S1-CD40L Fusion Protein in a Transgenic Human Dipeptidyl Peptidase 4 Mouse Model. *J Infect Dis* (2019) 220:1558–1567. doi:10.1093/INFDIS/JIZ137

317. Ávalos I, Lao T, Rodríguez EM, Zamora Y, Rodríguez A, Ramón A, et al. Chimeric Antigen by the Fusion of SARS-CoV-2 Receptor Binding Domain with the Extracellular Domain of Human CD154: A Promising Improved Vaccine Candidate. *Vaccines (Basel)* (2022) 10:897. doi:10.3390/VACCINES10060897/S1

318. Lao T, Avalos I, Rodríguez EM, Zamora Y, Rodriguez A, Ramón A, et al. Production and characterization of a chimeric antigen, based on nucleocapsid of SARS-CoV-2 fused to the extracellular domain of human CD154 in HEK-293 cells as a vaccine candidate against COVID-19. *PLoS One* (2023) 18:e0288006. doi:10.1371/JOURNAL.PONE.0288006

319. Marlin R, Godot V, Cardinaud S, Galhaut M, Coleon S, Zurawski S, et al. Targeting SARS-CoV-2 receptor-binding domain to cells expressing CD40 improves protection to infection in convalescent macaques. *Nat Commun* (2021) 12: doi:10.1038/S41467-021-25382-0

320. Coléon S, Wiedemann A, Surénaud M, Lacabaratz C, Hue S, Prague M, et al. Design, immunogenicity, and efficacy of a pan-sarbecovirus dendritic-cell targeting vaccine. *EBioMedicine* (2022) 80:104062. doi:10.1016/j.ebiom.2022.104062

321. Nguema L, Picard F, El Hajj M, Dupaty L, Fenwick C, Cardinaud S, et al. Subunit protein CD40.SARS.CoV2 vaccine induces SARS-CoV-2-specific stem cell-like memory CD8+ T cells. *EBioMedicine* (2025) 111:105479. doi:10.1016/j.ebiom.2024.105479

322. Study Details | NCT07113106 | Dose Escalation Trial of CD40.Pan.CoV Vaccine, Adjuvanted or Not, as a Booster in Adult Healthy Volunteers | ClinicalTrials.gov. Available at: https://clinicaltrials.gov/study/NCT07113106 [Accessed January 1, 2026]

323. Levy Y, Moog C, Wiedemann A, Launay O, Candotti F, Hardel L, et al. Safety and immunogenicity of CD40.HIVRI.Env, a dendritic cell-based HIV vaccine, in healthy

HIV-uninfected adults: a first-in-human randomized, placebo-controlled, dose-escalation study (ANRS VRI06). *EClinicalMedicine* (2024) 77:102845. doi:10.1016/j.eclinm.2024.102845

324. COVID-19 Global Risk Assessment. Available at: https://www.who.int/publications/m/item/covid-19-global-risk-assessment [Accessed January 1, 2026]

325. Fda. FDA Briefing Document Vaccines and Related Biological Products Advisory Committee Meeting Selection of the 2025-2026 Formula for COVID-19 Vaccines. (2025)

326. Young KM, Corrin T, Pussegoda K, Baumeister A, Waddell LA. Evidence brief on facilitators, barriers and hesitancy of COVID-19 booster doses in Canada. (2024) 50: doi:10.14745/ccdr.v50i10a02

327. Jacobs ET, Cordova-Marks FM, Farland L V., Ernst KC, Andrews JG, Vu S, et al. Understanding low COVID-19 booster uptake among US adults. *Vaccine* (2023) 41:6221–6226. doi:10.1016/J.VACCINE.2023.08.080

328. Wang Q, Guo Y, Tam AR, Valdez R, Gordon A, Liu L, et al. Deep immunological imprinting due to the ancestral spike in the current bivalent COVID-19 vaccine. *Cell Rep Med* (2023) 4:101258. doi:10.1016/J.XCRM.2023.101258

329. Semenzato L, Le Vu S, Botton J, Bertrand M, Jabagi MJ, Drouin J, et al. COVID-19 mRNA Vaccination and 4-Year All-Cause Mortality Among Adults Aged 18 to 59 Years in France. *JAMA Netw Open* (2025) 8:e2546822–e2546822. doi:10.1001/JAMANETWORKOPEN.2025.46822

330. Arunachalam PS, Lai L, Samaha H, Feng Y, Hu M, Hui HSY, et al. Durability of immune responses to mRNA booster vaccination against COVID-19. *J Clin Invest* (2023) 133: doi:10.1172/JCI167955

331. Roe MD, Coggins SA, Darcey ES, Goguet E, Haines-Hull H, Esposito D, et al. Estimating the decay of protective antibodies induced by SARS-CoV-2 mRNA vaccination and hybrid immunity. *npj Viruses 2025 3:1* (2025) 3:76-. doi:10.1038/s44298-025-00156-3

332. Park H, Nakamura N, Miyamoto S, Sato Y, Kim KS, Kitagawa K, et al. Longitudinal antibody titers measured after COVID-19 mRNA vaccination can identify individuals at risk for subsequent infection. *Sci Transl Med* (2025) 17: doi:10.1126/SCITRANSLMED.ADV4214;WGROUP:STRING:PUBLICATION

333. Doria-Rose N, Suthar MS, Makowski M, O'Connell S, McDermott AB, Flach B, et al. Antibody Persistence through 6 Months after the Second Dose of mRNA-1273

Vaccine for Covid-19. *New England Journal of Medicine* (2021) 384:2259–2261. doi:10.1056/NEJMC2103916

334. Maslow JN, Kwon I, Kudchodkar SB, Kane D, Tadesse A, Lee H, et al. DNA Vaccines for Epidemic Preparedness: SARS-CoV-2 and Beyond. *Vaccines 2023, Vol 11, Page 1016* (2023) 11:1016. doi:10.3390/VACCINES11061016

335. Ahn JY, Lee J, Suh YS, Song YG, Choi YJ, Lee KH, et al. Safety and immunogenicity of two recombinant DNA COVID-19 vaccines containing the coding regions of the spike or spike and nucleocapsid proteins: an interim analysis of two open-label, non-randomised, phase 1 trials in healthy adults. *Lancet Microbe* (2022) 3:e173–e183. doi:10.1016/S2666-5247(21)00358-X

336. Nakagami H, Matsumoto T, Takazawa K, Sekino H, Matsuoka O, Inoue S, et al. Long Term Follow-Up Study of a Randomized, Open-Label, Uncontrolled, Phase I/II Study to Assess the Safety and Immunogenicity of Intramuscular and Intradermal Doses of COVID-19 DNA Vaccine (AG0302-COVID19). *Vaccines 2023, Vol 11,* (2023) 11: doi:10.3390/VACCINES11101535

337. Nakagami H, Hayashi H, Sun J, Yanagida Y, Otera T, Nakagami F, et al. Phase I Study to Assess the Safety and Immunogenicity of an Intradermal COVID-19 DNA Vaccine Administered Using a Pyro-Drive Jet Injector in Healthy Adults. *Vaccines 2022, Vol 10,* (2022) 10: doi:10.3390/VACCINES10091427

338. Aurisicchio L, Brambilla N, Cazzaniga ME, Bonfanti P, Milleri S, Ascierto PA, et al. A first-in-human trial on the safety and immunogenicity of COVID-eVax, a cellular response-skewed DNA vaccine against COVID-19. *Molecular Therapy* (2023) 31:788–800. doi:10.1016/j.ymthe.2022.12.017

339. Haq MA, Roy AK, Ahmed R, Kuddusi RU, Sinha M, Hossain MS, et al. Antibody longevity and waning following COVID-19 vaccination in a 1-year longitudinal cohort in Bangladesh. *Sci Rep* (2024) 14:1–11. doi:10.1038/S41598-024-61922-6;SUBJMETA

340. Feliciano L-, Chapman C;, Hooper R;, Elma JW;, Zehrung K;, Brennan D;, et al. Improved DNA Vaccine Delivery with Needle-Free Injection Systems. *Vaccines 2023, Vol 11, Page 280* (2023) 11:280. doi:10.3390/VACCINES11020280

341. Han X, Pan H, Jin P, Wei M, Jia S, Wang W, et al. A head-to-head comparison of humoral and cellular immune responses of five COVID-19 vaccines in adults in China. *Front Immunol* (2024) 15:1455730. doi:10.3389/FIMMU.2024.1455730/BIBTEX

342. Yu J, Tostanosk LH, Peter L, Mercad NB, McMahan K, Mahrokhia SH, et al. DNA vaccine protection against SARS-CoV-2 in rhesus macaques. *Science (1979)* (2020) 369:806–811. doi:10.1126/science.abc6284

343. Prompetchara E, Ketloy C, Tharakhet K, Kaewpang P, Buranapraditkun S, Techawiwattanaboon T, et al. DNA vaccine candidate encoding SARS-CoV-2 spike proteins elicited potent humoral and Th1 cell-mediated immune responses in mice. *PLoS One* (2021) 16:e0248007. doi:10.1371/JOURNAL.PONE.0248007

344. Stevens TL, Bossie A, Sanders VM, Fernandez-Botran R, Coffman RL, Mosmann TR, et al. Regulation of antibody isotype secretion by subsets of antigen-specific helper T cells. *Nature 1988 334:6179* (1988) 334:255–258. doi:10.1038/334255a0

345. Khan MY, Aljehani ND, Abdulal RH, Ghazwani A, Alsulaiman RM, Eyouni M, et al. Intranasal CD40-targeted recombinant MERS-CoV S1 protein is superior to intramuscular immunization in eliciting systemic and mucosal immune responses in mice. *Vaccine* (2026) 69:127975. doi:10.1016/J.VACCINE.2025.127975

346. de Jong R, Vreman S, Wiese KE, Gerhards NM, Bewley KR, Hall Y, et al. Hamsters immunized with formalin-inactivated SARS-CoV-2 develop accelerated lung histopathological lesions and Th2-biased response following infection. *npj Vaccines 2025 10:1* (2025) 10:145-. doi:10.1038/s41541-025-01160-7

347. Zhang T, Magazine N, McGee MC, Carossino M, Veggiani G, Kousoulas KG, et al. Th2 and Th17-associated immunopathology following SARS-CoV-2 breakthrough infection in Spike-vaccinated ACE2-humanized mice. *J Med Virol* (2024) 96:e29408. doi:10.1002/JMV.29408;WEBSITE:WEBSITE:PERICLES;JOURNAL:JOURNAL:10969071;ISSUE:ISSUE:DOI

348. Ebenig A, Muraleedharan S, Kazmierski J, Todt D, Auste A, Anzaghe M, et al. Vaccine-associated enhanced respiratory pathology in COVID-19 hamsters after TH2-biased immunization. *Cell Rep* (2022) 40:111214. doi:10.1016/j.celrep.2022.111214

349. Brook B, Duval V, Barman S, Speciner L, Sweitzer C, Khanmohammed A, et al. Adjuvantation of a SARS-CoV-2 mRNA vaccine with controlled tissue-specific expression of an mRNA encoding IL-12p70. *Sci Transl Med* (2024) 16: doi:10.1126/SCITRANSLMED.ADM8451;PAGE:STRING:ARTICLE/CHAPTER

350. Wang L, Wan J, He W, Wang Z, Wu Q, Zhou M, et al. IL-7 promotes mRNA vaccine-induced long-term immunity. *Journal of Nanobiotechnology 2024 22:1* (2024) 22:716-. doi:10.1186/S12951-024-02993-5

351. Knorr DA, Dahan R, Ravetch J V. Toxicity of an Fc-engineered anti-CD40 antibody is abrogated by intratumoral injection and results in durable antitumor immunity. *Proc Natl Acad Sci U S A* (2018) 115:11048–11053. doi:10.1073/PNAS.1810566115;ISSUE:ISSUE:DOI

352. Vonderheide RH, Flaherty KT, Khalil M, Stumacher MS, Bajor DL, Hutnick NA, et al. Clinical activity and immune modulation in cancer patients treated with CP-870,893,

a novel CD40 agonist monoclonal antibody. *Journal of Clinical Oncology* (2007) 25:876–883. doi:10.1200/JCO.2006.08.3311;REQUESTEDJOURNAL:JOURNAL:JCO;WGROUP:STRING:PUBLICATION

353. Stone ML, Lee J, Herrera VM, Graham K, Lee JW, Huffman A, et al. TNF blockade uncouples toxicity from antitumor efficacy induced with CD40 chemoimmunotherapy. *JCI Insight* (2021) 6: doi:10.1172/JCI.INSIGHT.146314

354. Xu S, Hu Z, Song F, Xu Y, Han X. Lipid nanoparticles: Composition, formulation, and application. *Mol Ther Methods Clin Dev* (2025) 33:101463. doi:10.1016/J.OMTM.2025.101463

355. Le Guen YT, Pichon C, Guégan P, Pluchon K, Haute T, Quemener S, et al. DNA nuclear targeting sequences for enhanced non-viral gene transfer: An in vitro and in vivo study. *Mol Ther Nucleic Acids* (2021) 24:477–486. doi:10.1016/j.omtn.2021.03.012

356. Van Gaal EVB, Oosting RS, Van Eijk R, Bakowska M, Feyen D, Kok RJ, et al. DNA Nuclear Targeting Sequences for Non-Viral Gene Delivery. *Pharmaceutical Research 2011 28:7* (2011) 28:1707–1722. doi:10.1007/S11095-011-0407-8

357. Nong J, Gong X, Dang QM, Tiwari S, Patel M, Wu J, et al. Multi-stage-mixing to control the supramolecular structure of lipid nanoparticles, thereby creating a core-then-shell arrangement that improves performance by orders of magnitude. *bioRxiv* (2025)2024.11.12.623321. doi:10.1101/2024.11.12.623321

358. Andrews N, Stowe J, Kirsebom F, Toffa S, Rickeard T, Gallagher E, et al. Covid-19 Vaccine Effectiveness against the Omicron (B.1.1.529) Variant. *New England Journal of Medicine* (2022) 386:1532–1546. doi:10.1056/NEJMOA2119451;ISSUE:ISSUE:DOI

359. Kometani K, Kurosaki T. Differentiation and maintenance of long-lived plasma cells. *Curr Opin Immunol* (2015) 33:64–69. doi:10.1016/J.COI.2015.01.017

360. Pardi N, Hogan MJ, Naradikian MS, Parkhouse K, Cain DW, Jones L, et al. Nucleoside-modified mRNA vaccines induce potent T follicular helper and germinal center B cell responses. *Journal of Experimental Medicine* (2018) 215:1571–1588. doi:10.1084/JEM.20171450

361. Lederer K, Castaño D, Gómez Atria D, Oguin TH, Wang S, Manzoni TB, et al. SARS-CoV-2 mRNA Vaccines Foster Potent Antigen-Specific Germinal Center Responses Associated with Neutralizing Antibody Generation. *Immunity* (2020) 53:1281-1295.e5. doi:10.1016/j.immuni.2020.11.009

362. Nguyen DC, Hentenaar IT, Morrison-Porter A, Solano D, Haddad NS, Castrillon C, et al. SARS-CoV-2-specific plasma cells are not durably established in the bone

marrow long-lived compartment after mRNA vaccination. *Nat Med* (2025) 31:235–244. doi:10.1038/S41591-024-03278-Y;SUBJMETA

363. Patel MN, Tiwari S, Wang Y, O'Neill S, Wu J, Omo-Lamai S, et al. Safer non-viral DNA delivery using lipid nanoparticles loaded with endogenous anti-inflammatory lipids. *Nature Biotechnology 2025* (2025)1–11. doi:10.1038/s41587-025-02556-5

364. Public Health Agency of Canada. Guidance on the use of COVID-19 vaccines for 2025 to summer 2026. (2025)19.

365. Statement on the antigen composition of COVID-19 vaccines. Available at: https://www.who.int/news/item/15-05-2025-statement-on-the-antigen-composition-of-covid-19-vaccines [Accessed January 1, 2026]

366. Johnston TS, Li SH, Painter MM, Atkinson RK, Douek NR, Reeg DB, et al. Immunological imprinting shapes the specificity of human antibody responses against SARS-CoV-2 variants. *Immunity* (2024) 57:912-925.e4. doi:10.1016/j.immuni.2024.02.017

367. Reynolds CJ, Pade C, Gibbons JM, Otter AD, Lin KM, Sandoval DM, et al. Immune boosting by B.1.1.529 (Omicron) depends on previous SARS-CoV-2 exposure. *Science (1979)* (2022) 377: doi:10.1126/SCIENCE.ABQ1841;SUBPAGE:STRING:FULL

368. Tortorici MA, Addetia A, Seo AJ, Brown J, Sprouse K, Logue J, et al. Persistent immune imprinting occurs after vaccination with the COVID-19 XBB.1.5 mRNA booster in humans. *Immunity* (2024) 57:904-911.e4. doi:10.1016/j.immuni.2024.02.016

369. Wang Z, Li L, Du R, Chen X, Sun Y, Qin R, et al. Ancestral SARS-CoV-2 immune imprinting persists on RBD but not NTD after sequential Omicron infections. *iScience* (2025) 28:111557. doi:10.1016/j.isci.2024.111557

370. Yisimayi A, Song W, Wang J, Jian F, Yu Y, Chen X, et al. Repeated Omicron exposures override ancestral SARS-CoV-2 immune imprinting. *Nature 2023 625:7993* (2023) 625:148–156. doi:10.1038/s41586-023-06753-7

371. Yang X, Li G, Wang Y, Song T, Cui T, Luo J, et al. Immune imprinting toward SARS-CoV-2 XBB: implications for vaccine strategy and variant risk assessment. *Signal Transduction and Targeted Therapy 2025 10:1* (2025) 10:372-. doi:10.1038/s41392-025-02484-5

372. Kotaki R, Moriyama S, Oishi S, Onodera T, Adachi Y, Sasaki E, et al. Repeated Omicron exposures redirect SARS-CoV-2–specific memory B cell evolution toward the latest variants. *Sci Transl Med* (2024) 16: doi:10.1126/SCITRANSLMED.ADP9927

373. Wheatley AK, Fox A, Tan HX, Juno JA, Davenport MP, Subbarao K, et al. Immune imprinting and SARS-CoV-2 vaccine design. *Trends Immunol* (2021) 42:956–959. doi:10.1016/j.it.2021.09.001

374. Buchan SA, Chung H, Brown KA, Austin PC, Fell DB, Gubbay JB, et al. Estimated Effectiveness of COVID-19 Vaccines Against Omicron or Delta Symptomatic Infection and Severe Outcomes. *JAMA Netw Open* (2022) 5:e2232760–e2232760. doi:10.1001/JAMANETWORKOPEN.2022.32760

375. Wang L, Nicols A, Turtle L, Richter A, Duncan CJ, Dunachie SJ, et al. T cell immune memory after covid-19 and vaccination. *BMJ Medicine* (2023) 2:468. doi:10.1136/BMJMED-2022-000468

376. Montoya B, Melo-Silva CR, Tang L, Kafle S, Lidskiy P, Bajusz C, et al. mRNA-LNP vaccine-induced CD8+ T cells protect mice from lethal SARS-CoV-2 infection in the absence of specific antibodies. *Molecular Therapy* (2024) 32:1790–1804. doi:10.1016/j.ymthe.2024.04.019

377. Heitmann JS, Bilich T, Tandler C, Nelde A, Maringer Y, Marconato M, et al. A COVID-19 peptide vaccine for the induction of SARS-CoV-2 T cell immunity. *Nature 2022 601:7894* (2021) 601:617–622. doi:10.1038/s41586-021-04232-5

378. Heitmann JS, Tandler C, Marconato M, Nelde A, Habibzada T, Rittig SM, et al. Phase I/II trial of a peptide-based COVID-19 T-cell activator in patients with B-cell deficiency. *Nature Communications 2023 14:1* (2023) 14:5032-. doi:10.1038/s41467-023-40758-0

379. Jahantigh HR, Rezanavaz Gheshlagh S, Mafakher L, Ahmadi N, Shahbazi B, Ahmadi K. Advancing peptide-based vaccines against viral pathogens: a narrative review. *Ther Adv Infect Dis* (2026) 13:20499361251411188. doi:10.1177/20499361251411188

380. Clark JJ, Hoxie I, Adelsberg DC, Sapse IA, Andreata-Santos R, Yong JS, et al. Protective effect and molecular mechanisms of human non-neutralizing cross-reactive spike antibodies elicited by SARS-CoV-2 mRNA vaccination. *Cell Rep* (2024) 43:114922. doi:10.1016/J.CELREP.2024.114922

381. Goverdhana S, Puntel M, Xiong W, Zirger JM, Barcia C, Curtin JF, et al. Regulatable gene expression systems for gene therapy applications: progress and future challenges. *Molecular Therapy* (2005) 12:189–211. doi:10.1016/J.YMTHE.2005.03.022

382. Becher B, Waisman A, Lu LF. Conditional Gene-Targeting in Mice: Problems and Solutions. *Immunity* (2018) 48:835–836. doi:10.1016/j.immuni.2018.05.002

383. Day CL, Kaufmann DE, Kiepiela P, Brown JA, Moodley ES, Reddy S, et al. PD-1 expression on HIV-specific T cells is associated with T-cell exhaustion and disease progression. *Nature 2006 443:7109* (2006) 443:350–354. doi:10.1038/nature05115

384. Nakamoto N, Kaplan DE, Coleclough J, Li Y, Valiga ME, Kaminski M, et al. Functional Restoration of HCV-Specific CD8 T Cells by PD-1 Blockade Is Defined by PD-1 Expression and Compartmentalization. *Gastroenterology* (2008) 134:1927-1937.e2. doi:10.1053/j.gastro.2008.02.033

385. Boni C, Fisicaro P, Valdatta C, Amadei B, Di Vincenzo P, Giuberti T, et al. Characterization of Hepatitis B Virus (HBV)-Specific T-Cell Dysfunction in Chronic HBV Infection. *J Virol* (2007) 81:4215–4225. doi:10.1128/JVI.02844-06;WGROUP:STRING:PUBLICATION

386. Krawczyk PS, Mazur M, Orzeł W, Gewartowska O, Jeleń S, Antczak W, et al. Re-adenylation by TENT5A enhances efficacy of SARS-CoV-2 mRNA vaccines. *Nature* (2025) 641:984–992. doi:10.1038/S41586-025-08842-1;TECHMETA

387. Rood JE, Yoon SK, Heard MK, Carro SD, Hedgepeth EJ, O'Mara ME, et al. Endogenous antigen processing promotes mRNA vaccine CD4+ T cell responses. *bioRxiv* (2025)2025.03.11.642674. doi:10.1101/2025.03.11.642674

388. Pardi N, Tuyishime S, Muramatsu H, Kariko K, Mui BL, Tam YK, et al. Expression kinetics of nucleoside-modified mRNA delivered in lipid nanoparticles to mice by various routes. *Journal of Controlled Release* (2015) 217:345–351. doi:10.1016/J.JCONREL.2015.08.007

389. Kang DD, Marks A, Morla-Folch J, Dong Y, Brown BD, Teunissen AJP. Targeting and tracking mRNA lipid nanoparticles at the particle, transcript and protein level. *Nature Biomedical Engineering 2025 9:10* (2025) 9:1591–1609. doi:10.1038/s41551-025-01511-8

390. Hosseini-Kharat M, Bremmell KE, Prestidge CA. Why do lipid nanoparticles target the liver? Understanding of biodistribution and liver-specific tropism. *Mol Ther Methods Clin Dev* (2025) 33:101436. doi:10.1016/J.OMTM.2025.101436

391. Castaño D, Bettini E, Kumar B, Chudnovskiy A, Siv A, Protti G, et al. Distinct components of mRNA vaccines cooperate to instruct efficient germinal center responses. *Cell* (2025) 188:7461-7480.e23. doi:10.1016/j.cell.2025.11.023

392. Fair-Mäkelä R, Thorén P, Näsiaho J, Sundqvist P, Piiroinen I, Kähäri L, et al. COVID-19 vaccine type controls stromal reprogramming in draining lymph nodes. *Sci Immunol* (2025) 10: doi:10.1126/SCIIMMUNOL.ADR6787;REQUESTEDJOURNAL:JOURNAL:SCIIMMUNOL;PAGEGROUP:STRING:PUBLICATION

393. Takanashi A, Pouton CW, Al-Wassiti H. Delivery and Expression of mRNA in the Secondary Lymphoid Organs Drive Immune Responses to Lipid Nanoparticle-mRNA Vaccines after Intramuscular Injection. *Mol Pharm* (2023) 20:3876–3885. doi:10.1021/ACS.MOLPHARMACEUT.2C01024

394. Tam HH, Melo MB, Kang M, Pelet JM, Ruda VM, Foley MH, et al. Sustained antigen availability during germinal center initiation enhances antibody responses to vaccination. *Proc Natl Acad Sci U S A* (2016) 113:E6639–E6648. doi:10.1073/PNAS.1606050113;WEBSITE:WEBSITE:PNAS-SITE;WGROUP:STRING:PUBLICATION

395. Guimaraes LC, Costa PAC, Scalzo Júnior SRA, Ferreira HAS, Braga ACS, de Oliveira LC, et al. Nanoparticle-based DNA vaccine protects against SARS-CoV-2 variants in female preclinical models. *Nature Communications 2024 15:1* (2024) 15:1–19. doi:10.1038/s41467-024-44830-1

396. Xiao H, Feng B, Gao D, Shi S, Yang Y, Zhang Y, et al. A naturally derived lipopeptide lipid nanoparticle platform enabling multiple nucleic acids delivery. *Bioact Mater* (2025) 54:829–849. doi:10.1016/J.BIOACTMAT.2025.09.007

397. Barreira M, Kerridge C, Jorda S, Olofsson D, Neumann A, Horton H, et al. Enzymatically amplified linear dbDNATM as a rapid and scalable solution to industrial lentiviral vector manufacturing. *Gene Therapy 2022 30:1* (2022) 30:122–131. doi:10.1038/s41434-022-00343-4

398. Scott VL, Patel A, Villarreal DO, Hensley SE, Ragwan E, Yan J, et al. Novel synthetic plasmid and Doggybone^{TM} DNA vaccines induce neutralizing antibodies and provide protection from lethal influenza challenge in mice. *Hum Vaccin Immunother* (2015) 11:1972–1982. doi:10.1080/21645515.2015.1022008;CTYPE:STRING:JOURNAL

399. Chanani P, Rezaei N, Dormiani K, Shokatian M, Ata-abadi NS. Progress and prospect of minicircle as a minimized non-viral DNA vector in gene therapy and regenerative medicine. *Mol Ther Nucleic Acids* (2025) 36:102682. doi:10.1016/J.OMTN.2025.102682

400. Williams JA, Paez PA. Improving cell and gene therapy safety and performance using next-generation Nanoplasmid vectors. *Mol Ther Nucleic Acids* (2023) 32:494–503. doi:10.1016/j.omtn.2023.04.003

401. Walters AA, Kinnear E, Shattock RJ, Mcdonald JU, Caproni LJ, Porter N, et al. Comparative analysis of enzymatically produced novel linear DNA constructs with plasmids for use as DNA vaccines. *Gene Therapy 2014 21:7* (2014) 21:645–652. doi:10.1038/gt.2014.37

402. Barreira M, Kerridge C, Jorda S, Olofsson D, Neumann A, Horton H, et al. Enzymatically amplified linear dbDNATM as a rapid and scalable solution to industrial lentiviral vector manufacturing. *Gene Therapy 2022 30:1* (2022) 30:122–131. doi:10.1038/s41434-022-00343-4

403. Bai H, Lester GMS, Petishnok LC, Dean DA. Cytoplasmic transport and nuclear import of plasmid DNA. *Biosci Rep* (2017) 37: doi:10.1042/BSR20160616/57779

404. Akita H, Kurihara D, Schmeer M, Schleef M, Harashima H, Akita H, et al. Effect of the Compaction and the Size of DNA on the Nuclear Transfer Efficiency after Microinjection in Synchronized Cells. *Pharmaceutics 2015, Vol 7, Pages 64-73* (2015) 7:64–73. doi:10.3390/PHARMACEUTICS7020064

405. Lavelle EC, Ward RW. Mucosal vaccines — fortifying the frontiers. *Nature Reviews Immunology 2021 22:4* (2021) 22:236–250. doi:10.1038/s41577-021-00583-2

406. Vaca GB, Meyer M, Cadete A, Hsiao CJ, Golding A, Jeon A, et al. Intranasal mRNA-LNP vaccination protects hamsters from SARS-CoV-2 infection. *Sci Adv* (2023) 9: doi:10.1126/SCIADV.ADH1655

407. Pandey A, Kumar S, Mishra S. Intranasal mRNA vaccines: Targeting mucosal immunity through optimized delivery. *Mol Ther Nucleic Acids* (2025) 36:102654. doi:10.1016/j.omtn.2025.102654

408. Li M, Yi J, Lu Y, Liu T, Xing H, Wang X, et al. Modified PEG-Lipids Enhance the Nasal Mucosal Immune Capacity of Lipid Nanoparticle mRNA Vaccines. *Pharmaceutics* (2024) 16: doi:10.3390/PHARMACEUTICS16111423/S1

409. Yi J, Lu Y, Liu N, Wang Z, Zhang H, Xing H, et al. Chitosan and mannose-modified dual-functional mRNA-LNP vaccines for robust systemic and mucosal immune responses. *Journal of Controlled Release* (2025) 384:113891. doi:10.1016/J.JCONREL.2025.113891